Microbial Desalination Cells for Fresh Water Production:

Towards the Implementation of Sustainable Desalination Technology

Ph. D. Thesis

Marina Ramírez-Moreno

Programa de Doctorado de Hidrología y Gestión de Recursos Hídricos, 2023

UAH

Universidad de Alcalá

Escuela de Doctorado de la Universidad de Alcalá

Programa de Doctorado en Hidrología y Gestión de los Recursos Hídricos

TESIS DOCTORAL

Memoria presentada para optar al título de Doctor por Universidad de Alcalá por:

Marina Ramírez Moreno

Microbial Desalination Cells for Fresh Water Production:

Towards the Implementation of Sustainable Desalination Technology

Dirigida por:

Dr. Juan Manuel Ortiz Díaz-Guerra

Prof. Abraham Esteve Núñez

Departamento de Química Analítica, Química Física e Ingeniería Química

Universidad de Alcalá

Alcalá de Henares, 2023

Agradecimientos

En este trabajo queda reflejado la dedicación, la colaboración, el duro trabajo y el cuidado de todo un grupo de personas que han sido y serán muy importantes para mí a nivel tanto personal como profesional. Durante esta etapa he encontrado verdaderas figuras de referencia. Quiero agradecer esta tesis a todas y cada una de esas personas por su tiempo, apoyo, cariño y responsabilidad. Gracias por confiar más en mí que en lo que yo misma lo he hecho.

A mis directores Dr. Juan Manuel Ortiz Díaz-Guerra y Prof. Abraham Esteve Núñez por la oportunidad de poder integrarme en un grupo de investigación diverso, enriquecedor y en el cuál cada día es un reto distinto, de dónde me llevo grandes momentos, enseñanzas y amistades. No me olvido de la Prof. Doña Belén Batanero y el Prof. Don Fructuoso Barba, mis profesores de la Universidad de Alcalá que me concedieron la primera oportunidad que he tenido en el mundo de la investigación dentro de su grupo de Electrosíntesis Orgánica. Gracias a ellos pude comenzar este camino.

A todos los miembros pasados, presentes y futuros del grupo de BioE que se han convertido en mis amigos y familia para toda la vida, sin ellos no hubiera sido capaz de conseguir nada. Todas las personas que he conocido durante todos estos años en IMDEA Agua. Gracias a todos vosotros me he sentido acogida, querida y como en mi segunda casa. También quiero agradecer el trabajo y apoyo de las personas que han formado parte del proyecto MIDES del que me llevo grandes aprendizajes.

A toda mi familia que siempre está pendiente de mí. Gracias a mis padres, a ti mamá por tu fortaleza y cuidado. A mi familia alemana que les tengo siempre muy presentes.

Acknowledgements

Marina Ramírez-Moreno acknowledges the financial support of:

- Project “MIDES – H2020” which has received funding from the European Union’s Horizon 2020 research and innovation programme under grant agreement No 685793.
- Consejería de Educación e Investigación de la Comunidad de Madrid y Fondo Social Europeo (Ref: PEJD-2018-PRE/AMB-8721)." Grants for hiring pre-doctoral researchers and post-doctoral researchers, co-financed by the European Social Fund through the Youth Employment Operational Program and the Youth Employment Initiative (YEI)" Ref: IPRD 2018-04, Alcalá de Henares (Spain).
- CLEAN-CM project "Control and elimination of biological and chemical risks in the water cycle". (REACT-UE Resources of the Madrid Operational Program 2014-2020, in the line of action of R+D+ projects in response to COVID-19). Project financed by the Community of Madrid and the Regional Development Fund of the European Union, "A way of making Europe" (Funded as part of the Union's response to the COVID-19 pandemic).

I would like to express my gratitude to following entities for their collaboration, help, learning and scientific support, as well as their facilities to carry out this thesis: Bioe group, University of Alcalá, IMDEA Water Institute, Materials Research University of Alicante, Leitat Technological centre, REMTAVARES and Aqualia.

“Olvidamos que
el ciclo del agua
y el ciclo de la vida
son uno mismo”

Jacques Y. Cousteau

CONTENTS

SUMMARY

The discovery of the ability of some bacteria to exchange electrons with electrically conductive materials has given rise to a new field of study called electromicrobiology. Due to the capacity and versatility of these microorganisms, a platform of technologies called Microbial Electrochemical Technologies (MET) has been developed, with the potential to offer solutions to the challenge of limited resources such as energy and water. Although the birth of electromicrobiology aspired to recover the chemical energy present in organic contaminants, two decades of research have made possible the appearance of multiple applications, including water desalination.

Microbial Desalination Cell (MDC) technology is a sustainable and energy-self-sufficient bioelectrochemical technology that treats wastewater, produces power, and desalinates water simultaneously in the same device without external power input. The desalination process in the MDC device is driven by the energy provided by electroactive microorganisms through the degradation of organic matter contained in the wastewater. However, implementing MDC technology on a real scale depends on overcoming its current limitations. This requires a systematic study of these devices in the laboratory to be able to further study microbial processes, technological improvements, etc.

Currently, the desalination of seawater and the reuse of treated water have been proposed to alleviate the problems associated with the scarcity of water resources worldwide. Reverse osmosis (RO) is the most widely implemented desalination technology, but new approaches are still needed to decrease its high energy consumption (3-4 kWh m^{-3}). In this regard, Microbial Desalination (MDC) technology has been proposed as a pretreatment step for RO technology to reduce desalination energy from the RO process and increase potable water production using wastewater as a renewable energy source. With this objective,

the MIDES project (the research project in which this thesis has been framed) has developed the world's largest demonstration plant of MDC technology.

The memory of this thesis consists of 9 chapters, 5 of which are experimental. The main results presented served as a reference and a starting point for the subsequent scale-up of the technology within the MIDES-H2020 project, where this thesis is contextualized (Research Framework). ***Chapter 1*** (Introduction) provides an overview of the current situation of desalination technologies and the origin, rationale and state-of-the-art of METs. As a final part of this chapter, the MDC systems (mechanism, the main factors that worsen their performance) are detailed in-depth together with their state of the art. In addition, the current challenges that exist and can be overcome for implementing this technology on a real scale are presented.

The objectives of this thesis, collected in ***Chapter 2,*** have systematically investigated the MDC bioelectrochemical device on a laboratory scale (described in ***Chapter 3***) to deepen and understand the electrochemical behavior of this type of system and thus promote its use, development, design, and optimization to produce drinking water with low energy cost.

One of the current challenges of this technology is the choice of the cathode reaction used in the MDC system to carry out desalination. For this reason, the first experimental chapter (***Chapter 4***) deals with the comparison of the operation of two MDC systems under a different cathode strategy (air cathode versus the use of liquid catholyte) for the desalination of synthetic water (brackish water and seawater).

Once the performance of these systems without cathodic limitation was known, the study of the electrochemical behavior of the MDC system was carried out on a laboratory scale for the desalination of synthetic brackish water under the cathodic strategy of greater efficiency in desalination (***Chapter 5***). In this study, the main parameters of the MDC systems (desalinated water production

and generated energy) were under different values of external resistance. These treatment and production parameters are also affected by many other factors, such as the initial concentration of the saline stream (***Chapter 6***), which can vary depending on the scenario where this technology can be studied/implemented.

After the operation of the MDC system was studied in non-real conditions (synthetic waters), desalination was carried out operating with real waters, both residual (urban, industrial) and saline (brackish, seawater) to validate on a laboratory scale the system under real conditions (***Chapter 7***).

One of the crucial economic and performance factors, not only in MDC systems but also in bioelectrochemical systems in general, is carbonaceous conductive materials. Electroactive microorganisms use these materials for electron transfer. For this reason, the study of new materials that promise adhesion and electron transfer with electroactive biofilms is of great relevance in these technologies. The study shown in the last experimental chapter (***Chapter 8***) includes the physicochemical characterization of a commercial carbonaceous material that is subsequently activated through a CO_2 and temperature treatment. The influence of the activation of the material against electroactivity by electroactive bacteria that colonize its surface was learned.

Finally, a general discussion is presented to contextualize the results collected in the five experimental chapters exposed above, together with some general conclusions and future work that could be achieved in the future for the continuous development of MDC technology (***Chapter 9***).

RESUMEN

El descubrimiento de la capacidad que presentan algunas bacterias para intercambiar electrones con materiales conductores de la electricidad ha dado lugar a un nuevo campo de estudio denominado electromicrobiología. Debido a la capacidad y versatilidad de estos microorganismos se ha desarrollado una plataforma de tecnologías denominadas Tecnologías Electroquímicas Microbianas (en inglés, Microbial Electrochemical Technologies, MET), con potencial para ofrecer soluciones al reto de la limitación de los recursos como la energía y el agua. Aunque el nacimiento de la electromicrobiología aspiraba a recuperar la energía química presente en contaminantes orgánicos, dos décadas de investigación han hecho posible la aparición de múltiples aplicaciones, entre las que se encuentra la desalinización de agua.

La desalinización microbiana (en inglés, Microbial Desalination Cell, MDC) es una tecnología bioelectroquímica sostenible y energéticamente autosuficiente que trata aguas residuales, produce energía y desaliniza agua al mismo tiempo en el mismo dispositivo sin aporte de energía externa. El proceso de desalinización está impulsado por la energía que aportan los microorganismos electroactivos a través de la degradación de la materia orgánica contenida en las aguas residuales. Sin embargo, la implementación de la tecnología MDC a escala real depende de superar las actuales limitaciones que presenta. Es necesario el estudio sistemático de estos dispositivos MDC a escala de laboratorio para profundizar en el estudio de los procesos microbianos, en las mejoras tecnológicas, etc.

Actualmente, la desalinización del agua de mar y la reutilización del agua tratada se han propuesto para paliar los problemas asociados a la escasez de los recursos hídricos a nivel mundial. La ósmosis inversa (RO, por sus siglas en inglés) es la tecnología de desalinización más extendida, pero aún son necesarios nuevos enfoques para disminuir su alto consumo de energía (3-4 kWh m^{-3}). En este sentido, la tecnología de desalinización microbiana se ha propuesto como

una etapa de pretratamiento para la tecnología de RO para reducir la energía de desalinización del proceso de RO y aumentar la producción de agua potable utilizando aguas residuales como una fuente de energía renovable. Con este objetivo, el proyecto MIDES (proyecto de investigación en el que se ha enmarcado la presente tesis) ha desarrollado la planta demostrativa más grande del mundo de la tecnología MDC.

La memoria de esta tesis consta de 9 capítulos, 5 de ellos experimentales. Los principales resultados presentados sirvieron de referencia como punto de partida para el posterior escalado de la tecnología que se llevó a cabo dentro del proyecto MIDES-H2020 donde queda contextualizada esta tesis (Research Framework). El ***Capítulo 1*** (Introducción) proporciona una visión general de la situación actual de las tecnologías de desalinización, así como el origen, fundamento y estado del arte de las METs. Como parte final de este capítulo se detallan en profundidad los sistemas MDC (mecanismo, los factores principales que afectan a su desempeño) junto con su estado del arte. Además, se presentan los retos actuales que existen y que deberían superarse para la implantación de esta tecnología a escala real.

Los objetivos de esta tesis, recogidos en el ***Capítulo 2***, han sido investigar de forma sistemática el dispositivo bioelectroquímico MDC a escala de laboratorio ***(descrito en Capítulo 3)*** para lograr profundizar y entender el comportamiento electroquímico de este tipo de sistemas y así promover su desarrollo, diseño y optimización, con el objetivo de producir agua potable con bajo costo energético.

Uno de esos retos actuales de esta tecnología es la elección de la reacción catódica utilizada en el sistema MDC para llevar a cabo la desalinización. Por ello, el primer capítulo experimental (***Capítulo 4***) aborda la comparación del funcionamiento de dos sistemas MDC bajo una estrategia catódica diferente (cátodo de aire frente al uso de catolito líquido) para la desalinización de agua sintética (salobre y agua de mar).

Una vez conocido el desempeño de estos sistemas sin limitación catódica, se realizó el estudio del comportamiento electroquímico del sistema MDC a escala de laboratorio para la desalinización de agua salobre sintética bajo la estrategia catódica de mayor eficiencia en desalinización ***(Capítulo 5)***. En este estudio, los principales parámetros de los sistemas MDC (producción de agua desalinizada y energía generada) se obtuvieron bajo diferentes valores de la resistencia externa. Estos parámetros de tratamiento y producción se ven afectados, además, por otros muchos factores como por ejemplo la concentración inicial de la corriente salina (***Capítulo 6***), que puede variar dependiendo del escenario donde se pueda estudiar/implantar esta tecnología.

Una vez estudiado el funcionamiento del sistema MDC en condiciones no reales (aguas sintéticas), se realizaron desalinizaciones operando con aguas reales, tanto residuales (urbana, industrial) como salinas (salobre, agua de mar) con el fin de validar a escala de laboratorio el sistema en condiciones reales (***Capítulo 7)***.

Entre los factores cruciales a nivel económico y de rendimiento no sólo en los sistemas MDC sino en los sistemas bioelectroquímicos en general, se encuentran los materiales conductores carbonosos. Estos materiales son utilizados por los microorganismos electroactivos para la transferencia electrónica. Por esta razón, el estudio de nuevos materiales que promuevan la adhesión y la transferencia electrónica con las biopelículas electroactivas tiene gran relevancia en estas tecnologías. El estudio mostrado en el último capítulo experimental (***Capítulo 8***) comprende la caracterización fisicoquímica de un material carbonoso comercial que es posteriormente activado a través de un tratamiento de CO_2 y temperatura. Se estudió la influencia que tiene la activación del material frente a la electroactividad por parte de las bacterias electroactivas que colonizan su superficie.

Finalmente, se presenta una discusión general que pone en contexto los resultados recogidos en los 5 capítulos experimentales anteriores, junto con unas

conclusiones generales y trabajos futuros que podrían realizarse para el continuo desarrollo de la tecnología MDC (***Capítulo 9).***

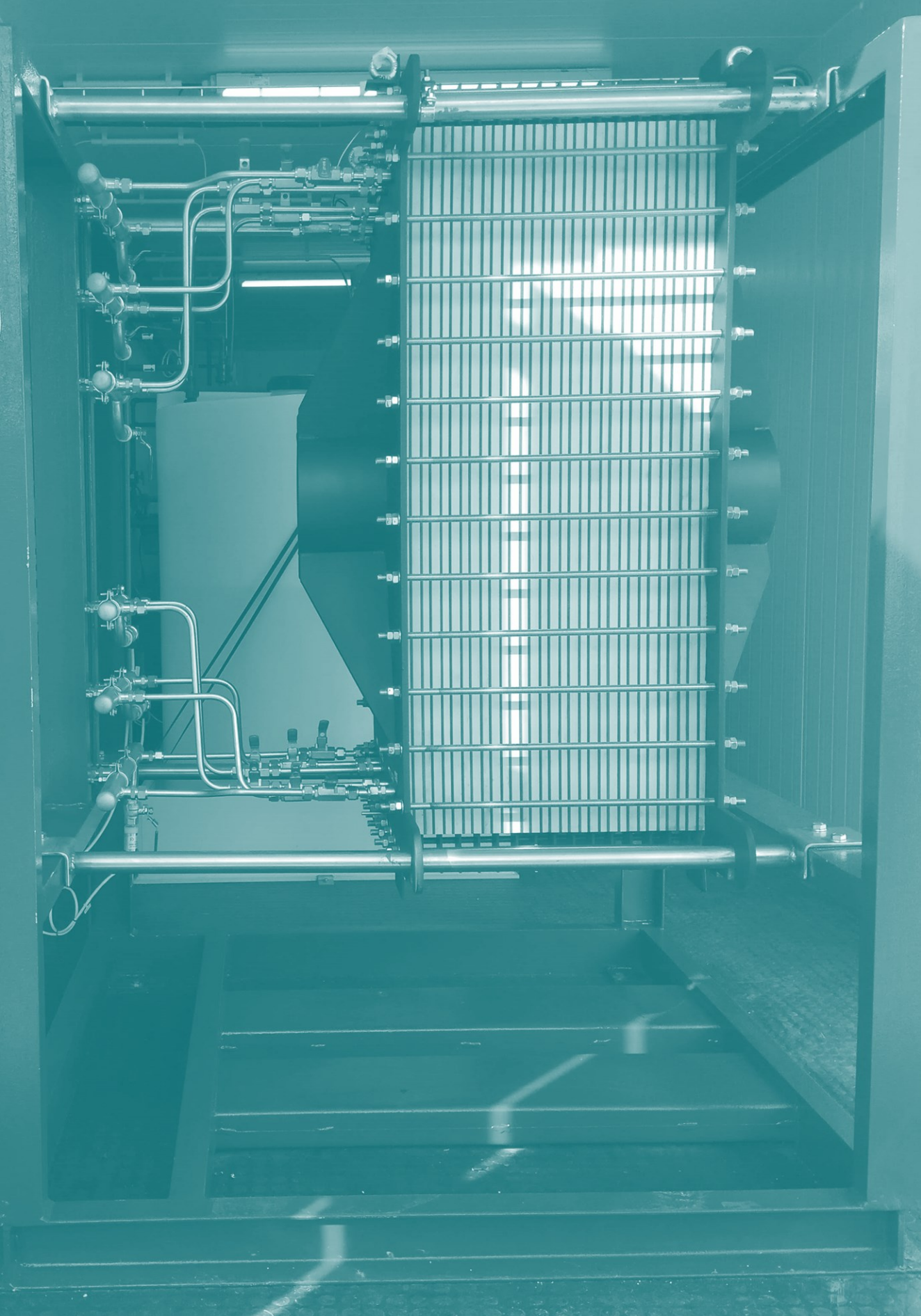

RESEARCH FRAMEWORK

The present thesis was developed within the framework of MIDES (Microbial Desalination for Low Energy Drinking Water) project. This project, implemented between 2016-2020, received funding from the European Union's Horizon 2020 research and innovation program under grant agreement No. 685793.

The objective of the project was to change the paradigm of desalination by developing a sustainable, low-energy process of producing safe drinking water, using the emerging technology of Microbial Desalination Cell (MDC) as a pre-treatment for Reverse Osmosis (RO). The project was comprised of an international consortium from seven countries: Austria, Germany, Hungary, the Netherlands, Portugal, Spain, and Tunisia, including 10 companies and research organizations, all experts in water and technology innovation.

The laboratory-scale studies shown in the experimental chapters of this thesis were carried out as part of the WP3 (Microbial Desalination Cell design and bioengineering assays) and WP4 (Process integration and prepilot validation) in the European MIDES project. The experimental results were key to scale up the technology and eventually to validate it at real scale.

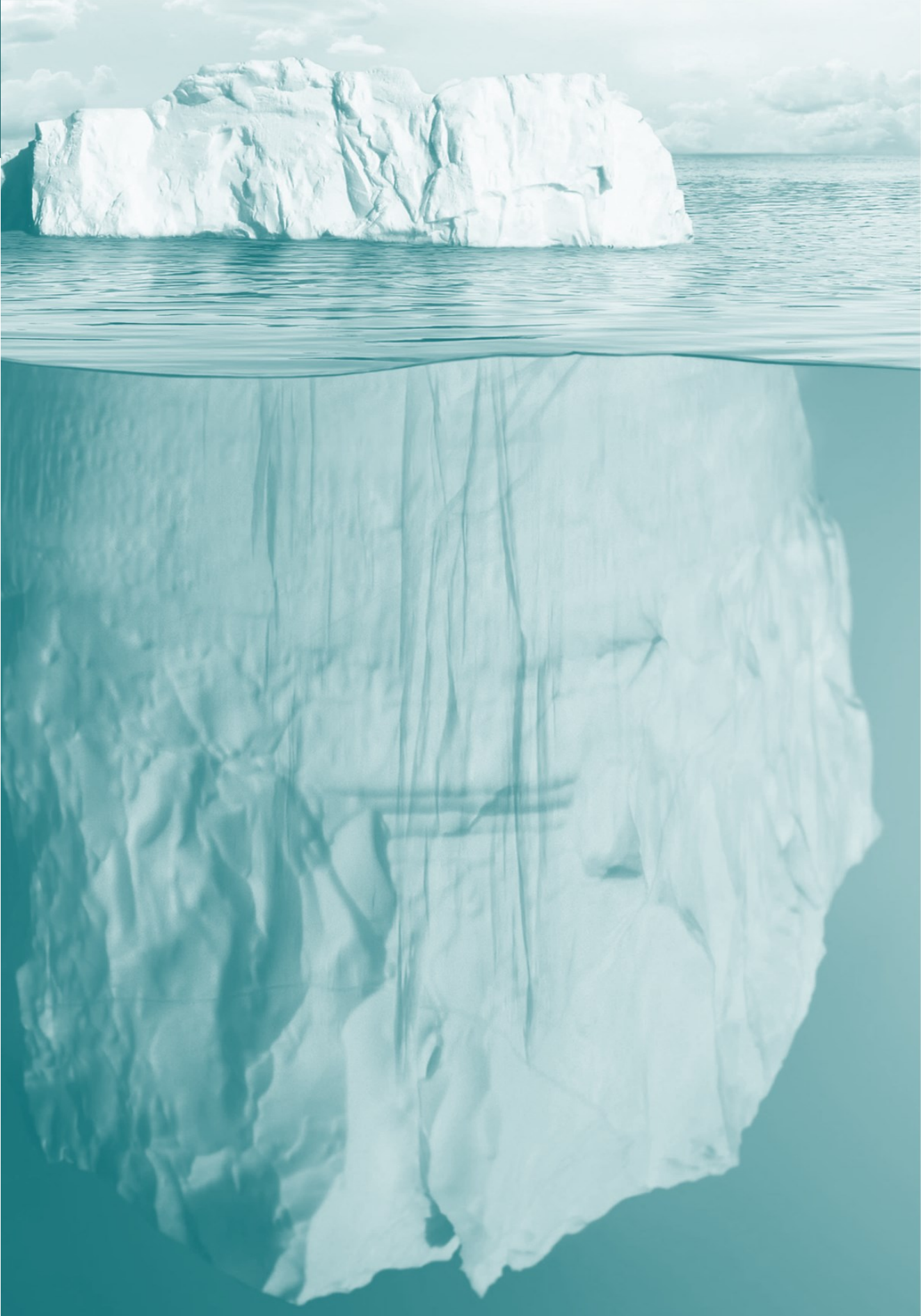

Chapter 1

Introduction:
towards the sustainable desalination

Introduction: towards a sustainable desalination

Chapter 1: Introduction

1.1 Towards a sustainable desalination

1.1.1 Water Shortage: The Main World Challenge

One of the most significant world challenges in the 21st century is water scarcity. Despite the broad natural water reserves on Earth, just 2.5% is freshwater, and only 1% of this freshwater is available for consumption (Sharma et al., 2019); the rest is in the form of deep underground or glaciers. Numerous studies predict that this shortage will continue to increase, with 52% of the population worldwide living in water-stressed regions by 2050 (Kölbel et al., 2018). This situation affects all continents **(Figure 1)**, where the Middle East is the most water-scarce region in the world. The increased water use, and an erratic supply will aggravate and generate water stress in regions with abundant water resources today. In addition, climate change is affecting the quantity, availability, and quality of water for basic needs, thus threatening the human rights of millions of people.

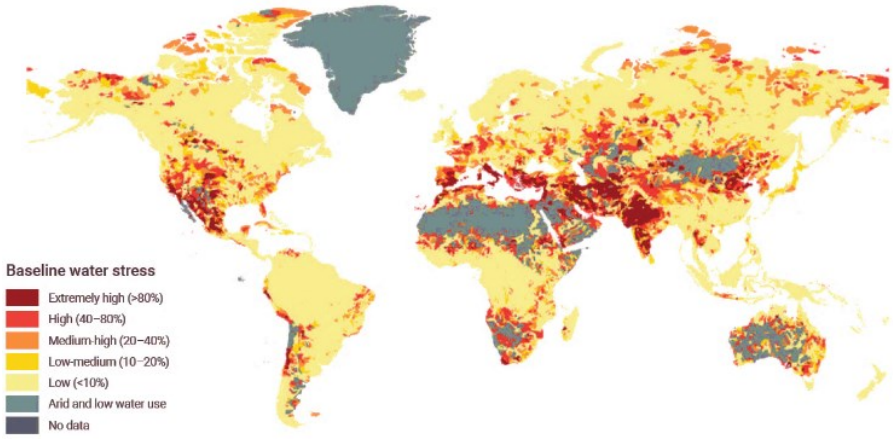

Figure 1. Water stress affect all continents (UNESCO/UN-Water, 2020). Source: (Global Water Intelligence, 2020).

In front of this situation, the adaptation and mitigation of climate change through water management is essential to achieve the United Nations 2030 Agenda for Sustainable Development (UNESCO/UN-Water, 2020). This Agenda is a universal roadmap and call to action to protect the planet and improve lives for everyone everywhere and establishes a 15-year plan to achieve 17 Sustainable Development Goals adopted by all UN member states in 2015. Among the goals, the objective SDG-6 is referred to freshwater and demands the availability and sustainable management of water and sanitation. It has become one of the main ones since other objectives depend on water (Schmidt, 2019).

1.1.2 Seawater and brackish water desalination

Given the limitless nature of seawater and the declining cost of renewable energy sources, desalination can improve freshwater supply for drinking, industrial use, and irrigation in the future (Elimelech and Phillip, 2011; Sood and Smakhtin, 2014). Desalination is the process of removal of salt from saline water to produce freshwater. Large-scale seawater desalination began in the 1960s, using thermal distillation processes such as multi-stage flash (MSF) and multi-effect distillation (MED). The membrane-based technology reverse osmosis (RO) was introduced in the 1970s into the market, mainly to treat brackish water and into 1980s for seawater applications. As a result of the membrane material and technology advancement, in 1999, membrane-based technologies, including RO, electrodialysis (ED) and nanofiltration (NF), have become the most dominant technologies for water desalination.

According to International Desalination Association (IDA Desalination & Reuse Handbook 2021–2022, 2022), in 2021, the currently installed desalination plants worldwide was around 19.000 and a high number of desalination plants have been installed in the Middle East, USA, Australia, China, Central Europe, the Mediterranean Region, and Japan. According to Global Water Intelligence (Global Water Intelligence, 2020) the total desalination capacity (installed and

projected, 2021) is about 115 Mm^3/d, of which 77% (~88 Mm^3/d) uses Reverse Osmosis technology being currently the most applied technology. This technology is used to produce drinking water and industrial water and seawater desalination. Almost half (53%) of the RO desalinated water is from seawater, and the rest is mainly from brackish, freshwater and treated wastewater (Dhakal et al., 2022).

The mechanism behind RO is diffusion **(figure 2)**; the water flows in the opposite direction of natural flow (i.e., osmosis) across a membrane (Khawaji et al., 2008). A flow of saline water (feed stream) is passed through a semi-permeable membrane where dissolved solutes (organic and inorganic) are rejected and are left behind with an increase in salt concentration on one side (concentrate) of the membrane and the production of high-quality water on the other side (permeate). This process is achieved due to the application of an external pressure higher than the osmotic pressure of the saline water. The process efficiency and energy consumption of the RO unit depends mainly on the salinity of the feed water and the recovery rate. In this sense, high salinity water contains higher osmotic pressure and requires a more significant amount of energy. In addition, the salt permeation through the membrane increases proportionally with the salt concentration of the feed water.

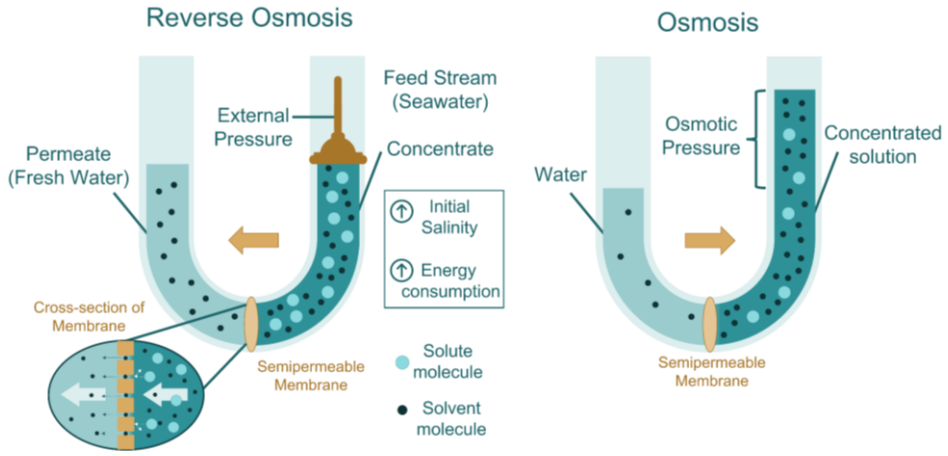

Figure 2. Reverse osmosis desalination plant (photography at the left), drawing water from the Marina Reservoir and the Singapore Strait. (IDA Desalination & Reuse Handbook 2021–2022, 2022). The reverse osmosis process (figure at the top) compared to the concept of osmosis occurring in nature.

1.1.3 Energy cost: the main problem

Challenges to the extended adoption of desalination exist, such as expense, the carbon footprint of facilities, greenhouse gas emissions (GHGs) if renewable energy sources are not used, chemical discharge (such as brine) and operational problems such as membrane fouling o scaling (Ihsanullah et al., 2021).

The conventional desalination processes are technologically feasible, but they currently maintain high energy consumption (electrical or thermal) powered mainly by fossil fuel combustion (Olabi et al., 2020). This high energy cost is a significant barrier to the comprehensive and sustainable implantation of the technology. The most efficient RO seawater desalination systems have achieved an energy requirement between 1.8–2.2 kWhm^{-3} (3-4 kWh m^{-3} considering the energy for pre-treatment or pumping)(Elimelech and Phillip, 2011; Al-Karaghouli and Kazmerski, 2013). This value is lower than the case of the thermal processes (5.5-40 kWh m^{-3})(Sharon and Reddy, 2015). RO is constantly evolving with new developments in configurations and membranes to reduce energy consumption and the associated emission of GHG (0.4–6.7 kg of CO_2 per m^3 of seawater). The most efficient RO achieved the value of 1.6 kWh m^{-3} with the best commercial membranes (MacHarg et al., 2008) which is near the value of the thermodynamic limit. This value limit is 1.09 kWh m^{-3} and is the minimum

energy required for seawater desalination at 50% recovery (ElMekawy et al., 2014; Salehmin et al., 2021).

New technologies and energy sources are emerging to address the challenges in the water-energy nexus (developing new energy resources requires significant water supplies and considerable energy resources for developing new water resources) (UNESCO/UN-Water, 2020). For the imminent need to increase freshwater production, an effort is needed to overcome the energy challenges in desalination technologies, which are still a mandatory option for drinking water supply in areas where freshwater sources are not available (Gude et al., 2010). This situation, in combination with the increase in the consumption and cost of fossil fuels (coal and gas) and the related GHG (Cornejo et al., 2014), has increased the interest in developing new sustainable strategies through the integration of renewable resources (Abdelkareem et al., 2018). However, despite the free cost of renewable energy (e.g., wind, solar), the capital cost of renewable energy systems is still very high, this makes the produced water cost high (Al-Karaghouli and Kazmerski, 2013). Due to this high cost, desalination systems incorporating renewable energy resources are currently only economic in rural areas without access to electric grid, where solar radiation or wind speed are appropriate. Furthermore, the renewable energy sources have an intermittent nature, for that requires the utilization of energy storage to secure energy supply during downtime (Rezk et al., 2019).

Therefore, there is a growing interest and urgency in finding cost-effective and renewable energy sources to complement or improve desalination technologies. One of these possible renewable energy sources is the chemical energy contained in wastewater which can be recovered and stored in diverse forms or used for different applications such as the desalination process. Wastewater contains about ten times more energy than required to treat it (requires 0.5-2 kWh of energy per m^3 depending on the process). This chemical energy contained in wastewater is mainly present in organic matter (~1.79 kWh

m^{-3}), nutrients such as nitrogen, phosphorous (~0.7 $kWhm^{-3}$), and thermal heat (~7 kWh m^{-3})(McCarty et al., 2011). Thus, wastewater treatment can be turned into an energy-producing process rather than an energy-consuming process while eliminating environmental pollution.

In that sense, a new desalination technology known as Microbial Desalination Cells (MDC) has offered an alternative approach that could provide a possible solution toward a greener, sustainable, and energy-efficient desalination. This self-powered technology reuses wastewater as a renewable source of energy and water source. Technologically, the MDC is a bioelectrochemical device where electroactive microorganisms oxidase organic substances present in wastewater and generate electricity, treated water and simultaneously achieve desalination of a saline stream (Cao et al., 2009).

It is estimated that MDC technology can produce around 1.8 kWh of bioelectricity from handling 1 m^3 of seawater that while RO technology requires 2.2 kWh of electricity for the same amount of water desalination (Jacobson et al., 2011b; Gude et al., 2013). Such produced energy can be directly used to remove the salt content in the saline stream without external energy input; or partially reduce the salinity to substantially lower the amount of energy for a subsequent desalination treatment. With this second point of view, the MDC technology has been proposed as a pre-treatment of RO to decrease the energy cost of conventional desalination plants (Mehanna et al., 2010c). This development idea materialized in 2016 with the MIDES Horizon 2020 project previously presented as the main framework of this thesis.

1.1.4 MIDES project

The objective of the European project MIDES (Microbial Desalination Cell for Low Energy Drinking Water, 2016-2020) was to develop a sustainable, low-energy process of producing drinking water using the technology of Microbial Desalination Cell (MDC) as a pre-treatment for conventional Reverse Osmosis (RO). To achieve this goal the project focused on overcoming the current limitations of MDC technology: low desalination rate, high manufacturing cost, biofouling and scaling problems on membranes, optimization of the microbial-electrochemical process, integration with RO, ceramic nano membranes as pre-treatment, system scale up and economic feasibility of the technology. The MIDES overall process scheme is shown in **figure 3** where the core technologies, MDC and RO, are integrated with other complementary technologies. The process includes the initial treatment of wastewater in an anaerobic reactor for using this effluent as a fuel for the MDC, which returns a treated wastewater with reduction of the initial chemical oxygen demand (COD). After pre-treatment by nano-coated ceramic, seawater entered the MDC unit where it was partially desalinated (70–90%) before it was fully processed in the RO unit. Since the RO process efficiency and energy requirement depends on feed water salinity, pre-desalination of the feed water with an MDC will reduce its salinity and thus energy demands for downstream RO (Salinas-Rodríguez et al., 2021). In this way, the energy consumption of the global desalination process would decrease from 3-4 kWh m^{-3} (energy consumed using RO) to approximately 0.5 kWh m^{-3} (energy consumed with a combination of MDC with RO in the MIDES project).

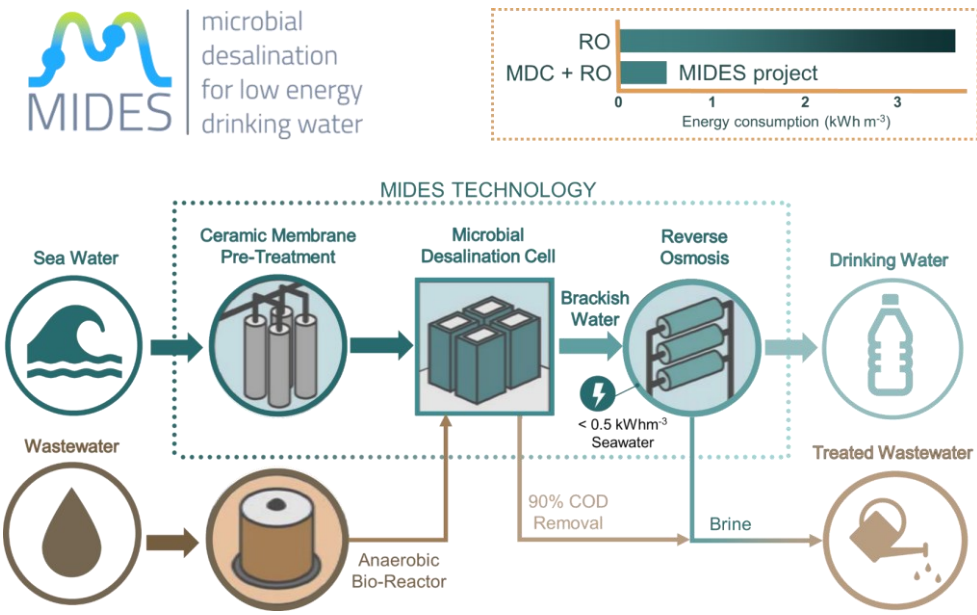

Figure 3. Overall process of MIDES project. Schematic representation of the reduction of energy consumption in the MIDES project compared to the energy consumption of conventional reverse osmosis (RO) technology.

The MDC technology was scaled from the laboratory scale to the pilot scale **(figure 4)** to connect it with the RO plant. The laboratory-scale studies shown in the experimental chapters of this thesis were carried out in the lab-scale MDC unit (100 cm^2). Pre-pilot unit and pre-pilot stack were also developed at IMDEA Water Institute. Finally, two pilot-scale MDC systems were implemented in Spain as demonstration sites: Demo Site 1 in Dénia (Alicante, Spain) (to validate brackish water desalination) and Demo site 2 in Tenerife (Spain) (to validate seawater desalination).

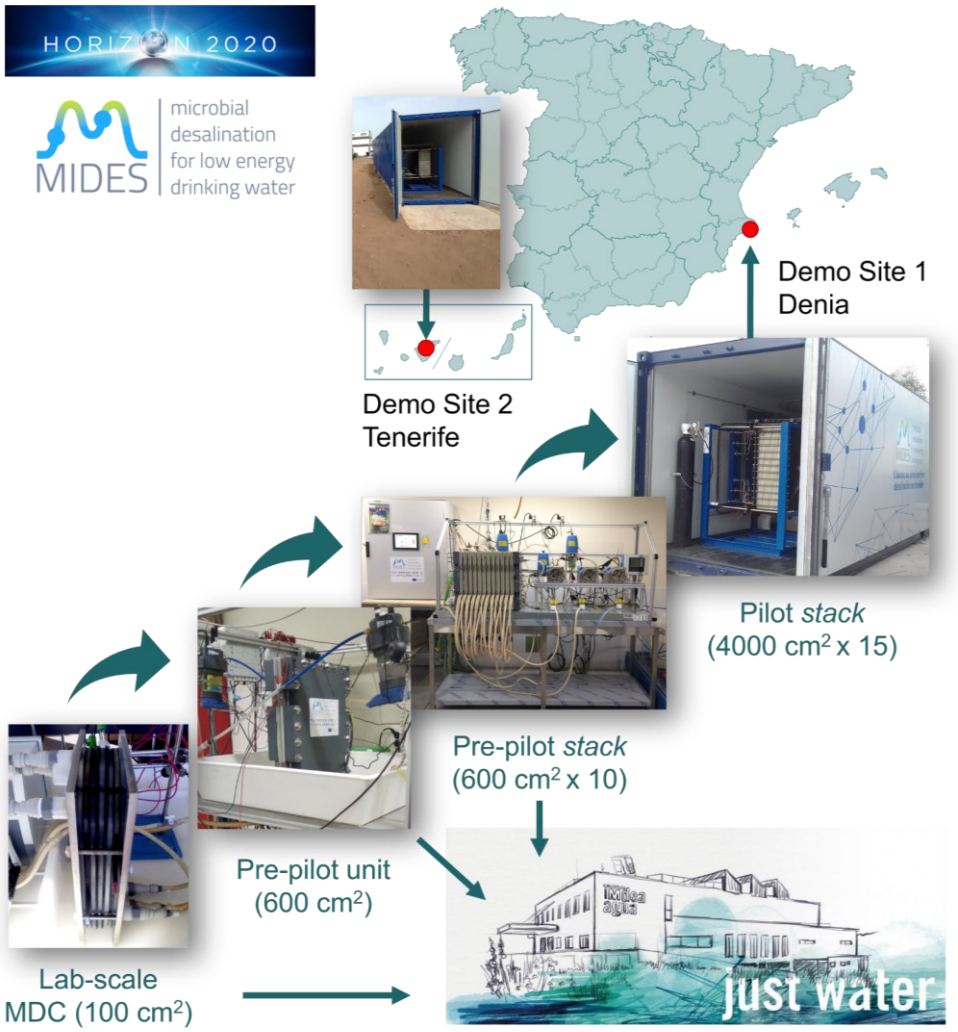

Figure 4. MDC device scale-up during the MIDES project. Scales: **a)** a 3-compartment configuration laboratory unit (100 cm^2); **b)** a 3-compartment configuration unit pre-pilot MDC (600 cm^2); **c)** stack pre-pilot (600 cm^2 x 10 units), an assembly of multiple MDC units with a 3-cell configuration **d)** stack pilot (4000 cm^2 x 15 units). Photos' source: (Salinas-Rodríguez et al., 2021). Draw from web page of IMDEA Water Institute.

Before starting the MIDES project, the desalinated water production in the most significant reported scaled-up MDC was 0.077 L m^{-2} h^{-1} (i.e., freshwater production per square meter of membrane and hour) for partial desalination synthetic seawater (Zhang and He, 2015). Although complete desalination in MDCs can be achieved without an external electrical source, the freshwater

production was still 200 times lower than in conventional desalination systems (for RO = 15–20 L m^{-2} h^{-1}). Preliminary results for the MDC pilot system (at Demo Site 1, Dénia) for complete synthetic brackish water desalination (with an initial electric conductivity of 4.2 mS cm^{-1}) showed a nominal desalination rate (NDR) of 4.1 L m^{-2} h^{-1} (Salinas-Rodríguez et al., 2021). In addition, this value was comparable to the laboratory (4.6 L m^{-2} h^{-1} for initial electric conductivity of 5.6 mS) and pre-pilot scale (6.2 L m^{-2} h^{-1} for initial electric conductivity of 3.2 mS cm^{-1}) MDC systems, showing good similarity for the future of the scale-up of the MDC system.

Together with other bioelectrochemical systems, the MDC system belongs to the innovative technology platform known as Microbial Electrochemical Technology (MET). This platform is a strategy that can contribute to developing more sustainable processes in various applications through the recovery, storage and efficient use of resources.


200
150
100
50
IKA
topolino
IKA
topolino

1.2 Microbial Electrochemical Technologies (MET): take advantage of alternative energy resources.

Microbial Electrochemical Technology (MET) is an emerging field in biotechnology that presents innovative solutions to current environmental challenges due to climate change and population growth. This technology is a sustainable platform that integrates the waste treatment/ valorization and energy production/recovery with biotechnological applications such as wastewater treatment (Aguirre-Sierra et al., 2020) bioremediation (Wang et al., 2020a; Rotaru et al., 2021), bioelectrosynthesis (Prévoteau et al., 2020), biosensing (Fernandez-Gatell et al., 2022) or desalination (Salinas-Rodríguez et al., 2021). These applications are based on concepts belonging to electromicrobiology. The electromicrobiology research field explore the ability of electroactive microorganisms to exchange electrons with conductive surfaces by performing an extracellular electron transfer (EET) mechanism (Logan et al., 2019) (**Figure 5**). Two decades after first MET was developed, a number of challenges still limit its direct implementation (Wang and Ren, 2013) so more significant efforts are necessary to tackle full scale applications.

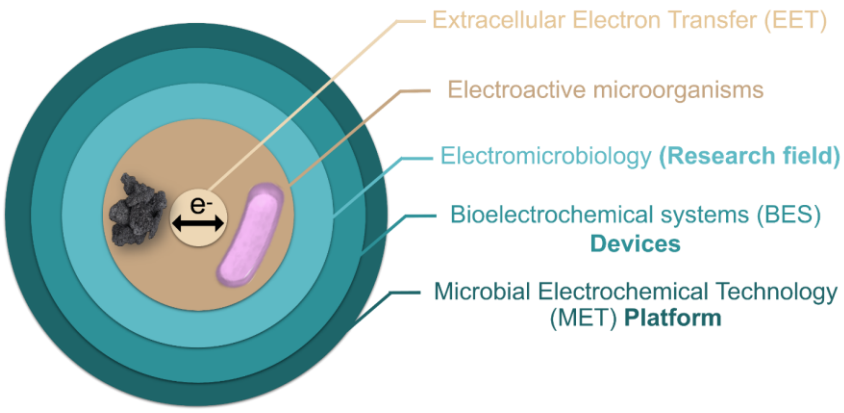

Figure 5. Conceptual map of concepts and terminology that encompass the platform of MET. Microbial Electrochemical Technology is the term that englobe the devices where the knowledge about electromicrobiology is applied.

1.2.1 Electromicrobiology: a connection between disciplines

The electrochemistry studies the heterogeneous redox (reduction/oxidation) reactions, i.e., the electronic transfer between a chemical species and a solid conductive material (electrode). When this phenomenon occurs, the chemical energy contained in the chemical species is transformed into electrical energy or vice versa. The fact that some microorganisms are involved in this chemical-electrical energy conversion make possible to merge electrochemistry and microbiology.

The electrical energy liberation from microorganisms was first observed more than 100 years ago (Potter, 1910, 1911; Cohen, 1931). More later, in the 21st century, is reported the presence of microorganisms capable of conserving the energy necessary for their growth through the oxidation of organic matter present in marine sediments and transferring the electrons resulting from their metabolism to an electrode, generating an electrical current (Reimers et al., 2001; Bond, 2002). Microorganism capable of developing such reactions are so-called electrochemically active bacteria (EAB).

The union between both disciplines **(Figure 6)** arised the electromicrobiology as an emerging field of research that studies the capacity of certain microorganisms to exchange electrons with insoluble conductive electron acceptors/ donors (Yee et al., 2020), such as conductive minerals or the electrodes used in biotechnological systems (Logan et al., 2019).

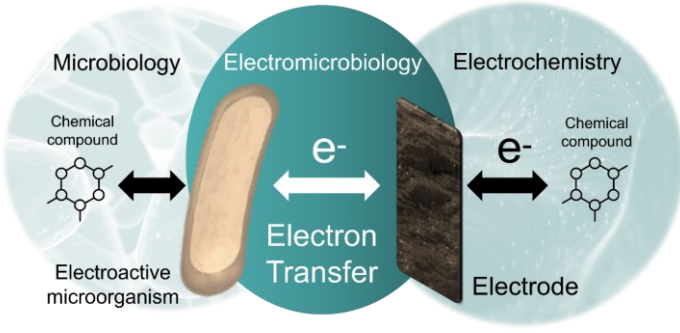

Figure 6. Electromicrobiology research field is the fusion between electrochemistry and microbiology.

Energetic concepts comparison (living cell vs. fuel cell)

All organisms show mechanisms to conserve energy, that is, to convert light or chemical energy into cellular energy in the form of adenosine triphosphate (ATP) (Russell and Cook, 1995) to maintain essential life functions. Microorganisms can produce that energy through two major metabolic pathways: respiration (energetically efficient complete oxidation, inorganic compound as final product) and fermentation (incomplete oxidation, organics molecules as final products)(Schröder, 2007; Kim and Gadd, 2019). During the respiration process the energy is extracted by transferring electrons via redox cascade (respiratory chain), from the oxidation of a reduced substrate with a low reduction potential such as organic compound (electron donor, EDN) to the terminal electron acceptors (TEA) such as oxygen molecule with a greater reduction potential (David White et al., 2012). The potential gradient between electron donor/acceptor determines the available energy for cell growth (Mathews et al., 2002). This amount of available energy is determined by the free Gibbs energy $\Delta G^{o\prime}$ (kJ mol^{-1}) of the process **(figure 7, equation 2)**(Schröder, 2007). Therefore, the higher positive redox potential of a terminal electron acceptor, the higher energy gain for an organism, been the aerobic respiration (oxygen molecule as TEA) the path with the highest energy gain **(figure 7, left).** In consequence, aerobic microorganism have more energy available to grow compared to anaerobic ones (when oxygen is unavailable the TEA used is a soluble oxidized form such as nitrates, sulfate…) (Schröder, 2007).

This respiration process to obtain energy could be compared with a more electrochemical concept: the fuel cell **(figure 7, right)**. A fuel cell is indeed an electrochemical energy conversion device where the chemical energy contained in a fuel (hydrogen, for example) is converted into electrical energy, heat and water (oxygen is reduced in the process). The energy input or output in electrochemical systems is determined by the Gibbs free energy change ($\Delta G^{0\prime}$, kJ mol^{-1}) of the overall reaction (at standard conditions of 1 atm, 273 K, 1 M a

neutral pH) and it is related to the cell voltage ($\Delta E^{0'}$) by **equation 1 (Figure 7)**, where *n* is the number of electrons transferred in the reaction and F is Faraday constant (96485 C mol^{-1}). In this device, also the higher the potential difference ($\Delta E^{0'}$), between two electrodes (anode and cathode) the higher available energy **(equation 3, Figure 7)** harvested by the fuel cell ($\Delta G^{0'}$). In the practice, (without standard conditions) when the fuel cell is at open circuit conditions (no charges flowing) the value of the open circuit voltage can be directly measured. This is named as open circuit voltage (OCV) or electromotive force (E_{emf}). It represents the maximum potential that the fuel cell can supply at open circuit conditions. This OCV can be calculated from the Gibbs free energy change of the overall reaction occurring at the electrodes (without standard conditions) **(equation 3, Figure 7)**. It is called also as theoretical cell voltage because the contribution of the partial voltage losses inside the device is not include (overpotential of electrodes, E_{η}, voltage lost across the membrane or due to the ionic resistance of the solutions, E_{Ω}). The real cell voltage **(equation 4, Figure 7)** considers these losses and is measured when the fuel cell is at closed circuit conditions (charges flowing through).

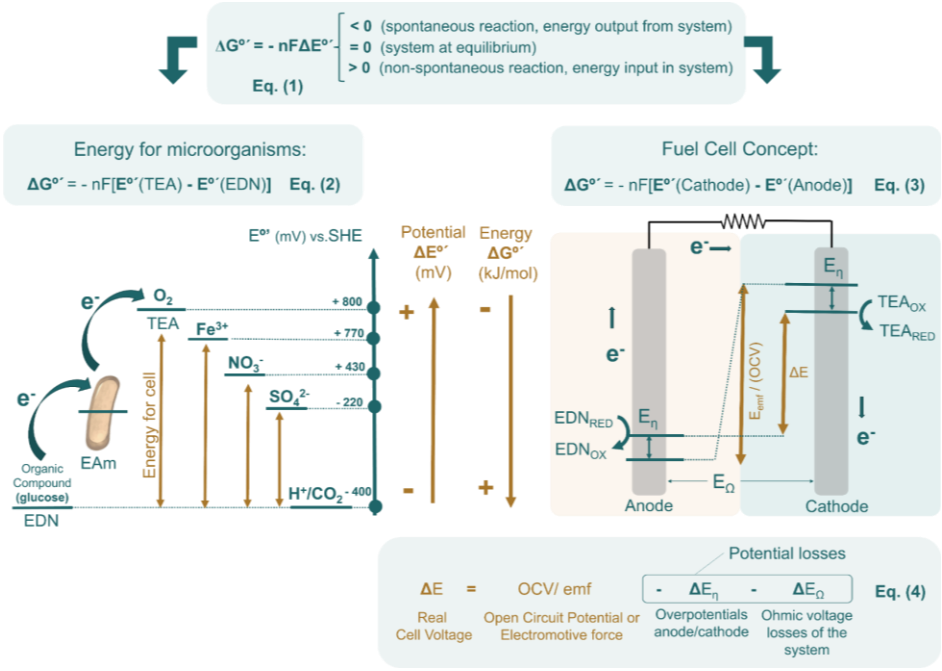

Figure 7. Left: Electron transfer from a substrate (EDN) such glucose with a low reduction potential, to a different final electron acceptor (TEA) with a greater reduction potential. The different between these potentials is the amount of energy for cell (Schröder, 2007). **Right:** The schematic fuel cell concept with the equations to consider. RED/OX: Reduced / Oxidized.

The way microorganisms can extract energy to maintain cellular functions is related to environment, the availability of nutrients and the interactions with other organisms (Haruta and Kanno, 2015; Sporer et al., 2017). Therefore, microorganisms that can generate cellular energy and also manage ambient requirements (redox ambient, temperature, pH) will maintain higher growth and survival rates and can exhibit more excellent ecological adaptative (Tejedor-Sanz et al., 2022).

In general, in aerobic environments, the respiration process, occurs intracellularly, i.e., the soluble TEA (oxygen, nitrate…) are reduced inside the outer cell membrane.

Among all electron acceptor that microorganism can respire those reduced inside the cell have been deeply studied (oxygen, nitrate, sulphate) in the last century. However, in environments without oxygen or alternative soluble electron acceptors (Richter et al., 2012), microorganisms have developed a number of strategies to connect internal respiratory chain to the external insoluble electron acceptors such as minerals that contain metals (Shi et al., 2016), carbonaceous conductive materials or even other microorganisms. Due to the microbial cell envelope is not physically permeable to minerals and not electrically conductive, this strategy is based on exchanging electrons extracellularly (outside the outer cell membrane) with insoluble TEA through a respiration process called extracellular electron transfer (EET) **(figure 8B).** Due to this adaptive mechanism of being able to "breathe" metals, these electroactive microorganisms are found in various environments, including lakes, rivers, seas, sludges, and sediments where Fe (III) oxides abound (Holmes et al., 2004). They have even been found in the human intestine (Cahoon and Freitag, 2018). From an evolutionary point of view, these microorganisms could be among the first organisms on earth's crust (Lovley et al., 2004) where iron was highly abundant and atmospheric oxygen was precisely very limited .

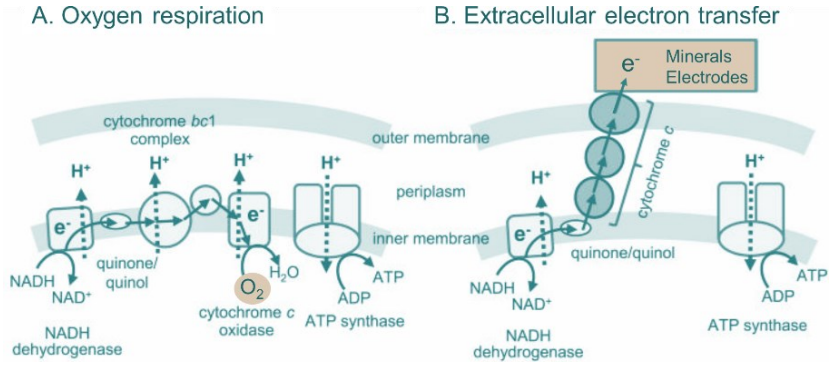

Figure 8. Scheme of microbial different respiration: **A)** Inner membrane, oxygen act as soluble electron transfer acceptor and **B)** Out-of-the-cell insoluble electron acceptor. Image from *Kato S., 2015* (Kato, 2015). ATP synthesis during respiration occurs via oxidative phosphorylation where electrons from electron carriers are transported by an electron transport chain, which creates a proton motive force for ATP generation (Kim and Gadd, 2019).

Extracellular Electron Transfer (EET): an adaptative mechanism

Extracellular electron transfer (EET) (Hernandez and Newman, 2001) is a type of microbial respiration that requires special molecular mechanisms for electrons to travel through the periplasm and outer membrane to be transferred to extracellular acceptors (TEA). Electroactive microorganisms exploit these EET mechanism in growth and information exchange with external environments (Xiao et al., 2017) or with other cells (cell-to-cell communication through quorum sensing or electron transfer by different pathways) (Paquete et al., 2022). In bioelectrochemical systems, the interactions between the microorganisms and electrodes are crucial to obtain efficient electron transfer, which is important in its performance (Wang et al., 2020a). In general, two mechanistic pathways of EET **(figure 9)** to a conductive material have been proposed, the direct (a) and indirect pathway:

(a) The direct physical contact pathway or **Direct Extracellular Electron Transfer (DEET)** occurs when cell-surface redox-active proteins (e.g., outer-membrane multiheme c-type cytochromes (OMCs) (Busalmen et al., 2008; Allen et al., 2009) or conductive cellular appendages located in the microbial outer membrane (Reguera et al., 2005; Gorby et al., 2006) (pili or nanowires are a proposal still under discussion) form a conduit in which electrons are transported from the cell to the electrode **(figure 9.a).**

When these cell-surface proteins conduce electrons directly to another cell (i.e., use another cell as the electron acceptor) the mechanism is called **Direct Interspecies electron transfer (DIET)**. This mechanism allows diversity in microbial communities to obtain energy from reactions that no microbe could catalyse (Summers et al., 2010; Rotaru et al., 2014, 2015; Shrestha and Rotaru, 2014; Holmes et al., 2021; Liu et al., 2021).

When DIET mechanism is produced through a conductive mediator like minerals (Kato et al., 2012) o carbon-based conductive surfaces (Liu et al., 2012; Chen et al., 2014a, 2014b) the mechanism is denominated **conductive-**

particle-mediated interspecies electron transfer or **CIET (Figure 9.a.2)** (Cruz Viggi et al., 2014; Li et al., 2015; Liu et al., 2015a; Viggi et al., 2020; Aulenta et al., 2021; Rotaru et al., 2021).

(b) The **indirect pathway** or **Indirect Extracellular Electron Transfer, IEET** occurs when electron transfer between microbial cells and solid materials is mediated by mobile or spatially fixed molecular redox shuttles (electron carriers or low molecular weight redox mediator) **(Figure 9.b)**. In this mechanism electron shuttles (e.g. quinones, flavins, phenazines) are reduced and/or oxidized by the cell and then reduced and/or oxidized for the electrode (Voordeckers et al., 2010; Kotloski and Gralnick, 2013; Costa et al., 2018). Also, via indirect, EET can be facilitated by extracellular enzymes, that catalyse the uptake of electrons from the surface of conductive material and conversion into substrates (e.g., formate, hydrogen) that can then be used by hydrogen-consuming methanogens or acetogens (Deutzmann et al., 2015; Tsurumaru et al., 2018).

Nowadays, extracellular polymeric substances (EPS, matrix biosynthesized by microorganisms where the cells are embedded forming the biofilms) are considered to play an important role in EET (Borjas Hernández, 2016; Borjas et al., 2017; Edel et al., 2019; Zhuang et al., 2020).

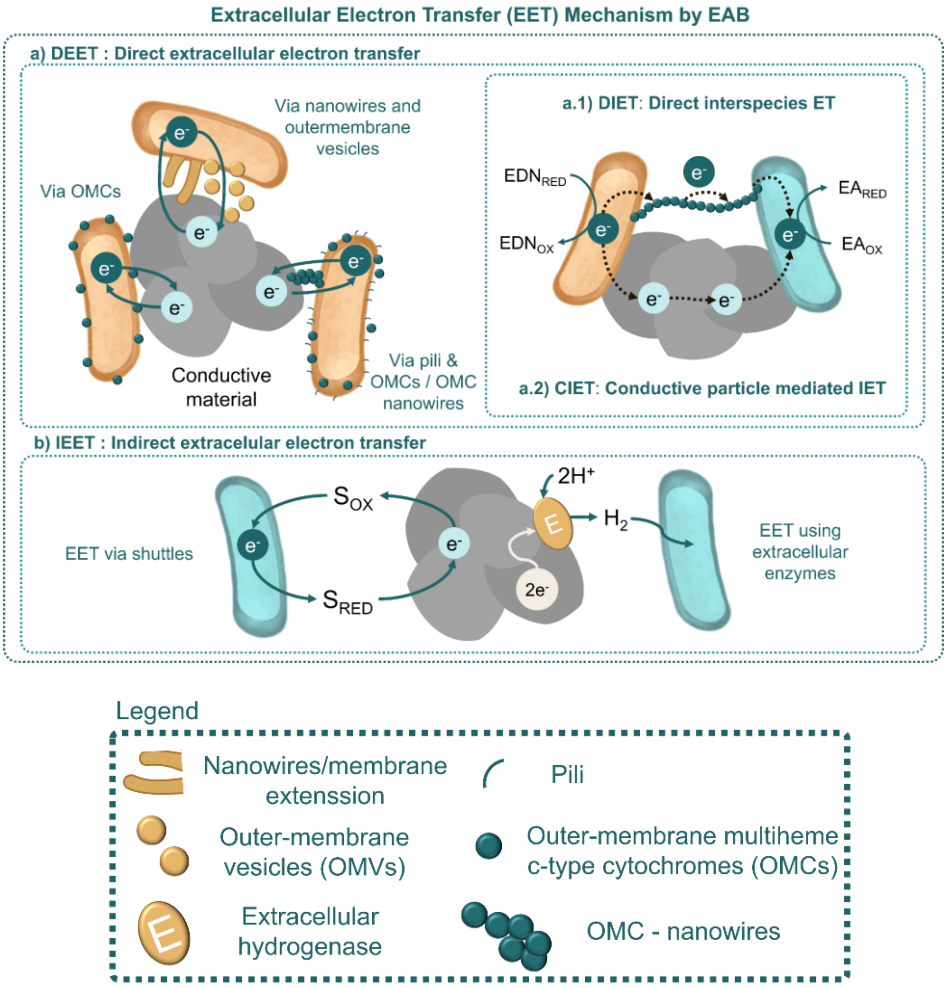

Figure 9. Proposed EET mechanisms performed by electroactive microorganisms: **a)** Electron exchange via direct surface contact (DEET, via membrane-bound cytochromes or conducting cellular appendages). **a.1)** Transfer electron interspecies by endogenous conductive proteins (DIET) or **a.2)** conductive material (CIET). **b)** Electron exchange via by an indirect process using electron shuttles or extracellular enzymes (IEET). Adapted from *Rotaru et al.,2021* (Rotaru et al., 2021) and *Paquete et al., 2022* (Paquete et al., 2022).

Electroactive microorganisms: Geobacter sulfurreducens as model

More than 100 organisms have been described as electroactive (Logan et al., 2019) and, mainly, differ in their ability to oxidize or reduce diverse organic or inorganic compounds using a conductive solid electron donor/acceptor (such as electrode).

Electroactive microorganisms capable of extracellularly transferring electrons to an electrode are named exoelectrogens (anode respiring microorganism)(Schröder et al., 2015). Most of them that have been reported belong to the taxonomic groups of iron and manganese reducing agents such as *Geobacter* and *Shewanella* (Lovley and Phillips, 1988; Myers and Nealson, 1988; Bretschger et al., 2007). Anodic microbes have a wide range of organic and inorganic substrates in anaerobic conditions to oxidase directly to obtain energy (for instance, volatile fatty acids, hydrogen, aromatic (Zhang et al., 2010; Tucci et al., 2021a) and chlorinated hydrocarbons (Aulenta et al., 2013), ammonium (Zhan et al., 2012; Zhu et al., 2016), metals (Wang and Ren, 2014; Pous et al., 2015). With complex organic substrates (organic macromolecules, natural polymers) electrogenic metabolism needs a partner to break these compounds (hydrolysis or fermentation) into simpler molecules (Ren et al., 2007; Logan and Rabaey, 2012).

Electroactive microorganisms that uptake electrons from a solid electron donor such as cathode electrode, are named electrotrophos (cathode respiring microorganism)(Schröder et al., 2015; Logan et al., 2019). These microorganisms, use cathode electrode such as electron donor to reduce a variety of non- metallic contaminants-nutrients such as nitrate (Gregory et al., 2004), nitrite (Puig et al., 2011), perchlorate (Thrash et al., 2007) or sulphate (Blázquez et al., 2016). Furthermore, these microorganisms can reduce metallic hexavalent ions (Gregory and Lovley, 2005; Huang et al., 2015), functionalized aromatics compounds (Wang et al., 2011) or perform reductive dechlorination (Strycharz et al., 2008;

Aulenta et al., 2010). Since most of the cited compounds represent a pollutant threat in water, groundwater, or sediments, the use of the capacity of these microorganisms is increasingly relevant in bioremediation applications (Pous et al., 2018; Wang et al., 2020a). Some autotrophic microbes, like acetogenic bacteria, can take electrons from the cathode (or from the H_2 produced at the cathode) and CO_2 as the only carbon source to produce organic compounds (Nevin et al., 2010, 2011). Methanogens can accept electrons directly from the cathodes (Clauwaert et al., 2008) to produce hydrogen (and then be converted to methane in an external anaerobic digester) or produce methane directly from electrical current (electromethanogenesis)(Cheng et al., 2009).

Within the broad group of electroactive bacteria known so far, *Geobacter genus* is one of the best-characterised and it is considered the model representative of a group known for coupling organic matter mineralization to metal reduction. First *Geobacter* strain, *Geobacter metallireducens* was isolated more than three decades ago (Lovley et al., 1987; Lovley and Phillips, 1988) from freshwater sediments of the Potomac River, Maryland. Nowadays, a more commonly used strain is *Geobacter sulfurreducens* (Caccavo et al., 1994; Coppi et al., 2001).

According to Tabares et al., *"Geobacter sulfurreducens electrified microbiology and set the foundation for the electromicrobiology subfield"* (Tabares et al., 2020). This bacteria is rod shaped, Gram-negative, anaerobic metal reducer, aerotolerant (Lin et al., 2004) and non-fermentative bacteria. Their natural habitat is soil and sediment where insoluble Fe (III) oxide is the most abundant and available as TEA (Lovley et al., 2011). Ferric iron, manganese oxides, fumarate, hexavalent uranium (Cologgi et al., 2011) or elemental sulphur are used by this bacteria for respiration process as TEA. In comparison with these possible TEAs, current-harvesting electrode or anodes provides a long-term, stable electron sink for *Geobacter* respiration and enhanced the formation of a biofilm on the conductive surface **(figure 10)**.

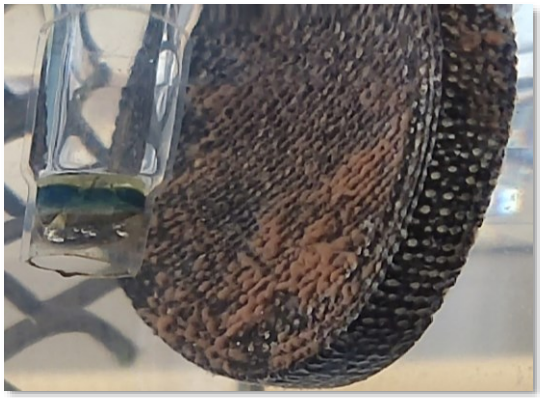

Figure 10. Picture take a *Geobacter sulfurreducens* biofilm on a working electrode acting as anode in an experimental set-up localized at IMDEA water Institute. Source: author's property.

The pioneer research at Derek Lovley´s lab (Bond and Lovley, 2003), represented the first report of microbial electricity production solely by cells colonizing and using a graphite electrode a sole electron acceptor. Hydrogen, lactate, formate or acetate are used as electron donors (EDN) by this specie being acetate molecule the preferential EDN for *Geobacter* bacteria and one of the few substrates used as carbon source (Speers and Reguera, 2012). However, under electron acceptor limitation, *G.sulfurreducens* is less efficient in converting acetate to cell carbon and has higher respiration rate (Esteve-Nunez et al., 2005). *Geobacter* species are among the most effective microorganisms for harvesting electrical current from organic compounds and *G. sulfurreducens* is reported to be one of the highest current producers (Rotaru et al., 2015), being this fact interesting for their application in biotechnology.

Geobacter sulfurreducens was the first *Geobacter* species for which methods for genetic manipulation were developed (Coppi et al., 2001) and its whole sequenced genome was reported in 2003 (Methé et al., 2003) where 73 multi-heme c-type cytochromes (MHC) were identified. This strain can developed highly structured multilayer biofilms on an electrode surface (Reguera et al., 2006) with an extracellular matrix containing molecules and biological structures, such as c-type cytochromes, able to perform EET mechanism to

insoluble electron acceptors under different ambient conditions (Reguera et al., 2005; Holmes et al., 2006; Inoue et al., 2011; Rollefson et al., 2011; Steidl et al., 2016). Indeed, EET performance and electrical current generation can be severely reduced in *Geobacter* strains impaired in c-cytochromes production (Estevez-Canales et al., 2015b). Furthermore, these c-type cytochromes have electron storage capacity (*capacitor effect*) to be used during periods in which an external electron acceptor is unavailable (Esteve-Núñez et al., 2008). This species also reduces iron oxides to magnetite and uses this conductive material to electronically connect with syntrophic partners, managing to couple acetate oxidation and nitrate reduction. (Kato et al., 2012). Recently, the synthesis of novel conductive biomaterials based on assemblies of *Geobacter* nanowire pili has been reported (Cosert and Reguera, 2019).

The diversity of electroactive microorganisms still to be discovered and the conditions under which they can exhibit electroactivity open new opportunities for biotechnological applications. Such microorganisms become "biocatalysts" by facilitating the transport of electrons between the electron donor/acceptor and the electrode (Rabaey et al., 2007). The presence of an electroactive biofilm colonizing the surface of an electrode changes the properties of that surface, allowing the reaction to occur.

1.2.2 MET platform: Bioelectrochemical Systems and applications

The MET platform consist of bioelectrochemical systems (BES) which are indeed engineering devices hosting electroactive microorganisms (Rabaey, 2009). A possible classification of MET **(figure 11)** is based on the electrochemical operation mode depending on their energy requirements (i.e., polarized or non-polarized systems). Some processes are based on spontaneous reactions ($\Delta G < 0$); accordingly, they are non-polarized systems because an external energy input is not necessary (microbial fuel cells, microbial snorkels or microbial desalination cells are some examples. On the other hand, other

processes imply non - spontaneous reactions ($\Delta G > 0$), so an external energy input is necessary, and systems are classified as polarized ones (eg. Microbial electrolysis cells).

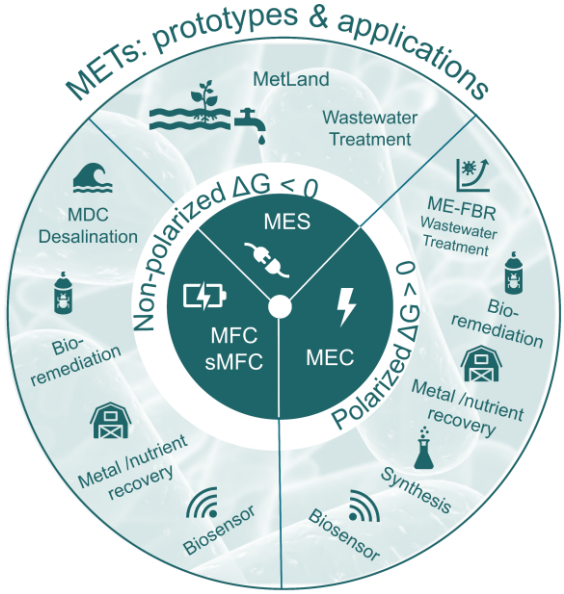

Figure 11. Possible scheme to organize the BES based on the electrochemical operation mode and applications. MES (Microbial electrochemical Snorkel); MFC (Microbial Fuel Cell); sMFC (Solid Microbial Fuel Cell); Microbial Desalination Cell (MDC); MEC (Microbial Electrolysis Cell); ME-FBR (Microbial Electrochemical-Fluidize Bed Reactor).

Non-Polarized Systems

a. Microbial Electrochemical Snorkel (MES)

In the first description of snorkel mode operation, an electrode (conductive material) was immersed in a sediment to take advantage of redox gradient along the height **(figure 12A)**: under anaerobic conditions, the anodic zone (bottom of sediment) of the electrode, develops an anaerobic electroactive biofilm on its surface where organic matter is oxidized and electrons are transferred to the conductive material. In the cathodic zone (upper most zone), where the electrode keep exposed to aerobic conditions, an electrochemical or biotic oxygen

reduction take place as counter reaction (Erable et al., 2011). The potential difference between the two environments causes electrons flow through the conductive material, from anaerobic zone (low redox potential) to aerobic zone (high redox potential). This process is similar to a short circuit mode in absence of the external resistance (Hoareau et al., 2019), where current flow is maximum. This configuration increases the rate of electrochemical reaction (oxidation of organic matter or removal of contaminants) without harvesting energy.

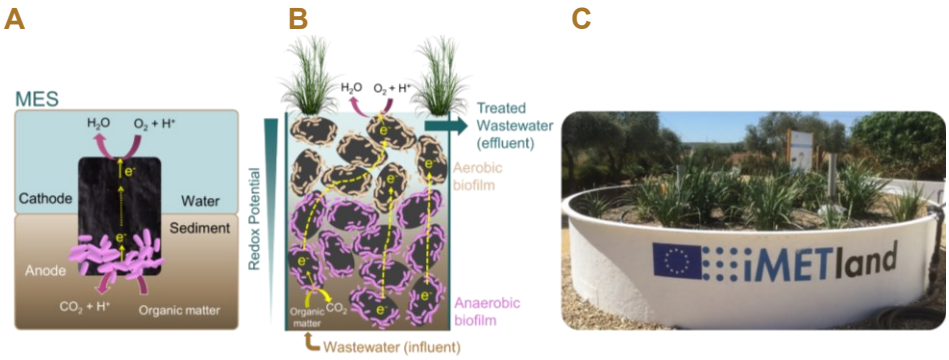

Figure 12. A) Schematic representation of MES using a single electrode to accelerate hydrocarbons (act as EDN for electroactive biofilm) with oxygen reduction reaction as counter reaction. **B)** MES concept applied to CW (METland® technology in flooded conditions and up-flow configuration). Picture adapted from (Ramírez-Vargas et al., 2018). **C)** Photography of METland® technology in Carrión de los Céspedes, Sevilla (from iMETland project).

Some applications of this mode of operation have enhanced the *in situ* removal of pollutants, e.g., for petroleum hydrocarbons in marine sediments (Cruz Viggi et al., 2015), nitrate removal and soil bioremediation (Hoareau et al., 2019). In addition, wastewater treatment is a potential niche for this operation mode. Indeed, the integration of MES system in a nature-based solution like constructed wetlands (CW), made possible a new born technological solution so-called METLand® (Aguirre-Sierra et al., 2016) **(figure 12C).** In METLand® a bed of carbonous-conductive material act as an unlimited electron acceptor, so the electroactive biofilms are stimulated to maximize substrate consumption (Ramírez-Vargas et al., 2019). In addition, this material act as single electrode

that connects all METland® zones incentivizing interaction between microbial communities (Wang et al., 2020a). As a result, greater efficiency in wastewater treatment was achieved overcoming performance of conventional CW. METland® systems can be operated under different modes but it was originally designed to operate under flooded conditions **(figure 12B)** which stimulate the natural redox gradient between the bottom of the system (anaerobic zone) and the naturally oxygenated surface, intensifying microbial reactions (Aguirre-Sierra et al., 2016); On the other hand, METland® has proven to be effective in non-flooded mode (and down-flow configuration), promoting passive aeration where oxygen acts as an electron acceptor (Aguirre-Sierra et al., 2020). In this operating mode, due to the presence of oxygen, nitrification is favoured, and micro-pollutants are efficiently eliminated (Pun et al., 2019). Conductive materials such as electroconductive coke (Aguirre-Sierra et al., 2016; Ramírez-Vargas et al., 2019) or electroconductive biochar (Prado et al., 2019; Schievano et al., 2019; Prado de Nicolás, 2021) have been investigated with a focus on sustainability and treatment efficiency. The difference in electrical profile (measured of the electric potential along the depth of the material) between gravel and conductive material (Ramírez-Vargas et al., 2019) shows the flow of electrons occurs only through the conductive material from the anaerobic zone towards the aerobic surface. In this sense, it has been proven that the flow of electrons can be altered by shifting the characteristics of the material or supplying alternative soluble TEAs inside some elements so-called e-sinks (Prado et al., 2020b). Furthermore, the METlands have recently undergone a geospatial study for optimal localization (Peñacoba-Antona et al., 2021a) and an techno-environmental study through life cycle assessment (LCA) study (Peñacoba-Antona et al., 2021b), validating full scale METland® solutions for decentralized sustainable wastewater treatment (Peñacoba Antona, 2021).

b. *Microbial Fuel Cell (MFC)*

The Microbial Fuel Cells (MFC) are devices that use electroactive bacteria as catalysts to oxidize organic or inorganic matter to generate electric current (i.e., converts chemical energy to electrical energy)(Logan and Regan, 2006b; Logan, 2007). The first MFC device was developed in 1962 (Davis and Yarbrough, 1962), fifty years later than the observation about electricity-producing bacteria. The conventional device **(figure 13A)** comprises two compartments separated by an ion-exchange membrane (IEM). The anode and cathode electrodes are placed in aqueous solutions in each compartment. Electroactive bacteria colonize the surface of the anode electrode and oxidize the reduced compound (EDN) that serves as fuel. This oxidation generates electrons and protons (or CO_2 in the mineralization of an organic compound). The bacteria transfer the electrons from this oxidation to the electrode surface, generating a potential difference between the surface electrode and solution (equilibrium anode potential). On the other hand, in the abiotic cathode chamber, dissolved oxygen in the aqueous medium generates a potential difference between the cathode electrode and the solution (equilibrium cathode potential). When an external resistance is connected between the electrodes, the circuit is closed Thus, the potential difference between anode and cathode allows the electrons to circulate through the external circuit (from the anode to the cathode). Conversely, the ions pass through the ion-exchange membranes (from the anode to the cathode when a cation exchange membrane is used). Finally, in the abiotic cathode chamber, electrons and protons are consumed on the surface cathode, reducing oxygen to water. MFC device can be considered the biotic equivalence of the galvanostatic cell (for example, Daniell Cell), which uses chemicals to generate electric energy from spontaneous reactions.

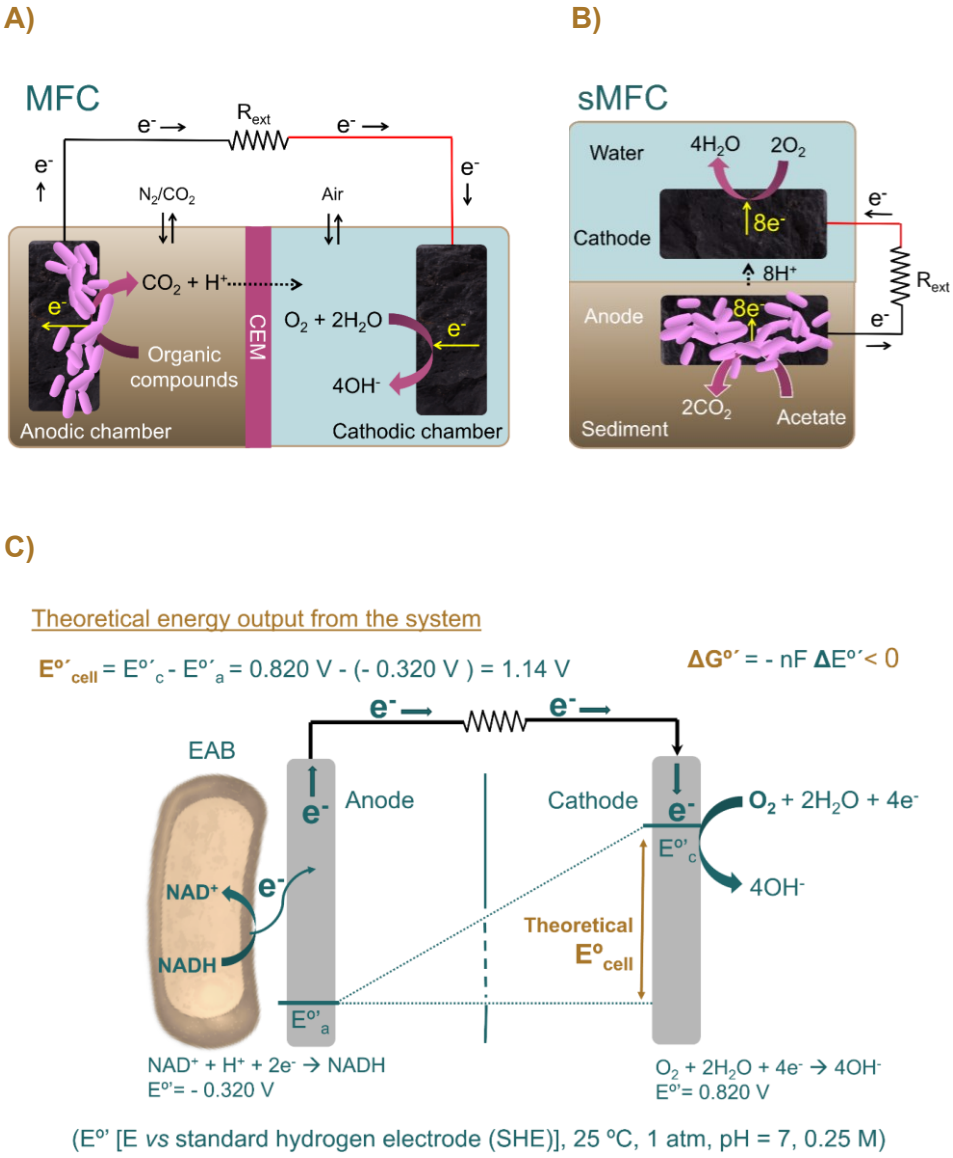

Figure 13. A) Schematic representation of 2-chambers microbial fuel cell (MFC) with cation exchange membrane (CEM) using the organic compound as fuel (EDN) and oxygen reduction reaction as counter-reaction. **B)** Schematic Sedimentary Microbial Fuel Cell (SMFC) used acetate as EDN and oxygen reduction as counter-reaction. **C)** The theoretical potential difference (the maximum energy gain that could be obtained) between the standard potential of the terminal metabolic electron donor NADH production (the intermediate electron carrier in microbial respiration) and oxygen reduction (TEA) is 1.14 V. The overall reaction in MFC is exergonic (i.e, negative ΔG). Due to potential losses through the system, this value is reduced to 0.51 V approximately (Schröder, 2007).

The ideal situation aims to maximise the power production, minimising the potential losses between the anode and cathode that occur along the device circuit (metabolic activation, ohmic drop). It is crucial to optimise conditions, materials, and configurations in order to minimize the energy loss. An example of the theoretical cell potential, or electromotive force (emf) is shown in **figure 13C** (Rozendal et al., 2008); however, the experimental potential obtained from the system (0.15 V) is low compared to the theoretical potential (Schröder, 2007).

The application of this system was primarily sustainable **direct bioenergy generation** (Rabaey and Verstraete, 2005), mainly from biodegradation of soluble organic matter present in a diverse waste sources such as urban wastewater (Liu and Logan, 2004; Capodaglio et al., 2013; Borjas et al., 2015) , industrial wastewater (Kelly and He, 2014; Angosto et al., 2015; Vilajeliu-Pons et al., 2017), hydrocarbon-contaminated groundwater (Wei et al., 2015), sludge (Chandrasekhar and Venkata Mohan, 2012), and biomass (Rozendal et al., 2008). This harvested energy can be used for **bioremediation** purposes (Wang et al., 2020a; Rotaru et al., 2021). This is an important environmental application where electrodes are used acting as electron acceptors or donors to accelerate the removal of pollutants from soils, sediments or groundwater (Pous et al., 2018) by overcoming the limiting factors of microbial metabolism (lack of electron donor/acceptor, nutrients, absence of capable organisms limitation in bioavailability of the pollutant). Some examples of the use of MFC configuration in bioremediation are: recover/conversion metals (with high reduction potentials) using abiotic cathodes (Gangadharan and Nambi, 2015; Rodenas Motos et al., 2015) or biocathodes (Tandukar et al., 2009; Shen et al., 2017). Also, this energy can be used for biologic denitrification (Clauwaert et al., 2007; Virdis et al., 2010; Pous et al., 2013) or perchlorate reduction (Jiang et al., 2017) in anaerobic biocathodes. In this biocathodes the microorganisms can use the electrode as a source of electron (He and Angenent, 2006). However, the power output in MFCs is low, and they can just have specific applications as **power supplies for small**

electrical devices in remote environments (Ren et al., 2012; Ieropoulos et al., 2013) or capacitors (Franks and Nevin, 2010).

A variant of the MFC devices is a **Sedimentary Microbial Fuel Cell (sMFC)** which are implement in natural ambient such as soil or sediment **(figure 13B)**. This device harvest energy from oxidation compounds by microorganism naturally presents in these environments. The anode is buried in sediment (acts as an anode chamber), and the cathode keep exposed in the aerobic aqueous phase, which covers the soil (acts as a cathode chamber). Both electrodes are connected by an external circuit. Some of these devices have been used to **harvest energy** in marine sediments (Reimers et al., 2001), or used to **clean up polluted soils** by incorporating the electrodes in soil for growing rice (Domínguez-Garay et al., 2013; Domínguez Garay, 2016), non-flooded soil contaminated by herbicides (Domínguez-Garay et al., 2016; Domínguez-Garay and Esteve-Núñez, 2018), pesticides (Cao et al., 2015) or polycyclic aromatic hydrocarbon (PAH)(Rodrigo et al., 2014; Rodrigo Quejigo, 2017).

Polarized Systems

c. *Microbial Electrolysis Cell (MEC)*

In this type of configuration, electrical energy is supplied externally to increase the potential difference between the anode and the cathode and allow or increase the speed of certain reactions on the surface electrodes (due to thermodynamic or kinetic constraints). Two instruments can be used to supply the energy (Kadier et al., 2016): **i)** a power source, or **ii)** a potentiostat **(figure 14A)**. If the energy supplied is through a potentiostat, then a potential difference is established between a working electrode (WE) and a reference electrode (RE) (potentiostatic mode) to control the value of the WE potential. In addition, a counter electrode (CE) or auxiliary electrode is needed to close the circuit, achieving a configuration of three electrodes **(figure 14B)**. This 3-electrode

configuration is widely used to control redox reactions and study the electrode-microorganism interaction.

A conventional example of 2-chambers configuration MEC for hydrogen production on the cathode and simultaneously organic compound oxidation on the anode is shown in **figure 14A** (Logan et al., 2008). Also is possible to operate in a single compartment without using a physical separator (Call and Logan, 2008), reducing the energy demand of the external power supply. In the case of MEC, the Gibbs free energy of the overall reaction (under standard biological conditions) that implicates, for example, the electron donor NADH oxidation and hydrogen production is positive (i.e., endergonic) the process is not spontaneously **(figure 14C)**.

The electromotive force (emf) or the theoretical potential difference between the standard potential of the NADH oxidation and water reduction is ca. - 0.1 V. This value of emf correspond with the minimum voltage required to drive an MEC. This voltage needs to be at least higher than the theoretical value to overcome the thermodynamic limits of hydrogen production and overcome the internal resistance of the different components of the system. Experiments have shown that the microbial electrolysis reactions typically occur at applied voltages above 0.2 V (Logan et al., 2008). The contribution of this additional amount of energy to the system allows water electrolysis on the cathode, forming hydrogen under anoxic conditions. This external energy supply is non-significant since most of the energy is harvested from substrates oxidation at the anode. The microbial catalysis on the anode electrode reduces the energy cost of this process compared to the voltage that must be applied to achieve it by conventional abiotic water electrolysis (1.7-2.2 V) (Carmo et al., 2013).

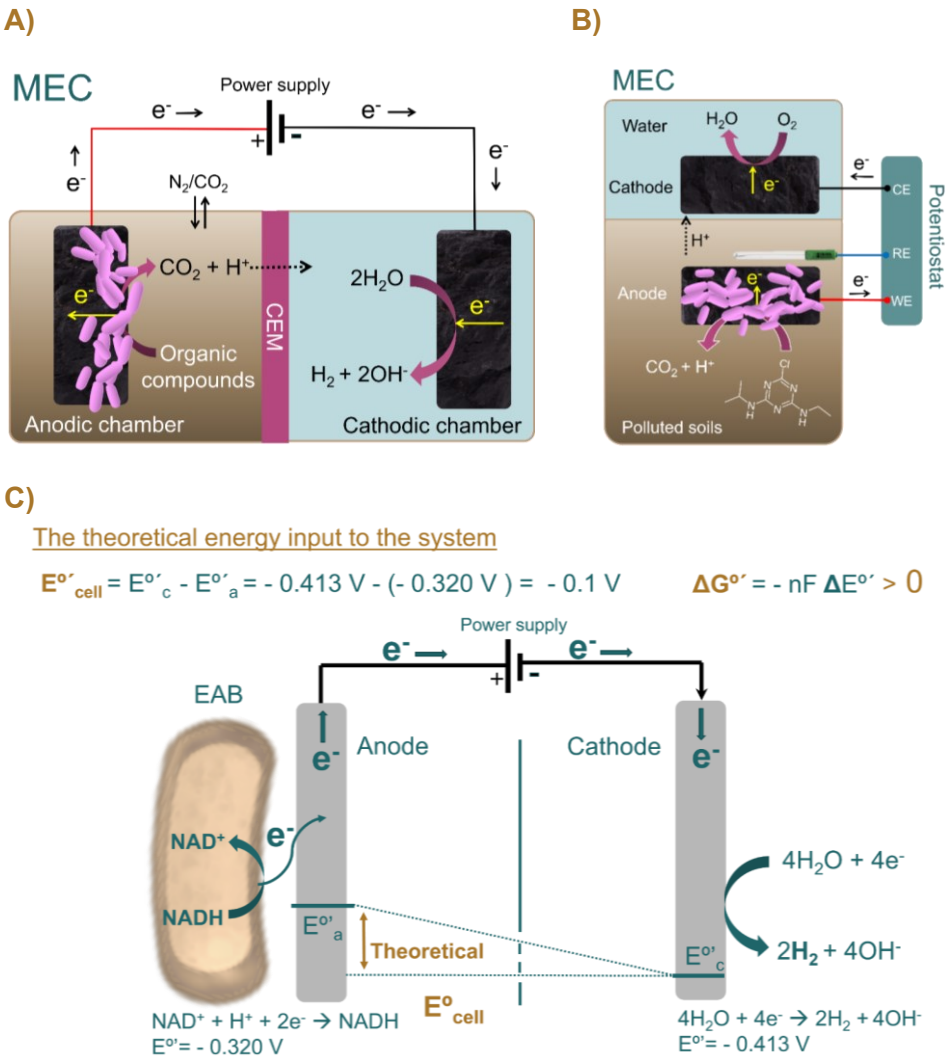

Figure 14. A) Schematic representation of 2-chambers microbial electrolysis cell (MEC) using organic compound as EDN. **B)** Three-electrode system controlled by a potentiostat for polarizing the anode (working electrode) versus reference electrode for cleaning-up atrazine polluted soils adapted from *Domínguez-Garay et al.,* (Domínguez-Garay et al., 2018). **C)** The overall reaction in MEC is endergonic (i.e., positive Δ*G*). The theoretical potential difference between the standard potential of the terminal metabolic electron donor NADH oxidation and water reduction is - 0.1 V approximately. A power supply is necessary to achieve the electrolysis water to produce hydrogen.

The main application for MEC configuration is to harvest energy from waste and storage it in various forms such as **hydrogen** (Logan et al., 2008), biofuels (Lu and Ren, 2016) and other value added products which need a small contribution of additional energy input in the system (Logan and Rabaey, 2012). This last estratergy known as **microbial electrosynthesis** (Nevin et al., 2011; Prévoteau et al., 2020) consists of capturing electrical energy in the carbon-carbon bonds, being an approach more easily storable than hydrogen storage. In this application, the microbial metabolism of biological cathodes is used to produce valuable products such as biofuels or chemicals (Mohanakrishna et al., 2015). The exoelectrogens uptake electrons from the cathode (or from cathode-mediated hydrogen, bio-hydrogen (Perona-Vico et al., 2020), or redox mediator to reduce carbon dioxide in a variety of organic compounds (Rabaey and Rozendal, 2010) such as acetate (Nevin et al., 2010; Patil et al., 2015) or ethanol (Steinbusch et al., 2010) as well as inorganic chemicals (Cusick and Logan, 2012)(Rozendal et al., 2009). Some examples of MEC configuration for **bioremediation** are applied for fast rates reduction of inorganic non-metallic contaminants, nutrients such as nitrate (Tejedor-Sanz, 2016; Cecconet et al., 2018) and perchlorate (Thrash et al., 2007). Electrobioremediation of metals with low reduction potential values (Gregory and Lovley, 2005; Qin et al., 2012) as well as herbicides **(figure 14B)**(Rodrigo Quejigo et al., 2016, 2018; Domínguez-Garay et al., 2018), aromatic hydrocarbons (Zhang et al., 2010; Tucci et al., 2021a), chlorinated compounds (Yu et al., 2016) or antibiotics (Quejigo et al., 2019) have been vastly explored.

An overview of the microbially-catalyzed reactions taking place at the anode and at the cathode of different systems (polarized or non-polarized) are shown in **Figure 15.**

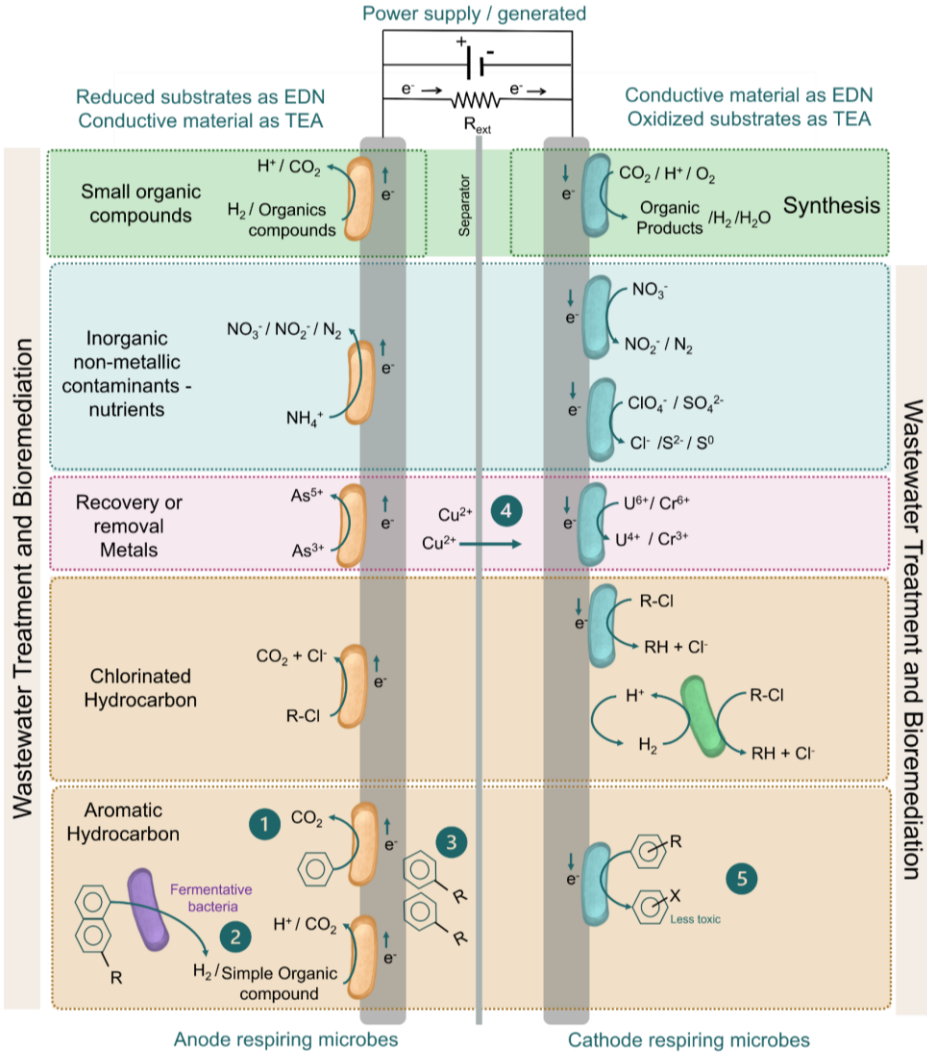

Figure 15. Schematic overview of microbially-catalyzed reactions taking place at the anode and at the cathode. Adapted from Pous et al.,(Pous et al., 2018), Wang et al., (Wang et al., 2020a) and Logan and Rabaey (Logan and Rabaey, 2012). Schematic overview of the main pollutant removal mechanisms in a MET-based electrobioremediation system: **1)** direct electricity-generating oxidation; **2)** cooperative electrogenic oxidation by syntrophic communities of fermentative and electroactive bacteria; **3)** adsorption onto the surface electrodes or within biofilm on the surface; **4)** electromigration and other electrokinetic transport mechanisms; **5)** direct electricity- consuming reduction. Adapted from Tucci *et al.*, (Tucci et al., 2021b).

One example of a bioelectrochemical systems operated under MEC configuration is **Microbial Electrochemical Fluidized bed reactor (ME-FBR)**. These devices achieve an enhancement in the removal of contaminants in aqueous media due to the increase in the area of electrode by using a electroconductive fluid-like bed (Tejedor-Sanz et al., 2017)**(Figure 16A)**. In addition, the system has a controlled upward flow that keeps these polarized particles in motion thus improving an optimal environment for improving the kinetics of the process and avoid mass transfer limitations (Tejedor-Sanz, 2016). These systems have been used to treat real wastewater from brewery **(Figure 16B)**(Tejedor-Sanz et al., 2018; Asensio et al., 2021b) or pharmaceutical industry (Asensio et al., 2021a) also for nitrate removal, biohydrogen production (Sara et al., 2020), or recovering nutrients as purple phototrophic bacteria (PPB) biomass (Manchon et al., 2023).

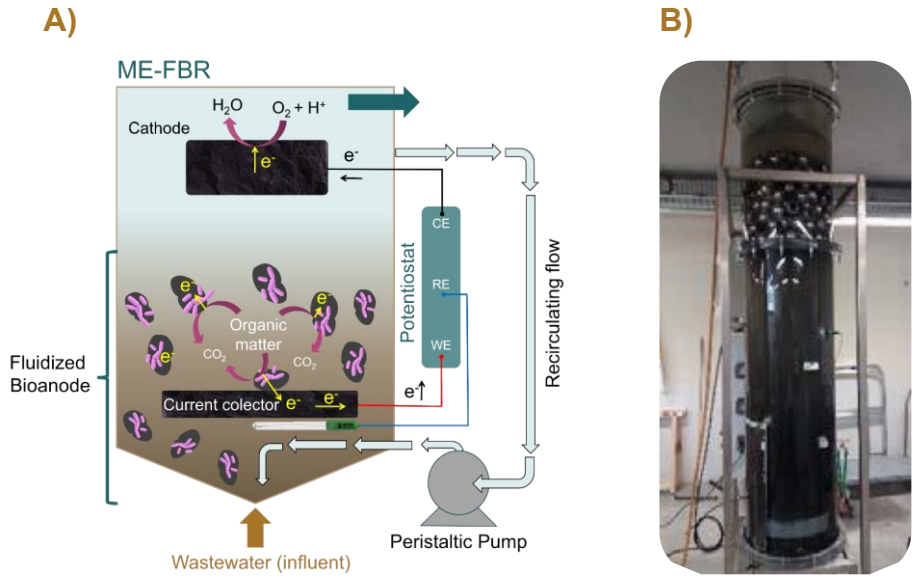

Figure 16. A) Schematic of Microbial Electrochemical Fluidized Bed Reactor (ME-FBR) Adapted from *Tejedor et al*.,(Tejedor-Sanz et al., 2017). **B)** Photo of ME-FBR pilot to treat brewery wastewater in ANSWER Life's Project.

Finally, a promising application is the biosensing (Fernandez-Gatell et al., 2022). The **EAB-based sensors** are bioelectrochemical devices that record an

electric current as a signal from electroactive metabolic activity in water. Thus, *in situ* real-time monitoring for environmental bioprocess can be self-powered under MFC mode (Li et al., 2011), or externally powered under MEC mode. The detection strategy depends on the analyte nature since it could stimulated or inhibit by toxicity the electrical output (Di Lorenzo et al., 2014). The positive electrical signal can be correlated with different factors: the concentration of VFAs (Prévoteau and Rabaey, 2017), matter susceptible to be oxidized by biological processes (biological oxygen demand, BOD) (Peixoto et al., 2011) as well as, some pollutants and specific toxic compounds (Webster et al., 2014) in wastewater. Most systems uses two electrodes to monitor anodic activity (Hassan et al., 2021) so, to avoid potential changes between them and achieve precision, a design based on 3 three electrodes, called IoT (Internet of Things) biosensing, has been developed (by Nanoelectra, Spain) operated in MEC mode allowing a control of the anodic potential **(Figure 17)**. In addition, ready-to-use artificial bioelectrodes have been constructed through the immobilization of *G. sulfurreducens* cells in silica gel and carbon felt (Estévez-Canales, 2016). Biosensors have also been developed to assess microbial electroactivity using screen-printed electrodes, a novel low-cost platform at the microscale level (Estevez-Canales et al., 2015a).

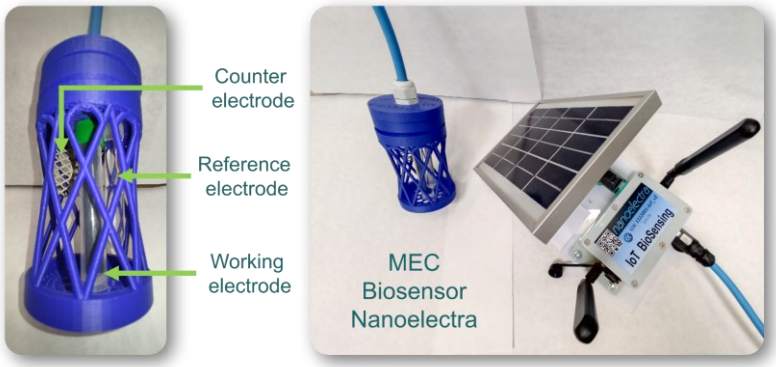

Figure 17. IoT biosensing device from Nanoelectra, Spain. Microbial electrochemical sensor monitors water quality in real time for natural, urban and industrial environments. Photo's source: author's own property .


AM-510-EUR
-0.48
V
Auto Range
>2Sec
HOLD
REL Δ
RANGE
Hz/%
SELECT
NCV
9V
1.5V
Hz
µA
mA
A
V
OFF
HzVΩ
COM
A
mAµA
FUSED
CAT III 600V
10Amax
VELP
ESP

1.3 Microbial Desalination Cell (MDC)

Among all the applications BESs can carry out, brackish or seawater desalination without external energy input was explored as a new application through microbial desalination cell (MDC) technology (Cao et al., 2009; Kim and Logan, 2013a). This technology arises from combining a membrane-based technology with bioelectrochemical systems.

The Microbial Desalination Cell (MDC) is an energy self-sufficient and sustainable technology that can address simultaneously wastewater treatment, bioenergy production and water desalination in a single device without external energy input (Cao et al., 2009; ElMekawy et al., 2014). The technology arisen from the combination of membrane-based technology such as electrodialysis (ED) cell with an MFC device in which a third camera has been added to act as a desalination chamber (Yang et al., 2019a). Some authors consider the MDC an upgrade of the MFC system since they obtained several improvements by adding the desalination compartment to the MFC device. This compartment can prevent the diffusion of oxygen from the cathode chamber to the bioanode producing an improvement in the performance (Yang et al., 2015; Ebrahimi et al., 2017).

1.3.1 Mechanism and force driving

The conventional MDC unit **(figure 18)** is composed of at least three chambers: **1)** An anaerobic anodic chamber hosting the electroactive microbial community which oxidises the organic compounds (fuel) (e.g., wastewater) and transfers the electrons to the anode. **2)** A central desalination compartment separated from the others by ion exchange membrane (anion exchange membrane, AEM and cation exchange membrane, CEM). **3)** A cathodic chamber where an electron acceptor (species with high redox potential, e.g., Fe^{3+} or oxygen) is electrochemically reduced to close the circuit. The potential difference between both electrodes is achieved when the anodic and cathode compartments are fed with organic matter

and an electron acceptor respectively. When an external load (R_{ext}) is connected to both electrodes, electric current flows through the system, enabling the migration of anions and cations through their respective ion-exchange membranes (IEM), thus decreasing the concentration of ions in the central saline compartment, and achieving freshwater production.

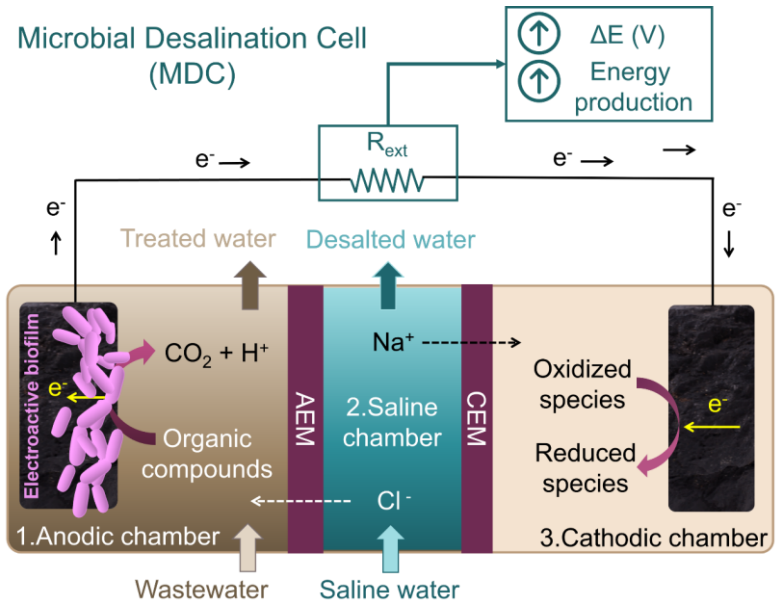

Figure 18. Scheme of a conventional 3-chamber Microbial Desalination Cell (MDC). R_{ext}: external resistance/load. AEM: anion exchange membrane. CEM: cation exchange membrane.

The driving force in ED technology for the migration of ions during the desalination process is the perpendicular electrical field to plane of both electrodes (this electrical field is developed by the application of a different potential). In this technology, an external electrical energy input is required (by power supply) to achieve the implicated electrochemical reactions **(figure 19)**. In the same manner, the driving force in MDC technology is the electric field which force the ion migration from the middle compartment to the adjacent in the cell due to spontaneous electrochemical reactions in the electrodes that developed a different potential (Jacobson et al., 2011b). However, in contrast with ED, in MDC technology, the achieved potential is generated by electroactive bacteria

that convert the chemical energy stored in wastewater into electric energy avoiding the need for externally applied energy.

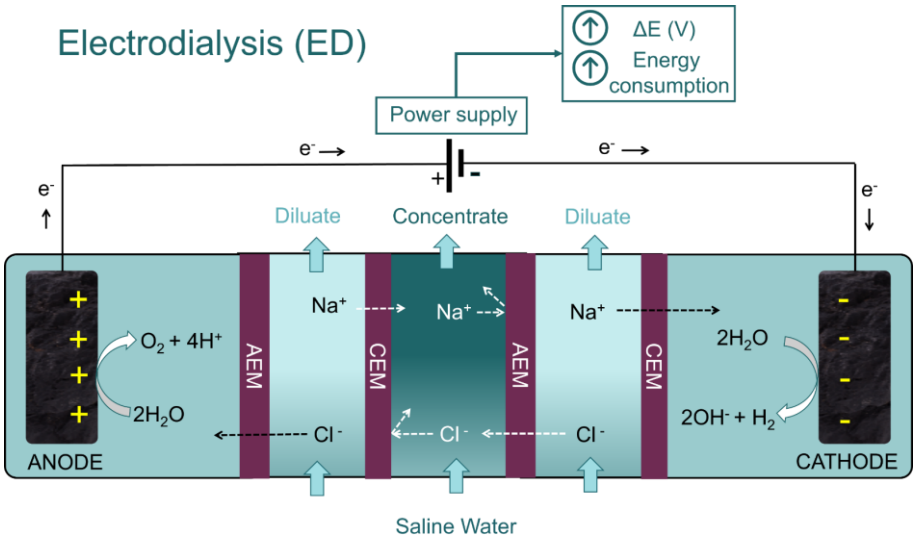

Figure 19. Schematic diagrams of electrodialysis unit with two cell pairs: a dilute compartment and a concentrate compartment which are composed of anionic (AEM) and cationic exchange membranes (CEM) and are placed between two electrodes (anode and cathode). The ED process involves transporting saline ions from one solution to another through IEM under an applied electrical potential difference.

The desalination process in MDC technology is attributed predominantly to ion migration. That means that an increase in the current density in the system directly benefits the desalination process (Ge et al., 2014). However, some researchers apply an external voltage to the system (Ge et al., 2014) to improve current density (and the desalination process as a consequence), but the process is no longer spontaneous, and there is energy consumption. In addition to ion migration, another transport phenomenon that can occur during the desalination process is ion diffusion (generated by the salinity gradient between compartments)(Kim and Logan, 2013a). Also, water transported across IEMs by osmotic pressure or electroosmosis play a part during the desalination process in MDCs (Mehanna et al., 2010c; Jacobson et al., 2011b).

1.3.2 Influence factors in MDC performance

Many factors affect the MDC performance **(figure 20)**, such as **A)** engineering factors (design and geometry of reactor, electrode material, membrane), **B)** desalination compartment factor (initial salinity or nature of saline water in the middle compartment) or **C)** electrochemical factors (composition of catholyte). Also, the **D)** operational factors (value of the external resistance, operation mode, an external voltage applied) or **E)** microbial and physicochemical factors (type of inoculum, buffer conditions and available substrate in the anolyte) are considered. From the scale-up point of view, the economic factors can determine a vast part of these factors. All of them must be considered together to develop of MDC system (Jingyu et al., 2017). Due to the wide variety of factors that can influence simultaneously in these devices, the direct comparison of MDC results reported in the literature is complex. Nevertheless, a positive approach is that various elements can be optimized to develop the technology and adapt it to large-scale applications.

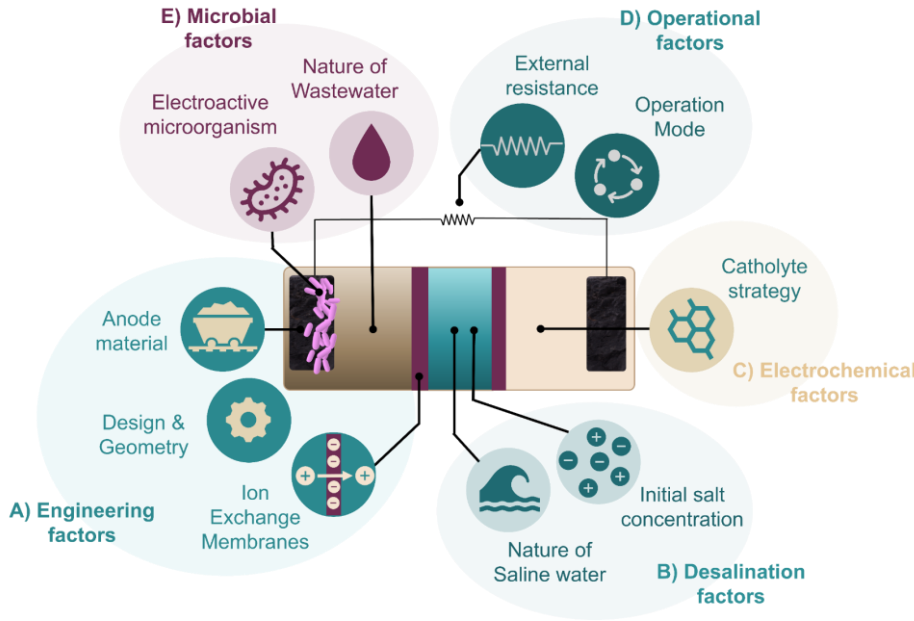

Figure 20. Scheme of influence factors in MDC performance.

A) Engineering factors: design and geometry reactor, membranes, and electrode materials

Several and different MDC configurations have been reported in the literature, with a different design, geometry and focus to avoid the main limitations of these systems and enhance the water treatment, desalination or generate energy. The first MDC proof-of-concept **(figure 21A and 21B)** was reported in 2009 by Cao *et al.,* (Cao et al., 2009) and it consisted in a *three-chamber device* (Luo et al., 2012b) that was able to remove the 90 % of salt and to generate a maximum power density of 2 W m^{-2}. The device used acetate as electron donor and ferricyanide as electron acceptor in batch mode with recirculation of anolyte and catholyte tanks. This configuration has some limitations such as, the increase of the internal resistance due to the decrease in electric conductivity in saline chamber, low desalination rate, pH imbalance in cathodic and anodic chamber, or chloride accumulation on the anode compartment. Each of these drawbacks led to the development of new configurations for MDC systems to overcome the limitations imposed by the 3-chamber configuration.

To improve the desalination rate *stacked microbial desalination cells (sMDC)* have been design (Chen et al., 2011b). The saline water stream passes through several desalination and concentration chambers **(figure 21C)** which are a series of stacked compartments separated by alternating anion and cation exchange membranes (Kim and Logan, 2011, 2013a). In this configuration, the efficiency of charge transfer and salt removal from the saline stream increases because the number of split ion-pair from saltwater increases for each electron circulating in the external circuit. Some results indicated that two is the optimal number of desalination compartments (Chen et al., 2011b). However current generation declined due to the increasing internal resistances and very thin desalination stacks need be applied (Kim and Logan, 2011) or applied voltage (Ge et al., 2014) to achieve higher desalination efficiencies and power densities.

Also, *tubular up-flow MDCs (UMDC)* configuration was developed to enhance desalination efficiency under continuous operation by enlarging the membrane surface to facilitate ion exchange. This tubular configuration consists of two compartments divided by IEM (Jacobson et al., 2011a, 2011b). An anodic inner compartment (filled with granular material) is sealed with an AEM, followed by another compartment (desalination chamber) sealed with a CEM **(Figure 21D)** although, recently, new proposed configurations has been reported (Jafary et al., 2020; Wang et al., 2020b). With this configuration, a large surface area is achieved in electrodes and membranes to increase the rate of desalination. Due to the up-flow mechanism, microorganisms are kept in suspension, efficiently carrying out the oxidation of organic matter. However, the operation cost of this design is high still (Sharma et al., 2019) and some works using applied voltage to enhanced the desalination process (Zhang and He, 2015).

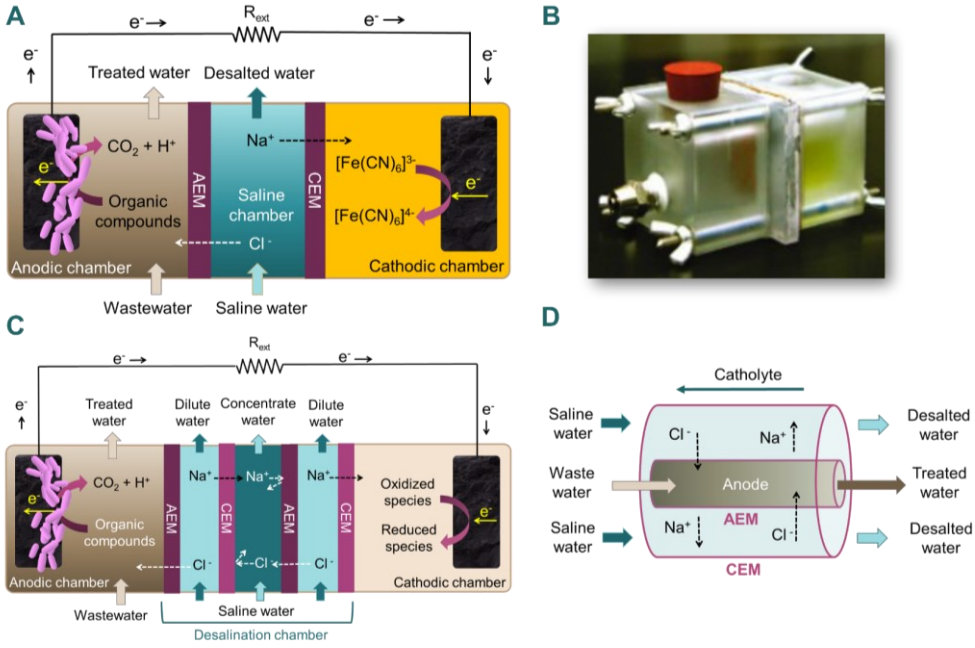

Figure 21. A) Scheme of 3-compartment configuration MDC and **B)** photo from Cao et al., (Cao et al., 2009) of 3-chamber configuration MDC with liquid catholyte of ferricyanide**. C)** Scheme of a stacked microbial desalination cell (sMDC). **D)** Schematic diagram of an tubular up-flow MDC adapted from (Jacobson et al., 2011a, 2011b).

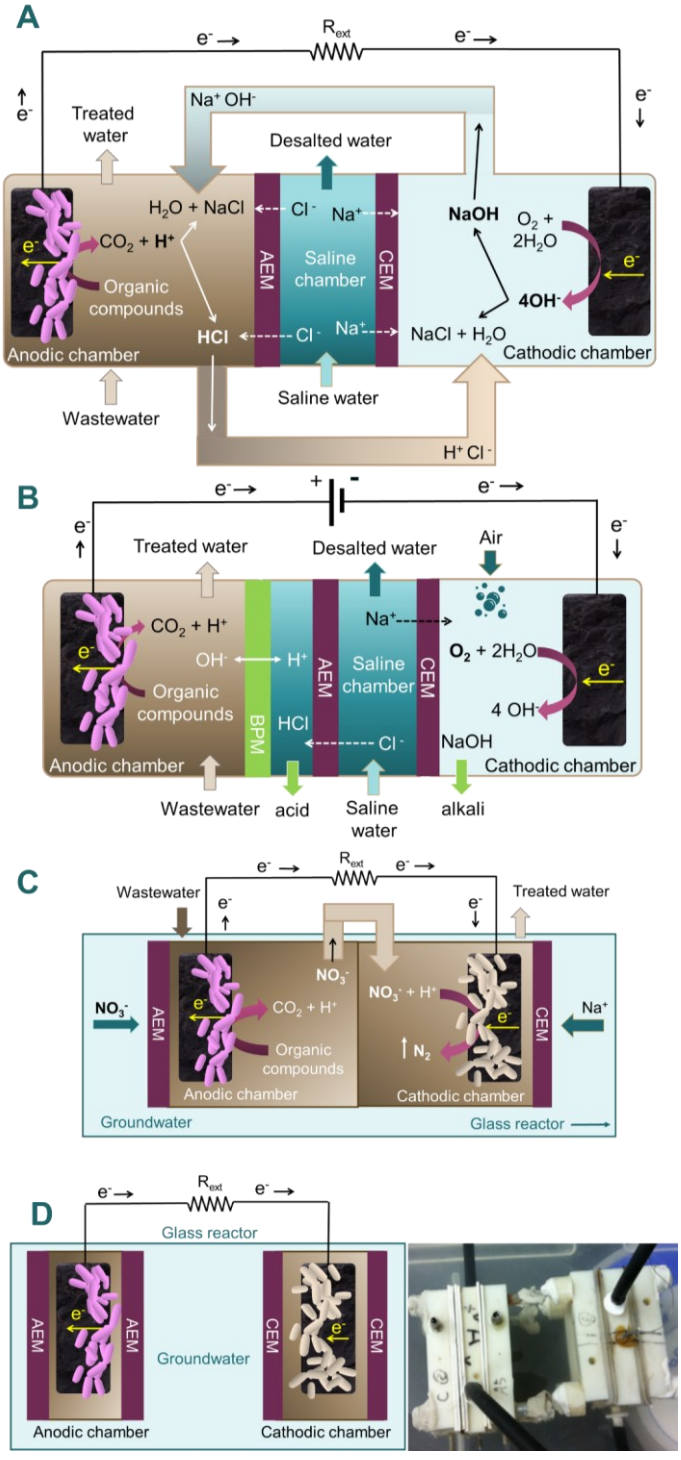
A
R_{ext}
e^-
Treated water
Na^+ OH^-
Desalted water
H_2O + NaCl
Cl^-
Na^+
NaOH
O_2 + $2H_2O$
CO_2 + H^+
AEM
Saline chamber
CEM
Organic compounds
4OH^-
HCl
NaCl + H_2O
Anodic chamber
Cathodic chamber
Wastewater
Saline water
H^+ Cl^-
B
Treated water
Desalted water
Air
CO_2 + H^+
OH^-
H^+
Na^+
O_2 + $2H_2O$
Organic compounds
BPM
HCl
4 OH^-
NaOH
Anodic chamber
Cathodic chamber
Wastewater
acid
Saline water
alkali
C
Wastewater
Treated water
NO_3^-
NO_3^- + H^+
N_2
Organic compounds
Groundwater
Glass reactor
D
Glass reactor
Groundwater
Anodic chamber
Cathodic chamber

Figure 22. A) Scheme of a Recirculation MDC adapted from Qu *et al.,* (Qu et al., 2012). **B)** Microbial Electrolysis desalination and chemical-Production Cell (MEDCC) scheme adapted from *Chen et al.,* (Chen et al., 2012a). **C)** Submerged microbial desalination-denitrification cell (SMDDC) Adapted from Zhang et al., (Zhang and Angelidaki, 2013). **D)** decoupled MDC. Draw adapted, and photo taken from Ping et al., (Ping and He, 2013).

In the 3-chamber configuration, pH changes can occur in the anodic compartments reducing microbial activity (acidification, due to the protons production of the fuel oxidation) and cathodic compartment with possible potential loss (basification by protons consumption or hydroxyl ions from oxygen reduction). It is due to the impossibility of the ion transport through the IEM (desalination chamber) between the anode and cathode chambers. To solve this problem high volumes by increasing the frequency of replacement anolyte and catholyte are used (Cao et al., 2009) or the addition of acids, bases (Cao et al., 2009; Chen et al., 2011b; Jacobson et al., 2011a) or buffers but this entails a higher operating cost (Kim and Logan, 2013a). Also, A direct proton transfer pathway could be installed between anode and cathode to alleviate pH changes (Yang et al., 2013). *Recirculation MDCs (rMDCs)* is other strategy that allowed control of the possible pH fluctuations (Qu et al., 2012). This configuration allows the recirculation of solutions between the anode and the cathode through very thin tubes to avoid equal potential at the anode and cathode chambers **(figure 22A)**. Some studies show that this method helps increase the power density and improve the efficiencies in desalination (Qu et al., 2012; Sevda et al., 2015). However, the activity of cathode catalysts could be hindered by bacterial growth on the cathode electrode having to add changes to the system (Chen et al., 2012c).

Another effect that could inhibit the metabolic activity of electroactive microorganisms is the accumulation of chloride ions although it is still a subject under study (Mehanna et al., 2010b; Yang et al., 2015; Yuan et al., 2017). To avoid this accumulation and the typical pH drop in the anode chamber a *Microbial Electrolysis Desalination and Chemical - Production Cell (MEDCC)* was constructed (Chen et al., 2012b). This configuration **(Figure 22B)** has an

additional chamber (called acid-production chamber) between the anode and desalination chamber by inserting a bipolar membrane (BPM). This membrane is a special kind of IEM able to dissociate water molecules into protons and hydroxyl groups. In this additional chamber acid is produced from chlorides, from the desalination chamber, and protons produced simultaneously in BPM. Apart from the production of hydrochloric acid and caustic soda (Chen et al., 2012a), organic acid also has been produced (Chen et al., 2012b; Liu et al., 2015b). The production of hydrogen gas or hydrogen peroxide, with simultaneously saline water desalination, is achieved in a *Microbial Electrodialysis Cell (MEDC)* where a potential difference is applied results in the production of these species at their cathodes (Mehanna et al., 2010b; Luo et al., 2011; Yang et al., 2014) . Another option for pH modulation and ion migration to anodic and cathodic chambers is the incorporation of capacitive deionization into an MDC system (Forrestal et al., 2012) creating a *Microbial Capacitive Desalination Cell (MCDC)*. The anode and cathode chambers are separated from the desalination chamber by CEM and activated carbon cloth layers. Saltwater is desalinated via electrical ion adsorption in capacitors without energy input. The protons, produced in the anode chamber, can move to the cathode chamber through CEM.

Some configurations have been developed for more specific applications such as nitrate removal in groundwater "in situ" (Zhang and Angelidaki, 2013). Is the case of submergible modular-type MDC which is called as a *Submerged Microbial Desalination-Denitrification Cell (SMDDC)* **(figure 22C)**. This device consisting of an AEM and CEM installed at the end of the anode and cathode chambers, respectively. The nitrates, which pass through the AEM, flow with the wastewater stream through the tube which hydraulically connect the anodic and cathodic chamber and these ions are used as electron acceptors for the biocathode. Other types of submerged modular-type MDC is a Decoupled MDC (Ping and He, 2013) where the anode and cathode chambers are spatially decoupled to

improve the flexibility of MDC construction and operation. One decoupled MDC consists in an anode chamber unit comprised of two AEMs and an anode electrode and a cathode unit made of two CEMs and a cathode electrode **(figure 22D).** Configurations dedicated to denitrification and nutrients recovery are being developed that only needs wastewater as sole water input. An example is the *Multi - stage MDCs (M–MDC)* which is fabricated for desalination and biologically denitrifying high-strength industrial wastewater flowing through the multiple anode and cathode chambers in series (Zuo et al., 2017). Other configuration with this purpose is *HFM-MDC* which is an MDC with bio-cathodes integrated with a hollow fiber microfiltration membrane (HFM) (Zuo et al., 2018).

Different type of configuration is the *Osmotic Microbial Desalination Cell (OsMDC)* that combines MDC technology with Forward Osmosis (FO) mechanism by replacing the AEM with a FO membrane to recover water by osmosis (Zhang and He, 2012). In an FO system, water flux is created between the feed solution and draw solution (with a higher osmotic pressure than the feed solution) due to the concentration gradient) (Cath et al., 2006). However, the OsMDC to allow the water to pass through the FO membrane (achiving a dilution in the middle chamber) but reducing the transport of ions from the middle chamber to either electrode chamber (Zhang and He, 2013) due to the high resistance of FO membranes and the possible fouling (the salts of the middle chamber are not removed but are concentrated). In conventional MDC, the desalination of low-concentration saltwater or the decrease of conductivity in saline stream during desalination process causes a greatly increase of the ohmic resistance in the system. This fact reduces the electricity production and, consequently the desalination rate (Cao et al., 2009). For the aim of the reduction of this ohmic resistance and achieved higher desalination rate with low energy consumption MDCs have been packed with ion-exchange resin (IERs) packed *(R-MDC)* inside desalination chamber. These resins can operate as ionic

conductors with high conductive (Morel et al., 2012; Zhang et al., 2012). This block of reported configurations for MDC systems is summarized in the following **table 1**, together with its main characteristics, disadvantages, and advantages.

Table 1. Summary of different configurations of microbial desalination cells reported in the literature.

Reported MDC reactor configuration	✓ Advantages	✗ Desadvantages
Rectangular 3-chamber		
Stacked (sMDC)	Increased charge transfer efficiency	Increased internal resistance
Tubular up-flow (UMDC)	Increased surface of contact	Longer retention time
Recirculation (rMDC)	Stabilised pH in the cell	Biofouling membranes
Microbial Electrolysis desalination and chemical - Production Cell (MEDCC)	Valuable products production	Non-spontaneous process
Microbial Electrodialysis Cell (MEDC)	Hydrogen Production	Non-spontaneous process
Microbial Capacitive Desalination Cell (MCDC)	Stabilised pH in the cell	
Osmotic Microbial Desalination Cell (OsMDC)	cheaper membrane cost	High internal resistance
Ion-exchange resin (IERs) packed (R-MDC)	Reduced ohmic resistance	Scaling in resin surface
Submerged Microbial Desalination-Denitrification Cell (SMDDC)	Nitrate removal “in situ”	
Decoupled MDC	Easy to repair	
Multi-stage MDCs (M–MDC)		
Hollow fiber Membrane - MDC (HFM-MDC)		

The ***ionic exchange membranes (IEMs)*** allow ion separation in the desalination chamber and physically separation of the anode, cathode, and desalination chambers. These membranes are used in most electrodialysis processes. One of the most important properties in these membranes is their permselectivity, which is the ability to allow the passage of certain ionic species while preventing the passage of other species (Davis et al., 1997). In addition to other types, there are two basic types of IEMs, as they show a selective

permeability to cations but not to anions, or vice versa: The cation exchange membranes (CEM) are formed by negatively charged functional groups chemically fixed to the polymer matrix, which allow the pass of cations (counter-ion) while anions (co-ions) are rejected **(figure 23)**. In contrast, the anion exchange membrane (AEM) are formed by positively charged functional groups chemically fixed to a polymer matrix, which allow the anions (counter-ions) to pass through while cations (co-ions) are rejected (Gubler, 2018). The exclusion of the co-ions is the result of the two *Donnan* potentials (potential different between membrane and solution) one on each face of the membrane or also named as *Donnan* exclusion (Donnan, 1995).

$$\text{Current efficiency (\%)} = \frac{charge\ transfer\ across\ membranes}{Circulated\ charge\ across\ external\ circuit} = \frac{ion\ migration + diffusion}{ion\ migration}$$

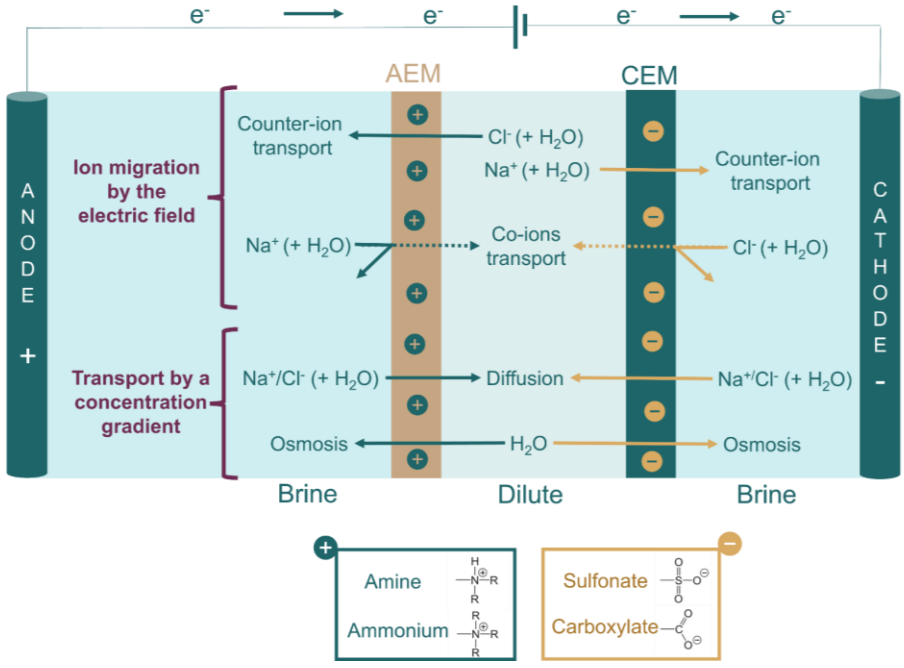

Figure 23. Selective permeability of cation exchange membrane (CEM) and anion exchange membrane (AEM) with the main functional groups fixed to the polymer matrix. Illustration of the transport process that can occur simultaneously during the electrodialysis process.

Counter-ion transport **(Figure 23)** or ion migration constitute the main electric movement in the process. This solvates ions transport a certain amount of water by electroosmosis. The co-ion transport (also can transport water molecules) is relatively negligible but it is dependent of the membrane selectivity quality. When two solutions with different ion concentration are separated by permselectivity membrane, a different potential is established between these two-solution named "potential membrane" which can be measured. This potential is composed by the two *Donnan* potential and the diffusion potential (this last potential is negligible for ideal membrane and is the potential gradient that is opposed to counter-ions transport by concentration gradient inner membrane). The electrolyte diffusion transport, or back-diffusion (co-ion and counter-ion) take place for concentration gradient from brine to dilute compartment (also with water transport association) and act in contrast to ion migration. This transport is controlled by the concentration gradient between the two surfaces of membrane (more saline concentration different, more diffusion rate) (Ping et al., 2016). In MDC systems, is possible substrate leakage through the AEM by diffusion (Davis et al., 2013; Werner et al., 2013) to desalinated water causing reduction in the desalination efficiency and contamination with an elevation in microorganism growth (Ping et al., 2013). Finally, the water transport by osmosis take place from low solute concentration compartment to high solute concentration compartment. The desalination efficiency in MDC can be reduced for some of the presents transports e.g., co-ions transport, diffusion, water transport associated with counter-ion transport or osmosis phenomenon. These non-deseable process can be reduced by membrane selection and operative process. The membranes do not show ideal ionic selectivity and deviation from ideal performance in desalination process is expressed by *current efficiency* **(Figure 23)**.

Another critical membrane-related issue is membrane fouling which can increase capital costs and decrease system performance (Judd, 2008; Logan and Elimelech, 2012). In long-term tests of MDCs, the biofouling on an AEM (in

contact with anode chamber) (Luo et al., 2012b) and inorganic scaling on the CEM (in contact with cathode chamber) (Ping et al., 2013) due to divalent cations (Ca^{2+} and Mg^{2+}) inhibits ion transfer and increases system resistance leading to significant performance declines such current density (Chen et al., 2012a; Luo et al., 2012a). Replacing the membranes recovers the performance of the system, but this increases costs (Zhang et al., 2016b) therefore, is needed to improve resistance to biological fouling such as antibiotic coating or carbon-based nanomaterials.

For suitable performance, these membranes should have next characteristics: low electrical resistance (it influences on the ohmic resistance of unit MDC); high permselectivity (Güler et al., 2013) (i.e., co-ions negligible permeability) that will allow low diffusion rates. A low osmotic permeability as well as high mechanical and chemical stability. Therefore, to improve the performance and scability of MDC technology is necessary continue development of IEMs (Moruno et al., 2018b, 2018a)(Mehanna et al., 2010c) and their production must have a compromise between selectivity and low resistance, low production cost (Strathmann, 2010) and useful lifetime. In that sense, the development of processes for recycling this type of membrane can contribute to a more sustainable desalination system that is more compatible with the circular economy system (Lejarazu-Larrañaga et al., 2020b, 2020a).

Respect to ***construction for the desalination chamber*** a variety of factors have been investigated. Some can contribute to increased internal resistance of system: width between membranes (Chen et al., 2012b; Lu et al., 2017), spacers installed in in desalination compartment to ensure turbulent flow (Shehab et al., 2014) as well as the number of desalination chambers in stacked MDC (Ge et al., 2014; Chen et al., 2016). Although the increase of number of desalination cells exhibits an increase in charge transfer efficiency and desalination rate, more water losses (from dilution to concentration chambers) occurs and the electrical current and desalination ratio decrease. Others factors can contribute to decrease

internal resistance: filling inside desalination compartment such as ion exchange resins (IERs) (Morel et al., 2012; Zhang et al., 2012).

Electrodes constitute essential components in MDC as they determine the magnitude of the potential gradient which drives the desalination process (Salinas-Rodríguez et al., 2021). In terms of materials, new anode electrodes have been developed to enhance the performance of MDC: unusual materials such as granular coconut shell (Sophia and Bhalambaal, 2015) or graphite plate with a photocatalyst hematite nanostructure (on one side in the anode) used in a called photo-microbial desalination cell (Liang et al., 2016). Respect to cathode materials, carbon felt was used in the first MDC with liquid catholyte (ferricyanide) (Cao et al., 2009). In air-cathodes platinum-coated carbon paper have been studied (Mehanna et al., 2010c, 2010b; Luo et al., 2012a; Qu et al., 2013) as well as non-precious Fe-N-C catalyst electrode (Santoro et al., 2017) for oxygen reduction reaction (ORR). In addition to having high electrical conductivity and high surface area, carbonaceous materials must be biocompatible, flexible, chemical/mechanical resistant, and cost-effective to implement. Further studies of innovative materials with more outstanding microbial adhesion to the surface and a specific porous structure that improves microbial colonization would be necessary.

B) Desalination chamber factors: initial saline concentration, the composition and hydraulic retention time (HRT)

The ***initial concentration of saline water*** in the desalination chamber affects the energy production, desalination performance (Mehanna et al., 2010b; Yang et al., 2015) or anodic microbial community structure (Yuan et al., 2017). Some studies about three-chambered MDCs reported an increase of power density related to that the increase of initial salt concentration, mainly due to a reduction of internal resistance in the system and an improvement in the junction potential generated by the concentration gradient across the IEMs (Yang et al., 2015; Yuan

et al., 2017). Not only the ionic concentration affects the efficiency of the desalination process, but also the ***ionic composition***. The use of synthetic saline medium containing sodium bicarbonate and sodium chloride in the desalination chamber (Luo et al., 2012b, 2012c) allows to achieve good results due to the increase in buffer capacity and conductivity achieved in the anodic compartment as desalination occurs (migration of HCO_3^- from saline chamber to anode chamber). However, using real seawater exhibits much lower power density and desalination efficiency (Jacobson et al., 2011b). For example, the presence of divalent cations deteriorates the MDC performance (Luo et al., 2012a; Zuo et al., 2013) because although they are removed faster due to their ionic charge (Chen et al., 2015) they can precipitate, which leads to membrane scaling. Furthermore, real saline water could contain high concentrations of inorganic compounds such as nitrate or sulphate ions that could have a negative impact when they pass to the anode compartment. These anions could act as a final electron acceptor instead of the electrode with the corresponding loss of coulombic efficiency. For configurations that work under continuous conditions, the ***hydraulic retention time (HRT)*** factor of water determines the desalination efficiency of the system. Higher HRT allows for greater efficiencies (Qu et al., 2013).

C) Electrochemical factor: catholyte strategy, the importance of terminal electron acceptor.

As with any other microbial electrochemical system (Cheng et al., 2006), MDC also shows a limitation in the cathodic reaction and the choice of electron acceptor is important to improve the performance of the MDC system. Different ***cathodic strategies*** have been used in the literature on MDC systems (**Figure 24**).

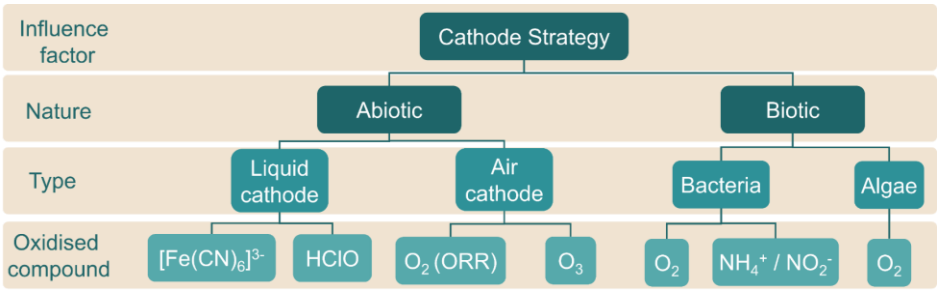

Figure 24. Different cathode strategies for MDC devices. Classification for its nature, type and oxidized species that suffer the reduction reaction.

C1. Abiotic Cathodes: Liquid cathodes

These cathodes are based on redox compound dissolved in water. The use of ***potassium ferricyanide*** (mediator redox) as a liquid cathode (i.e., $[Fe(CN)_6]^{3-} + 1e^- \rightarrow [Fe(CN)_6]^{4-}$, $E^{0'} = 0.37$ V) was used in the first proof of concept MDC (Cao et al., 2009; Luo et al., 2012b; Zhang and He, 2012; Liang et al., 2016). This cathode reaction has fast reaction kinetics and allows reached high cathodic potentials allowing obtaining high performance in desalination without the use of precious catalysts such as platinum (Kondaveeti et al., 2018). Other example is the use of hypochlorite as an electron acceptor (Borjas et al., 2017). The use of these redox mediators in the MDC literature is proper to test a concept (Cao et al., 2009), analyse the maximum potential of the technology or analysis of the functioning of these systems to understand their behaviour in different experimental conditions in case the cathode is not a limitation. The high operating costs and toxic characteristics for some liquid cathodes make its implementation on a large scale difficult (He and Angenent, 2006). However, could be interesting if low-cost redox mediators are used and an easy and low energy method is developed for regeneration of depleted redox mediator solutions (for example, using renewable energies or biocathodes).

C2. Abiotic Cathodes: Air-diffusion cathode

The air-diffusion cathode **(figure 25)** use the ***oxygen reduction reaction (ORR)*** as a cathodic reaction, where atmospheric oxygen as the final electron acceptor (Gude et al., 2013; Borràs et al., 2021). The use of ORR was adopted as a main cathodic reaction in MDC systems (Yang et al., 2019a) because it was a more an environmentally friendly and sustainable approach compare to the use of dissolved redox pairs. However, this strategy limits the performance of MDC, decreasing freshwater and energy production even using external voltage (Zhang and He, 2015). The ORR has a very high reduction potential (i.e., $O_2 + 2H_2O + 4e^- \rightarrow 4OH^-$, ($E^{0'}$= 0.815 V vs. SHE or $E^{0'}$= 0.605 V vs. Ag/AgCl at pH 7) but, in practice, this is not reflected by oxygen diffusion problems or slow reaction kinetics at neutral pH (has a high overpotential). This limitation is because the ORR in aqueous solution is a multistep irreversible process with low kinetic due to the high activation energy required to break the double covalent bonding of the O_2 molecule (Wang et al., 2014). Consequently, the reaction must be catalyzed and its kinetic depends on architecture, the cathode material (carbon materials for example), the metal catalyst of the air-cathode or medium characteristics (pH). Regarding the catalyst, platinum is considered the best catalyst for the ORR with high stability but is an expensive strategy for the scale-up implementation (Mehanna et al., 2010c). Iron subgroup metals (Ni, Co, Fe) (Bosch-Jimenez et al., 2017) or manganese oxides (Fujimoto et al., 2020) represent suitable alternatives as catalyst. Furthermore, high energy is required to maintain dissolved oxygen concentration what it entails to use using high-surface-area carbon substrates, or exposing the MDC to atmosphere, or using passive methods to achieve transfer of oxygen in the cathodes (Sharma et al., 2019).

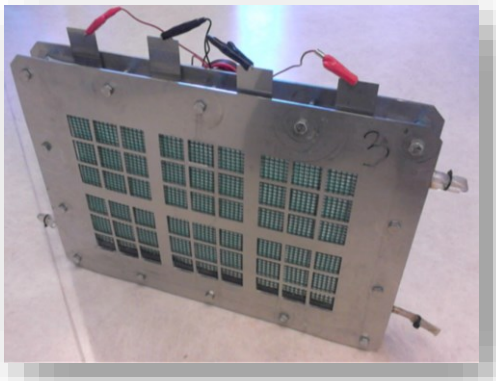

Figure 25. Photo of an air cathode MFC cell from Bosch-Jimenez et al., (Bosch-Jimenez et al., 2017).

Respect to the medium characteristics, during ORR significantly increases the catholyte pH and the thermodynamic and kinetic of the reaction suffer variation. Some MDC works reported using PBS (Mehanna et al., 2010c; Chen et al., 2011b; Ping et al., 2013; Lu et al., 2016) acidified water (Jacobson et al., 2011a; Zhang and He, 2013; Sevda et al., 2017) or saline water (to enhance the conductivity) (Ping and He, 2013; Ebrahimi et al., 2018a) with ORR as cathodic reaction. Another proposed new final electron acceptor has been the ozone molecule, which with a high redox potential increases current density and desalination rate but dramatically increases operating costs (Gholizadeh et al., 2017).

C3. Bio-cathodes:

On the other hand, instead of modifying the electrode materials with precious metals to ORR, a cheaper and more sustainable alternative is a bio-cathode (Wen et al., 2012) or a photosynthetic biocathode (Kokabian and Gude, 2013, 2015; Ashwaniy and Perumalsamy, 2017; Khazraee Zamanpour et al., 2017; Arana and Gude, 2018; Kokabian et al., 2018c; Ewusi-Mensah et al., 2021). ***Aerobic biocathodes*** is based on electroactive aerobic consortia that bio-catalyze the ORR. The catholyte solutions tested are nutrient mineral buffer (Wen et al., 2012),

wastewater (Ebrahimi et al., 2018a) or MDC anode effluent (Ebrahimi et al., 2018b) for instance. Some studies reported the better performance of biocathode than air-cathode in desalination and energy production (Wen et al., 2012) since in a biocathode the final acceptor (electroactive biofilm) is more available than an oxygen molecule (Ebrahimi et al., 2018a). However, can lead to biofouling during long-term operation (Wen et al., 2012) and degraded MDC performance (Zhang et al., 2016b). Also, have been reported ***anaerobic biocathode*** applied in MDC systems (Kokabian et al., 2018b). ***Photosynthetic MDC systems*** (P-MDC) (Bejjanki et al., 2021) are characterized by the use of microalgae in the cathode that consumes carbon dioxide and produce oxygen (Kokabian and Gude, 2013) for the use ORR as a counter-reaction on the cathode (Ewusi-Mensah et al., 2021). These biocathodes can show superior wastewater treatment as it can use the remaining dissolve organic matter and nutrients of wastewater treated to produce microalgae biomass that could be used for bioenergy production. They are sustainable and environmentally friendly systems but the performance in desalination is still low (Kokabian and Gude, 2015; Kokabian et al., 2018c, 2018a).

D) Operational factors: start-up, modes operation, and external load value

Most of the studies on MDC follow the same ***start-up protocol***: a pre-growth of the anodic biofilm under a MFC configuration (Cao et al., 2009; Kim and Logan, 2013b), and then a conversion of MFC into MDC device by adding a third chamber (saline compartment) that requires the disassembly of the whole system and time-consuming procedure (almost 20 days) (Meng et al., 2014) and does not favour reproducible experimental results at the lab scale. The work of Borjas et al., (Borjas et al., 2017) implemented an efficient start-up protocol where a filter press-based MDC prototype is inoculated with electroactive bacteria under MEC configuration. This protocol allowed obtaining an optimal biofilm in the MDC achieving 90 % desalination in just 72 hours without power supply. This start-up

protocol optimizes for time and simplifies operational procedures making it a more feasible strategy for future scaling-up of MDCs (Borjas Hernández, 2016).

The ***external resistance value*** allows choose between two main options in an MDC system: obtain the highest power density or obtain the highest desalination rate. With a low external resistance value, high current density is achieved, and a higher desalination rate is achieved because ion removal by migration is improve (Ebrahimi et al., 2017). However, if MDCs operates with the maximum current density, then the maximum power density cannot be obtained. The application of an ***external voltage*** to the MDC system, increases the current density and the desalination rate is improved (Ge et al., 2014; Lu et al., 2016; Ye et al., 2017) however, the process stops being spontaneous, and energy is wasted.

Batch or continuous ***modes of operation*** significantly affect the performance of the MDC, with continuous flow mode (Qu et al., 2013) as a recommendation for the implementation of these systems, although it is the least studied (Sophia et al., 2016). Another factor to consider is the ***ratio of the volumes*** used as anolyte, catholyte and saline solution ($V_{anolyte}$:V_{saline}:$V_{catholyte}$). This ratio will have an impact on the performance of the system. Considering the conductivities of the solution and physical transports that could occur, using larger volumes of anolyte and catholyte with respect to saline are more favourable (Rahman et al., 2021b). On the other hand, due to there being biological processes involucrate, an optimal ***temperature*** range (25-30°C) is needed (Malakootian et al., 2018).

E) Microbial and physicochemical: Biocatalyst, biofilm environmental and substrate in anode compartment

The general role of electroactive microorganism in MDCs is to oxidize the organic substrate present in the wastewater and transfer the electrons to the conductive surface of the electrode. This phenomenon causes a specific anode potential that, together with the potential obtained at the cathode, achieves a potential difference responsible of electric field that promotes the ionic migration

from the salt compartment. Different types of mixed cultures have been used as ***anode inoculums*** for MDC systems; anaerobic biofilms from the MFC (Cao et al., 2009; Mehanna et al., 2010c), or from different types of sludges (Wen et al., 2012; Kalleary et al., 2014; Meng et al., 2014; Pradhan and Ghangrekar, 2014; Sabina et al., 2014; Shinde et al., 2018). Also have been used pure cultures such as *Geobacter sulfurreducens* (Borjas et al., 2017). The ***bacterial community structure*** reported for MDC is different and less diverse than MFC, due to the salinity achieve in anode environment during desalination process (Luo et al., 2012c; Zhang et al., 2016b; Yuan et al., 2017). Some studies (Luo et al., 2012b; Zhang et al., 2016b) reflects the evolution of anodic bacterial community from early stage of MDC operation to its long-term operation: dominant species *Actinobacteria* and *Chlamydiae* (along with a diverse bacterial species) are substitute in dominance by *Proteobacteria* (along with a reduced of diversity bacterial species). In addition, anodes of MDC systems for low initial saline concentration (5 g L^{-1} NaCl) showed such as dominant species *Pelobacter propionicus* but, for a higher initial concentration (20 g L^{-1} NaCl), *Geobacter sulfurreducens* was the predominant (Mehanna et al., 2010b). Yuang et al., reported that *Pseudomonas, Acinetobacter*, and *Arcobacter* as the significant electrochemically active microorganisms in the MDC anode community structure and, they demonstrated how the community in an MDC anode is shaped by salinity and dominated by these shuttle-mediated electrochemically active microorganisms. Interestingly, halophilic microorganisms were not dominant in the communities even at the highest NaCl concentration (>0.8 M in the anode), possibly because the electrochemically active bacteria developed mechanisms to cope with osmotic pressure (Yuan et al., 2017).

An important operation factor is the ***availability of easily oxidative substrate*** in wastewater for optimal MDC performance. For a complete high saline concentration desalination, high amount of charge from organic compounds is necessary (desalination without depleting substrate). Some studies reported that

an excess (Mehanna et al., 2010c) or poor substrate concentration (Lu et al., 2016) could inhibit the activity of anodic bacteria. Although several MDC studies utilize acetate as an organic fuel (Cao et al., 2009; Mehanna et al., 2010c; Luo et al., 2012a; Zhang and He, 2012; Chen et al., 2015; Ebrahimi et al., 2017; Santoro et al., 2017) or synthetic wastewater (Malakootian et al., 2018) other types of organic carbon sources have been tested: xylose (Qu et al., 2013), leachate (Iskander et al., 2018), sludge (Meng et al., 2014, 2017; Ebrahimi et al., 2018b), petroleum refinery (Abu Reesh et al., 2016), domestic (Luo et al., 2012b; Zuo et al., 2018), steel plant (Shinde et al., 2018), urban (Luo et al., 2012c; Ebrahimi et al., 2018a), industrial (Zuo et al., 2017) or dairy industrial wastewater (Khazraee Zamanpour et al., 2017). Some studies have employed actual wastewater (Luo et al., 2012b; Sophia and Bhalambaal, 2015; Sevda et al., 2017) which resulted in a reduced desalination performance, maximum power densities and COD removal rates compared to those with the use of acetates. MDCs, like other BESs, have difficulty degrading complex carbon compounds. With the aim of solving this worse performance of these systems, when actual wastewater and seawater are applied, is suggested the combination with current commercially available processes. For example, MDC installed after an anaerobic digestion process which supply easily degradable carbon sources (e.g., volatile fatty acids). Within the physicochemical parameters, ***the buffer capacity*** of the environment of the anodic chamber directly affects the performance of the MDC system since a decrease in pH in anode chambers can lead to inhibition of anode bacterial metabolism (Davis et al., 2013; Lu et al., 2016).

1.3.3 Scale-up MDC and new applications

Although most of the MDC prototypes to date only perform at lab-scale, i.e., millilitres (Sayed et al., 2020) a few studies have designed and evaluated the performance of greater than litre-scale reactors. Up-flow MDCs was scaled up to a litre scale (total volume 2.75 L) using artificial seawater (Jacobson et al., 2011b)

with comparable performance to the smaller-scale up-flow MDC. Also, a stacked MDC **(figure 26A)** with 10 litre (as total volume) was fabricated with a membranes sectional area of 675 cm^2 to desalinate 0.5 gL^{-1} NaCl (Zuo et al., 2014). One strategy to scale-up, is the assembly of multiple units of same MDC configuration, for example, serially assembly of 4 stacked MDC **(figure 26B)** (Kim and Logan, 2011; Qu et al., 2013) or 30 up-flow tubular MDC reactors constituting a 100-L pilot-scale MDC **(figure 26C)**. This last system, with ORR as cathode strategy, achieves partial desalination of 15 L synthetic seawater (Zhang and He, 2015), but the performance was found to be much lower than that achieved in millilitre-scale MDC. Another strategy is coupling MDC systems with other types of desalination technologies (e.g., forward osmosis or membrane capacitive deionization) (Zhang and He, 2013; Wen et al., 2014; Yuan et al., 2015). Although these multiple-unit systems enhanced the performance of wastewater and desalination compared to the stand-alone system, the scale and performances are not sufficient yet. For the scale-up of MDC reactors, installation in existing treatment or desalination plants should be considered, with footprint minimization and simplicity for operation and maintenance. In addition, modelling is a powerful tool for understanding phenomena that can affect performance although pilot scale operational data is currently scarce and operational factors must be systematically investigated.

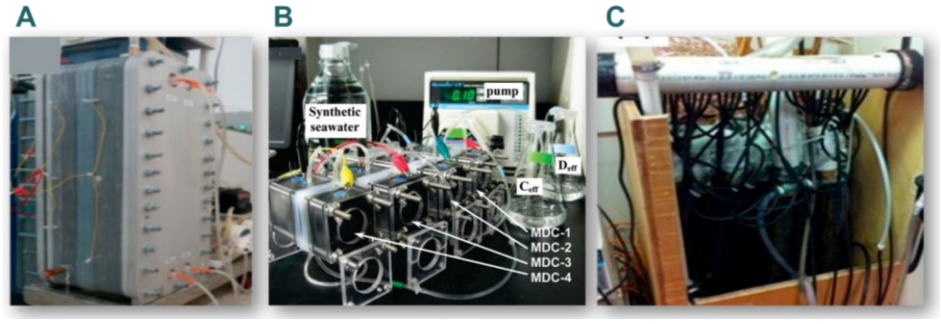

Figure 26. A) Photo of 10-L stack MDC system from Zuo *et al.,* (Zuo et al., 2014). **B)** Photo of desalination system with 4 MDCs operated in series from *Kim and Logan* (Kim and Logan, 2011). **C)** Photo of up-flow scaled system with a total liquid volume of 105 L from Zhang *et al.,*(Zhang and He, 2015).

Several authors agree that the most important ***potential application*** for MDCs **(Figure 27)** is as ***pretreatment*** for desalination processes (RO and ED) to reduce their energy requirements (Mehanna et al., 2010c; Jacobson et al., 2011b; Dong et al., 2017) although, this technology also have been proposed as ***post-treatment*** of concentrate discharge from RO (Luo et al., 2017).

Apart of this main applications, some MDC configurations are used to ***valuable chemical production*** such hydrogen gas or hydrogen peroxide (Mehanna et al., 2010b; Luo et al., 2011; Yang et al., 2014), hydrochloric acid and caustic soda (Chen et al., 2012a) or organic acids (Liu et al., 2015b; Lu et al., 2017). Other application is the ***removal harmful heavy metals*** (Cr^{6+} / Cu^{2+}) (An et al., 2014b, 2014a; Dong et al., 2017) and ***hardness*** (Ca^{2+} / Mg^{2+}) (Brastad and He, 2013; Hemalatha et al., 2017) using the cathodic reduction reaction and ion migration in desalination chambers.

Denitrification (Zhang and Angelidaki, 2013) and ***nutrient recovery*** such nitrogen and phosphorus from wastewater (Mehanna et al., 2010a; Chen et al., 2017) are achieved in modified MDC systems. MDC technology could increase the circularity of essential resources presented in industrial wastewater streams, allowing effective and sustainable wastewater treatment. In addition, it could be a viable alternative for the desalination of industrial saline waters such as the electroplating, mining, petrochemical, and agri-food industries. These systems have been proposed as a treatment for industrial or domestic wastewater: the energy required to carry out the treatment is less than conventional treatment technologies, and no aeration of the wastewater or external energy input to the system is required. In addition, it is also proposed as a pretreatment for conventional biological wastewater treatments since these are not efficient when the salt concentration is high, which can affect microorganisms, producing the effect of plasmolysis inhibiting its action.

Finally, another possible application is as ***biosensors*** used to monitor the concentration of VFA in anaerobic digestion processes in real-time (Jin et al., 2016).

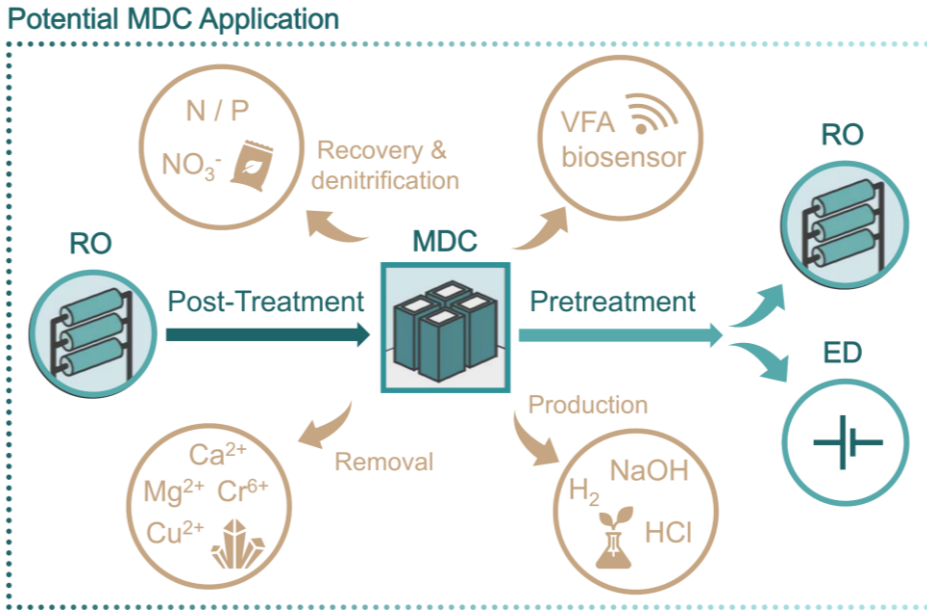

Figure 27. Summary of potential MDC application.

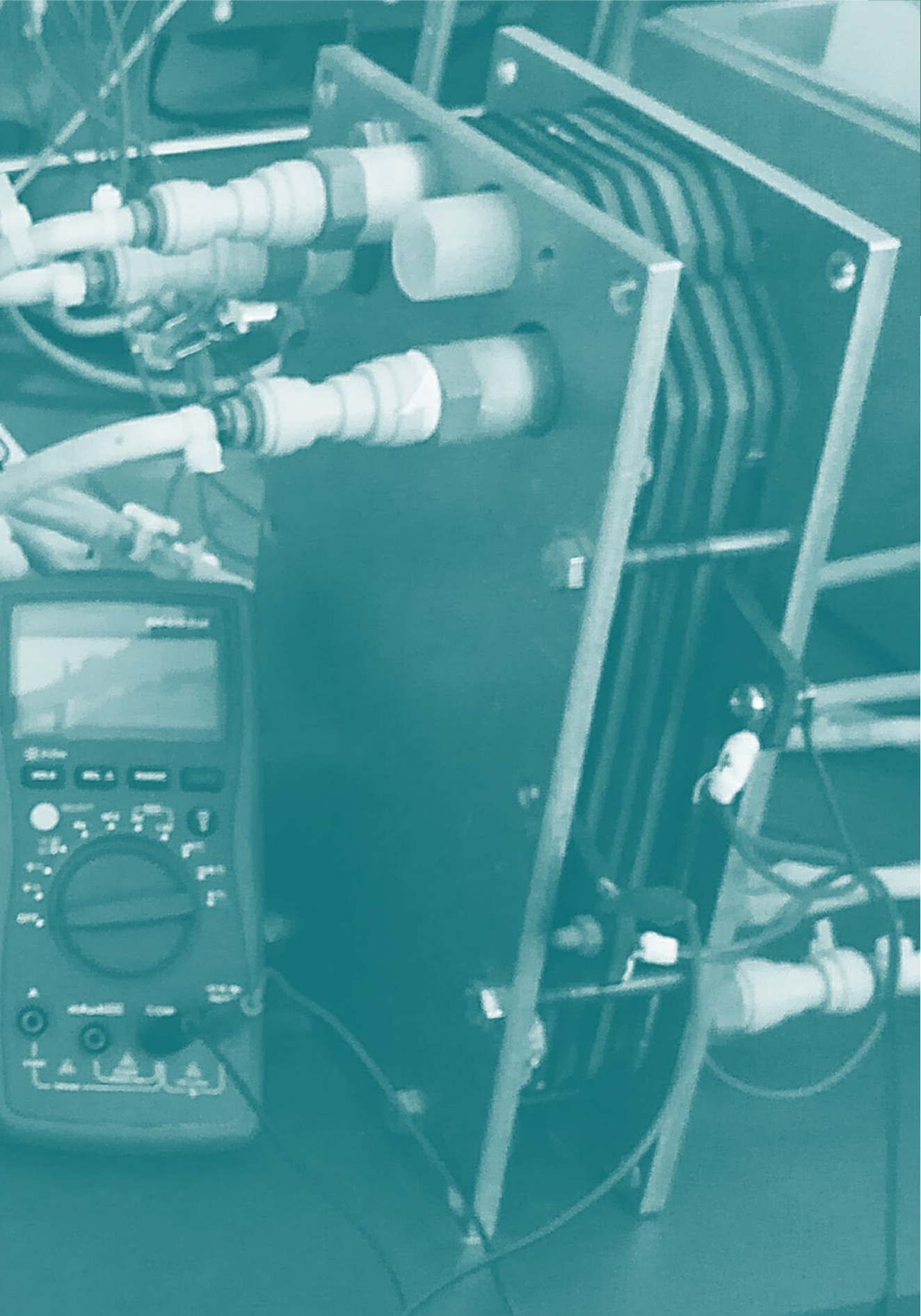


100
60
20

Chapter 2

Objectives and thesis Outline

Objectives and Thesis Outline

Chapter 2: Objectives and thesis outline

This doctoral thesis aims to investigate water desalination in a lab-scale bioelectrochemical device called Microbial Desalination Cell (MDC). This work is providing key information for developing, designing, and optimising water desalination to produce drinking water with low energy cost. The **general objective** of this work is to deeply understand the behaviour of this type of technology and how different disciplines (microbiology, engineering, chemistry, materials science) can be merged a single system. A number of experiments were carried out in a bioelectrochemical filter-press reactor in order to achieve a better electrochemical understanding during desalination, pollutant removal and energy production. In addition, the main limitations of the technology were identified to support the scale-up process. The **specific objectives** of this thesis are summarised below (**figure 28**):

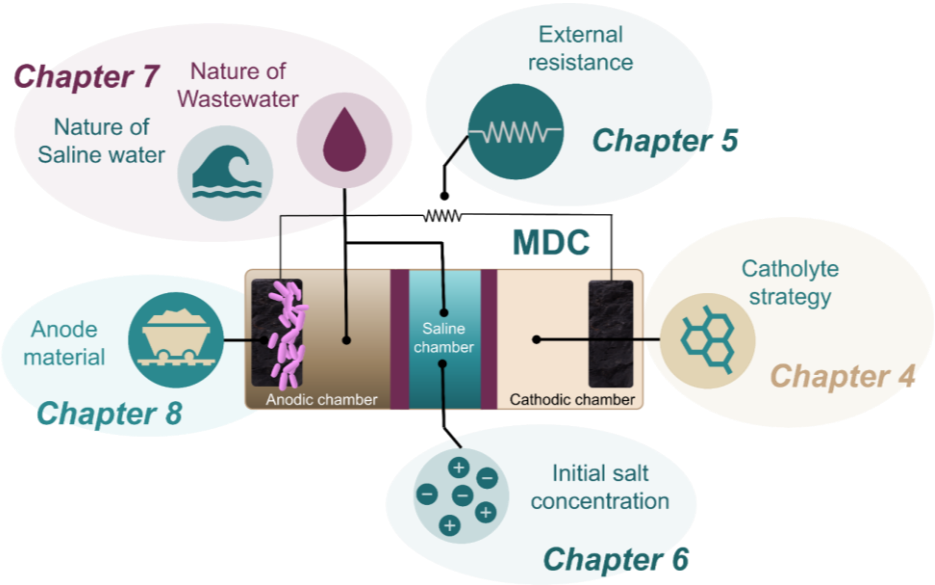

Figure 28. Summary scheme of the main factors that will be addressed in each of the experimental chapters (4-8).

- ***Chapter 4*** investigated the cathodic reaction, one of the most important limiting factors of MDC systems. Two cathodic strategies (oxygen reduction reaction and ferricyanide complex reduction) were studied, including both advantages and disadvantages for a possible large-scale implementation of this technology.
- In ***Chapter 5*** the electrochemical behaviour of an MDC device during brackish water desalination was studied. The influence of the external resistance on its performance was discussed. This study aims to suggest that the MDC device can adapt its primary function (eg. desalinated water production or energy production) depending on the value of external resistance.
- The main objective of ***Chapter 6*** was to study the impact of different saline scenarios on the performance in terms of **i)** desalinated water production, **ii)** wastewater treatment and **iii)** energy production.
- The objective of ***Chapter 7*** was to demonstrate the feasibility of the MDC using real water matrix. The main objective was to compare the performance of MDC for desalinating **i)** river, **ii)** brackish well and **iii)** seawater with the use of real wastewater as anolyte (industrial, municipal wastewater…). These experiments represented a screening of different wastewater to optimize the desalination of real saline waters.
- Finally, in ***Chapter 8***, the main objective was to explore the impact of nanoscale porosity of an activated-surface material on the microbial colonization. This chapter provided a study of new conductive carbonaceous material which could be used successfully in bioelectrochemical systems, including MDC systems, promoting the performance, and reducing costs of these systems (today 30-40% of the total assembly cost).

Throughout the thesis, different microbial desalination cycles have been carried out under different operating conditions (different salinity, nature of solutions, value of external resistance). A chronological diagram of the different

desalination cycles that have been carried out **(Figure 29)** have given rise to some of the different experimental chapters of the thesis. The starting point was the inoculation of the filter press type MDC system whose protocol is described in ***Chapter 3*** in experimental section. Synthetic solutions were used in all compartments (anolyte, saline and catholyte) in the first desalination cycles that were carried out without the need for an external energy supply (desalination cycles that appear in ***Chapters 4-6***). The following desalination cycles (corresponding to those that appear in ***Chapter 7***) are carried out first, with synthetic brackish water (7 g L^{-1} NaCl) using real wastewater from different sources and natures as fuel for the system (industrial, municipal…). As a final step, ***chapter 7*** also includes desalination cycles with a single type of wastewater (industrial wastewater) as fuel to carry out the desalination of brackish water and seawater. The real saline water has been collected in the vicinity of an existing desalination plant in Racons (Dénia, Alicante).

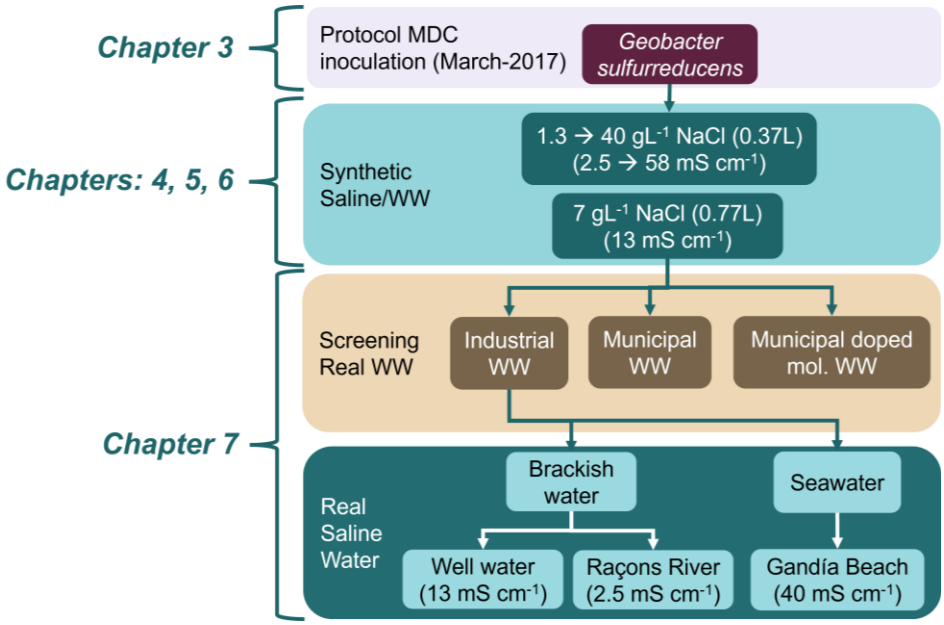

Figure 29. Scheme of the chronological diagram or road map of desalination cycles followed for finding the optimal conditions in MDC and corresponding Chapters number; WW: wastewater; Municipal doped. Mol.: Municipal doped with molasses wastewater.

In parallel, the results obtained from the road map (**Figure 29**) with the lab-scale MDC device, will serve as an experimental platform for the design and development of the scaling of this technology towards a pre-piloting stage within the European MIDES project.

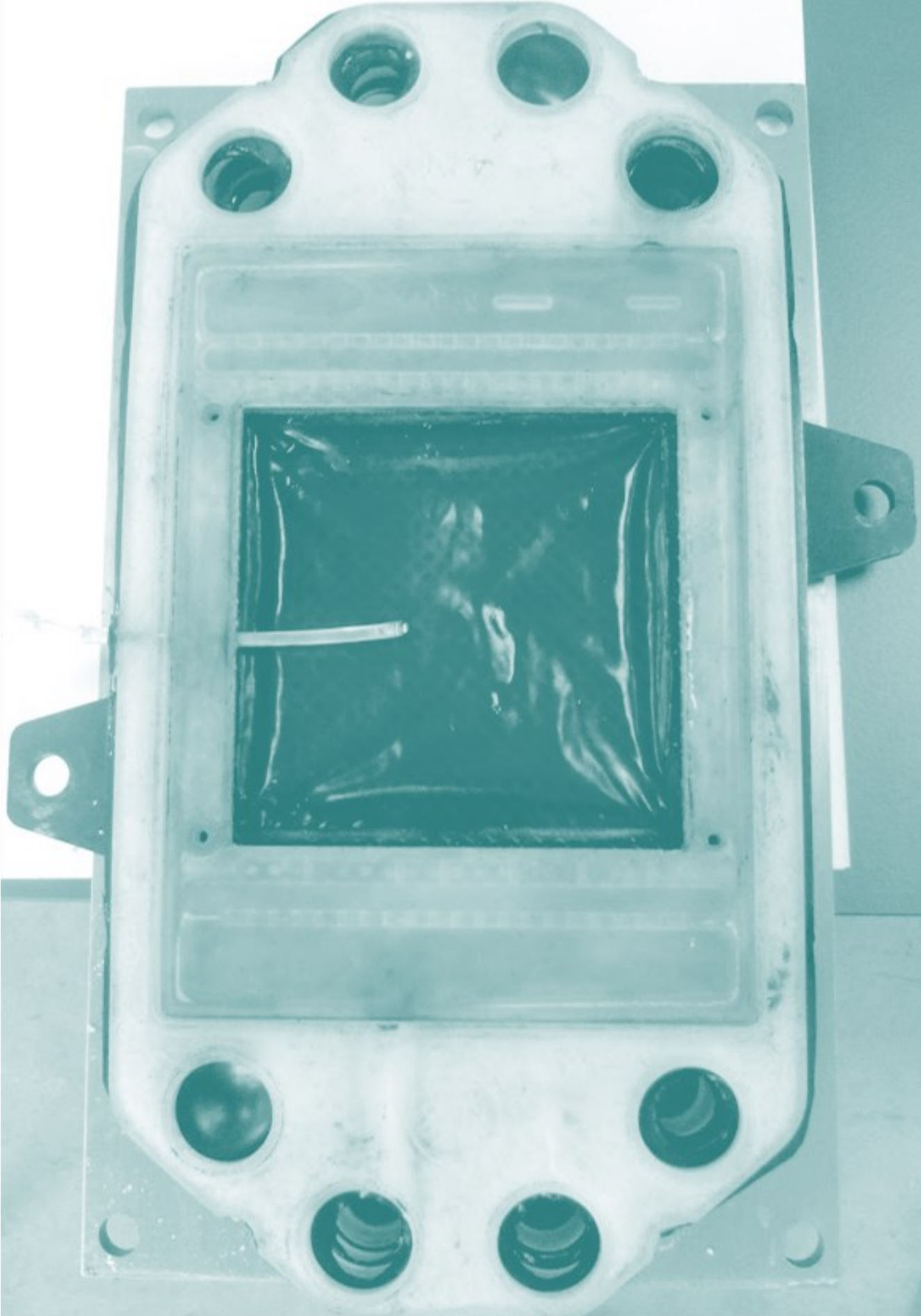


www.duran-group.com

Chapter 3

Electrochemical Techniques & Microbial Desalination Cell Process Parameters

Chapter 3: Electrochemical techniques for bioelectrochemical systems and MDC process parameters

Several basic electrochemical techniques such **voltammetry techniques** are used to study the electron transfer mechanisms between the electrogenic bacteria and the electrodes, characterization of biofilms and to evaluate the kinetics of bioelectrochemical reactions (Marsili et al., 2008). Also, other electrochemical techniques are used to study the electrochemical performance of a bioelectrochemical system, such a **polarization curve.**

3.1.Voltammetry techniques

Voltammetry techniques encompass basic electroanalytical techniques that are used to analyse the reactivity of an electroactive analyte of an electrochemical half-reaction (oxidation or reduction reaction) on the surface of an electrode. The experimental system used for these techniques consists of a three-electrode configuration: the working (WE), the counter (CE) and the reference (RE) electrodes. These electrodes are immersed in an electrolyte solution with a determinate electroactive analyte/s. This system includes a potentiostat as a control and measurement instrument (**figure 30**).

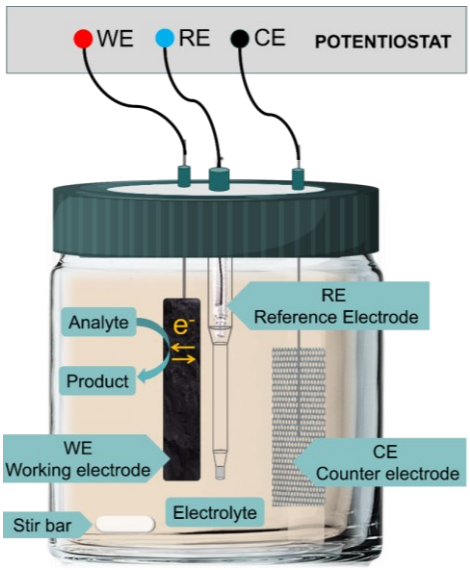

Figure 30. Scheme of the set-up of the three-electrode system: WE, CE and RE immersed in electrolyte solution connecting with a potentiostat instrument.

- Working electrode (WE): electrode surfaces in contact with the electroactive analyte, where the reaction under study takes place (i.e., surface colonized by electroactive bacteria in our case); its potential can be controlled, with the help of a reference electrode, to facilitate electron transfer to and from the analyte of interest. The potential drop between the WE and the electrolyte solution is controls by the potentiostat.
- Reference electrode (RE): this non-polarizable electrode (stable) has a constant potential and is used to established or measured a determinate potential at WE. One of the most used reference electrodes include silver/silver chloride electrode (Ag/AgCl; 0.2V vs SHE).
- Counter electrode (CE): To complete the circuit is used the counter electrode by passing the current required to control the potential at the WE. Its potential depends on the flow of current circulating through the system. In its surface the counter-reaction occurs allows the desired reaction in WE.

With the use of this configuration system the method is the following: the potentiostat applies the desired potential (E_{app}) to the WE, and the resulting current (I) (i.e., the electron transfer between electroactive analyte and surface electrode) is monitored. The obtained I-Eapp curve is known as a voltammogram (Varanasi et al., 2017). Depending on whether the potential applied to WE vary with time or not, two types of voltammetry differ, providing different information on the electroactive biofilm under study:

3.1.1. Chronoamperometry (CA) (*I vs t*)

If the potential applied to WE remain constant, the voltammetric technique is called chronoamperometry (CA). In that technique, a potential value is applied in WE, and the resulting current (positive ion movement due to electron transfer with the electrode) is monitored over a determinate time. In bioelectrochemical systems such as microbial fuel cell, CA technique has been used for the identification of electrogenic species in the natural environment (Parot et al.,

2008), formation of electroactive biofilms on electrode surfaces (Cercado-Quezada et al., 2010), to differentiate between the capacitive and Faradaic currents (Khilari et al., 2015) etc.

3.1.2. Cyclic Voltammetry (CV) *(I vs E)*

If the applied potential varies cyclically with time, the technique is called cyclic voltammetry (CV). This electrochemical analysis consists of recording the current production (positive ion movement due to electron transfer with the electrode) while a potential sweep is carried out along a specific window of potentials. CV is a tool for estimating the nature of electron transfer mechanisms, reversibility and formal potentials of electroactive species, mass transfer influence and kinetic behaviour of microbe-electrode interactions (Harnisch and Freguia, 2012).

The principle of CV recording **(Figure 31A)**, as well as a typical CV recorded (under non-turnover conditions or absence of substrate) using a *Geobacter*-dominated EAB **(Figure 31B)** is shown below (Zhang et al., 2017). In a typical CV, the potential is swept linearly with time from an initial potential (E_i) to a final potential (E_f). In this first interval, towards positive potentials, an electrochemical reaction taking place (i.e., oxidation reaction: $C_{red} - e^- \rightarrow C_{ox}$) and an oxidation current peak (j_{pa}) is recorded (due to the electron transfer between electrochemical species and electrode surface). A transient peak is observed if mass transport is limiting and bulk concentration of electroactive species decreasing. The potential is then swept back from the final potential (E_f) to initial potential (E_i) towards negative potentials, causing electron transfer (reduction current peak, j_{pc}) in the opposite direction (i.e., reduction reaction: $C_{ox} + e^- \rightarrow C_{red}$) and the reformation of initial redox states of the electrochemical species is achieved. The apparent midpoint potential or formal potential ($E^{0'}$) is characteristic of redox pairs (redox center) responsible of the heterogeneous electron transfer.

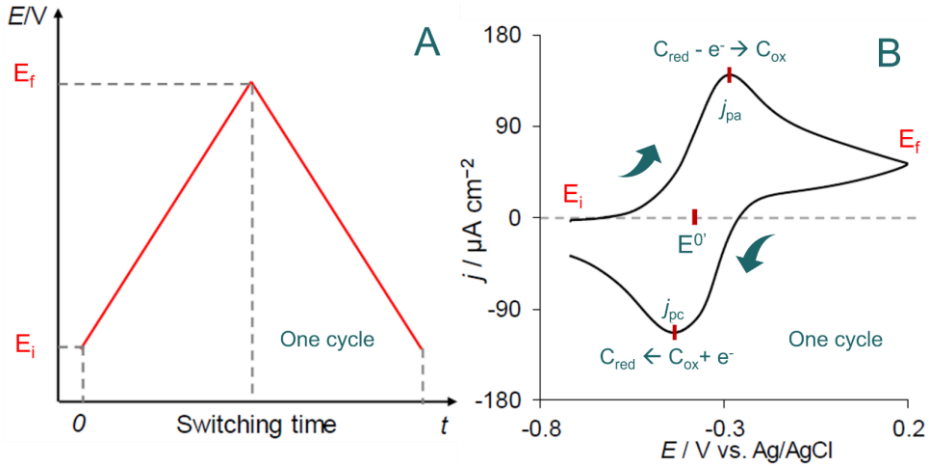

Figure 31. (A) Principle of a CV. **(B)** Cyclic voltammogram from a mature electroactive bacteria under non-turnover conditions on a surface electrode (Zhang, 2019). Under non-turnover conditions, biofilm is deprived of electron donor and oxidation or reduction current peak by each redox centre accessible to the electrode can be observed.

3.2. Polarization curves

The polarization study is used to characterize the performance of fuel cells, in which the cell voltage (or individual electrode potentials employing a reference electrode) is plotted as a function of the current density. Experimentally, the commonly performed is manually varies the value of external resistance and records the stable voltage using a multimeter or a voltage monitoring device (Logan et al., 2006). Then, using Ohm's law, the current density can be calculated for the different resistances values and plotted against voltage. shows a typical polarization curve and the main regions (A, B…) caused by certain effects that influence the fuel cell performance is shown in **Figure 32**. This curve shows how well the MFC maintains a voltage as a function of the current production. Under ideal conditions where there would be no potential losses (complete transformation of chemical energy into electricity with perfect electrodes, infinite rates electrochemical reactions, negligible internal resistance…) the value of the theoretical cell voltage ($E^{0'}$) would remain constant with the increase in current

(yellow line). For that, the knowledge of the individual electrochemical losses must be reduced for the optimization of performance system.

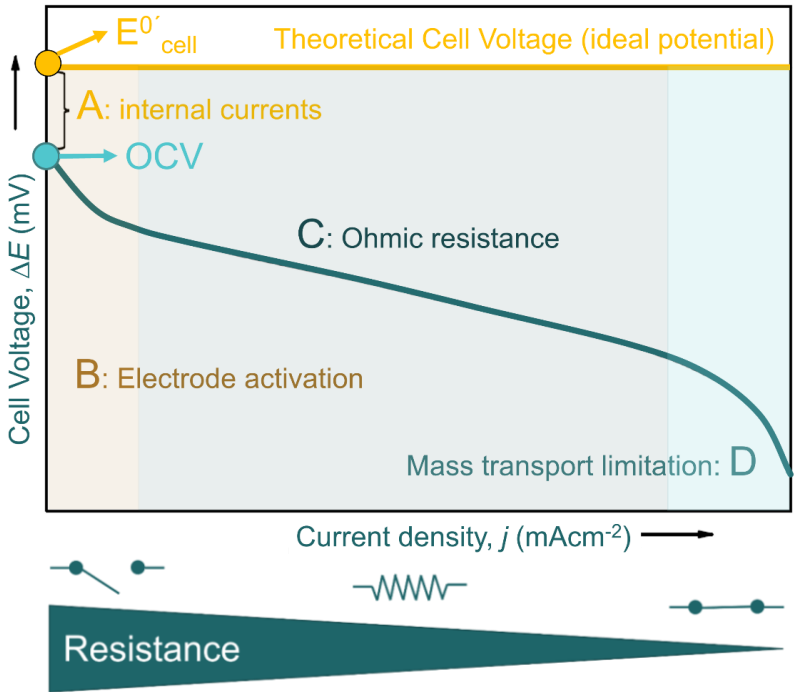

Figure 32. Typical polarization curve for a MFC showing regions where different types of losses caused by certain effects reduce the useful current: **(A)** "internal currents" **(B)** electrode activation, **(C)** ohmic resistance, **(D)** mass transport. Figure adapted from Rabaey, 2009 (Rabaey, 2009), and Logan, 2008 (Logan, 2007).

The different regions, identified with letters **(Figure 32)**, represent the potential loss caused by various limitations of an electrochemical nature:

The decrease of the calculated theoretical cell voltage ($E^{0\prime}$) until open circuit voltage (OCV), the **A region**, is caused by so-called "internal currents" (Rabaey, 2009). The maximum voltage value that the cell can be supplied is the potential value obtained in open circuit conditions (OCV; infinite resistance, no current), due to limitations imposed by microorganisms community and the cathode potential (Logan, 2007). The **region B** is a rapid potential loss at low current

caused by the activation energy required to initiate the oxidation and reduction reactions at electrodes (electrode kinetics).

The **region C** corresponds to a steady decline in the voltage with an increase in the current and is caused by the ohmic resistances of the system components (membranes, electrodes, electrolyte…). The **region D** corresponds to the region at high currents where the voltage falls drastically due to losses by the limitation of mass transport (substrate limitation, lower diffusion rates of the reaction species).

3.3 Materials and methods for desalination cycles with Microbial desalination cell device (MDC)

3.3.1 Microbial Desalination cell device: reactor and configuration

The device used as the MDC in this thesis was a commercial multipurpose electrochemical reactor (Electro MP-1, Electrocell) with a projected electrode area of 100 cm^2 (laboratory-scale MDC device). This type of reactor has a compact stack design **(figure 34)** with individual polypropylene compartments and neoprene gaskets (for an optimal hermetic seal), which allows different cell configurations. In this thesis, the prototype used as the MDC device showed a three-chamber configuration **(figure 33)**: the desalination chamber (compartment volume: 70 cm^3) flanked by the anodic and the cathodic chamber (the volume of both compartments: 70 cm^3) and separated from them by an anionic exchange membrane (AMX Neosepta, Astom Corporation) and a cation exchange membrane (CMX Neosepta, Astom Corporation). Both membranes with 100 cm^2 of membrane surface. The anode and cathode electrodes (projected area of 100 cm^2) were composed of RVG 4000 carbon felt (MERSEN Ltd.), both attached to graphite plates acting as electrical collectors (Isostatic Graphite Plate, MERSEN Ltd.). The device was tightened with stainless steel screws to avoid any leakage from the system.

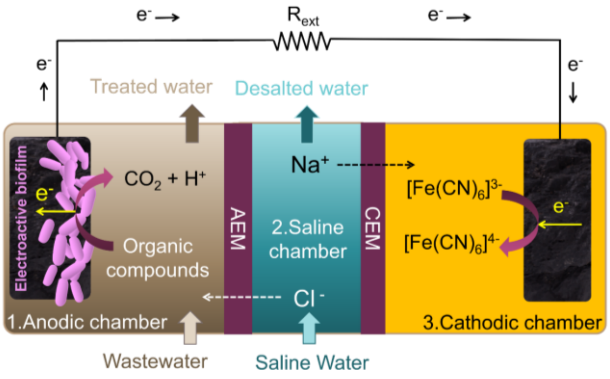

Figure 33. Diagram of an MDC unit. AEM, anion exchange membrane; CEM, cation exchange membrane. R_{ext}: external load or resistance.

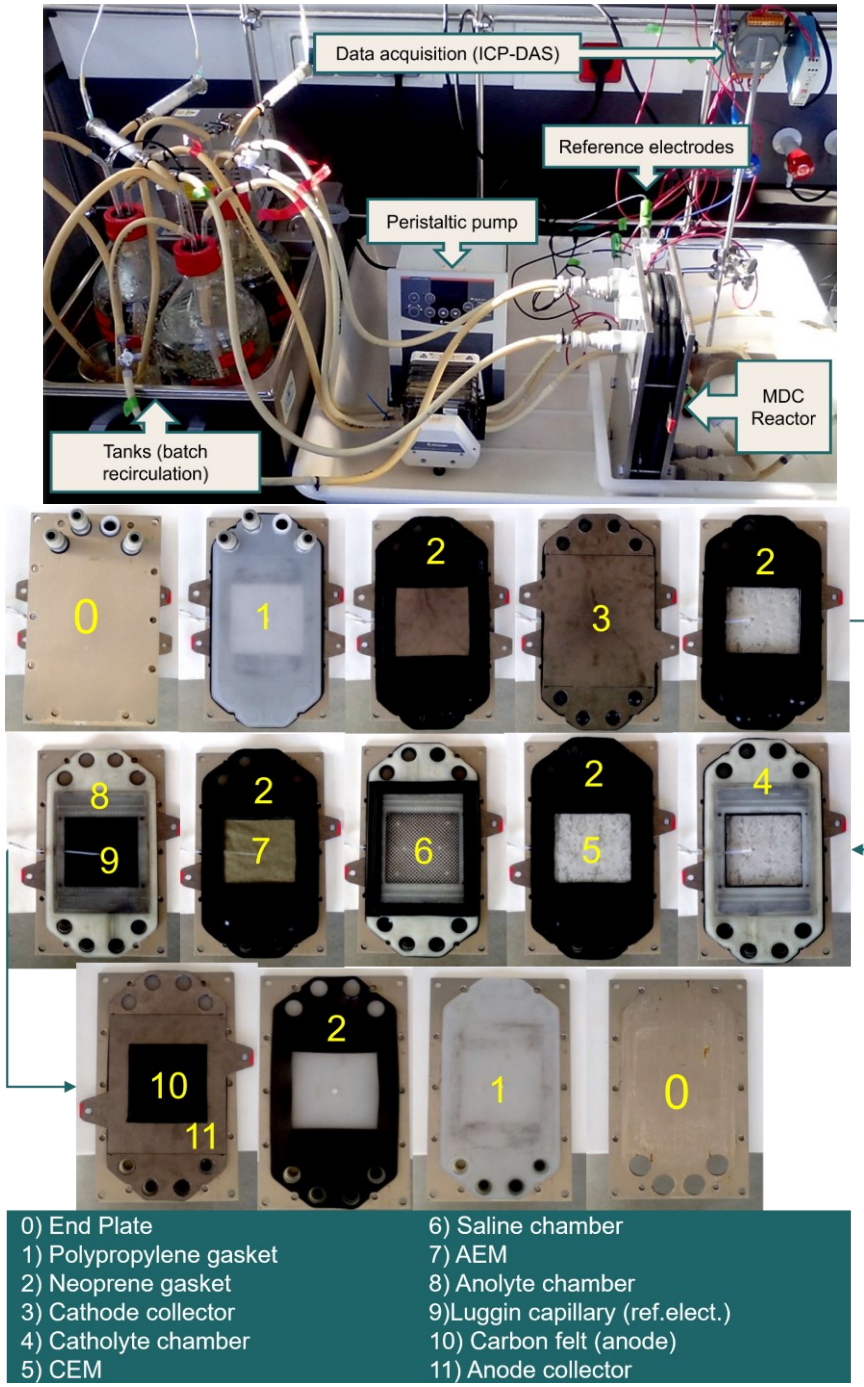

Figure 34. The laboratory-scale MDC system with batch operation mode with recirculation (picture at the top). Elements and layers inside of MDC reactor (picture at the bottom).

A real photography of lab-scale MDC experimental set-up is shown in **Figure 34** and the flow diagram of this experimental set-up is shown in **Figure 36**. Three streams, corresponding to the anolyte, catholyte, and saline solution, were recirculated (flow rate 95 mL min^{-1}) through the MDC system from 3 different tanks (batch recirculation). The MDC reactor was connected to tanks using PharMed BTP Tubing (Saint-Gobain) with an internal diameter of 1/4" and using a three-channel peristaltic pump (Model PD 5206 with a C8 multi-channel pump head, Heidolph). Tanks were placed in a temperature-controlled bath at 30°C, and the anolyte tank was kept under anaerobic conditions by flushing a mixture of N_2/CO_2 (80:20) during the start-up and desalination cycles.

3.3.2 Electrochemical equipment

To monitor the anode and cathode potential, respectively, two reference electrodes (Ag/AgCl, KCl 3.5 M, CRISON) were placed in the geometric centre of the anodic and cathodic compartment, using a Teflon Luggin capillary (internal diameter 3/16", Cole-Parmer) **(element nº 9 in Figure 34)**. The data acquisition from the anode, cathode and cell potential during start-up and desalination cycles was performed using a custom Visual Basic program and ModBus modules (ICP-DAS) **(Figure 35)**. The electric current was measured by the voltage drop through the external resistance in the system.

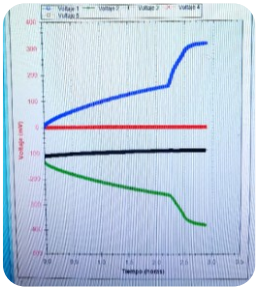

Figure 35. Visual Basic program.

3.3.3 MDC operation: Process Parameters

The main parameters, with their equations, definitions, and units, used to determine the MDC performance are collected in **table 2** and **figure 36** encompasses all these parameters and equations in a schematic picture of the MDC system.

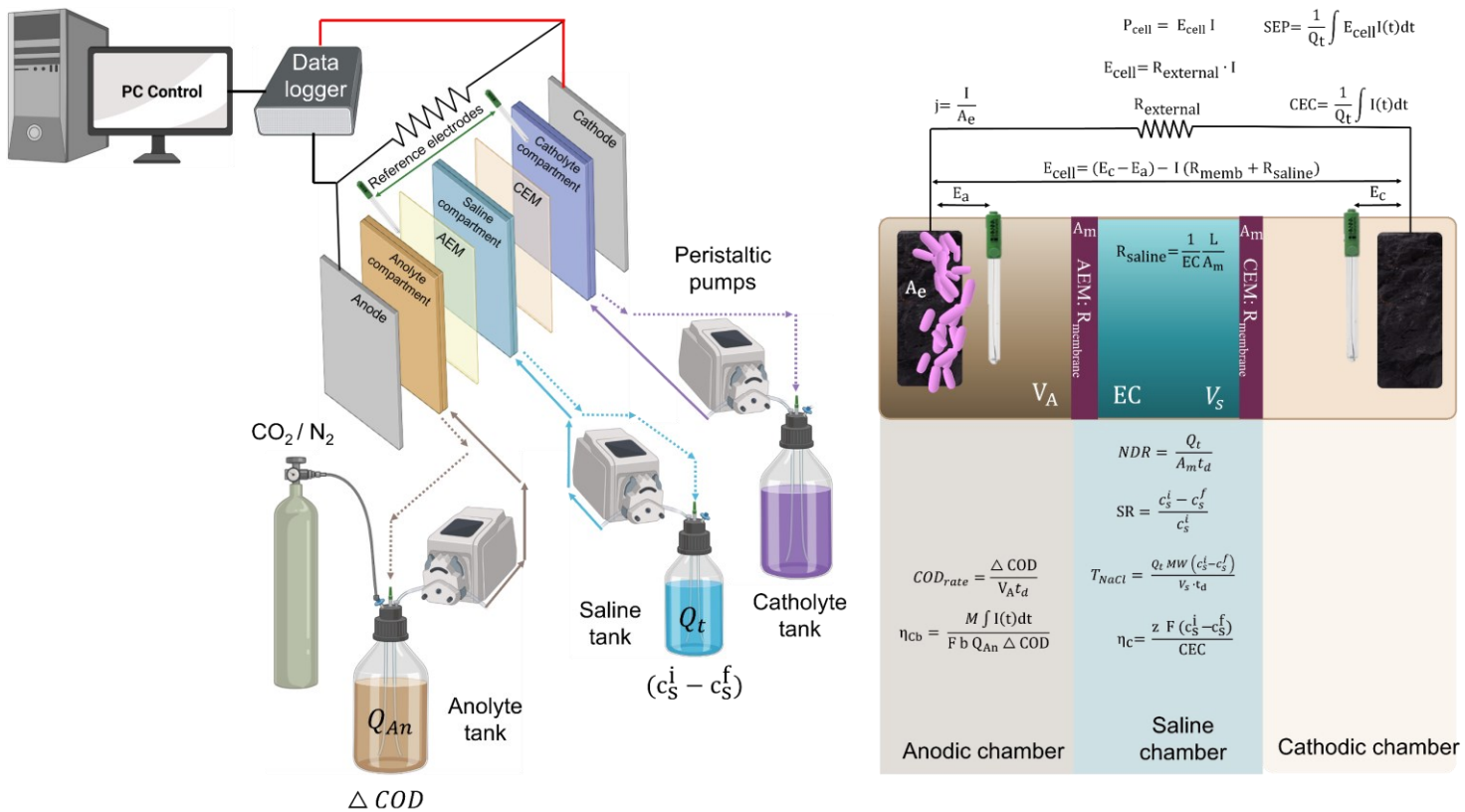

Figure 36. Diagram of MDC set-up (draw made with Biorender.com) with the main parameters and equations used to determine the MDC performance. All the parameters and equations are described in **table 2**.

Table 2. Parameters, equations, definitions and unit used for determining the MDC performance:

Parameter	Equation		Definition (Unit)
Current density	$j = \frac{I}{A_e}$	(1)	where I is the electric current (A) and A_e is the geometric electrode surface area (cm^2). **Units: mA cm^{-2}**
	$E_{cell} = R_{external}\, I$	(2)	where $R_{external}$ (Ω) is the external load resistance connected to the MDC. **Units: V**
MDC potential	$E_{cell} = (E_c - E_a) - I(R_{memb} + R_{saline})$	(3)	This equation could be used for the calculation of MDC potential, where E_c and E_a represent the cathode and anode potential, respectively (V), R_{memb} is the sum of the electric resistances of both anionic and cationic exchange membranes (Ω), and R_{saline} is the electric resistance due to the saline compartment (Ω). **Units: V**
Saline Resistance	$R_{saline} = \frac{1}{EC}\frac{L}{A_m}$	(4)	R_{saline} could be calculated when the geometry and conductivity of the saline compartment is known (Ortiz et al., 2005). Where EC is the electric conductivity of the saline stream (mS cm^{-1}), L is the thickness of the saline compartment (cm) and A_m is the geometric area of the membrane (cm^2). **Units: Ω**
Electrical power output	$P_{cell} = E_{cell} \cdot I$	(5)	The electric power can be calculated with this equation. **Units: W**
Specific energy production	$SEP = \frac{1}{Q_t}\int E_{cell} I(t)dt$	(6)	The amount of energy produced by MDC when a cubic metre of fresh water is produced (Lee et al., 2002). In conventional desalination systems, such as RO, this parameter indicates the energy consumed per volume of water produced. E_{cell} is the measured electric potential provided by the MDC device (V), and Q_t is the desalinated water volume (m^{-3}) and $E_{cell} \cdot I = P_{cell}$ is the electric power. **Unit: kWh m^{-3}**

Current efficiency	$\eta_c = \frac{\upsilon \; z \; F \; (c_s^i - c_s^f)}{CEC}$	**(7)**	Percentage of electric energy efficiently used for desalination (i.e., ion migration). The ratio between the charge associated with the salt removed from saline compartment and the circulated electric charge (CEC, C m^{-3}) through external circuit of the MDC system. $\boldsymbol{\upsilon}$ and z represent the stoichiometric coefficient and the salt ion valence, respectively, and F is the Faraday constant (96485 C mol^{-1} of electrons). The terms c_s^i *and* c_s^f are molar salt concentrations in the saline tank (mol m^{-3}) at the beginning and final desalination cycle, respectively. **Unit: %**
Circulated electric charge	$CEC = \frac{1}{Q_t} \int I(t)dt$	**(8)**	The circulated electric charge (CEC) represents the circulated charge across external circuit. **Unit: C m^{-3}**
Total circulated charge	$Q = \int I(t)dt$	**(9)**	Total circulated charge. **Unit: C (coulombios)**
Salt removal	$SR = \frac{c_s^i - c_s^f}{c_s^i}$	**(10)**	This parameter is related to the percentage of salt removed in a complete desalination cycle. **Unit: %**
Nominal desalination rate	$NDR = \frac{Q_t}{A_m \cdot t_d}$	**(11)**	The normalised amount of freshwater produced in a complete desalination cycle using the MDC system. Where Q_t is the desalinated water volume (L), A_m is the geometric membrane surface (m^2) and t_d is the desalination time (h) (if considered when the saline tank conductivity is below 1 mS cm^{-1}). **Unit: L $m^{-2}h^{-1}$**

Salt removal rate	$T_{NaCl} = \frac{Q_t \ MW\left(c_s^i - c_s^f\right)}{V_s \ t_d}$	(12)	The amount of transferred salt from saline compartment where *MW* is the molecular weight of NaCl (kg mol^{-1}) and V_s is the volume of the desalination chamber (m^3). **Unit: kg NaCl m^{-3} d^{-1}**
	$T_{NaCl} = \frac{Q_t \ MW\left(c_s^i - c_s^f\right)}{t_d}$	(13)	The amount of transferred salt from saline compartment. **Unit: kg NaCl h^{-1}**
COD removal rate	$COD_{rate} = \frac{\triangle \text{ COD}}{V_A t_d}$	(14)	Δ COD is the change in chemical oxygen demand (kg) in one desalination cycle and V_A is the volume of liquid in the anode compartment (m^3). **Unit: kg COD m^{-3} day^{-1}**
Coulombic efficiency	$\eta_{Cb} = \frac{Pm\ (O_2) \int \mathrm{I(t)dt}}{\mathrm{F \cdot b \cdot Q_{An}} \cdot \triangle\ COD}$	(15)	The ratio of total electric charge transferred to the anode from the consumed organic substrate or the ratio of organic substrate that is effectively converted into electricity by electrogenic microorganisms in anode surface. **Unit: (%)** where Pm (O_2) is the molecular weight of oxygen (32 g mol^{-1}), *b* is the number of moles of electrons per mole of oxygen (b= 4 moles), Q_{An} is the volume of anolyte tank (L), and Δ COD is the change in chemical oxygen demand (COD) in one desalination cycle (g O_2 L^{-1})(Logan et al., 2006).
	$\eta_{Cb} = \frac{Pm\ (Ac) \int \mathrm{I(t)dt}}{\mathrm{F \cdot b \cdot Q_{An}} \cdot \triangle\ [Ac]}$	(16)	where Pm (Ac) is the molecular weight of acetate (59 g mol^{-1}), *b* is the number of moles of electrons produced per mole of acetate oxidised (b= 8 moles of electrons per mol of acetate oxidised to CO_2) and Δ[Ac] is the change in concentration of acetate (g L^{-1}) in one desalination cycle (Lefebvre et al., 2012).

3.3.4 MDC inoculum: Bacterial strain and culture condition

A pure culture of *Geobacter sulfurreducens* (strain DL1) was used as the inoculum for the MDC start-up protocol and performance assays. This strain was grown at 30°C in septum-sealed serum bottles **(figure 37)** (50 mL working volume) containing freshwater medium (FWM, pH= 6.9; EC (25°C) = 11.4 mS cm^{-1}) supplied with the following salts: $NaHCO_3$ 2.5 gL^{-1}; NH_4Cl 0.5 g L^{-1}; $NaH_2PO_4.6H_2O$ 0.6 gL^{-1}; KCl 0.1 gL^{-1}. A trace mineral cocktail and a vitamin solution described elsewhere (Esteve-Nunez et al., 2005) were also added (rate 1:100). Sodium acetate ($C_2H_3NaO_2$, 20 mM) was supplied as the sole carbon source and electron donor, while disodium fumarate ($C_4H_2Na_2O_4$, 40 mM) was supplied as the sole electron acceptor. Culture media was degassed in the serum bottle using a mixture of N_2/CO_2 (80:20, ALIGAL-12, Air Liquide) prior to inoculation. Traces of oxygen were removed from the gas phase by passing the gas through an oxygen filter (Gas Clean Filter System, Agilent Technologies). Exponential-phase culture with an optical density, at 600nm, of 0.4 (OD_{600} nm=0.4) was used for inoculating the anode chamber as part of the start-up protocol.

Figure 37. Real photo of culture of *Geobacter sulfurreducens* in septum-sealed serum bottles.

3.3.5 MDC Start-up protocol

A previously reported start-up protocol (Borjas Hernández, 2016; Borjas et al., 2017) was followed to obtain the operative MDC for this thesis **(Figure 38)**.

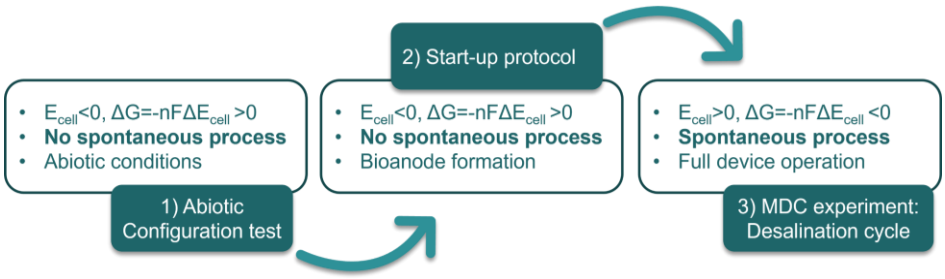

Figure 38. Schematic diagram: start-up protocol for MDC study at lab scale.

1) Abiotic desalination cycle

First, an abiotic desalination cycle was completed using the MDC to remove salts from a saline stream (5 g L^{-1} $NaHCO_3$) under the control of a conventional power supply (Fullwat Premier 3.0, 0-30 V, 0-3 A). FWM with 20 mM acetate (electron acceptor-free) and Na_2SO_4 (0.025 M) were used as an anolyte and catholyte, respectively. A power supply applied a cell potential of 3 V between anode (positive terminal) and cathode (negative terminal). This initial essay ensured that the MDC device operated correctly as an electrochemical reactor before hosting electroactive microorganisms.

2) Start-up protocol

Before any biological treatment, the whole system (MDC reactor and tubing) was sterilised by recirculating 70% w/w ethanol/water solution and then gassed with a filtered gas mixture (N_2/CO_2) for 2 hours to guarantee ethanol evaporation and an anoxic environment inside the device. Three sterilized and continuously deoxygenated tank solutions were placed in a thermostatic (30 °C) bath: the anolyte was 2 L of FWM with 1.64 g L^{-1} sodium acetate (20 mM, pH = 6.95, EC at 25^0C= 5.95 mS cm^{-1}, electron acceptor-free), and the catholyte was 2 L of 3.55 g L^{-1} Na_2SO_4 (0.025 M, pH = 7.87, EC at 25^0C= 5.24 mS cm^{-1}). The saline solution was 2 L of 5.0 g L^{-1} sodium bicarbonate (60 mM, pH = 8.70, EC at 25^0C = 5.1 mS cm^{-1}).

The cell potential was fixed at 1.0 V (i.e., the potential between the anode and the cathode). The three tanks were recirculated overnight before anode inoculation to remove any dead volumes inside the system. After this, pump recirculation was switched off to inoculate the anodic chamber with 300 mL of exponential-phase *Geobacter sulfurreducens* culture. After injection, the system was incubated overnight without recirculation to ensure cell adhesion to the anode. After incubation overnight, the pump was activated to recirculate the tank solutions again through the system. The cell potential (i.e., 1.0 V) was maintained until the anode potential, and the current density was constant i.e., at steady state (~45 h). After that time, the cell potential was increased to 1.5 V to enhance biofilm growth on the anode surface (~70 h). This part of the protocol involved sodium bicarbonate desalination in a Microbial Electrolysis Cell configuration (cell potential of 1.0-1.5 V using an external power supply). Bicarbonate was used to avoid pH changes in the anodic compartment during biofilm growth. The anode potential (which decreases as the biofilm grows) and electric current (which increases as the biofilm grows) were recorded during this inoculation period to monitor biofilm growth over time (Borjas et al., 2017).

3) Spontaneous desalination operation

When the current was stabilised (i.e., the biofilm was properly grown on the anode) the MDC was ready to operate without any additional energy supply for desalination under different experimental conditions. Then, the power supply is disconnected, and the electrode collectors are connected to an external load that allows the monitoring of the electric current. The three tank solutions are replaced to start each spontaneous desalination experiment. The system was thermostated at 30 °C and maintained under anaerobic conditions in the anolyte tank during all the experiments. The conductivity of saline tank was measured during the desalination process. The desalination cycles are considered completed when the conductivity of the saline tank was below 1 mS cm^{-1} (Council Directive

75/440/EEC of 16 June 1975 concerning the quality required of surface water intended for the abstraction of drinking water in the Member States (OJ L 194 25.07.1975 p. 26), 2006). Initial anolyte and catholyte samples were collected after 10 min of recirculation through the MDC system to homogenisation. Final anolyte and catholyte sample were collect at the end of desalination cycle (final EC saline tank = 1mS cm^{-1}). The samples were kept at -20 ^{0}C until analysis.

3.3.6 Analytical methods

pH and electric conductivity (EC) were measured using a BASIC pH metre (CRISON, at 21 °C) and a GLP31 conductivity metre (CRISON, at 25 °C), respectively. The salt concentration in the saline stream was calculated using an experimental correlation **(Figure 39)**. For total chemical organic demand (COD) determination, 50 mL of sample was collected and kept at -20 °C until analysis by APHA method 5520 (EspectroQuant PHARO 100 Merck). The samples used to measure the acetate content in the anolyte were filtered with a 0.22-micron PVDF filter before being kept at -20 °C in an opaque glass until analysis by liquid chromatography (HPLC-UV). A N°. 55 Supelcogel C-610 (30 cm x 7.8 mm) column was used with a N°.55 Supelguard H Guard column (5 cm x 4.6 mm). The mobile phase used was 4.74 mM H_2SO_4 + 2% ACN with a flow rate of 0.5 mL min^{-1} (Isocratic mode). Acetic acid was detected using a UV detector at 210 nm (Validation method from IMDEA Water Institute).

Calibration curve for NaCl concentration

The calibration curves used in this thesis are given below: electric conductivity **(Figure 39)**. These calibration curves can vary slightly with the salinity range, equipment condition (e.g., time interval of maintenance/cleaning) and environmental factors (e.g., room temperature). To ensure the validity of the calibration curves and minimise the impacts of the factors mentioned above on

the accuracy of the sample analysis, the standard calibration solutions were always made fresh on the same day of sample analysis. The R- squared of the calibration curves used for sample analysis was greater than 0.99.

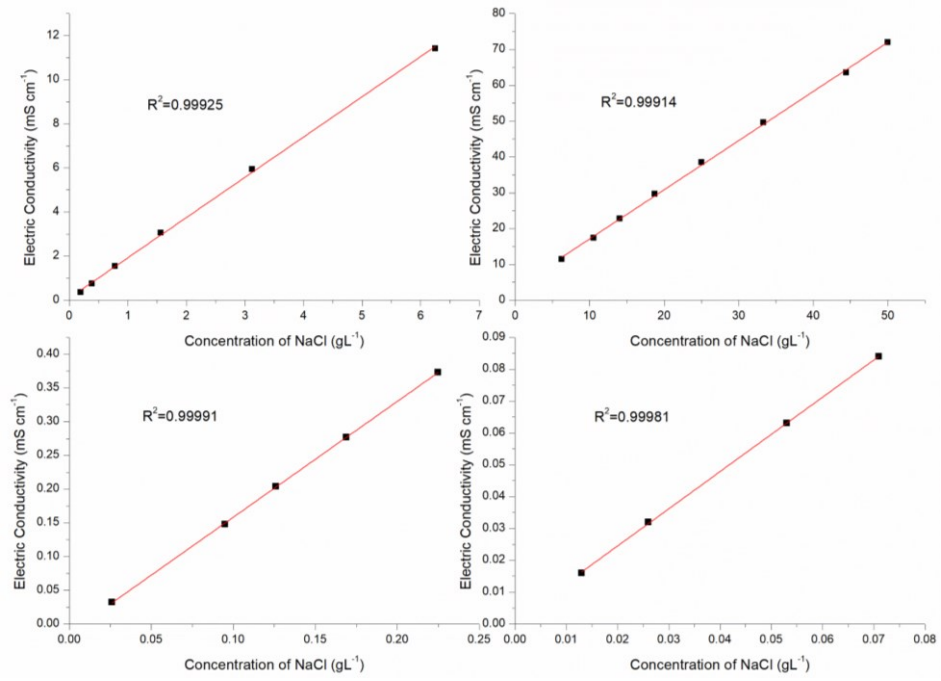

Figure 39 NaCl calibration curve made using the electric conductivity metre at 25 ± 0.5 °C for different ranges: 0.01-0.07 g L^{-1}, 0.02-0.22 g L^{-1}, 0.20-6.25 g L^{-1}, and 6.25-50 g L^{-1}.

Chapter 4

Comparative Performance of Microbial Desalination Cells Using Air Diffusion and Liquid Cathode Reactions: Study of the Salt Removal and Desalination Efficiency

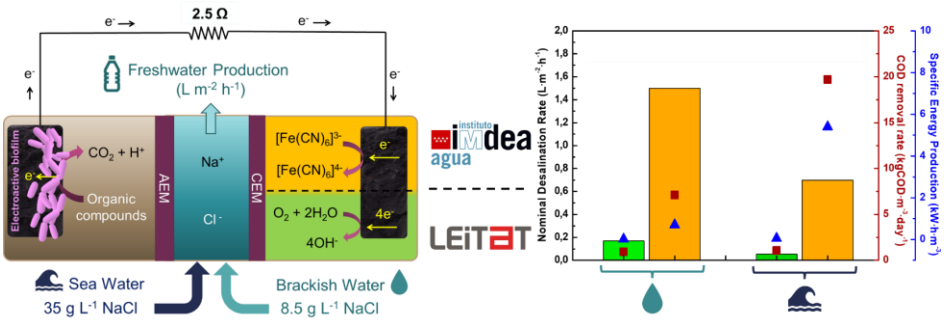

This chapter has been published and redrafted for this thesis:

Ramírez-Moreno, M., Rodenas, P., Aliaguilla, M., Bosch-Jimenez, P., Borràs, E., Zamora, P., et al. (2019). Comparative Performance of Microbial Desalination Cells Using Air Diffusion and Liquid Cathode Reactions: Study of the Salt Removal and Desalination Efficiency. *Front. Energy Res.* 7, 135. doi:10.3389/fenrg.2019.00135.

Chapter 4. Comparative Performance of Microbial Desalination Cells Using Air Diffusion and Liquid Cathode Reactions: Study of the Salt Removal and Desalination Efficiency

Abstract

The use of oxygen reduction (i.e., $O_2 + 2H_2O + 4e^- \rightarrow 4\ OH^-$, $E^{0'} = 0.815$ V, pH = 7) was usually implemented as cathodic reaction in most of the MDCs reported in literature, whereas other strategies based on liquid catholytes have been also proposed, for example, ferro-ferricyanide redox couple (i.e., $Fe(CN)_6^{3-} + 1e^- \rightarrow Fe(CN)_6^{4-}$, $E^{0'} = 0.37$ V). As the MDC designs in the literature and operation modes (i.e., batch, continuous, semi-continuous, etc.) are quite different, the available MDC studies are not directly comparable. For this reason, the main objective of this work was to have a proper comparison of two similar MDCs operating with two different catholyte strategies and compare performance and desalination efficiencies. In this sense, this study compares the desalination performance of two laboratory-scale MDCs located in two different locations for brackish water and sea water using two different strategies. The first strategy consisted of an air cathode for efficient oxygen reduction, while the second strategy was based on a liquid catholyte with Fe^{3+}/Fe^{2+} solution (i.e., ferro-ferricyanide complex). Both strategies achieved desalination efficiency above 90% for brackish water. Nominal desalination rates (NDR) were in the range of 0.17–0.14 L m^{-2} h^{-1} for brackish and seawater with air diffusion cathode MDC, respectively, and 1.5–0.7 L m^{-2} h^{-1} when using ferro-ferricyanide redox MDC. Organic matter present in wastewater was effectively removed at 0.9 and 1.1 kg COD m^{-3} day^{-1} using the air diffusion cathode MDC for brackish and sea water, respectively, and 7.1 and 19.7 kg COD m^{-3} day^{-1} with a ferro-ferricyanide redox MDC. Both approaches used a laboratory MDC prototype without any energy supply (excluding pumping energy). Pros and cons of both strategies are discussed for subsequent upscaling of MDC technology.

4.1 Introduction

Cathode reaction is considered one of the main bottlenecks in microbial electrochemical technologies (METs) (Freguia et al., 2008). Most of the MDC studies have been carried out by implementing oxygen reduction in the cathodic compartment by taking advantage of the gained experience in the field of microbial electrochemical systems using oxygen as electron acceptor (i.e., O_2 + $2H_2O + 4e^- \rightarrow 4OH^-$, $E^{0'}$= 0.815V, pH = 7). Current challenges are to develop air-cathodes with high oxygen reduction reaction (ORR) performance, long term stability and low cost (Freguia et al., 2007b; Lu and Li, 2012). Zhao et al. studied three main factors that affect air cathodes performance: the solution pH, the catholyte concentration and the catalyst load (Zhao et al., 2006). Precious metals (Pt, Pd, Au, or Ag) are used as catalysts in electrochemical devices to reduce oxygen in different pH conditions (Ge et al., 2015). Liu et al. showed operative oxygen reduction potential on MFCs between 0.17 to 0.26V using MnOx as alternative catalyst instead of precious metals (i.e., Pt, Pd) (Zhao et al., 2006; Liu et al., 2010). Also other metal oxides or metal-organic catalysts from the transition metal group (FeOOH, CoOOH, MnOx, WO_3, Co-PPY) have been developed to reduce the capital costs (Bashyam and Zelenay, 2006; Lu and Li, 2012; Wang et al., 2015a; Zhang et al., 2016a). Among these transition metals, nickel has been shown good performance when surface properties are modified to facilitate ORR (Vij et al., 2017). Additionally, iron is also another promising transition metal for ORR on microbial electrochemical devices (Lefèvre et al., 2009). For example, Harnish et al. demonstrated the versatility of iron phthalocyanine as catalyst for oxygen reduction on MFCs at neutral pH (Harnisch et al., 2009). Activated carbons, carbon fibers, carbon black and graphene are also use on ORR due to their tuneable surface properties and high surface (Yuan et al., 2016b). More recently, air diffusion cathodes using nanofibers doped with transition metal (Bosch-Jimenez et al., 2017) has been proposed for microbial fuel cells.

Despite the extensive use of oxygen as electron acceptor in METs, the proof of concept of MDC was developed using a ferricyanide catholyte (i.e., $Fe(CN)_6^{-3} + 1e^- \rightarrow Fe(CN)_6^{-4}$, $E^{0'} = 0.36V$) (Cao et al., 2009). Salt removal up to 94%, and energy production of 2 Wm^{-2} were achieved, thus significantly increasing the performance of the system compared to that when using ORR as cathodic reaction. Nevertheless, due to high cost of reagents, the use of ferro-ferricyanide catholyte (or other redox mediators/compounds) would be only feasible from a technical point of view in MDCs if: **(i)** the redox mediator is low cost or **(ii)** an easy and cheap strategy is developed for regeneration of catholyte solution once depleted.

This chapter presents the results obtained in parallel in two laboratories (LEITAT and IMDEA Water) for the development of MDC technology for low-energy drinking water production. Similar MDC configurations and experimental methodology have been implemented in both locations to compare two different approaches:

a) MDC operating using oxygen reduction as cathodic reaction.

b) MDC operating using the ferro-ferricyanide redox couple as cathodic reaction.

For the first approach, an air diffusion cathode made of carbon nanofibers and iron nanoparticle as catalyst (produced by electrospinning and pyrolysis) was developed as suitable low-cost electrode for environmental applications (i.e., no use of Pt as catalyst). In the second approach, a ferro-ferricyanide redox catholyte was studied as an alternative to oxygen reduction, to enhance the available potential in the MDC and allow for an improved performance. Finally, salt removal (SR), nominal desalination rate (NDR), current efficiency (η_c), specific energy production (SEP), COD removal rate (COD_{rate}), coulombic efficiency (η_{Cb}), total circulated charge (Q), and water transport are discussed to compare the pros and cons of the afore mentioned MDC approaches.

4.2 Materials and Methods

4.2.1 Microbial Desalination Cell Set Up

The main features for both MDCs used in this study are shown in **Table 3**.

Table 3. Main characteristics for MDC experimental setups.

Strategy	Air-diffusion cathode MDC	Ferro-ferricyanide redox MDC
Location	LEITAT Lab	IMDEA Water Lab
Cross section (cm^2)	100	
Dimensions active area (cm)	10 x10	
Number of unit cells	1	
Anode		
Electric collector	Stainless steel	Isostatic graphite plate (Grade 2114 - 45)
Electrode	SGL Unidirectional Carbon Fiber	RVG 2000 MERSEN Carbon Felt
Electrode thickness (mm)	5.0	4.6
Compartment thickness (mm)	8.7	9
Cathode		
Electric collector	Stainless steel 316 frame + carbon fibers mesh	Isostatic graphite plate (Grade 2114 - 45)
Electrode	Carbon nanofibers doped with iron nanoparticles	RVG 2000 MERSEN Carbon Felt
Electrode thickness (mm)	0.6	4.6
Compartment thickness (mm)	8.7	9
Saline compartment		
Compartment thickness (mm)	8.7	9
Ion exchange membranes		
Anionic membrane	Neosepta AMX	
Electric resistance (Ω cm^2) *	2.4	
Permselectivity **(%)	>93	
Thickness (µm)*	0.14	

Cationic membrane	Neosepta CMX	
Electric resistance (Ω cm^2) *	3.0	
Permselectivity **(%)	>90	
Thickness (µm)*	0.17	
Operational conditions		
Operation mode	Batch (3 streams)	
Flow rate (mL min^{-1})	95	
Temperature (ºC)	25 - 30	
External load (Ω)	2.5	
Streams		
Anolyte	FWM + Sodium Acetate	
Catholyte	PBS	$K_3[Fe(CN)_6]$
Saline stream	NaCl	
Tanks		
Anolyte Volume (mL)	2500	2100
Catholyte Volume (mL)	2500	2100
Saline Volume (mL)	500	370
Rate $V_{anolyte}$:V_{saline}:$V_{catholyte}$	5:1:5	5:1:5
Start-up operation		
Initial inoculum	Electroactive biofilm from an operating MFC	Pure culture *Geobacter sulfurreducens*
Period (hours)	158	140

NOTE: *Equilibrated with 0.5M-NaCl solution, at 25ºC (Data provided by manufacturer). ** Measured at the laboratory. Membrane equilibrated with 0.1 M NaCl and 0.5 M NaCl solutions.

The laboratory MDCs consisted of a three-compartment compact stack design with neoprene gaskets for a hermetical seal **(Figure 40)**. Graphite felt RVG 2000 (MERSEN) and Unidirectional Carbon Fiber (UDCF) felt (SGL) were used as anode electrodes, and isostatic graphite (Grade 2114-45, MERSEN) and stainless steel AISI 316 as anode electric collector. In the first approach, a novel air diffusion cathode using carbon nanofibers with iron nanoparticles as catalyst was implemented (see section Start-up protocol in this chapter), and metal frame (stainless steel frame with UDCFs mesh (SGL) as electric collector-was used in the cathodic compartment. For the second approach (i.e., ferro-ferricyanide redox MDC), the materials were the same of the anode compartment. Finally, two

stainless steel end plates were used to close the cell on both ends with a Torque of 10 N m and 6 N m for the liquid and air cathode MDCs, respectively. The diagram of the MDC experimental setup at IMDEA Water's and LEITAT's facilities is shown in **Figure 36 (in chapter 3).** The pictures of both set up are shown in **Figure 40.** In both cases, the systems were operated in batch mode with recirculation at flow rate of 95 mL min^{-1} (for all streams), and in temperature-controlled room at 30 ºC.

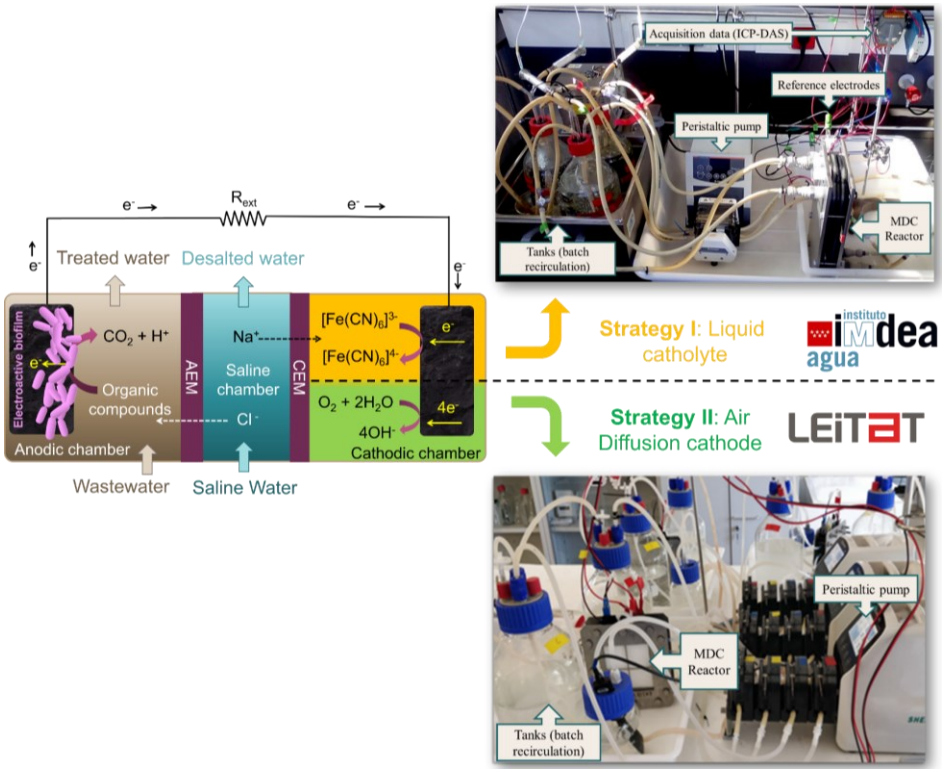

Figure 40. Left: Diagram of an MDC unit with both catholyte strategies. AEM, anion exchange membrane; CEM, cation exchange membrane. **Right:** MDC set-up at IMDEA water facilities (picture above) and LEITAT facilities (picture at the bottom).

The anolyte solution used at LEITAT consisted of a solution containing 0.45 g L^{-1} NaCl, 0.165 g L^{-1} $MgCl_2 \cdot 6H_2O$, 0.0136 g L^{-1} $CaCl_2$, 0.0153 g L^{-1} Mg_2SO_4, 8.4 g L^{-1} $NaHCO_3$, 0.128 g L^{-1} KH_2PO_4, 0.925 mL L^{-1} of NH_4Cl 1M solution, 1 mL L^{-1} of trace element solution and 0.5 mL L^{-1} of Wolfe's vitamins solution with

20 mM sodium acetate as organic substrate. The catholyte solution consisted of 100 mM Phosphate Buffered Solution (PBS). Saline media was prepared by dissolving 10 g L^{-1} NaCl for brackish water solution and 35 g L^{-1} NaCl for seawater solution. Similarly, the anolyte solution used at IMDEA Water consisted of freshwater media (FWM) containing 0.1 g L^{-1} KCl, 2.5 g L^{-1} $NaHCO_3$, 0.6 g L^{-1} KH_2PO_4, 0.5 g L^{-1} NH_4Cl, 10 mL L^{-1} of trace element solution and 10 mL L^{-1} of Wolfe's vitamins solution with 20 mM sodium acetate as organic substrate for brackish water desalination and 40 mM for seawater desalination. The catholyte solution consisted of 0.04 M $K_3[Fe(CN)_6]$ solution for brackish water and 0.2 M for seawater desalination. Saline media was prepared by dissolving 7 g L^{-1} NaCl for brackish water solution and 35 g L^{-1} NaCl for seawater solution. The equations used to determine the main parameters of the MDCs performance are collect in **table 2** (***Chapter 3, section 3.3.3***).

4.2.2 Air diffusion cathode

Air cathode was composed of three parts as depicted in **Figure 41**: **(i)** an external membrane (high density polyethylene fibers textile), impermeable to water and permeable to oxygen; **(ii)** a conductive material, in this case carbon nanofibers with iron nanoparticles to allow ORR; and **(iii)** an internal semipermeable membrane (treated high density polyethylene fibers textile) to allow proton exchange.

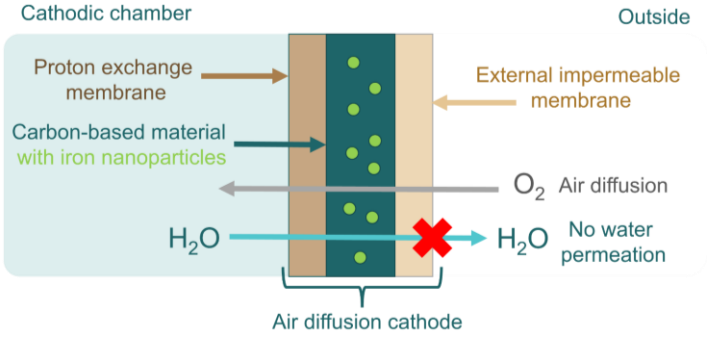

Figure 41. Air diffusion cathode configuration.

4.2.3 Start-up protocol

A previously reported start-up procedure was followed for both MDCs under study (Borjas et al., 2017). This start-up protocol is deeply described in ***section 3.3.5*** in ***Chapter 3***. The anolyte, saline and catholyte streams were firstly sterilised and recirculated through the lab-MDCs. Then, 200 mL of inoculum containing electrogenic bacteria was introduced in the anodic chamber of the MDCs by recirculation with a peristaltic pump.

For the air cathode MDC approach, as initial inoculum for start-up, an anodic-electroactive mixed culture from a long term (>3 years) operating Microbial Fuel Cell (MFC) was employed. Initial microbial population content, characterized by MiSeq Ilumina platform, accounted for a mixture of *Bacteroidetes* (6.7%), *Fermicutes* (3.1%), *Proteobacteria* (65.9%), *Spirochaetes* (4.8%), *Thermotogae* (2.8%) and *Verrucomicrobia* (9.0%). A selective pressure through a redox potential gradient was applied to the anode in order to promote the growth and attachment of electroactive bacteria onto the electrode. Anode was properly inoculated when current density achieved values higher than 0.15 mA cm^{-2}. After that, it was transferred to the MDC. In the case of the ferro-ferricyanide redox MDC, a pure culture of *Geobacter sulfurreducens* (strain DL1) was used as inoculum. Exponential-phase culture (OD_{600nm} = 0.4) was used for the inoculation into the anode compartment in the start-up protocol.

After inoculation of the anodes, the peristaltic pump was switched off overnight, allowing the microorganism to start growing on the anode surface (i.e., graphite felt). After incubation, the pumps were switched on to recirculate the anolyte, catholyte and saline solutions through the system.

Once the bioanode was considered stable (i.e., no significant variation of electric current), the first desalination cycle was performed with newly prepared solutions to ensure reproducibility among subsequent desalination cycles. The desalination cycles were finished when the conductivity of saline tank was below

of 1 mS cm^{-1}, as this threshold could be considered as optimum value for water quality (Council Directive 75/440/EEC of 16 June 1975 concerning the quality required of surface water intended for the abstraction of drinking water in the Member States (OJ L 194 25.07.1975 p. 26), 2006).

4.3 Results of cathode strategies comparative: ferricyanide vs oxygen

Both MDC strategies (i.e., ORR as cathodic reaction, ferro-ferricyanide redox system as cathodic reaction) were compared using laboratory-scale MDCs with 100 cm^2 of cross section (or geometric electrode surface, A_e). Experimental results are showed in **Figure 42**. Experiments were carried out at two different initial saline concentrations: brackish water range (NaCl 7.5–10 g L^{-1}) with an initial electric conductivity of 13.9 and 17.5 mS cm^{-1} for ferro-ferricyanide redox and air cathode approach, respectively, and seawater range (NaCl 35 g L^{-1}), with an initial electric conductivity of 51.5 and 53.3 mS cm^{-1} for ferro ferricyanide redox and air cathode approach. Nominal desalination rate, salt removal, current efficiency and COD removal rate were compared between both strategies to compare the feasibility of MDC technology, understand its limitations, describe its advantages and disadvantages, and elucidate which strategy is more convenient for scaling up of the technology in real environments.

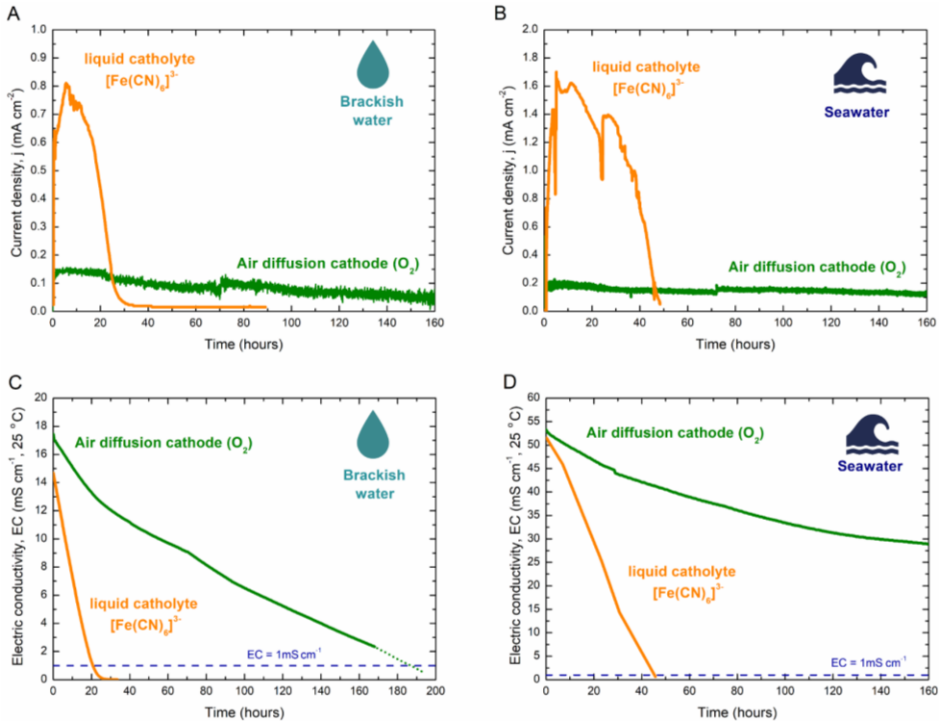

Figure 42. Experimental results for air diffusion cathode MDC (green) and ferro-ferricyanide redox MDC (orange). **(A, B)** Current density vs. time for brackish and seawater desalination. **(C, D)** Conductivity vs. time for brackish and sea water desalination. Horizontal dash line shows the threshold for conductivity 1 mS cm^{-1}. The dotted line for the air diffusion cathode MDC results from an interpolation of the electric conductivity below 1 mS cm^{-1} for comparative purposes.

4.3.1 Brackish Water Desalination

The electric current for brackish water desalination experiments using the aforementioned strategies is shown in **Figure 42A**. Maximum current densities for air diffusion and ferro-ferricyanide cathode were 0.14 and 0.81 mA cm^{-2}, respectively. As both devices used the same external load (2.5 Ohmios) and analogous anodes and configurations, the higher electric current obtained when using the ferro-ferricyanide redox MDC may be directly related to the cathode reaction, which provide higher available potential to drive the desalination process.

In general, it could be stated that from the thermodynamic point of view, the available potential in the MDC to perform the desalination process is higher when oxygen reduction is used in the cathode [$E^{0\prime}_{MDC} = E^{0\prime}_{cathode} - E^{0\prime}_{anode} = 0.81V - (-0.3V) = 1.11V$]. However, oxygen reduction reaction provides less potential than expected in the range of current densities (i.e., 0.2-1.5 mA cm^{-2}) used for desalination in MDC systems, and it is mainly related to slow kinetics associated to this reaction at pH = 7 (or neutral), that is common in microbial electrochemical systems. On the other hand, regardless the lower thermodynamic potential when ferri-ferrocyanide reduction is used in the cathode compartment [$E^{0\prime}_{MDC} = 0.36 - (- 0.3V) = 0.66V$], fast kinetic provides more available potential when implemented in MDC systems. Thus, the lower potential available is the reason behind the poor desalination performance when oxygen reduction is used as cathodic reaction. The electric conductivity (EC) for brackish water desalination using the aforementioned strategies is shown in **Figure 42C**. As the electric current is also directly related to migration of ion species, the desalination time (i.e., time required to achieve the threshold conductivity of 1 mS cm^{-1}) for the ferro-ferricyanide redox MDC is lower compared to the air cathode MDC.

As shown in **Figure 42A**, the current density in ferro-ferricyanide redox cathode experiment decreased from 0.81 mA cm^{-2} in 16 h to 0.08 mA cm^{-2}. This decrease is attributable to the drop in conductivity of the salinity compartment from 14 to 0.56 mS cm^{-1}. In the case of the air cathode experiment, the current density dropped from 0.14 to 0.08 mA cm^{-2} in 160 h, decreasing the conductivity in the saline compartment from 16 to 2.4 mS cm^{-1}.The decrease of current density in both MDC cases could be linked to the increase of the internal resistance of the MDC, as electric conductivity decreases during the experiments. These observations are in accordance with previous MDC behavior operating in batch mode (Borjas et al., 2017). It is worthwhile to mention that the air diffusion cathode developed in this study (Fe-doped C-NF) displayed higher current densities compared with analogous studies in the literature (in the range of 0.084

mA cm^{-2}, using Pt coated air diffusion cathode when desalinating 10 g L^{-1} brackish water) (Jafary et al., 2018). **Table 4** shows the main experimental performance parameters for brackish water desalination using both cathodic reactions.

Table 4. Initial and final salinity, salt removal, desalination time, current efficiency, nominal desalination rate (NDR), COD removal rate, anode coulombic efficiency, specific energy production, total circulated charge, and volume variation for air diffusion cathode and ferro – ferricyanide redox MDC experiments for **brackish water desalination.**

Parameters	Air-diffusion cathode MDC	Ferro-ferricyanide redox MDC
Initial salinity (g L^{-1})	10.7	7.4
Final salinity (g L^{-1})	0.5	0.5
Salt removal (%)	93.6	93.3
Desalination time (h)	205	23
NDR (L m^{-2} h^{-1}) *	0.17 **	1.5
Current efficiency (%)	162	81.1
COD removal rate (kg COD m^{-3} day^{-1}) ***	0.94	7.1
Coulombic efficiency (%)	6.5	84.00
Specific Energy production (kWh m^{-3})	0.02	0.7
Total circulated charge (C)	5086	5165
Volume variation (%)	-36	-8.1

NOTE: * Calculated considering the final volume of saline tank. ** Extrapolated from experimental results. *** Considering the volume of anolyte compartment.

For both desalination cycles the salt removal exceeded 90%, indicating proper performance of both MDCs as desalination devices. Regarding nominal desalination rate (NDR), the ferro-ferricyanide redox MDC was able to produce almost six times higher amount of desalinated water (1.54 L m^{-2} h^{-1}) compared to that of the air diffusion cathode MDC (0.17 L m^{-2} h^{-1}). Current efficiencies were 162% and 81.1% for air diffusion cathode and ferro-ferricyanide redox MDC, respectively. As current efficiency determines the rate of current that is used for ion migration, values above 100% means that an additional transport phenomenon occurred during the experiment, i.e., diffusion from saline to adjacent compartments.

From the point of view of wastewater treatment, COD removal rates for both air diffusion cathode and ferro-ferricyanide redox MDCs were 0.94 and 7.14 kg COD m^{-3} day^{-1}. This parameter is related to the current density and desalination performance, as consumption of COD provides the electric current to drive the desalination process. The coulombic efficiency decayed at longer desalination times (t_d), as it is the case of the air diffusion cathode MDC experiment. This fact may be due to a competition between electrogenic and anaerobic microorganism since the latter do not contribute to electric current generation. Specific energy production (SEP) was 0.02 and 0.7 kWh m^{-3} for air diffusion cathode and ferro-ferricyanide redox MDC, respectively. This fact indicates that in both cases it is possible to generate a significant amount of electric energy simultaneously with desalinated water production and wastewater treatment, as reported in the literature (Sophia et al., 2016; Sevda and Abu-Reesh, 2018).

Finally, the water transport was measured by determining the change in the final volume of the saline tank. Water transport across membranes was remarkable for air diffusion cathode MDC experiment, accounting for 36% decrease (v/v). In the case of the ferro-ferricyanide redox MDC, the volume decrease remained below 10% (v/v). Water transport may be attributable to osmosis and/or electroosmosis phenomena (i.e., water transport due to electric charge). As the desalination conditions were similar for both cases (i.e., electric charge to perform desalination, see **Table 4**), the water transport could be attributed to osmosis. In this sense, for a similar water flux due to osmosis, a higher desalination time allows for a higher osmosis water transport, as indicated in **Table 4** for the air diffusion cathode experiment.

4.3.2 SeaWater Desalination

The electric current for seawater desalination experiments is shown in **Figure 42B**. In this case, air diffusion cathode MDC and ferro-ferricyanide redox MDC experiments achieved maximum current densities of 0.20 and 1.70 mA cm^{-2},

respectively. Similarly, to the previously discussed results, the current density for ferro-ferricyanide redox MDC decreased from 1.7 to 0.1 mA cm^{-2} in 48 h due to the drop in the conductivity of the salinity compartment (from 50 to 0.6 mS cm^{-1}) as depicted in **Figure 42B**. For the air cathode MDC experiment, the current density dropped from 0.2 to 0.12 mA cm^{-2} in 160 h, while decreasing the salinity from 51 to 28 mS cm^{-1}. The electric conductivity for seawater desalination is shown in **Figure 42D**. In this case, the air diffusion cathode MDC was not able to accomplish complete desalination (i.e., electric conductivity below threshold value of 1mS cm^{-1}). **Table 5** shows the main experimental performance parameters for the seawater desalination experiment.

Table 5. Initial and final salinity, salt removal, desalination time, current efficiency, nominal desalination rate (NDR), COD removal rate, anode coulombic efficiency, specific energy production, total circulated charge, and volume variation for air diffusion cathode and ferro – ferricyanide redox MDC experiments **for seawater desalination.**

Parameters	Air-diffusion cathode MDC **	Ferro-ferricyanide redox MDC
Initial salinity (g L^{-1})	33.5	35.0
Final salinity (g L^{-1})	17.4	0.5
Salt removal (%)	48.2	98.6
Desalination time (h)	-	43
NDR (L m^{-2} h^{-1}) *	0.14	0.7
Current efficiency (%)	145	108
COD removal rate (kg COD m^{-3} day^{-1})	1.07	19.7
Coulombic efficiency (%)	10.3	61.0
Specific Energy production (kWh m^{-3})	0.06	5.4
Total circulated charge (C)	8994	19354
Volume variation (%)	-2	-19

NOTE: * Calculated considering the final volume of saline tank. ** Calculated for partial desalination.

It is important to note that for the air diffusion cathode MDC, the salt removal was around 48%, indicating that only partial desalination was achieved. The partial desalination has been also reported in the literature with similar MDC configuration using oxygen reduction as cathode reaction (decrease of 58 to 22

mS cm^{-1}, salt removal 50%) (Zhang and He, 2015; Moruno et al., 2018b). This effect could be attributed to the low available potential to drive the migration of the ions. When the electric conductivity increased in the anodic/cathode chamber due to the migration of the ions from the saline compartment during the desalination cycle, back-diffusion transport of salt started to be significant, and eventually this ionic transport was equal to the ionic transport due to migration. This resulted in a zero net balance of salinity in the saline compartment (Ping et al., 2016). This effect could be observed in **Figure 42D** from the asymptotic trend of the electric conductivity for the air diffusion cathode MDC (28 mS cm^{-1}). In the case of ferro-ferricyanide redox MDC, complete desalination was achieved, being the desalination time 43 h (td).

NDR values were 0.14 L m^{-2} h^{-1} for partial desalination (air diffusion cathode MDC), and 0.7 L m^{-2} h^{-1} for the ferro-ferricyanide redox MDC. This latter value is slightly higher compared to analogs MDC systems operating with ferro-ferricyanide catholyte (Cao et al., 2009; Luo et al., 2012b; Kalleary et al., 2014; Chen et al., 2015) likely due to recirculation, thickness of the saline compartment and low external load value. Current efficiencies were above 100%, indicating higher ion migration which could be attributed to the electric current achieved. Thus, diffusion from saline compartment to adjacent compartments was more significant for seawater desalination compared to brackish water desalination (see **Tables 4, 5**). Regarding volume variation, it could be attributed to osmotic processes due to the longer duration in the air cathode MDC configuration as well as different initial conductivity in catholyte solutions in both configurations. The main experimental results for both MDC strategies for brackish and seawater desalination is summarizes in **Figure 43**.

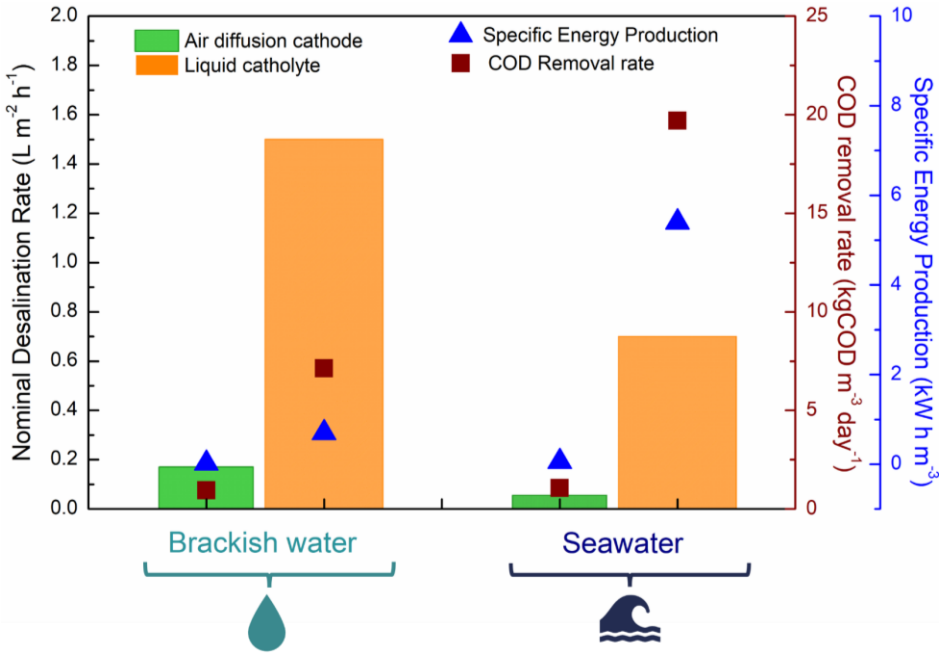

Figure 43. Nominal desalination rate (NDR) (bar plot), COD removal rate (red squares), and specific energy production (SEP) (blue triangles) for both MDC strategies.

As stated, NDR was higher for brackish and seawater when the ferro-ferricyanide redox MDC was used, and only complete desalination could be achieved using air diffusion cathode MDC for brackish water desalination (i.e., partial desalination for seawater). From the point of view of COD removal rate, desalination of seawater increased the wastewater treatment capacity of the MDC, and this effect was related to the increase in the generation of electric current. Similarly, specific energy production (SEP) was higher for seawater desalination compared to brackish water's.

From the point of view of real application, brackish water desalination can be accomplished by both strategies. As oxygen is a simple and available reagent, air diffusion cathode MDC is more suitable for brackish water desalination, but water production (i.e., NDR) should be maximized by complete optimization of the system. In the case of seawater desalination, only ferro-ferricyanide redox MDC could achieve complete desalination, so air diffusion MDC strategy could be

adopted as a suitable approach for pre-desalination step applications, for example, coupled to a RO conventional plant (ElMekawy et al., 2014). Obviously, even if ferro-ferricyanide redox catholyte allows the increase of the desalination efficiency, wastewater treatment, fresh water, and energy production in the MDC device, it should be regenerated when depleted due to the high costs of reagents, as previously discussed in the literature (Cao et al., 2009). For this reason, low-cost and effective strategies for regeneration of the redox mediator catholyte need to be explored in next studies, for instance, using renewable energy (i.e., photovoltaic, wind energy) or other microbial electrochemical processes (i.e., biocathodes).

Finally, the experimental results of this study have been obtained in two different laboratories, with systematic experimental approach and in close collaboration. The consistent and reproducible experimental results shall help the further development of MDC technology and to speed up their scaling-up for operation in real environments.

4.4 Conclusions

Microbial Desalination Cell constitutes an innovative technology where microbial fuel cells and electrodialysis merge in the same device for obtaining fresh water with no energy-associated costs, while treating wastewater and producing energy. One of the main limitations for MDC technology is the low available potential for desalination when oxygen reduction is used as cathodic reaction, as partial desalination is obtained when sea water is used as feed stream. The ferro-ferricyanide redox MDC strategy has been proposed in the literature in order to enhance the performance of MDC technology and provide total desalination of seawater. Two analogous MDC experimental setups with different cathode strategy (air diffusion and ferro-ferricyanide redox) allow to compare the desalination performance of both systems, and to understand the main limitations

for the technology development. Air cathode approach may be suitable for brackish water desalination, even though nominal desalination rates are near one order of magnitude lower than those obtained using a ferro-ferricyanide redox mediator. Seawater desalination could be better addressed by a ferro-ferricyanide redox MDC; however, catholyte regeneration routes should be explored to reduce costs and allow for low-cost and efficient desalination. A compromise between MDC performance and costs should be made for further upscaling and application in real environments. Finally, the proposed methodology could be an interesting approach for interlaboratory collaboration for further MDC studies.

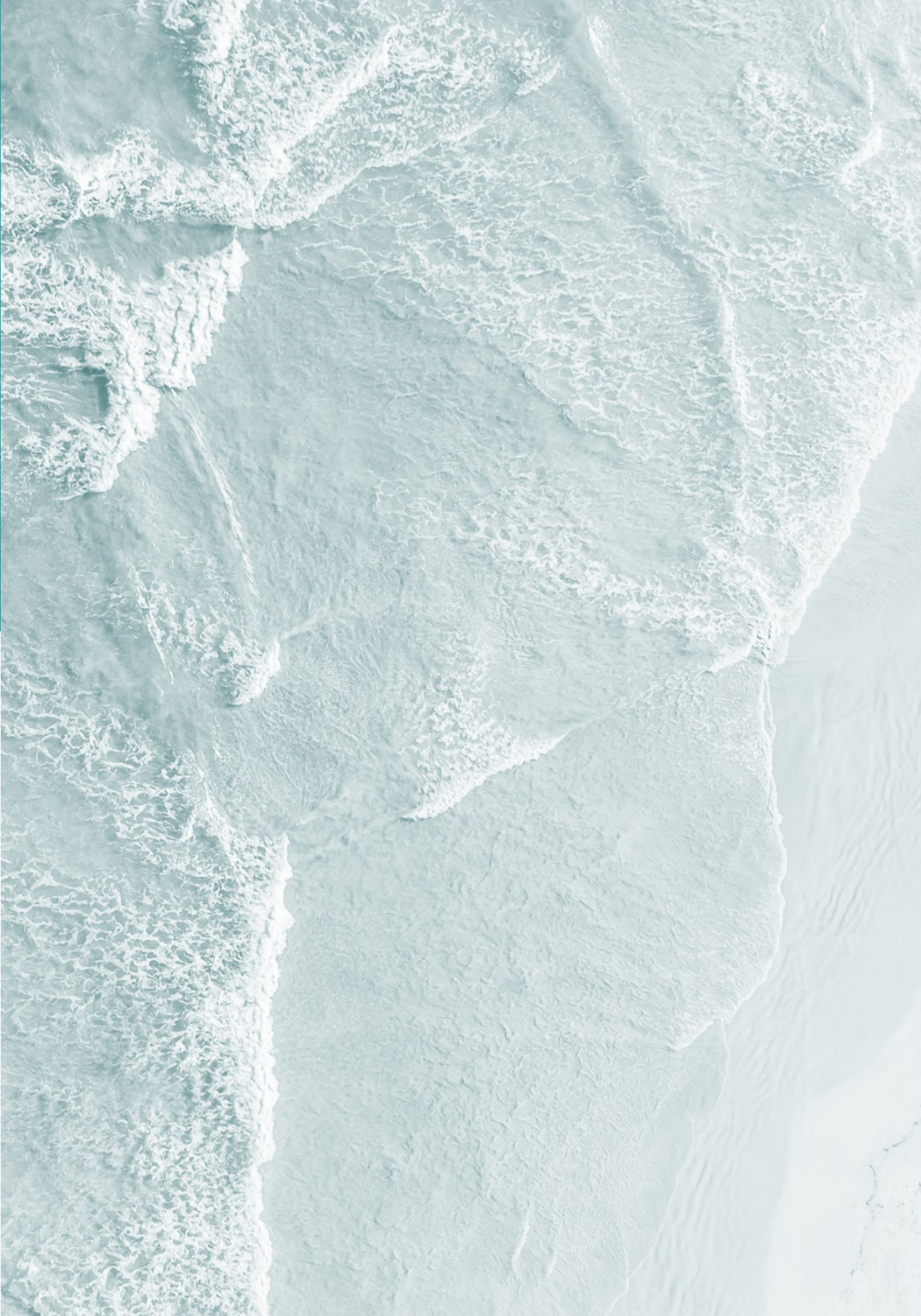

Chapter 5

Desalination of brackish water using a microbial desalination cell: Analysis of the electrochemical behaviour

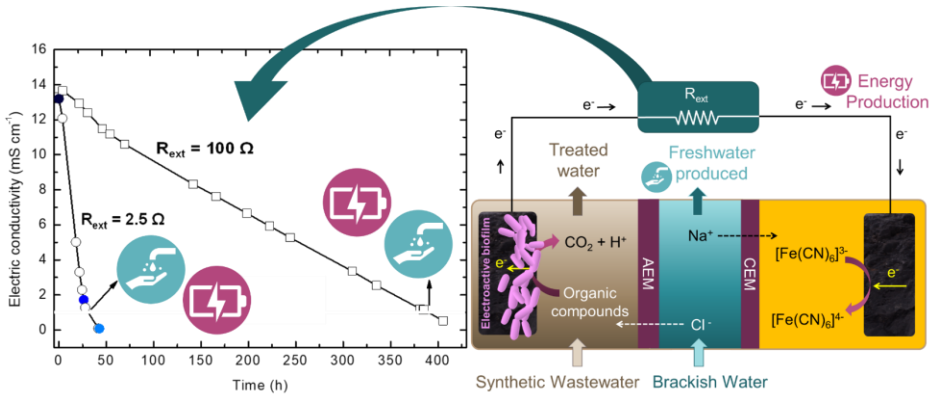

This chapter has been published and redrafted for this thesis:

Ramírez-Moreno, M., Esteve-Núñez, A., and Ortiz, J. M. (2021). Desalination of brackish water using a microbial desalination cell: Analysis of the electrochemical behaviour. *Electrochim. Acta* 388, 138570. doi:10.1016/j.electacta.2021.138570.

Chapter 5. Desalination of Brackish water using a Microbial Desalination Cell: Analysis of the electrochemical behaviour

Abstract

Most previously reported studies of MDC used oxygen reduction as the primary cathodic reaction. In contrast, we have explored brackish water desalination (7 g L^{-1}) and energy production using a laboratory MDC system (cross-section 100 cm^2, batch mode) and ferricyanide as the catholyte. Furthermore, a rational explanation of desalination performance when using a catholyte is presented, and, additionally, the impact of producing electrical energy on desalination performance is discussed. Interestingly, conductivity variation in the saline chamber can be used to predict electrochemical performance. In summary, this study provides the basis for the development, design, and optimisation of low-energy desalination using MDC technology.

5.1 Introduction

5.1.1 MDC catholyte, the control point

As with any other microbial electrochemical system (Cheng et al., 2006), MDC also shows a fundamental limitation in the cathodic reaction. The catholyte of choice should fulfil two technical requirements: **i)** a reasonable cost and **ii)** an easy and cost-effective strategy for regeneration of depleted catholyte solution. Some authors have suggested the use of biocathodes as a sustainable and environmentally friendly option, but these can certainly lead to biofouling during long-term operation (Wen et al., 2012; Kokabian and Gude, 2013; Bejjanki et al., 2021). Considering the 3-chamber configuration as a model design, a vast number of assays using synthetic media, including air diffusion cathodes or potassium ferricyanide as a liquid catholyte have been reported in the last decade (**Table 6**).

Interestingly, the first study carried out by Cao *et al.* used a ferricyanide catholyte (i.e., $Fe(CN)_6^{3-} + 1e^- \rightarrow Fe(CN)_6^{4-}$, $E^0 = 0.36$ V) to demonstrate the feasibility of the MDC process, providing just enough electric potential in the system to reach complete desalination (i.e., salt removal 88-94%, energy production 2 W m^{-2}). Less frequent is the use of hypochlorite as an electrochemical acceptor, but the results were promising (0.308 L m^{-2} h^{-1}) for desalinating brackish water (Borjas et al., 2017). However, in subsequent studies (Yang et al., 2019a), the use of oxygen reduction was adopted as a cathodic reaction, despite the decreased production of both freshwater and energy (i.e., 0.07 L m^{-2} h^{-1}, salt removal rate 3.7 to 9.2 kg m^{-3} d^{-1}, using external voltage for seawater desalination)(Zhang and He, 2015). Probably one of the biggest challenges regarding the cathode is the development of materials for enhancing oxygen reduction. In this sense, metallic nanoparticles using iron and nanofibers have been recently proposed as catalysts in air diffusion cathodes for brackish water desalination using MDC. However, a similar test using ferricyanide catholyte showed a nominal desalination rate one order of magnitude higher (0.7 L m^{-2} h^{-1}, for seawater desalination)(Ramírez-Moreno et al., 2019).

Table 6. Summary of conventional three-chambered MDC studies using synthetic solutions and ferricyanide or air diffusion cathodes.

Operation Mode (R_{ext})	V_{an}: V_{desl}: V_{cat}*	MDC Chamber					Main Parameters			Ref
		Anodic	**Cathodic**	**Desalination Chamber**			**Desalination**	**Treatment**	**Energy**	
		Electrode/ Inoculum/ Electron Donor	Electrode/ Catholyte	Vdesl. (mL)	Initial Salinity (g L^{-1} NaCl)	End desal. cycle	Salt Removal*	COD Removal	Power Density / Current density	
Batch **(200 Ω)**	100:1:33	Carbon felt (9 cm^2)/ MFC anode/ Acetate (1.6 g L^{-1}; 5 mL min^{-1})	C. felt/ Ferricyanide + PBS (5 mL min^{-1})	3	5	E_{cell} < 50 mV	88%	-	31 Wm^{-3} (Total reactor Vol.); 2 Wm^{-2}	(Cao et al., 2009)
					20		94%			
					35		93%			
Batch **(1 Ω)**	2.5:1:1.4	Graphite Brush (7 cm^2)/ MFC Anode/ Acetate (1 g L^{-1})	C. Cloth (7 cm^2)/ Ferricyanide (50 mM)	10	0.17mol L^{-1} Ionic solution	Current < 0.05 mA	1.07mmol L^{-1} h^{-1}	-	0.1 W m^{-2}	(Chen et al., 2015)
Batch **(1000 Ω)**							0.02mmol L^{-1} h^{-1}		0.07 W m^{-2}	
Batch **(1000 Ω)**	1:1:1	C. Cloth (7 cm^2)/ culture *B. subtilis*/ dye	C. Cloth (7 cm^2)/ Ferricyanide + PBS	14	35	E_{cell} < 30 mV	62 %	35-90%	3 mW m^{-2} / 0.15 W m^{-3}	(Kalleary et al., 2014)
Batch, recirculation **(1 Ω)**	10:1:10	C. Brush/ -/ Acetate (4 g L^{-1} 0.17 mL min^{-1})	C. Brush/ Ferricyanide + PBS (0.17mL min^{-1})	75 (15 mL min^{-1})	5	-	100 % conductivity	-	-	(Zhang and He, 2012)
					10		70 %			
					20		41 %			

Batch, recirculation (3 streams) 95 mL min^{-1} **(2.5 Ω)**	5:1:5	Isostatic graphite plate + C. felt (100 cm^2)/ *Geobacter sulfurreducens* Sodium Acetate (1.65 - 3.2 g L^{-1})	Isostatic graphite plate + C. felt / Ferricyanide (0.04 - 0.2 M)	370	7.3	0.5 g L^{-1} NaCl	93.3 %	7.14 kg COD m^{-3} d^{-1}	0.7 $kWhm^{-3}$	(Ramírez-Moreno et al., 2019)
					35	0.5 g L^{-1} NaCl	98.6 %	19.7 kg COD m^{-3} d^{-1}	5.4 $kWhm^{-3}$	
		Stainless steel + C. fiber felt (100 cm^2)/ MFC anode Sodium Acetate (2.5 g L^{-1})	Stainless steel + C. fiber mesh+ c. nanofibers doped iron nanoparticles / O_2 (0.1 M PBS)	500	10.7	0.5 g L^{-1} NaCl	93.6 %	0.94 kg COD m^{-3} d^{-1}	0.02 $kWhm^{-3}$	
					33.5	17.4 g L^{-1} NaCl	48.2 %	1.07 kg COD m^{-3} d^{-1}	0.06 $kWhm^{-3}$	
4 MDCs series continuous flow **(10 Ω)**	2:1:1	Treated C. Brush (7 cm^2)/ MFC anode/ xylose 1 g L^{-1} (0.25 mL min^{-1})	Pt/Air-cat 7 cm^2/ (O_2 / PBS)	14	20 g L^{-1} NaCl (0.04 mL min^{-1})	5 g L^{-1}	76 % (5.2 g L^{-1} d^{-1})	60 % (1.15 kg COD m^{-3} d^{-1})	-	(Qu et al., 2013)
					20 g L^{-1} NaCl (0.02 mL min^{-1})	1 g L^{-1}	97 % (3.36 g L^{-1} d^{-1})		-	
					20 g L^{-1} NaCl (1 mL min^{-1})	-	-	-	0.7-0.8 Wm^{-2}	
Batch **1000 Ω**	1:1:1	C. Cloth 7 cm^2 / MFC anode/ Acetate (1 g L^{-1})	Pt/Air-cat (7cm^2) O_2 / PBS (50 mM)	14	5 g L^{-1} NaCl	Ecell < 40 mV	43-60% conductivity	77 - 82%	0.5 Wm^{-2}	(Mehanna et al., 2010c)
		Acetate (2 g L^{-1})			20 g L^{-1} NaCl		50 % conductivity		0.2 Wm^{-2}	

recirculation **200 Ω**	2.6:1:1.8	Porous graphite/ Anaerobic sludge/ peptone 25 g L^{-1} 0.05 mL min^{-1}	Pt-C. Cloth/ O_2 /PBS	38	20 g L^{-1} NaCl	-	55% 2 mg TDS h^{-1}	-	0.37 Wm^{-2}	(Gholizadeh et al., 2017)
Batch **100 Ω**	4:1:4	Roughened graphite/ MFC Anode/ Acetate 1.6 g L^{-1}	Air C. Cloth without Pt/ O_2 /PBS	50	35 g L^{-1} NaCl	-	78 %	85 %	11 Wm^{-3}	(Ebrahimi et al., 2017)
Batch **100 Ω**	3:1:3	C. Brush 9 cm^2/ activated sludge/ Acetate 3.0 g L^{-1}	Air cathode Fe-NCB 7 cm^2/ O_2 /PBS (0.023 M)	11	30 g L^{-1} NaCl	20 mS cm^{-1}	55 % conductivity	83%	0.5 Wm^{-2}	(Santoro et al., 2017)
Batch **(1.5 Ω)**	3:3:1	Treated graphite Brush/ MFC anode / Acetate (2 g L^{-1})	Pt/Air-cat/ O_2 / PBS (100 mM)	150	Cation sol. (50 mM)	$j = 0$	29%	-	660 mAm^{-2}	(Luo et al., 2012a)
					Anion sol. (50 mM)		24% 8.4 TDS L^{-1} d^{-1}	25%	2200 mAm^{-2}	
Recirc* 5mL min^{-1} **(1.5 Ω)**	3.3:1:3.3				Anion solution (50 mM)		90% 21.1 g TDS L^{-1} d^{-1}	-	2600 mAm^{-2}	

Although oxygen reduction is a convenient option, with regard to low cost and sustainability, for cathode reactions in MDC systems, it is necessary to study the impact of using a redox mediator (such as ferro-ferricyanide) on desalination performance (i.e., salt removal and energy production). Even if redox mediators (i.e., ferro-ferricyanide catholyte) would limit the operation of the MDC because of depletion, they could be interesting if low-cost redox mediators are used and an easy and low energy method is developed for regeneration of depleted redox mediators solutions (for example, using renewable energies).

In the current work, the microbial electrochemical behaviour of a lab-scale MDC system was deeply explored for simultaneous brackish water desalination and energy production. Moreover, the impact of the catholyte nature and electrical energy production on the desalination performance is described. Furthermore, a short discussion is presented on the possible scenarios for MDC technology: i) low-energy production and high desalination performance or ii) high-energy production and low desalination performance.

5.2 Materials and Methods

The bacterial strain and culture condition, microbial desalination cell device, electrochemical equipment, analytical methods, as well as process parameters used in this study are described in ***Chapter 3 (section 3.3).***

5.2.1 Desalination operation

To operate the MDC experimental setup, a start-up protocol (Borjas et al., 2017) was performed as described in ***Chapter 3 (section 3.3.5).*** After this start-up protocol, once the current was stable and the biofilm was properly grown in the anode, the MDC operates autonomously without any additional energy supply for desalination under different experimental conditions. The brackish solution was replaced to start the first spontaneous desalination cycle. Thus, the anolyte

was replaced with 2 L of fresh water medium (FWM) containing sodium acetate (20 mM) as the sole electron donor and 60 mM of $NaHCO_3$ (pH=7.7, EC=8.9 mS cm^{-1}); the catholyte was replaced with 2 L of a potassium ferricyanide solution (0.06 M, pH=7.4, EC=23 mS cm^{-1}), and the saline solution was replaced with 600 mL of NaCl (7 g L^{-1}, pH=5.8, EC=13.2 mS cm^{-1}). The volume ratio of the solutions was approximately 3:1:3 (V_{an}: V_{desal}: V_{cat}). The electrode collectors were connected to an external load (resistance value= 0.1, 2.5, or 100 Ω). The system was operated at 30°C, maintaining anaerobic conditions in the anolyte tank during the experiment. Desalination time was calculated as the experimental time for saline tank conductivity below 1 mS cm^{-1} (Council Directive 75/440/EEC of 16 June 1975 concerning the quality required of surface water intended for the abstraction of drinking water in the Member States (OJ L 194 25.07.1975 p. 26), 2006). **Table 7** summarises the experiment performed using the MDC lab setup.

Table 7. Summary of microbial desalination cell (MDC) experiments.

		Saline stream		Anolyte stream		Catholyte stream		
	R_{ext}	Tank Vol.*	[NaCl]	Tank Vol.*	[Acetate]	Tank Vol.*	$K_3[Fe(CN)_6]$	Flow Rate
Id	Ω	mL	gL^{-1}	mL	mM	mL	M	mL min^{-1}
1	2.5	770	6.80	2150	20	2150	0.06	95
2	100	770	6.90	2150	20	2150	0.06	95
3	0.1	770	6.80	2150	20	2150	0.06	95
4	2.5	770	6.80	2150	20	2150	0.06	190
5	2.5	370	7.40	2150	20	2150	0.06	95

NOTE: *compartment volumes and dead volumes (approx. 150-170 mL) have been considered to calculate the total volume of the anolyte, catholyte, and saline streams. **Rext:** value of external load; **Vol.**: tank volume. $K_3[Fe(CN)_6]$: Potassium Ferrycianide.

5.2.2 MDC characterisation (anode/cathode curves)

To characterise the electrochemical behaviour of the system, both anodic and cathodic curves (i.e., the anode/cathode potential versus the current density) were measured just after reaching a steady state. For this task, different values of external resistance (from 0.1 to 500 Ω) were connected to the MDC system, and the potential and current density were registered after a stabilisation period (30-60 min).

5.3 Results and Discussion

An in-depth exploration of all electrochemical parameters controlling MDC performance has generated a series of useful results to evaluate the impact of using ferricyanide as a catholyte.

5.3.1 Impact of the cathodic reaction on MDC performance: air versus liquid

MDC operations classically use two kinds of reactions for the cathode: **a)** oxygen reduction primarily through air diffusion cathodes (Mehanna et al., 2010c; Luo et al., 2012a; Qu et al., 2013; Moruno et al., 2018b, 2018a; Ramírez-Moreno et al., 2019), and **b)** the reduction of soluble redox compounds, mainly ferricyanide (Cao et al., 2009; Luo et al., 2012b; Kalleary et al., 2014; Chen et al., 2015; Sophia and Bhalambaal, 2015; Zuo et al., 2016; Ramírez-Moreno et al., 2019) or hypochlorite (Borjas et al., 2017). From a thermodynamic point of view, the available potential in the MDC to drive the desalination process is higher when oxygen reduction is used in the cathode ($E^{0'}_{MDC} = E^{0'}_{cathode}-E^{0'}_{anode}$= 0.81 V - (-0.3 V) = 1.11 V), see **Table 8**, (Logan, 2007).

Table 8 The anode and cathode potentials for different anodic and cathodic reactions.

Reaction	E^0 vs HSE reference*	$E^{0'}$, pH=7 vs HSE reference	$E^{0'}$, pH=7 vs AgCl/Ag KCl 3.5 M reference
Anodic reaction			
$2HCO_3^- + 9H^+ + 8e^- \rightarrow CH_3COO^- + 4H_2O$	0.187 V	- 0.3 V	- 0.5 V
Cathodic reaction			
$Fe(CN)_6^{3-} + e^- \rightarrow Fe(CN)_6^{4-}$	+0.36 V	+0.36 V	+0.155 V
$O_2 + 4e^- + 4H^+ \rightarrow 2H_2O$	+1.23 V	+0.81 V	+0.605 V

NOTE: *Hydrogen Standard Electrode (HSE). Potential of AgCl/Ag KCl 3.5 M reference electrode vs HSE= 205 mV.

However, the potential curve for oxygen reduction provides less potential than expected when implemented in an MDC reactor and is primarily related to the slow kinetics associated with this reaction at neutral pH (pH=7 (or neutral), which is commonly used for growing electroactive microorganisms like those from the *Geobacter* genus (Bond and Lovley, 2003). Conversely, regardless of the lower thermodynamic potential for ferricyanide ($E^{0'}_{MDC}$ = 0.66 V), fast kinetics provide more available potential in the range of typical current densities (i.e., 0.2-1.5 mA cm^{-2}) used for desalination. To verify this hypothesis, we measured the anodic potential curve to confirm the microbial colonisation of the anode. Furthermore, we also measured cathodic potential curves for both **i)** oxygen reduction (i.e., the air diffusion cathode) and **ii)** ferricyanide reduction (i.e., the liquid catholyte).

Our results **(Figure 44 and table 9)** revealed that $E_{MDC\text{-}Ferri} > E_{MDC\text{-}Oxygen}$ in the range j = 0.2 - 1.4 mA cm^{-2}. The kinetic limitation observed in oxygen diffusion cathodes may explain the low freshwater production previously reported in the literature (Saeed et al., 2015). Consequently, the oxygen-based MDC required an external energy supply to achieve complete seawater desalination.

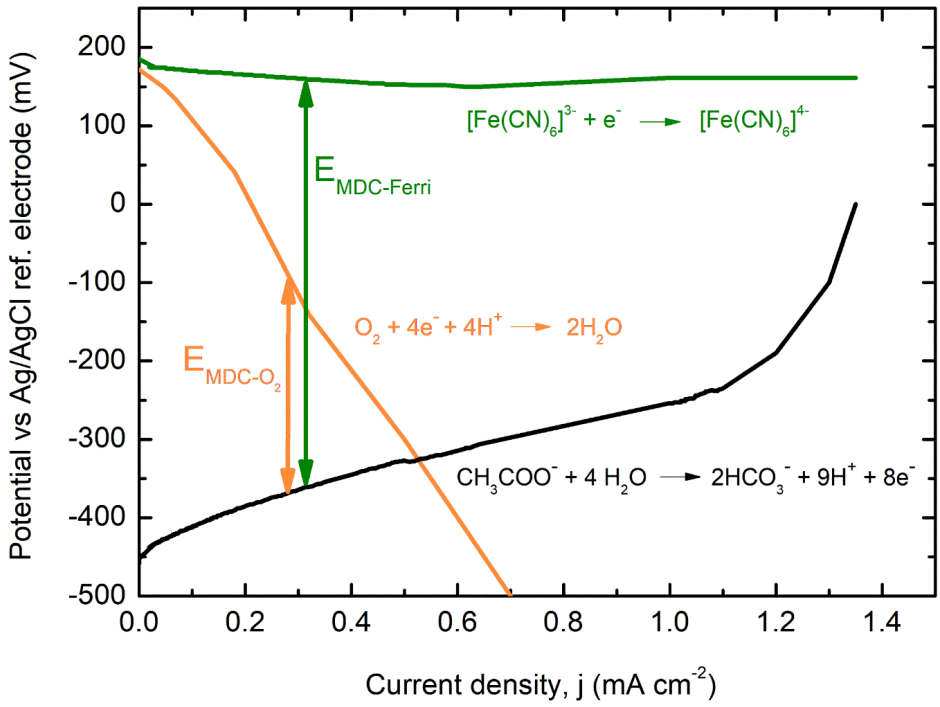

Figure 44. The anode and cathode potential diagram for MDC at steady-state: anode potential: black; liquid catholyte potential: green; air-diffusion cathode potential: orange. Experimental conditions: saline volume of 770 mL; saline concentration of NaCl 7 g L^{-1}. The air diffusion cathode was a commercial Type E4 (Electric fuel Ltd.) **NOTE: Figure S-52** in the Supplementary Information shows air diffusion curves in other experimental conditions.

Table 9 Conclusions summary from the potential diagram in **figure 44**.

Cathodic Reaction	$E^{0'}$, pH=7 vs HSE reference	Thermodynamics ($\Delta G^{0'} = - nF\Delta E^{0'}$)	Kinetics	$E_{cathode}$ for j ($mAcm^{-2}$) = 0.3
$Fe(CN)_6^{3-} + e^- \rightarrow Fe(CN)_6^{4-}$	+0.36 V	- 34.7 kJ	Fast	+ 0.160 V
$O_2 + 4e^- + 4H^+ \rightarrow 2H_2O$	+0.81 V	-312.6 kJ	Low	- 0.140 V

5.3.2 Evolution of conductivity in the saline compartment: impact on the potential drop

The optimal performance of MDC can be severely affected by the evolution of the conductivity from the saline compartment. The impact on electrochemical efficiency can be represented by the anode (E_a) and cathode (E_c) potentials, and the term, potential drop (E_{drop}). Such term can be obtained from the following equation (**Table 2, *Chapter 3***):

$$E_{cell} = (E_c - E_a) - \mathbf{I(R_{memb}+R_{saline})} \qquad \textbf{(3)}$$

$$\boldsymbol{E_{drop} = I\,(R_{memb}+R_{saline})}$$

being E_c and E_a, the cathode and anode potential, respectively (V), R_{memb}, the sum of the electric resistances of all exchange membranes (Ω), and R_{saline} is the electrical resistance due to the saline compartment (Ω). R_{saline} could be easily calculated when the geometry and conductivity of the saline compartment is known, using the **equation 4 (*Chapter 3, section 3.3.3*)** where *EC* is the electric conductivity of the saline stream (mS cm $^{-1}$), *L* is the thickness of the saline compartment (cm) and A_m is the membrane area (cm^2):

$$\mathbf{R_{saline}} = \frac{1}{EC}\frac{L}{Am} \qquad \textbf{(4)}$$

The typical performance of the MDC setup leads to a decrease in the conductivity for the saline chamber during the desalination process **(Figure 45a)**.

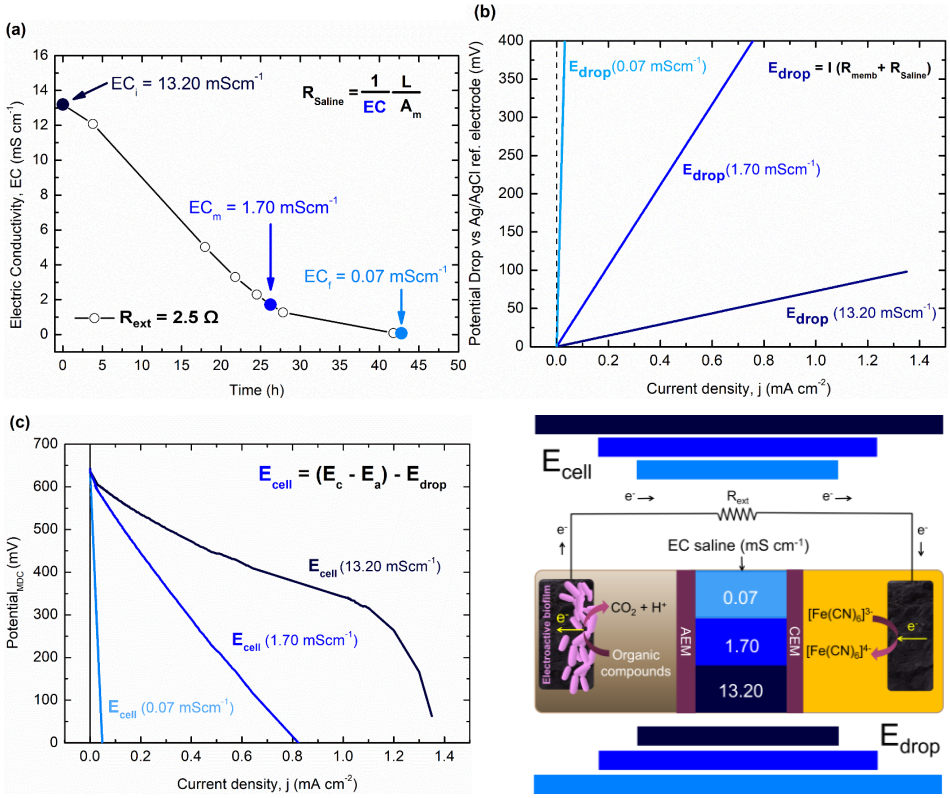

Figure 45. The microbial desalination cycle using R_{ext} = 2.5 Ω. **(a)** Electric conductivity versus time. The coloured dots represent the values of EC from saline samples (chosen for the equation of R_{saline}) at a different time during the desalination cycle (EC_i: initial sample; EC_m: intermediate; EC_f: final). **(b)** The potential drop in the system when the saline stream was 13.20, 1.70, 0.07 mS cm^{-1} in EC **(c)** The potential cell when the saline stream was 13.20, 1.70, 0.07 mS cm^{-1} in EC. **(d)** Figure drawing is added to visualize this process.

Interestingly, the potential drop in the saline compartment, E_{drop}, shifts according to the electric conductivity in the saline stream and, consequently, with current density. Thus, the conductivity in the saline chamber can be used as a tool for predicting electrochemical performance. To validate this hypothesis, we developed a series of assays to quantify the E_{drop} in response to the saline compartment **(Figure 45b)**. Our results revealed that the E_{cell}-based electrochemical performance was reduced by 74-fold at the end of the desalination process.

If the anolyte and catholyte compositions do not significantly change during the desalination process (i.e., the organic substrate and redox intermediate are in excess in comparison to the saline concentration), then the electrochemical behaviour of the MDC unit is governed by the electric conductivity from the saline stream. The cell potential-current density curve can be calculated using the formula $E_{cell} = (E_{cathode} - E_{anode}) - E_{drop}$ **(Figure 45c)**.

5.3.3 Electrochemical behaviour of MDC at different external resistance loads

A standard MDC unit is typically operated using an external load to measure electric current during simultaneous desalination and wastewater treatment. Therefore, it is useful to determine the electric current density and cell potential to study the influence of the external resistance load value on MDC performance (i.e., desalination rate, the energy produced, and wastewater treatment capacity).

In this context, E_{load} ($E_{load} = I\ R_{ext}$) appears as an interesting parameter to monitor the impact of the external resistance load (R_{ext}). The intersection between E_{cell} and E_{load} **(figure 46-4a)** determines the operative point for each moment in the desalination process. For example, A1 (j_{A1}, E_{A1}), A2 (j_{A2}, E_{A2}), and A3 (j_{A3}, E_{A3}) represent the initial, medial, and final points for an MDC operation using an external load of 2.5 Ω.

It is important to note that current density is directly related to both the desalination rate (i.e., the circulated electric charge) and wastewater treatment. Thus, MDC performance is higher when a low external load is used. Conversely, high-value external loads (i.e., >100 Ω) usually produce higher power output (as discussed in the next section). So, despite not harvesting energy externally, the load should be near short circuit conditions (i.e., R_{ext}~0) to maximise the desalination rate (i.e., production of freshwater). Remarkably, producing freshwater using MDC represents indirect energy savings in comparison with a conventional desalination system (i.e., the RO system consuming 1.5-2.5 kWh m^{-}

^{3} for brackish water desalination (Al-Karaghouli and Kazmerski, 2013), 2.8-3 kWh m^{-3} in the case of seawater desalination (MacHarg et al., 2008).

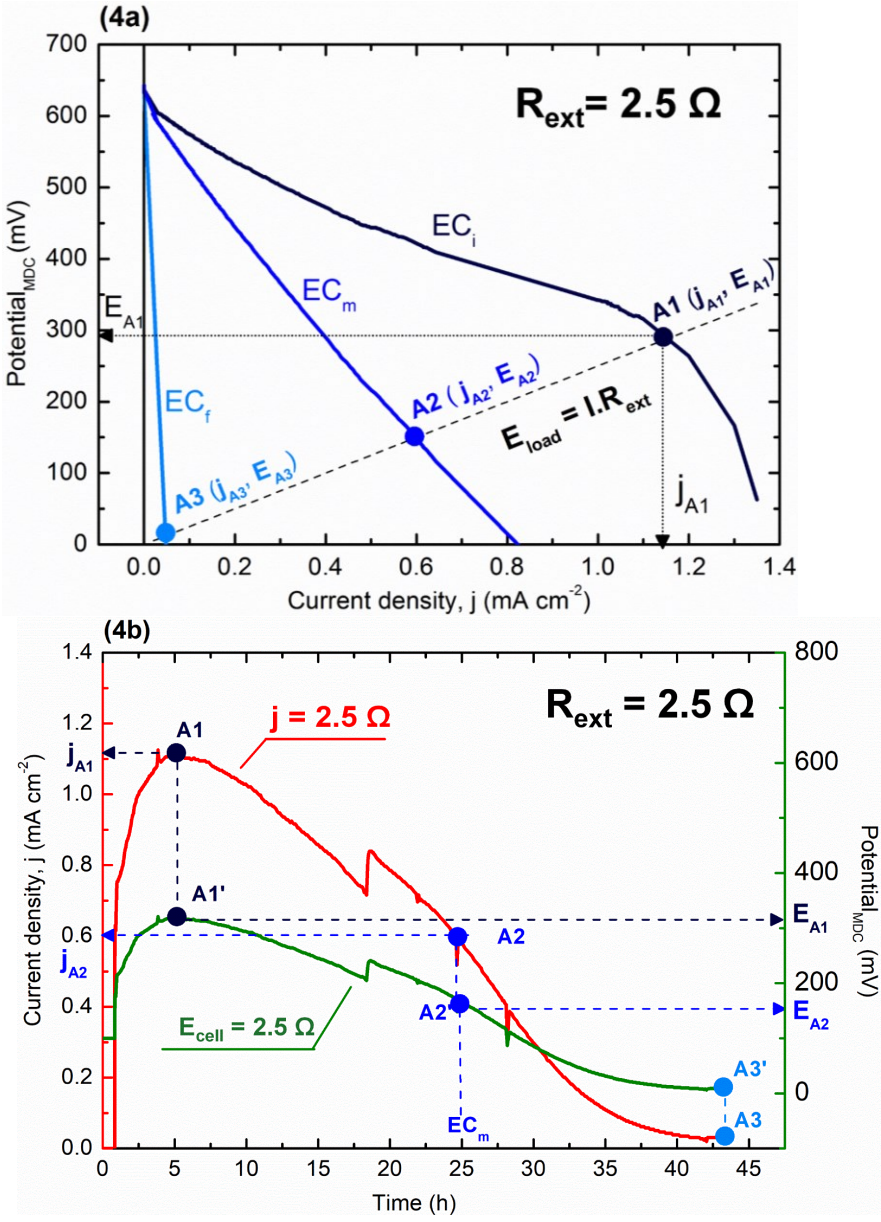

Figure 46. Validation of predictions for a microbial desalination cycle, **(4a)** Electrochemical predictions at R_{ext} = 2.5 Ω. **(4b)** Experimental performance at R_{ext} = 2.5 Ω; Initial conductivity = 13.3 mS cm^{-1}, C_0=7 g L^{-1} NaCl.

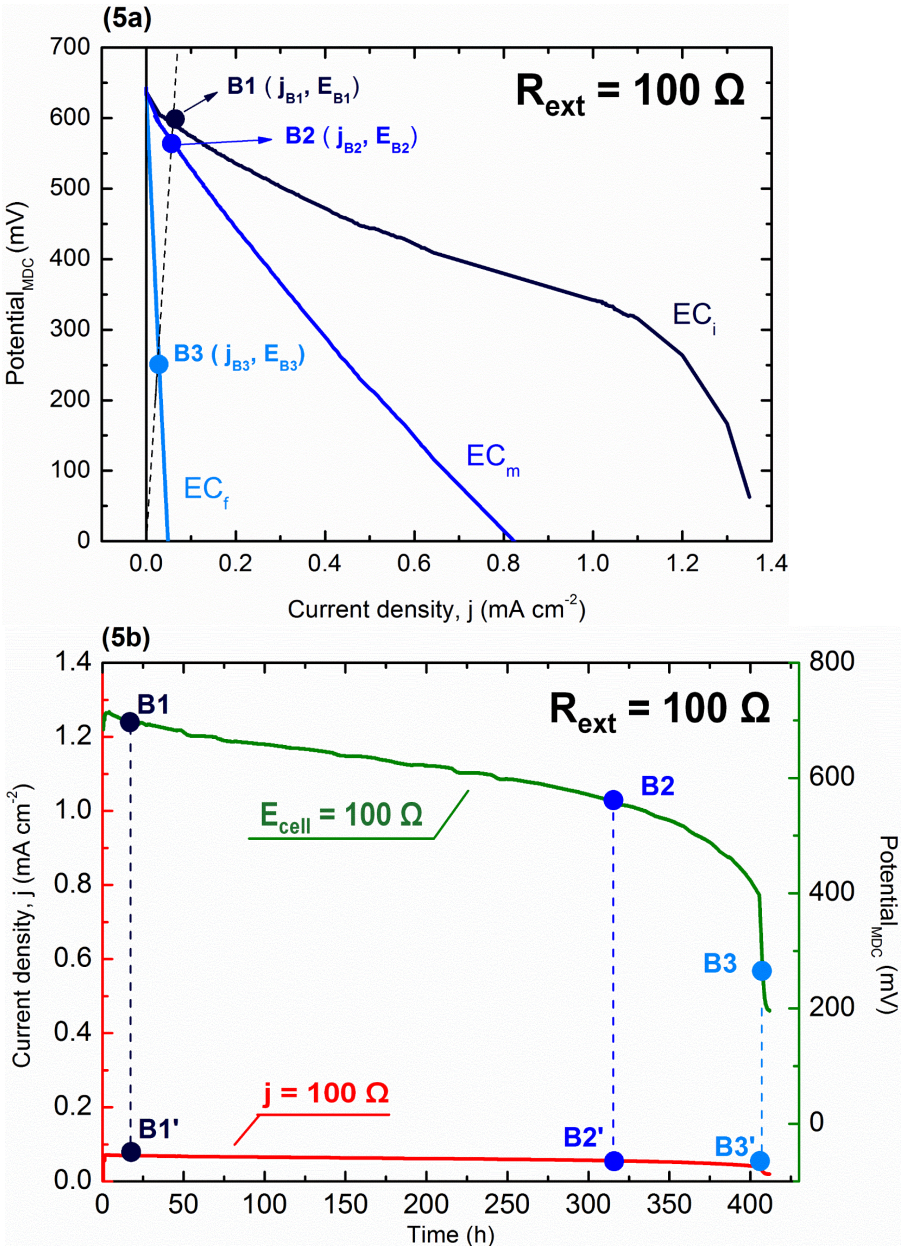

Figure 47. Validation of predictions for a microbial desalination cycle, **(5a)** Electrochemical predictions at R_{ext} =100 Ω. **(5b)** Experimental performance at R_{ext} = 100 Ω; Initial conductivity = 13.3 mS cm^{-1}, C_0=7 g L^{-1} NaCl.

Validating our electrochemical predictions using experimental performance

Our successful set of desalination assays (93% EC removal) generated an attractive scenario for experimental validation of predictions based on EC from the saline chamber.

To validate our predictions based on the E_{load} method from the previous section **(Figure 46-4a and 47-5a)**, we performed brackish water desalination to measure experimental current density (j) and potential cell (E) during desalination time with different external resistance loads (2.5 Ω and 100 Ω) **(Figure 46-4b and 47b-5b)**. The predicted points A1 (j_{A1}, E_{A1}), A2 (j_{A2}, E_{A2}), and A3 (jA_3, E_{A3}) **(Figure 46-4a)** were also presented in the real experimental data **(Figure 46-4b)** to illustrate the behaviour of the MDC as an electrochemical device. Thus, the predicted high current density in **Experiment 1** (R_{ext} 2.5 Ω) at the beginning of the assay **(Figure 46-4a**, j_{A1}, E_{A1}) was related to the operational point A1/A1' **(Figure 46-4b)**, and, analogously, the low current predicted at the end of the desalination process (jA_3, EA_3 in **Figure 46-4a)** were related to point A3/A3' **(Figure 46-4b).** Similarly, the high potential and low current during **Experiment 2** (R_{ext} 100 Ω) (j_{B1}, E_{B1}, and j_{B3}, E_{B3} in **Figure 47-5a)** could be related to operational points B1/B1', B2/B2', and B3/B3' **(Figure 47-5b).**

The relationship between energy and desalination in the MDC context

Our results **(figure 46-4b and 47-5b)** revealed that the current density for $DS_{2.5\ \Omega}$ (a desalinating cycle at 2.5 Ω) was higher in comparison to $DS_{100\ \Omega}$ (a desalinating cycle at 100 Ω). Thus, the more electric charge was circulating through the external circuit of MDC unit and, consequently, more ions were migrating from the saline compartment (desalination). Conversely, the cell potential revealed the opposite trend in those desalination cycles governed by external loads (higher E_{cell} in $DS_{100\ \Omega}$). Therefore, the desalination time **(Figure 48)** significantly decreases for the $DS_{2.5\ \Omega}$ (t_{d1}= 28.9 h) compared with $DS_{100\ \Omega}$ (t_{d2}=

390.3 h), and consequently, the nominal desalination rate for $DS_{2.5\,\Omega}$ (NDR_{exp1} = 2.50 L m^{-2} h^{-1}) was higher than for $DS_{100\,\Omega}$, (NDR_{exp2} = 0.14 m^{-2} h^{-1}). Regarding the energy production, $DS_{100\,\Omega}$ showed higher electrical power output (i.e., $P_{cell} = E_{cell} \cdot I$) resulting in a higher SEP (1.91 kWh m^{-3}) in comparison to $DS_{2.5\,\Omega}$ (0.78 kWh m^{-3}). In this sense, it would be possible to analyse theoretically the optimal load for maximum power production in the MDC system, as suggested in the literature (Weiner et al., 2015; Moya, 2016). A scheme to illustrate this relationship between NDR, SEP and external load is shown in **Figure 49.**

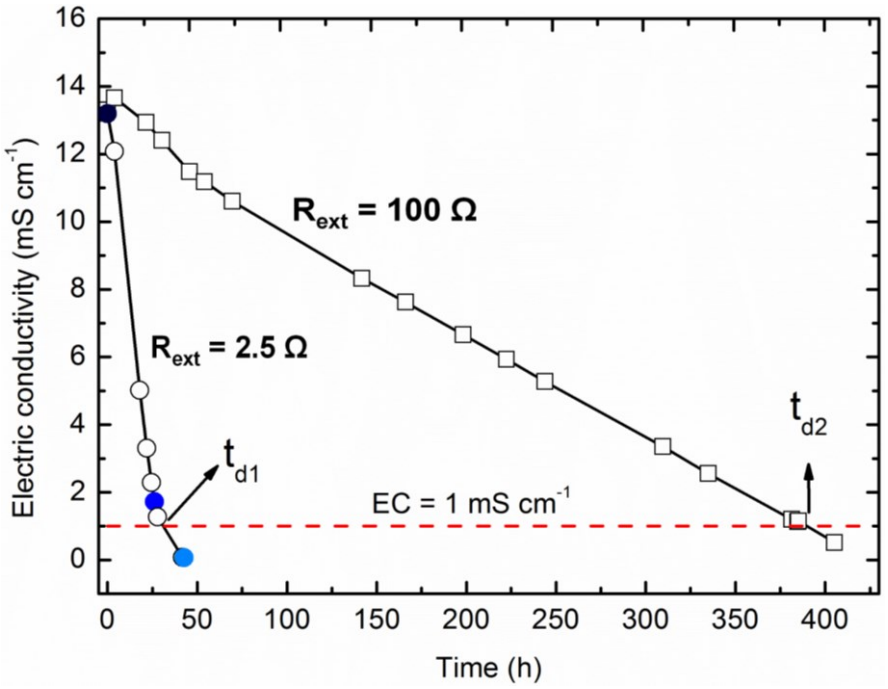

Figure 48. Electrical conductivity versus time for an MDC desalination cycle (7 g L^{-1} / 13 mS cm^{-1}) with 2.5 Ω (circles) and 100 Ω (squares). $t_{d1,2}$: desalination time in the equations. The dashed line shows 1 mS cm^{-1} as the conductivity value to fulfil the legal limits for drinking water (The Environmental and Protection Agency, 2014).

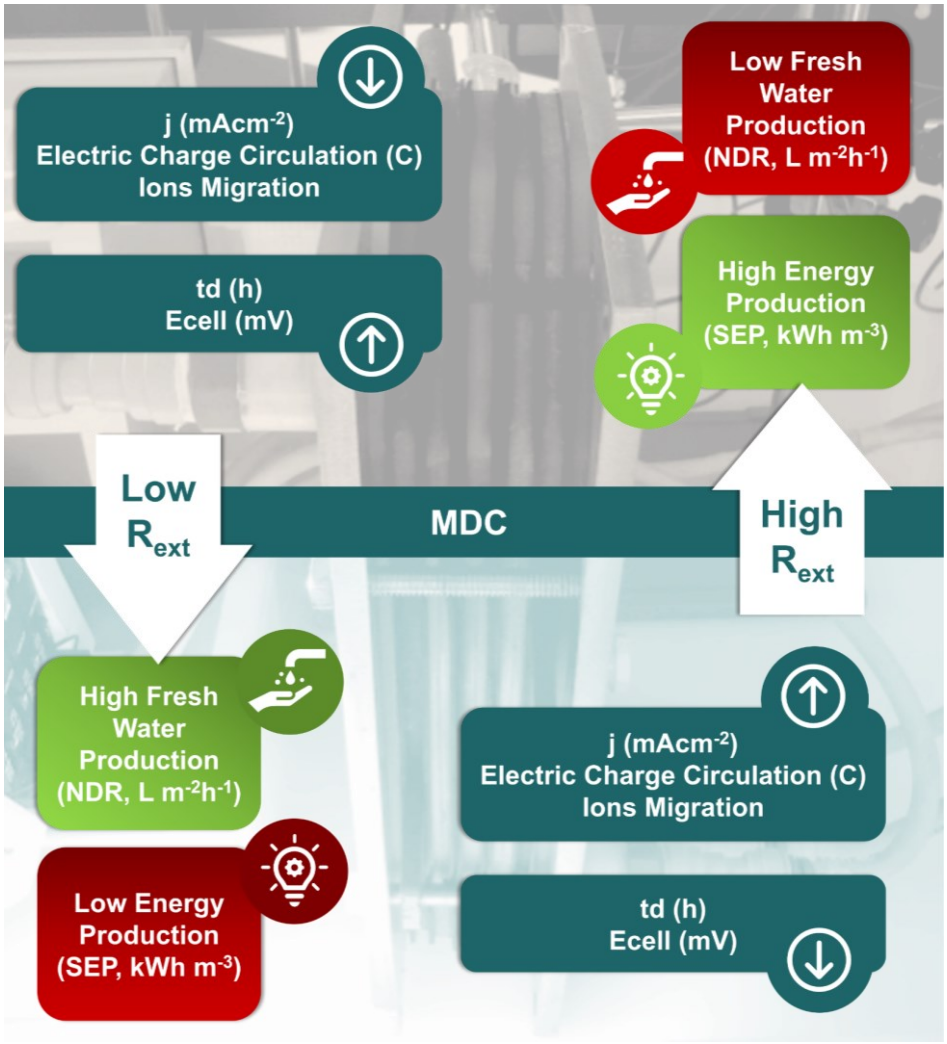

Figure 49. Scheme illustrating the relationship between the nominal desalination rate (NDR), specific energy production (SEP), and the external load.

Five brackish water desalination cycles at three independent external loads **(Table 10)** were performed to generate information about the circulated electric charge, salt removal, the current efficiency, the nominal desalination rate (NDR), specific energy production (SEP), the salt transfer rate, water transport, the COD removal rate, and coulombic efficiency.

Table 10 Experimental conditions and results for brackish water desalination using the MDC lab setup.

Id.	Circulated charge (kC m^{-3})	Salt removal (%)	Current efficiency (%)	Nominal Desalination Rate (NDR)** (L m^{-2} h^{-1})	Specific Energy Production (SEP) (kWh m^{-3})	Salt transfer rate** (NaCl kg m^{-3} d^{-1})	Water transport (%)	COD removal rate (kg COD m^{-3} d^{-1})	Coulombic efficiency (%)
1	11095	93	94.5	2.50	0.78	58.42	6.50	8.08	71.50
2	11108	93	95.6	0.14	1.91	4.44	28.60	1.74	30.35
3	11752	93	88.2	4.32	0.23	100.05	6.50	14.00	81.17
4	11307	93	92.0	2.86	0.97	67.50	7.80	13.88	60.00
5	13961	93	81.1	1.47	0.71	38.00	8.11	7.14	84.00

Exp. 1: R_{ext} =2.5 Ω; Q_t= 770 mL; c_s^i = 7 g L^{-1}. **Exp. 2:** R_{ext} =100 Ω; Q_t= 770 mL; c_s^i = 7 g L^{-1}. **Exp. 3:** R_{ext} =0.1 Ω; Q_t= 770 mL c_s^i = 7 g L^{-1}. **Exp. 4:** R_{ext} =2.5 Ω Q_t= 770 mL c_s^i = 7 g L^{-1} *Flow rate=190 mL min^{-1}. **Exp. 5:** R_{ext} =2.5 Ω Q_t= 370 mL c_s^i = 7.35 g L^{-1}.

NOTE: the compartment volumes and dead volumes (approx. 150-170 mL) have been considered for calculating the total volume of the anolyte, catholyte, and saline streams. *Flow rate=95 mL min^{-1}, except for **Id.4**. ** Calculated considering the final volume of the saline tank. $\boldsymbol{c_s^i}$ (initial saline concentration).

The trend of NDR, energy production and the COD removal rate **(Figure 50)** revealed an increase in NDR when low-value external loads were used, and inversely, the MDC energy production diminished. In this context, the trend of COD removal rate was consistent with the nominal desalination rate (NDR) because COD biodegradation is typically co-related to current density in the MDC. Our COD removal rates were similar to values previously reported in the literature (Luo et al., 2012b; Zhang and He, 2013), demonstrating that MDC technology could perform efficiently for both wastewater treatment and desalination. Nevertheless, these results were validated at lab scale using synthetic wastewater. Moreover, validation using real wastewater should be part of future actions.

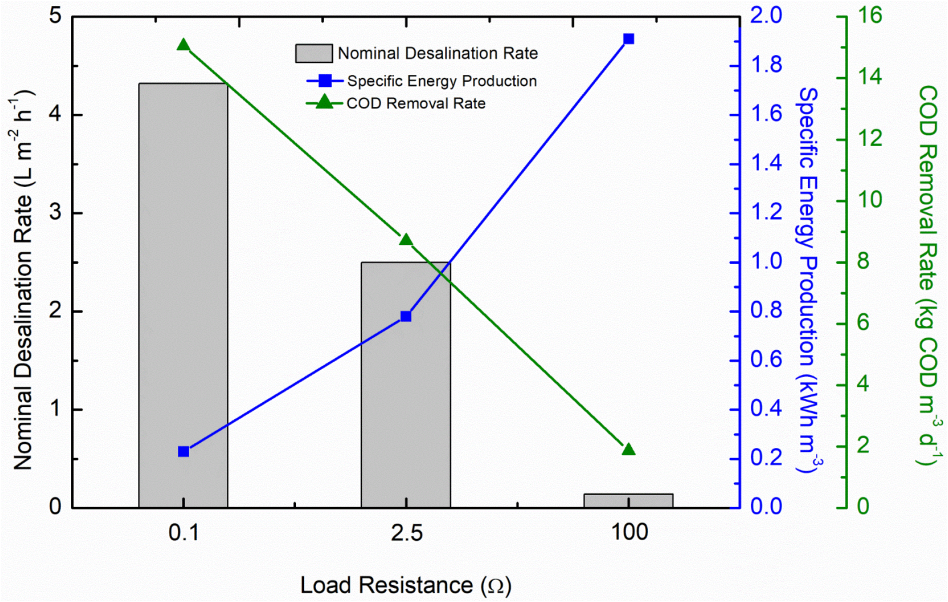

Figure 50 The nominal desalination rate (grey columns), specific energy production (blue squares), and the COD removal rate (green triangles) versus different external load values for $DS_{0.1\,\Omega}$; $DS_{2.5\,\Omega}$, $DS_{100\,\Omega}$.

Besides energetic issues, external load also influences both current and coulombic efficiency. The current efficiency was >90% in all cases **(Figure 51).** Interestingly, this is a similar value than conventional electro membrane

processes (Ortiz et al., 2005), indicating that the MDC system operates properly from the electrochemical point of view (i.e., the ion exchange membrane efficiency transport number for ions is approximately 85-95%). Also, the decrease in the desalination efficiency **(Figure 51)** could be explained by back diffusion between the anodic/cathodic and saline compartment, as reported in (Ping et al., 2016).

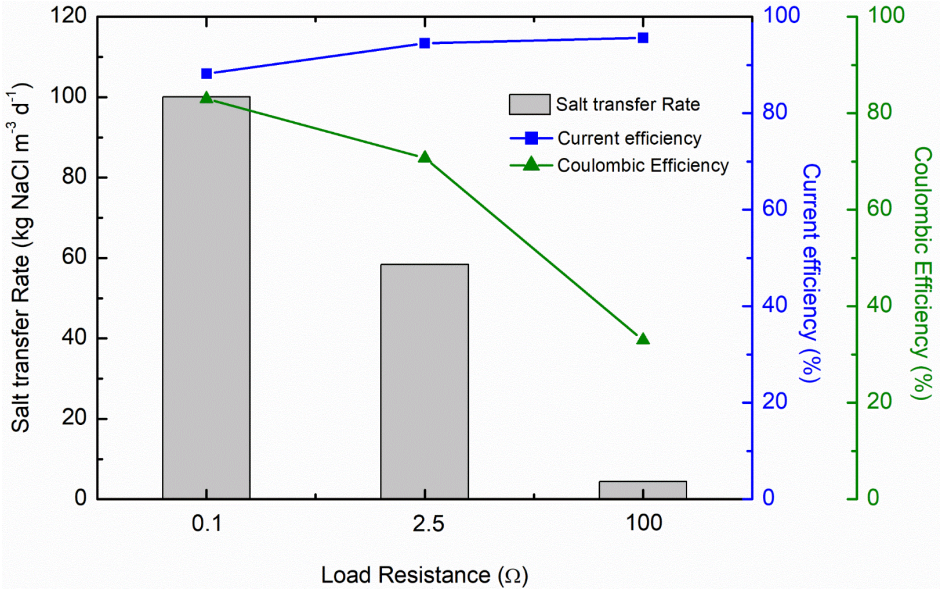

Figure 51 The salt transfer rate (grey columns), current efficiency (blue squares), and coulombic efficiency (green squares) versus different external load values for $DS_{0.1\ \Omega}$; $DS_{2.5\ \Omega}$, $DS_{100\ \Omega}$.

This proper performance of all MDC assays was also confirmed by measuring the electric charge per volume or circulated electric charge **(Table 10)** and produced very similar results (i.e., 11095-13961 kC m^{-3}). Since salt transfer is directly related to the current density, its value was higher when the low-value external load was used. Regarding coulombic efficiency, this parameter was higher when desalination time (t_d) was lower, indicating a competition between electroactive bacteria and those anaerobic ones not contributing to electric current production **(Experiment 2 in Table 10).**

The increasing flow rate **(Experiment 4 in Table 10)** revealed a slight improvement in the performance of the MDC (SEP, NDR), probably due to better homogenisation in the anode compartment. The volume of the saline chamber was also assayed, and its reduction (**Experiment 5**, approximate volume ratio: 6:1:6 / V_{an}:V_{desal}:V_{cat}) led to a slight decrease in the MDC performance, from NDR_1=2.50 L m^{-2} h^{-1} to NDR_5=1.47 L m^{-2} h^{-1}.

Another critical issue is the potential transfer of water through the membrane. Our results **(Table 10)** revealed how water transport increased in relation to desalination time (td), and this effect was mainly due to water transport osmosis (Qu et al., 2013).

MDC technology represents a sustainable and disruptive approach in which vast energy savings is produced during wastewater treatment and freshwater production, in contrast with conventional processes that typically consume 0.5-2.0 kWh m^{-3} for wastewater treatment, and 2.2 kWh m^{-3} for RO-based desalination (Gude et al., 2013), and generate greenhouse gas emissions (i.e., 300 g CO_2 kWh^{-1} in the average European Union energy mix (European Environment Agency (EEA), 2019).

5.4 Conclusions

Microbial Desalination Cells constitute an innovative technology where microbial fuel cells and electrodialysis merge in the same device for obtaining fresh water with no energy-associated cost and greenhouse gas emissions. MDC concept was firstly proposed by Cao et al. (Cao et al., 2009) using ferro-ferricyanide reaction in cathode compartment (i.e., liquid catholyte), and subsequent studies implemented oxygen reduction as cathodic reaction because its sustainability. However, oxygen reduction decreases the available potential due to slow kinetics, and thus desalination rate and energy production. This effect

could be easily explained taking into account the potential curves of the anode, cathode and saline compartment, and the external load operative curve at steady state, as described in *Section 5.3.1*, where MDC potential and electric current density is related to MDC main parameters (i.e., Nominal Desalination Rate, Specific Energy Production, COD Removal Rate, Coulombic Efficiency). The electrochemical behaviour shown in this work could be useful for further development, design and optimization of low energy desalination using MDC technology.

Finally, even if the use of liquid catholyte is used (i.e., ferricyanide solution) could allow the increase of the desalination rate, wastewater treatment, freshwater and energy production, this liquid catholyte has to be regenerated when depleted. For this reason, it could be convenient in further studies to establish a rationale method for regeneration of the liquid catholyte, including sustainable use of renewable energy (i.e., photovoltaic, wind energy) or coupling microbial electrochemical reactions (i.e., biocathodes) for regeneration.

Supplementary data *Chapter 5*

Air diffusion cathodes: experimental data

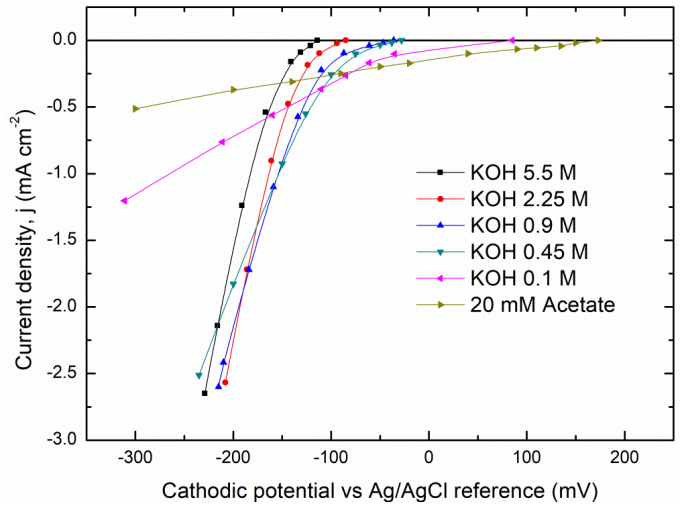

Figure S-52 Air diffusion cathode potential curves for various experimental conditions. (Type E4, Manufacturer: Electric fuel Ltd., https://electric-fuel.com). Active layer: Manganese-based catalysed carbon).

As observed in **figure S-52**, alkaline conditions increase the performance of oxygen reduction reactions in the air diffusion cathode as expected, due to faster kinetics. In the case of freshwater medium (FWM, pH=6.95, CE=5.95 mS cm^{-1}), the open circuit potential (OCP, the potential when the current density is zero) is higher compared with the alkaline conditions, as expected using the next equation (oxygen reduction reaction: $O_2 + 4e^- + 4H^+ \rightarrow 2H_2O$ $E^\circ = +1.23$ V):

$$E = E^0 - \frac{RT}{nF} ln\left(\frac{a_{H_2O}^2}{a_{O_2} a_{H^+}^4}\right) = E^0 - 0.059pH - \frac{0.059}{4} log\left(\frac{1}{p_{O_2}}\right)$$

Thus, a decrease in pH produces higher values of equilibrium potential (i.e., pH=6.95 for 20 mM Acetate, compared with alkaline conditions). However, the potential values provided at different current densities are lower compared with alkaline conditions (i.e., higher overpotential due to slow kinetics) for the reaction of oxygen reduction.

Experimental pH and conductivity data (initial and final values for each desalination cycle)

	Anolyte stream				Catholyte stream				Saline stream			
Id.	pH_i	pH_f	EC_i (mS cm^{-1})	EC_f (mS cm^{-1})	pH_i	pH_f	EC_i (mS cm^{-1})	EC_f (mS cm^{-1})	pH_i	pH_f	EC_i (mS cm^{-1})	EC_f (mS cm^{-1})
1	7.70	6.92	8.99	10.09	7.45	7.50	23	23.20	5.76	5.40	13.19	0.072
2	7.92	7.25	8.27	10.06	7.5	7.43	22.8	22.40	5.92	6.38	13.30	0.51
3	7.60	7.36	8.29	9.56	9.17	7.06	21.80	-	5.85	6.30	13.09	0.33
4	7.34	7.08	8.50	9.86	8.79	6.67	20.70	21	6.00	6.12	13.12	0.67
5	8.07	7.95	6.16	6.86	5.97	8.19	13.3	13.9	6.40	5.87	13.88	0.56

*Initial samples ($_i$) were collected after 10-20 min of recirculation in the MDC system for their homogenisation.

Chapter 6

Study of Microbial Desalination Cell performance with different saline streams: Analysis of current efficiency and freshwater production

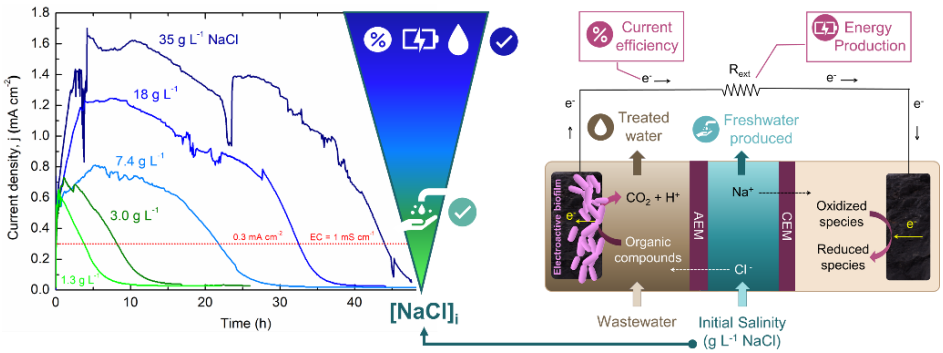

This chapter has been published and redrafted for this thesis:

Ramírez-Moreno, M., Esteve-Núñez, A., and Ortiz, J. M. (2023). Study of microbial desalination cell performance with different saline streams: Analysis of current efficiency and freshwater production. *J. Environ. Chem. Eng.* 11, 109240. doi:10.1016/j.jece.2022.109240.

Chapter 6. Study of Microbial Desalination Cell performance with different saline streams: Analysis of current efficiency and freshwater production

Abstract

The optimal desalination process in MDC technology depends on the potential generated in the system, which is mainly limited by cathode reaction, high external load values used, initial salinity of saline stream, or other conditions such as anolyte buffer concentration. As transport processes (i.e., migration and diffusion) in the device overlap under such conditions, it is difficult to identify the factors that affect desalination performance. Most of the existing MDC studies have used oxygen reduction (at neutral pH) as a cathode reaction limiting the performance. The removal of the cathode reaction limitation could help to clarify the operation of the MDC and identify different transport phenomena and their influence on the performance (current efficiency, freshwater production, and salt removal rate). This study presents a systematic analysis of a laboratory-scale MDC (cross-section 100 cm^2, batch mode) behaviour under different initial saline concentrations from slightly brackish water (1.3 g L^{-1} NaCl) to seawater (40 g L^{-1} NaCl) without limitation in the desalination process (i.e., using a low value of external resistance and potassium ferricyanide as a liquid catholyte). For each initial salinity, the parameters of wastewater treatment capacity, energy and freshwater production are discussed and compared with the literature. The values of freshwater production between 0.5 and 10.6 L m^{-2} h^{-1} for each initial saline concentration in the saline compartment are achieved with optimal current efficiency values (80–100%). Additionally, the influence of anolyte buffer capacity on current density in the MDC system (from 0.8 to 1.2 mA cm^{-2}) is analysed. Furthermore, the behaviour of the system during a seawater desalination process is discussed in terms of treatment capacity and Coulombic efficiency. This study could help understand the performance of these systems in

possible natural saline scenarios where MDC technology can be implemented in the future.

6.1 Introduction

Currently, the low production capacity could be considered the main limitation of MDC technology due to the low available energy in the bioelectrochemical system, mainly due to the use of the oxygen reduction reaction as a common cathodic strategy (Zhao et al., 2006; Ashwaniy and Perumalsamy, 2017; Khazraee Zamanpour et al., 2017). The application of this strategy could be enhanced with the application of cheap nanomaterials in cathodes development (Mashkour et al., 2021). As the anode potential established by the bacteria ($E^{0'}$ = - 0.29 V vs HSE, in the case of *Geobacter sulfurreducens*) is limited, the study of the cathode reaction performance could be the key to improving the water production capacity. Thus, considering a redox mediator for the cathode reaction in the MDC system (for example, ferricyanide) would open up the possibility of carrying out a rational study of the MDC system behaviour since the cathode limitations are removed (i.e., low cathode potential due to oxygen reduction reaction at pH = 7) (Ramírez-Moreno et al., 2021a). The main drawback of using ferricyanide catholyte is that it must be regenerated when depleted. It is convenient for further studies to establish an easy and cost-effective procedure for regenerating depleted catholyte solution, including integrating renewable energy or using biocathodes for regeneration.

MDC systems are versatile and complex devices, as many factors influence their performance (Jingyu et al., 2017). The initial saline composition (e.g., initial ion concentration), anolyte composition (e.g., available substrate, buffer capacity and conductivity), and catholyte composition (e.g., final electron acceptor or conductivity) could determine the overall system performance. These factors will affect the internal resistance, electrochemical performance of the system,

bacterial community present in the anode, membrane scaling and biofouling processes, and other driving forces of desalination, such as diffusion and osmotic pressure. Most laboratory-scale studies show a variable efficiency attributed to the different conditions in which they operate. Systematic studies could be helpful to address the limitations of these systems and improve their development and application.

Saline intrusion could occur in areas in which underground aquifers are in contact with seawater, producing issues for its use, for example, in irrigation (**Table S-13** is included in Supplementary Information, which collects a classification of water according to its saline concentration and its possible use). Due to this possible variability in the saline scenario, it is essential to validate the MDC system and know its behaviour in the range from brackish to seawater (i.e., different grades of saline intrusion).

In that sense, this work presents an extensive study on the behaviour of a laboratory-scale MDC system for the desalination of a wide range of initial salinity concentrations. The objective is to determine how the initial salinity of the saline compartment influences the main parameters, such as freshwater production, treatment capacity or energy production without limitations in the system. To remove the limitations in the performance of system a low value of external resistance (2.5 Ohms) is used to maximise freshwater production. Additionally, potassium ferricyanide (i.e., $K_3[Fe(CN)_6]$) is used as a liquid catholyte to study the MDC system under different experimental conditions without cathode potential limitation (i.e., when using an oxygen reduction reaction). The initial salt concentrations cover the range of water salinity from slightly brackish water (1.3 g L^{-1} NaCl) to seawater (35–40 g L^{-1} NaCl).

The main parameters of desalination performance of our MDC system, such as nominal desalination rate (NDR) and current efficiency, are discussed and compared with those of the 3-chamber MDC configurations available in the literature. Additionally, the wastewater treatment capacity and energy production

are discussed. A comparison of two desalination cycles of the same initial salt concentration but under different buffer conditions of synthetic wastewater used as an organic matter source is shown. Finally, the behaviour of our MDC system for water desalination with a high salt concentration is discussed. The experimental results could be useful to understand the performance of the MDC systems in different possible scenarios where the MDC technology can be implemented to derive irrigation or drinking water from the desalination of brackish or seawater.

6.2 Materials and methods

The microbial desalination cell device description, electrochemical equipment, the microbial desalination cell inoculum, start-up protocol, analytical methods, and the calculation of microbial desalination cell performance indicators used in this study are described in ***Chapter 3 (section 3.3).***

6.2.1 Spontaneous desalination operation

After the start-up protocol followed (Borjas Hernández, 2016; Borjas et al., 2017) (described in ***Chapter 3, section 3.3.5***) and when the current was stabilised (i.e., the biofilm was properly grown on the anode), the MDC was ready to operate without any additional energy supply for desalination under different experimental conditions. Then, the first desalination cycle was performed; three tank solutions were replaced to start the first spontaneous desalination experiment.

The saline solution was replaced by 200 mL of NaCl (1.3 g L^{-1}, pH = 6.4, EC = 2.5 mS cm^{-1}). The anolyte was replaced by 2 L of FWM with sodium acetate (20 mM) as the sole electron donor and 30 mM of $NaHCO_3$ (pH = 8.6, EC = 6.7 mS cm^{-1}); the catholyte was replaced by 2 L of a potassium ferricyanide solution (0.04 M, pH = 6.7, EC = 14.4 mS cm^{-1}). The volume relation of the solutions was

approximately 5:1:5 (V_{an}: V_{sal}: V_{cat}) (V_{an}= anolyte volume, V_{cat}= catholyte volume, V_{sal}= saline water volume) with a dead volume account. The power supply (used during start-up protocol) was disconnected, and the electrode collectors were connected to an external load (R_{ext} = 2.5 Ω). The system was thermostated at 30 °C and maintained under anaerobic conditions in the anolyte tank during all the experiments. The desalination cycles were considered completed when the conductivity of the saline tank was below 1 mS cm^{-1} (Council Directive 75/440/EEC of 16 June 1975 concerning the quality required of surface water intended for the abstraction of drinking water in the Member States (OJ L 194 25.07.1975 p. 26), 2006). Desalination performance was assessed compare the different parameters, summarized in **Table 2** of ***Chapter 3, section 3.3.3.***

Table 11 summarises the initial conditions for each desalination cycle using the MDC device described in ***Chapter 3 (section 3.3.1).***

Table S-13 (in supplementary data of this ***Chapter 6***) shows the comparison between the initial salt concentrations selected for this study and the general classification of saline water (based on salt concentration and electrical conductivity) with its possible application. This table could help to visualise that the present study covers all possible salinity scenarios where the behaviour of the MDC device could be studied.

Table 11 Summary the initial conditions for each desalination cycle using the microbial desalination cell.

	Saline stream				Anolyte stream				Catholyte stream			
Id.	Tank Volume*	[NaCl]	Initial conductivity	Charge necessary**	Tank Volume*	[Acetate]	Charge added	[$NaHCO_3$]	Tank Volume*	[Ferricyanide]	Charge added
	mL	g L^{-1}	mS cm^{-1}, 25 °C	Coulombs	mL	mM	C	mM	mL	M	C
1	370	1.3	2.5	505	2150	20	33190	30	2150	0.04	7680
2	370	3.0	5.6	1546	2150	20	33190	30	2150	0.04	7680
3	370	7.4	13.9	4190	2150	20	33190	30	2150	0.04	7680
4	370	18	28.0	10486	2150	20 20	66382	30 30	2150	0.04 0.04	15094
5	370	18	29.0	11205	2150	20	33190	60	2150	0.06 0.04	21102
6	370	35	51.5	21085	2150	40	66382	120	2150	0.2	38600
7	370	40	57.8	23914	2150	20 20 20	99573	30 30 30	2150	0.04 0.04 0.04	23447

NOTE: *compartment volumes and dead volumes (approx. 150-170 mL) were considered to calculate the total volume in the anolyte, catholyte and saline streams. The external load used in all the experiments was 2.5 Ω, and the flow rate was 95 mL min^{-1}. ** Necessary charge to desalinate until 1 mS cm^{-1}, calculated in the supplementary information **(Table S-14)**. The feeding cycles in Experiments **4** and **7** are indicated.

6.3 Results and discussion

6.3.1 Analysis of freshwater production and current efficiency

The lab-scale MDC system studied achieved complete desalination over a wide range of initial salinities from 2.5 mS cm^{-1} to 60.0 mS cm^{-1} (1.3 g L^{-1} to 40.0 g L^{-1} NaCl). In all cases, the electrical conductivity (EC) at the end of the desalination cycle was below 1 mS cm^{-1} (corresponding to 0.5 g L^{-1} NaCl, confirming the feasibility of MDC technology).

The measured electric current vs. time for each desalination cycle is shown in **Figure 53A**. A different value of maximum current density was obtained for each one. For a concentration of 1.3 g L^{-1} NaCl in the saline stream (which corresponds to 2.5 mS cm^{-1}), the maximum current density obtained was 0.63 mA cm^{-2}, while for the desalination of 35.0 g L^{-1} NaCl (51.5 mS cm^{-1}), the maximum current density was 1.70 mA cm^{-2}.

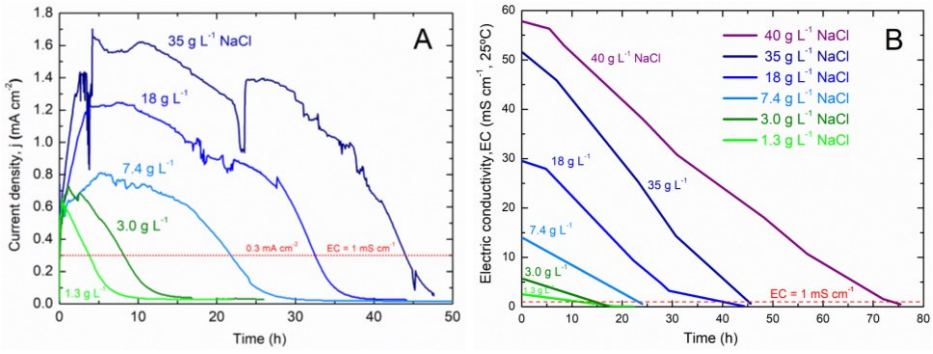

Figure 53. Experimental results for lab-scale MDC during independent desalination cycles. **A)** Current density vs. time measured in the system through an external 2.5-Ohms resistance **(Exp. 1-3, 5-6)**. The red dotted line marks the current density value that can be measured when the electrical conductivity of the saline tank equals 1 mS cm^{-1}. **B)** Electrical conductivity (at 25 °C) vs. time measured in the saline tank during desalination cycles **(Exp. 1-3, 5-7)**. The red dashed line marks the electrical conductivity value corresponding to 1 mS cm^{-1}.

All desalination cycles were carried out with the same value of external resistance (2.5 Ohms) and conditions of an excess of substrate (acetate as electron donor) and redox mediator for counterreaction (potassium ferricyanide as the final electron acceptor), thus maintaining the available potential to drive the desalination process in the MDC system. Under these conditions, the current density is mainly affected by the internal resistance of the system (Ramírez-Moreno et al., 2021a). In experiments where the initial electric conductivity of the saline stream was high, the initial internal resistance due to the central compartment was low, and higher current densities were reached at the beginning of the process. Additionally, the available potential in the MDC could be slightly increased due to the difference in salinity between the saline compartment and the adjacent compartments (i.e., membrane potential) at the beginning of the desalination process, as reported by Yang et al. (Yang et al., 2015).

The EC of the saline tank is shown in **Figure 53B** for all experiments. Complete desalination was achieved in all the different desalination cycles (i.e., electrical conductivity was below 1 mS cm^{-1}). The desalination of 1.3 g L^{-1} NaCl, with an initial conductivity of 2.5 mS cm^{-1}, ended the process with 0.04 mS cm^{-1} and a salt removal value of 63%. The desalination of 40 g L^{-1} NaCl (initial conductivity = 58 mS cm^{-1}) reached 0.5 mS cm^{-1} after the desalination process with a salt removal value of 98.7%. **Table S-15** (supplementary data of this chapter) summarises the main parameters of the desalination experiments using the MDC system proposed in this study. **Figure 54** shows the nominal desalination rate (NDR) and the current efficiency vs. the initial concentration of NaCl for all experiments.

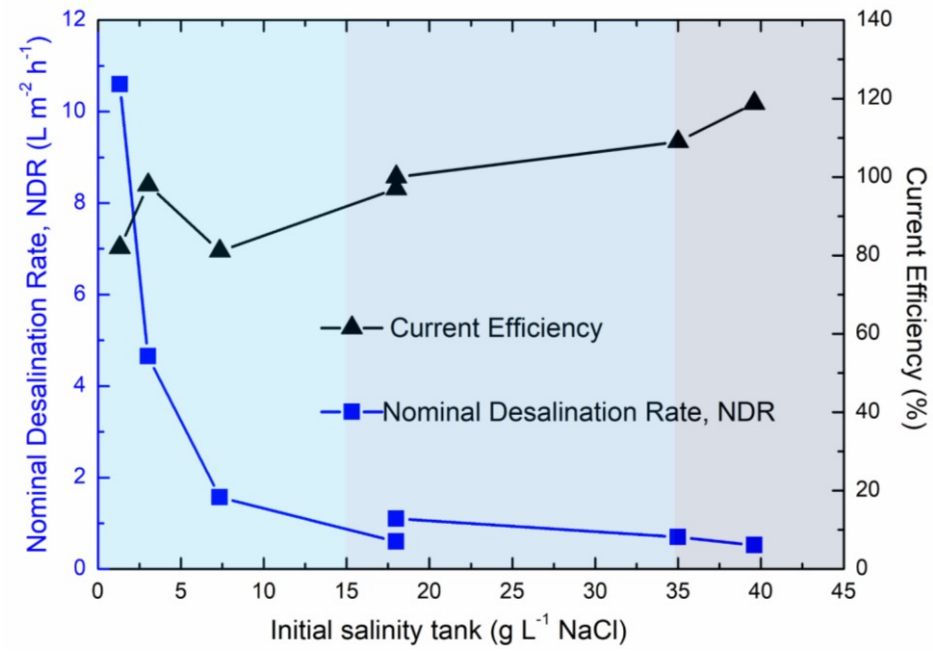

Figure 54. Nominal desalination rate, NDR (blue square symbols) and current efficiency (black triangle symbols) for each independent desalination cycle.

Regarding current efficiencies (percentage of electric energy efficiently used for desalination., i.e., ion migration), it is possible to obtain 80–100% in the range of 1–20 g L^{-1} of initial NaCl concentration, indicating a proper operation of the MDC system as an electrochemical device, as the electric charge is properly used for desalination (i.e., ion migration). Current efficiency values below 100% could be obtained in low initial saline concentration desalination where low current densities are achieved (as seen in **Figure 53A**).

In these cases, back-diffusion is expected from the anode/cathode compartment to the saline compartment (due to the difference in ion concentrations between compartments). Therefore, the desalination process would need a surplus of electric charge in comparison to the theoretical value (electric charge needed for complete desalination), and consequently, the current efficiency is lower than 100%. Similar results have been reported in the literature. For example, Chen et al. (Chen et al., 2015) indicated that for the desalination of

5 g L^{-1} NaCl to occur as described in Mehanna et al. (Mehanna et al., 2010c), the current efficiency value must have been between 23 and 42% if only the effect of ion migration was considered. Other studies using gas diffusion electrodes have achieved current efficiencies of 47% for the desalination of 10 g L^{-1} NaCl (Borràs et al., 2021).

Interestingly, when the initial salt concentration was high (35-40 g L^{-1} NaCl), the current efficiency was significantly above 100%, indicating that the ion diffusion process, which does not implicate electric charge circulation across the external circuit, is also responsible for ion transport from the saline compartment to adjacent compartments due to the difference in concentrations among compartments (Jacobson et al., 2011a). Similarly, high values of current efficiency were reported in works desalinating a high initial salt concentration (35 g L^{-1} NaCl) with an air cathode (129-241%) (Rahman et al., 2021a) or biocathode (113-129%) (Zhang et al., 2016b). According to these results, the desalination of high saline concentrations can be carried out through the diffusion process taking advantage of salinity-gradient power such as concentration cells, or the reverse electrodialysis technologies (Post et al., 2007; Veerman and Vermaas, 2016), which are energetically advantageous since the ion transport process does not need external energy. However, even if the current efficiency is high in these cases, the production of fresh water and the salt removal rate are poor (i.e., the value of NDR), as the diffusion transport phenomenon is slow and is stopped once the concentration is equilibrated in the compartments (no driving force for diffusion).

The nominal desalination rate (NDR) is a parameter that considers the time required for the entire desalination process and helps compare systems in terms of desalinated water production. The highest NDR value achieved was 10.6 L m^{-2} h^{-1} for an initial salinity of 1.3 g L^{-1} NaCl, in contrast to the lowest value of 0.5 L m^{-2} h^{-1} for the 40 g L^{-1} NaCl. This parameter decreases for high concentrations, as complete desalination requires more time.

One of the phenomena that could affect the NDR value is the transport of water by the osmosis effect from the saline compartment to the anode or cathode compartment, calculated as the water transport (%) through the membranes. This parameter increased in the desalination of high initial salt concentrations (such as 35 g L^{-1} NaCl), which required more time and a high concentration of ferricyanide to reach complete desalination (i.e., the charge that must migrate/circulate to complete desalination is high). For this reason, in these cases, where the conductivity of the catholyte tank was higher, there was a greater transfer of water by osmosis from the saline compartment to the catholyte compartment, producing a decrease in water production. To avoid this effect, it is advisable to work with a much higher catholyte-saline volume ratio. In addition, it is essential to choose commercial ion exchange membranes that minimise the passage of water molecules. To support this result, **Table S-16** (in supplementary information) provides the EC and pH values for the saline, anolyte and liquid catholyte tanks at the beginning and the end of each desalination cycle.

Table 12 compares different desalination experiments with 3-chamber configuration MDCs, especially it compares the desalinated water production (i.e., final volume after water transport effect and NDR values) of this study with previous work. The initial desalination conditions, such as the catholyte strategy, the value of external resistance used, the volume ratio, and the initial salinity, are compared among studies **(Table 12)**. Moreover, some of the results obtained in this study are compared: the final desalinated water volume (after water transport effect), removal salinity and desalination rate, current densities reached, and the time employed in a desalination cycle, which can vary according to the criteria of the authors (end desalination cycle). The NDR parameter is shown when the calculation was possible (from the data available in the text).

Table 12 Comparison of desalination performances of 3-chamber configuration MDCs.

R_{ext} (Ω)	Cathode reaction	V_{an}:V_{sal} :V_{cat}*	Initial [NaCl] g L^{-1}	Initial EC (mS cm^{-1})	Final desalinated water (mL)	End desal. cycle	Removal salinity/Total desalination rate (% /mg NaCl h^{-1})	Max. current density* (mA cm^{-2})	Desal time* (h)	NDR* (L m^{-2} h^{-1})	ref
200	Ferricyanide	100:1:3 3	5	-	3	E_{cell} < 50 mV	88	-	-	-	(Cao et al., 2009)
			20	-			94	0.3	20-30	0.1	
			35	-			93	-	-	-	
200	Biocathode	11:1:9	35	52	39	1.50 g L^{-1}	92 (2.8 mg NaCl h^{-1})	0.76	450	0.04	(Wen et al., 2012)
	Air cathode	13:1:10				5.46 g L^{-1}	77 (2.3 mg NaCl h^{-1})	0.59			
	Ferricyanide	13:1:13				8.06 g L^{-1}	77 (2.2 mg NaCl h^{-1})	0.80			
1.5	Air cathode fed-batch	3:3:1	Cationic sol.	22.4	150	I = 0 mA	29	0.07	166	-	(Luo et al., 2012 a)
			Anionic sol.	17.5			24	0.25	71		
	Air cathode r-MDC a*	3.3:1: 3.3	Anionic sol.	17.5	150		90	0.26	110	-	
100	Air cathode	2:1:2	5	-	90	I < 0.05 mA	-	0.11	87	0.40	(Yang et al., 2015)
			20	-			-	0.12	65	0.55	
			30	-			-	0.13	55	0.65	

R_{ext} (Ω)	Cathode reaction	V_{an}:V_{sal} :V_{cat}*	Initial [Na Cl] (g L^{-1})	Initial EC (mS cm^{-1})	Final desalinated water (mL)	End desal. cycle	Removal salinity/Total desalination rate (% / mg NaCl h^{-1})	Max. current density* (mA cm^{-2})	Desal time* (h)	NDR* (L m^{-2} h^{-1})	ref
1	Ferricyanide	4:1:4	5	-	10	0.3 g L^{-1}	96	0.40	6.3	1.28	(Liang et al., 2016)
			10	-		0.2 g L^{-1}		0.80	7.8	1.02	
			20	-		0.5 g L^{-1}			22.0	0.36	
			40	-		1.3 g L^{-1}			47	0.17	
200	Biocathode	10:1:8	35	-	39	EC < 10 mS cm^{-1}	84 (3-2.2 mg h^{-1})	0.14	400	0.05	(Zhang et al., 2016b)
100	Air cathode	4:1:4	35	54	50	EC < 12.1 mS cm^{-1}	78	6.45 mA	72	-	(Ebrahimi et al., 2017)
0.5	Ferricyanide	2:1:2	10	17.7	125	-	> 99 (16.5 mg h^{-1})	0.47	73	-	(Ma and Hou, 2019)

R_{ext} (Ω)	Cathode reaction	V_{an}:V_{sal}:V_{cat}*	Initial [NaCl] (g L^{-1})	Initial EC (mS cm^{-1})	Final desalinated water (mL)	End desalcycle	Removal salinity/Total desalination rate (% /mg NaCl h^{-1})	Max. current density* (mA cm^{-2})	Desal time* (h)	NDR* (L m^{-2} h^{-1})	ref
1	Air cathode	-	35	53.2	32	Salt removal > 99%	> 99 (9.85 mg h^{-1})	0.26	120	0.2	(Rahman et al., 2021a)
2.5	Ferricyanide	6:1:6	1.3	2.5	370	EC = 1 mS cm^{-1} (0.5 g L^{-1})	63 (87.5 mg NaCl h^{-1})	0.58	3.5	10.6	This study**
		6:1:6	3.0	5.6	370		84 (117.5 mg NaCl h^{-1})	0.7	7.9	4.6	
		6:1:6	7.4	14	350**		93 (118.4 mg NaCl h^{-1})	0.8	21.6	1.6	
		12:1:12	18	28	370		97 (134.2 mg NaCl h^{-1})	0.9	47	0.6	
		6:1:12	18	29	320**		97.4 (210 mg NaCl h^{-1})	1.25	32.4	1.0	
		6:1:6	35	52	300**		98.6 (297.8 mg NaCl h^{-1})	1.6	43	0.7	
		17:1:17	40	58	370		98.7 (202.5 mg NaCl h^{-1})	1.1	71.5	0.5	

*Data calculated according to figures presented in corresponding articles. **Final actual volume of desalinated water at the end of a desalination cycle (after water transport effect). [a]*Anolyte-catholyte recirculation. The ratio V_{an}:V_{sal}:V_{cat} is calculated to consider the number of fed cycles necessary to one desalination cycle (V_{an}=anolyte volume, V_{cat}= catholyte volume, V_{sal}= saline water volume).

As shown in **Table 12**, extensive information in the literature on 3-chamber configuration MDC systems exists to compare results. However, these results may be disparate due to a lack of agreed criteria (such as the same criterion for ending a desalination cycle), making the comparison difficult between them. For this reason, the objective of this work was to carry out a systematic study of desalination at different salinities with the same criterion for the end of a desalination cycle (the final electrical conductivity of the salinity tank was equal to 1 mS cm^{-1}). Some of the lower values of the NDR parameter shown in **Table 12** may be due to air-cathode strategies where the potential available during the desalination process can be low compared to ferricyanide as a liquid cathode (Ramírez-Moreno et al., 2019). On the other hand, the low NDR values obtained using the liquid catholyte could be due to a high value of external resistance in the system (achieving a lower current density in the process) or the design of the device itself. In this work, assuming the effect of water transport during some cycles, the volume of final desalinated water is remarkable (almost 0.4 L).

6.3.2 Influence of anolyte buffer capacity on water production

A desalination cycle in these systems comprises the time necessary for the total or partial elimination of a specific initial salt concentration from the saline stream. The replacement of the anolyte and/or catholyte tank (electron donor and acceptor) without changing the saline tank is a feeding cycle.

The replacement of the anolyte and catholyte tank to perform the desalination process is a common strategy used in previous MDCs studies. For example, in Wen et al. (Wen et al., 2012), 39 mL of 35 g L^{-1} NaCl (initial EC = 50 mS cm^{-1}) was desalinated using a 10 - feeding cycle for one desalination cycle (11:1:9 V_{an}: V_{sal}:V_{cat}) with different catholyte strategies: biocathode, air cathode and ferricyanide (3-chambers, resistance external of 200 Ω). In this case, the anolyte (1.6 g L^{-1} acetate and initial pH = 6.5) and catholyte were replaced every 48 h, and the calculated NDR values in all 3 cases had the same value of 0.04 L m^{-2} h^{-}

[1] (without considering a specific final value of electrical conductivity in the saline compartment).

In the present work, the feasibility of the desalination of 35 g L^{-1} NaCl solution in one feeding cycle (6:1:6 V_{an}: V_{sal}: V_{cat}) is demonstrated, obtaining 10 times more production of freshwater (NDR = 0.7 L m^{-2} h^{-1}) **(see Table 12, Table S-15)** compared to the study mentioned above. In that case, the difference in freshwater production could be mainly due to the external resistance value used in the desalination process (200 Ω vs. 2.5 Ω), which affects the current density achieved (Ramírez-Moreno et al., 2021a).

However, the initial conditions of the feeding cycle have a notable influence on the MDC performance, even if the device design maximises freshwater production. In **Experiment 4 (see Table 11)**, a volume of 0.37 L with an initial salt concentration of 18 g L^{-1} NaCl (initial conductivity = 28 mS cm^{-1}) was desalinated using two feeding cycles (12:1:12 V_{an}:V_{sal}:V_{cat}) for total desalination. This desalination cycle started by recirculating a tank of 2 L of anolyte (20 mM acetate, 30 mM $NaHCO_3$, pH_i = 7.8, EC_i = 6.4 mS cm^{-1}) and 2 L of 0.04 M ferricyanide catholyte **(see Table 11)**. At 25 h, the anolyte and catholyte tanks were replaced with the same initial conditions (empty arrows in **Figure 55A**) to supplement the electron donor and acceptor. In **Experiment 5**, similar experimental conditions were used, but the $NaHCO_3$ concentration was increased to 60 mM (pH_i = 8.3, EC_i = 8.6 $mScm^{-1}$), and ferricyanide catholyte was 0.06 M. Only the catholyte tank was replaced in this case (coloured arrow in **Figure 55A**) for complete desalination. The final volume ratio for **Experiment 5** was 6:1:12 (V_{an}: V_{sal}: V_{cat}).

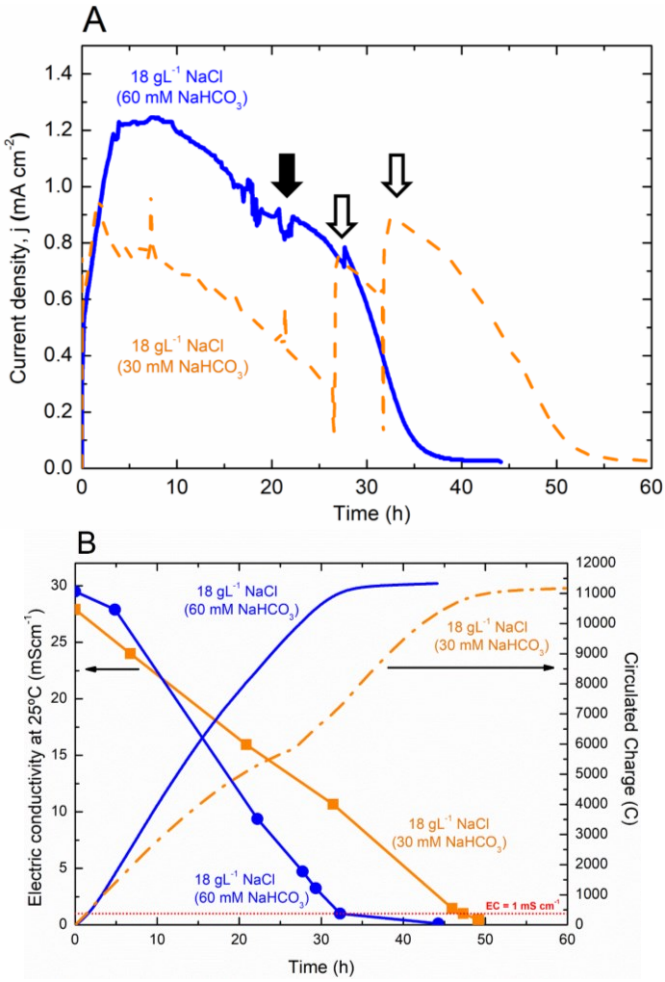

Figure 55. A) Current density **B)** Electrical conductivity (in the saline tank at 25 °C) and circulated charge vs. time during desalination cycles of **Exp. 4** (orange squares/dash-dot) and **Exp. 5** (blue circles/continue line) with an initial salt concentration of 18 g L^{-1} NaCl. **Figure A:** Arrows corresponding to the replaced catholyte tank in **Exp. 5** (coloured arrow) and replaced the anolyte and catholyte tank in **Exp. 4** (empty arrow). **Figure B**: The red dashed line marks the electrical conductivity value corresponding to 1 mS cm^{-1}.

Although the initial saline concentration of both experiments was the same (approximately 18 g L^{-1} NaCl), the maximum current densities in each case were different, as shown in **Figure 55A**. The maximum current densities reached were 0.9 mA cm^{-2} and 1.25 mA cm^{-2} for **Exp. 4** (discontinued orange line) and **Exp. 5** (continuous blue line), respectively. The highest current in **Exp. 5** could be due

to the higher initial conductivity and buffering capacity of the anolyte. Desalination cycles with a high initial salt concentration in the desalination chamber achieve a high current density in the first hours of the process (the system has no potential losses due to internal resistance). The ability to neutralise the protons from bacterial metabolism should be faster in those first hours. **Figure 55B** shows the difference in the charge circulation between the two experiments, where the experiment that obtained a higher current **(Exp. 5)** managed to reach the amount of charge circulated for total desalination in less time (approximately 11000 Coulombs for 18 g L^{-1} NaCl, see **Table S-15**) and consequently affected the drinking water production (0.6 L m^{-2} h^{-1} and 1.1 L m^{-2} h^{-1} for Experiments **4** and **5**, respectively). This difference is also reflected in the values obtained for the specific energy production (1.6 and 2.4 kWh m^{-3} for Exp. **4** and Exp. **5,** respectively), and the value of the treatment capacity (6.0 and 9.1 kg COD m^{-3} d^{-1} for Experiments **4** and **5**, respectively), as shown in **Table S-15**.

The better electrochemical behaviour of the anode in **Exp. 5** compared with that of **Exp. 4** is shown in the supplementary information, i.e., monitoring the anodic potential during the desalination process **(Figure S-58)** or the anodic polarization curves **(Figure S-59)**. This fact highlights the importance of the buffer in the medium to counteract the acidification of the biofilm during the process, especially in desalination with high salt concentration, in which high current densities could produce a greater production of protons from the oxidation of acetate and consequently acidification of the biofilm. Similarly, in previous works (Borjas et al., 2015), buffer bicarbonate addition to wastewater increased the current obtained in an MEC system while maintaining the constant electric conductivity in the anode compartment.

6.3.3 Influence of salinity on treatment capacity and energy production

The amount of acetate (and ferricyanide) used in this study was always in excess compared to the electric charge needed to perform the desalination

process. The calculation of theoretical charge as a function of the initial concentration of ions to desalinate is shown in **Table S-14**. The amount of acetate consumed experimentally (green circles) and the Coulombic efficiency (%) in each complete desalination cycle (i.e., $EC_{saline} < 1$ mS cm^{-1}) are shown in **Figure 56A**.

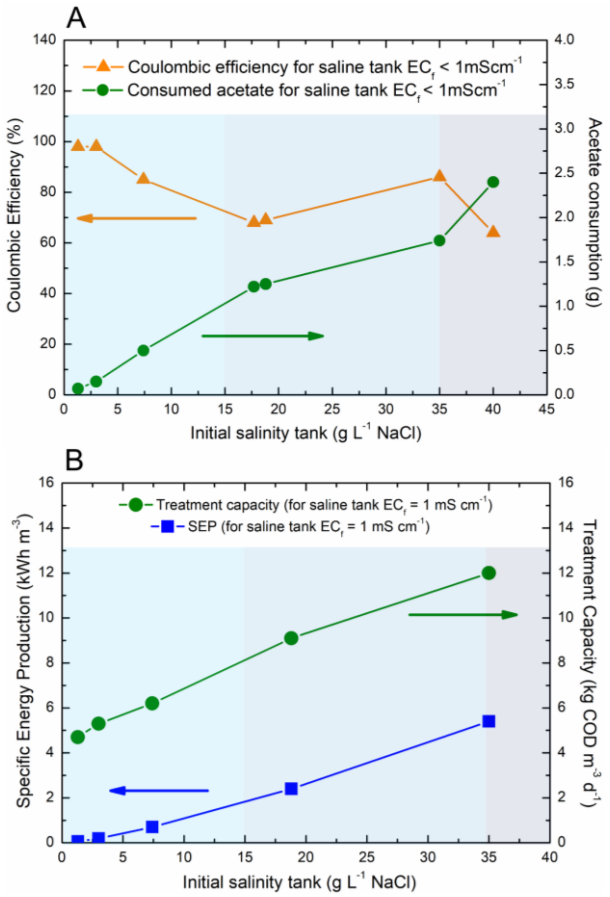

Figure 56. A) The Coulombic efficiency (%) and acetate consumption (g acetate) for each of the independent desalination cycles with different initial salt concentrations (1.3, 3.0, 7.4, 18, 18, 35, and 40 g L^{-1} NaCl). Experimental consumed acetate for $EC_{saline\ tank} <$ 1 mS cm^{-1} (green circle symbols); Coulombic efficiency for $EC_{saline\ tank} < 1$ mS cm^{-1} (orange triangle). **B)** Treatment capacity (kg COD m^{-3} d^{-1}; green circles) and specific energy production (kWh m^{-3}; blue squares) for each initial salt concentration for a final value of saline tank EC = 1 mS cm^{-1}. ***NOTE:** Treatment capacity values obtained according to the circulated charge for a final value of saline tank EC equal to 1 mS cm^{-1} (See **Figure S-60** in Supplementary Information).

A more significant amount of electric charge was required to achieve complete desalination for cycles with high initial salinities (18–40 g L^{-1} NaCl); then, the acetate consumption was higher. Concerning the Coulombic efficiency, it was almost 100% for low salinities (i.e., when the resistance of the saline compartment is high), while for higher initial salinities, the efficiency lowered to values between 68-86%. This adverse effect may be due to possible contamination of the anolyte tank by non-electroactive bacteria, which consume organic matter without electron transfer to the electrode during the long desalination cycle. Additionally, the electroactive behaviour of the anodic biofilm could be negatively affected by the accumulation of ions in the anolyte in those high initial salinity experiments (Yang et al., 2015).

The COD removal rate (kg COD m^{-3} d^{-1}) has been used to compare the treatment capacity results of this system with the literature values. This treatment parameter and the energy production achieved for each initial saline concentration desalination cycle are presented in **Figure 56B.** As a general trend, the treatment capacity and the energy production of the MDC system linearly increased as the salinity of the saline compartment increased (except in the case of 40 g L^{-1} desalination discussed below). For the desalination of 1.3 g L^{-1} NaCl, a COD removal rate of 4.7 kg COD m^{-3} d^{-1} was achieved (final saline tank EC = 1 mS cm^{-1}). In contrast, for desalination of 35 g L^{-1} NaCl, the COD removal rate achieved was 12 kg COD m^{-3} d^{-1}, indicating a great performance of MDC technology for the degradation of organic matter in the range of other reported microbial electrochemical systems for water treatment (Asensio et al., 2021b).

The energy production achieved (considering final saline tank EC = 1 mS cm^{-1}) is 0.064 kWh m^{-3} and 5.4 kWh m^{-3} for the desalination of 1.3 g L^{-1} and 35 g L^{-1} NaCl, respectively. These values indicate that it is possible to generate a significant amount of energy simultaneously with wastewater treatment and freshwater production (Qu et al., 2012), as indicated in the description of this technology.

6.3.4 Seawater desalination: Evolution in each feeding cycle

In **Experiment 7**, the complete desalination of 0.37 L with an initial salt concentration of 40 g L^{-1} NaCl was achieved (initial conductivity of the saline stream 58 mS cm^{-1}). This desalination cycle was started by recirculating a tank of 2 L of anolyte (20 mM acetate and 30 mM of $NaHCO_3$, pH_i = 7.7) with an initial conductivity of 6.2 mS cm^{-1} and 2 L of catholyte (0.04 M, 14.6 mS cm^{-1}) (see Supplementary Information, **Table S-16**). These tanks were replaced at 25 h to supplement the electron donor/acceptor, using three feeding cycles (17:1:17 V_{an}:V_{salt}:V_{cat}) for complete desalination (final saline EC = 1 mS cm^{-1}). Total desalination was achieved in 72 hours with a maximum current density of 1.0-1.1 mA cm^{-2} **(Figure 57A)**.

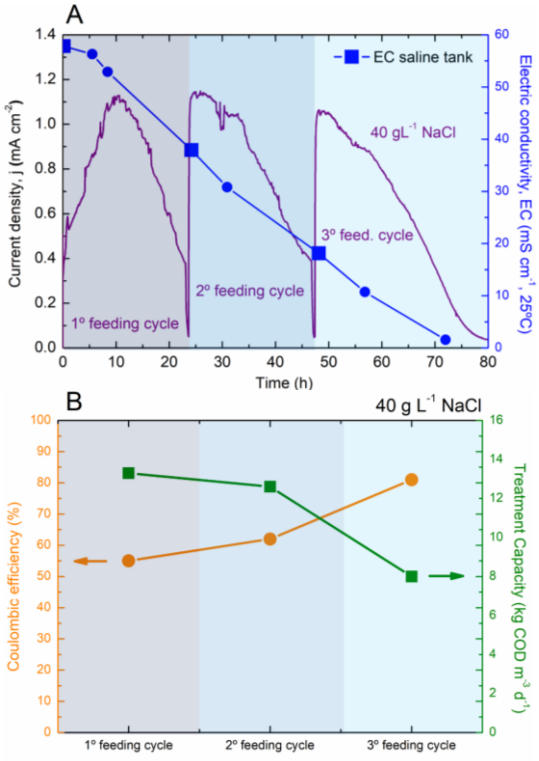

Figure 57. A) Current density (mA cm^{-2}) vs. time of desalination (h), and **B)** treatment capacity (kg COD m^{-3} d^{-1}) and Coulombic efficiency (%) for each feeding cycle in a 40 g L^{-1} NaCl desalination cycle.

Each feeding cycle could be considered an independent desalination cycle of 58, 38 and 18.1 mS cm^{-1} (blue squares, **Figure 57A**). The electrical conductivity in the saline compartment decreased by 19.8, 19.8 and 18 mS cm^{-1} for each of the feeding cycles. Although the system had different internal resistance in each feeding cycle, due to the desalination of the salinity stream, the maximum current density achieved was similar (1.1 mA cm^{-2} for the first and second feeding cycles and 1.0 mA cm^{-2} for the third feeding cycle). In that case, the current density appears limited by the internal resistance caused by adjacent anolyte and catholyte compartments (Liang et al., 2016).

The COD removal rate and Coulombic efficiency were calculated for each feeding cycle to discuss the evolution inside the system. In the first feeding cycle **(Figure 57B)** (high salinity in the saline compartment), a high COD removal rate (13.3 kg COD m^{-3} d^{-1}) was obtained with low Coulombic efficiency (55%). The COD removal parameter decreased in the following two feeding cycles, but the Coulombic efficiency increased (12.6 kg COD m^{-3} d^{-1}, 62% and 8 kg COD m^{-3} d^{-1}, 81% for the second and third feeding cycles, respectively). These results are similar to those obtained with the other desalination cycles of this study (low initial saline concentration, high internal resistance, low COD removal rates and high Coulombic efficiencies). The value of treatment capacity for the total desalination cycle in this experiment (7.6 kg COD m^{-3} d^{-1}) was less than that expected for a high salinity concentration desalination **(Table S-15)**. This fact indicates that operating conditions also have great importance regardless of the saline scenario for the MDC system.

The circulated charge through the external circuit for the three feeding cycles was similar (same current density for approximately the same time); therefore, the value of Coulombic efficiency is conditioned by the amount of substrate consumed in each feeding cycle **(Eq. 16, *Chapter 3*, section 3.3.3)**. A similar effect occurs in the work of Yuan et al. (Yuan et al., 2015), where the authors

argue that a higher organic loading rate might encourage the growth and metabolic activity of organisms other than exoelectrogens.

The Coulombic efficiency obtained in bioelectrochemical systems, in general, increases with power density because there is less time for the substrate to be lost through competing physical and biological processes (Logan and Regan, 2006a). However, in MDC systems, the anode receives significant chloride anions from the saline compartment that could initially affect the physiology of the electroactive anaerobic community of the anode (Mehanna et al., 2010b; Lefebvre et al., 2012). For this reason, the Coulombic efficiency in the first feeding cycle (first 24 h) could be adversely affected due to the punctual increase in the concentration of chlorides reaching the anode quickly. An increase in anolyte conductivity in each feeding cycle (due to chlorides from the saline compartment) was appreciable even using a volume ratio for each feeding cycle of 6:1:6 (V_{an}:V_{salt}:V_{cat}). For the first feeding cycle, the conductivity increase was 1.62 mS cm^{-1}, while for the second and third cycles, the increase was low: 1.45 mS cm^{-1} and 0.84 mS cm^{-1}, respectively.

6.4 Conclusions

This work achieved energy-free complete desalination for a wide range of initial salinities in a lab-scale MDC, thereby confirming their technical feasibility in possible natural salinities scenarios. The low external resistance value and potassium ferricyanide complex as catholyte allowed high values of freshwater production (NDR) similar to those found in other works reported in the literature under similar conditions. Accordingly, exploring paths towards the regeneration of redox mediators could bring this technology closer to implementation on real scale. The current efficiencies obtained (80 - 100 %) for the desalination of a range of 1 - 20 g L^{-1} of initial NaCl concentration indicate a proper operation of the MDC system. For higher initial NaCl concentrations, current efficiency over

100% shows a significant ion diffusion transport process that does not implicate electric charge circulation across the external circuit (i.e., diffusion).

The complete desalination of high saline streams requires a long desalination time, leading to higher water transport from the saline chamber to the cathode chamber due to the osmotic pressure between the two solutions, which decreases the production capacity of desalinated water. Therefore, to avoid this undesirable effect in batch modes, the volume ratio of the catholyte (which contained the charge necessary to complete desalination) compared to the saline solution should be increased. Due to the lack of agreed criteria to consider that a desalination cycle is complete, comparing the performance of the MDC systems reported in the literature could be difficult. Thus, more systematic studies under the same criteria should be carried out.

The initial conditions of the feeding cycles (electric conductivity and buffer capacity) had a notable influence on the MDC performance in the desalination of high salt concentrations. During the first hours of desalination (i.e., when the system reached high current densities), the anolyte buffer capacity was the key to proper anode operation to mitigate the acidification of bioanode. These initial conditions also affected the capacity for treatment and energy production, but in general, these parameters increased linearly with increasing initial salinity under study. Finally, the COD removal rate (or treatment capacity) and the Coulombic efficiency were calculated during the evolution of the MDC system in the seawater desalination cycle. A decrease in the Coulombic efficiency was shown at the beginning of the desalination experiment when the increase in the conductivity of the anolyte produced by chloride ions was significant.

From the point of view of future perspectives, MDC technology has a promising potential as a sustainable process for water desalination, compared to more conventional technologies of desalination, i.e., Reverse Osmosis or thermal processes. MDCs could be either employed as a stand-alone technology for distributed water treatment and recycle or integrated with the traditional

membrane-based Reverse Osmosis plants as strategy for reducing energy requirements by decreasing salinity of the feed water.

Nevertheless, there are some issues that should be addressed before the real practical application of MDCs, and then, future efforts should be focused in order to demonstrate the economic and technical feasibility of MDC technology, as for example membranes and electrodes development (including air diffusion cathodes), catholyte regeneration (when redox-mediators are used), capital and operation costs, and to find appropriate niches for MDC technology application.

In this sense, future works focused on described technology constrains will contribute to step forward toward the implementation of microbial desalination and bringing new ideas for a more sustainable future in the water sector.

Finally, while MDC technology development reaches pilot plant scale, validation at real scale could bring new information for subsequent design and optimization of commercial prototypes. For this reason, further efforts should also be focused on economic analysis of the proposed approaches, in order to provide insights for production of economically viable solutions based on MDC technology.

Supplementary data of ***Chapter 6***

Table S-13 General classification of saline water based on the electrical conductivity (EC) and salt concentration (g L^{-1}).

The salt concentration used in this study	Classification of salinity water	Salt concentration range	EC range	Application
g L^{-1} NaCl		g L^{-1}	mS cm^{-1}, 25 °C	
0.5	Fresh Water	0.5	0.8	Drinking water
1.3	Slightly brackish	1	1.7	Irrigation water
3.0	Medium brackish	1-5	1.7-8	-
7.4	Brackish	5-15	8-25	-
18 18	Strong brackish	15-35	25-58	-
35	Seawater	35	58	-
40	Brine	> 35	> 58	-

*Adapted and calculated from: (Saline Agriculture Worldwide).

Charge (C) calculation for one desalination cycle

This section presents an example calculation for estimating the necessary charge (theoric charge) to desalinate a determined initial concentration salt (1.32 g L^{-1} NaCl) until complete desalination (0.5 g L^{-1} NaCl ≡ EC = 1 mS cm^{-1}).

Table S-14 Calculations to obtain the theoretical charge associated with the initial concentration of NaCl (saline tank), added acetate (anolyte tank), and added potassium ferricyanide (catholyte tank).

Saline Information		Saline volume (tank + dead volume) (L)	0.37
		Pm NaCl (g mol^{-1})	58.44
		Cte Faraday (C mol^{-1})	96485
		mol e^-	1
Theorical charge equation: $\frac{\textbf{salt concentration } (\textbf{g L}^{-1}) \times \textbf{Saline volume (L)}}{\textbf{Pm NaCl } (\textbf{g mol}^{-1})} \times \frac{\textbf{mol}(\textbf{e}^-)}{\textbf{mol NaCl}} \times \textbf{Cte Faraday } (\textbf{C } (\textbf{mol e}^-)^{-1})$			
NaCl concentration (g L^{-1})	1.32	Necessary charge for total desalination (C)	805
	0.5	Necessary charge to desalination 1 mS cm^{-1} (C)	300
	0.82	Necessary charge for one desalination cycle (C) until 1 mS cm^{-1}	505

Anolyte Information		Anolyte volume (tank + dead volume) (L)	2.15
		Cte Faraday (C mol^{-1})	96485
		mol e^- (per mol of acetate oxidated)	8
Theorical charge equation: $\textbf{Acetate concentration } (\textbf{M}) \times \textbf{Anolyte volume (L)} \times \frac{\textbf{mol } (\textbf{e}^-)}{\textbf{mol acetate}} \times \textbf{Cte Faraday } (\textbf{C } (\textbf{mol e}^-)^{-1})$			
Sodium Acetate (M)	0.02	Theorical charge added (C)	33190

Catholyte Information		Catholyte volume (tank + dead volume) (L)	2.15
		Cte Faraday (C mol^{-1})	96485
		mol e-	1
Theorical charge equation: $[\textbf{Fe(CN)}_6]^{3-}\textbf{concentration } (\textbf{M}) \times \textbf{Catholyte volume (L)} \times \frac{\textbf{mol } (\textbf{e}^-)}{\textbf{mol } [\textbf{Fe(CN)}_6]^{3-}} \times \textbf{Cte Faraday } (\textbf{C } (\textbf{mol e}^-)^{-1})$			
$K_3[Fe(CN)_6]$ (M)	0.04	Theorical charge added (C)	7622

Table S-15 Experimental conditions and results for saline water desalination using the MDC lab setup.

Id.	Initial NaCl concentration	Current efficiency	Nominal desalination rate (NDR)*	Water transport	Circulated charge	Circulated electric charge (CEC)	Specific energy production (SEP)	COD removal rate	Coulombic efficiency
	g L^{-1}	%	L m^{-2} h^{-1}	%	C	kC m^{-3}	kWh m^{-3}	kg COD m^{-3} d^{-1}	%
1	1.3	82	10.6	0	613	1658	0.06	4.7	101
2	3.0	98	4.6	0	1574	4254	0.2	5.3	99
3	7.4	83	1.6	5.4	5054	13660	0.7	6.2	85
4	18	97	0.6	0	10788	29157	1.6	6.0	68
5	18	102	1.0	13	11021	29786	2.4	9.1	69
6	35	109	0.7	19	19402	52440	5.4	12	86
7	40	117	0.5	0	20359	55024	3.9	7.6	64

NOTE: All the experiments used: R_{ext} = 2.5 Ω; Q_t (initial saline volume) = 370 mL; and flow rate = 95 mL min^{-1}.

*Calculated considering the final volume of the saline tank (not the same as the initial volume due to the effects of osmosis).

The data shown were calculated for desalination up to a saline tank conductivity value of 1 mS cm^{-1} (corresponding to a concentration of 0.5 g L^{-1} NaCl) except for the Coulombic efficiency parameter.

Table S-16 Experimental data of pH and electric conductivity (EC). Initial (i) and final (f) values.

		Anolyte stream				Catholyte stream				Saline stream			
Id.	Tank replacement	pH_i*	pH_f	EC_i* (mS cm^{-1})	EC_f (mS cm^{-1})	pH_i*	pH_f	EC_i* (mS cm^{-1})	EC_f (mS cm^{-1})	pH_i*	pH_f	EC_i* (mS cm^{-1})	EC_f (mS cm^{-1})
1	N°1	8.6	7.8	6.7	6.5	6.7	5.4	14.4	14.4	6.4	5.9	2.5	0.04
2	N°1	8.6	7.8	6.5	6.8	5.4	6.4	14.3	14.8	6.0	6.6	5.6	0.1
3	N°1	8.0	7.9	6.2	6.9	6.0	8.2	13.3	13.9	6.4	5.9	13.9	0.05
4	Tank N°1	7.8	6.1	6.4	7.8	6.6	7.6	13.3	14.1	7.3	6.9	27.9	0.4
	Tank N°2	7.2	6.9	5.9	6.8	6.9	7.2	13.3	13.9				
5	Tank N°1	8.3	7.23	8.6	10.34	9.8	7.6	20.9	22.2	7.5	6.8	29.5	0.1
	Tank N°2					6.6	7.0	13.3	14.8				
6	N°1	8.8	7.3	12	16.6	9.9	7.2	54.4	54.6	6.4	7.2	51.5	0.6
7	Tank N°1	7.7	6.5	6.2	7.9	7.2	7.7	14.6	15.5	6.1	6.7	57.8	0.5
	Tank N°2	7.4	6.0	6.0	7.4	7.1	7.2	14.0	15.1				
	Tank N°3	7.4	6.8	6.2	7.0	7.1	7.1	13.5	14.5				

*All the initial values were taken when the tank solutions were recirculated for 10 minutes in MDC to collect a homogenous sample. Before recirculation of the solutions, the tanks were degassed and adjusted to neutral pH.

Different anode behaviours in desalination cycles of 18 g L^{-1} NaCl (Exp. 4 and 5)

Figure S-58 shows the anodic, cathodic, and cell potentials that were monitored during the desalination process of Experiments **4** and **5** (for the desalination of 18 g L^{-1} NaCl). The records make it possible to visualise, in real time, the electrochemical behaviour of the system and its evolution throughout the desalination process. Additionally, this monitoring is helpful to intervene in the event of a deterioration in the functioning of the system (increase in the value of the anode potential or decrease in the cathode potential). Additionally, the polarization curves for Experiments **4** and **5** under the corresponding initial conditions are shown **(Figure S-58)**.

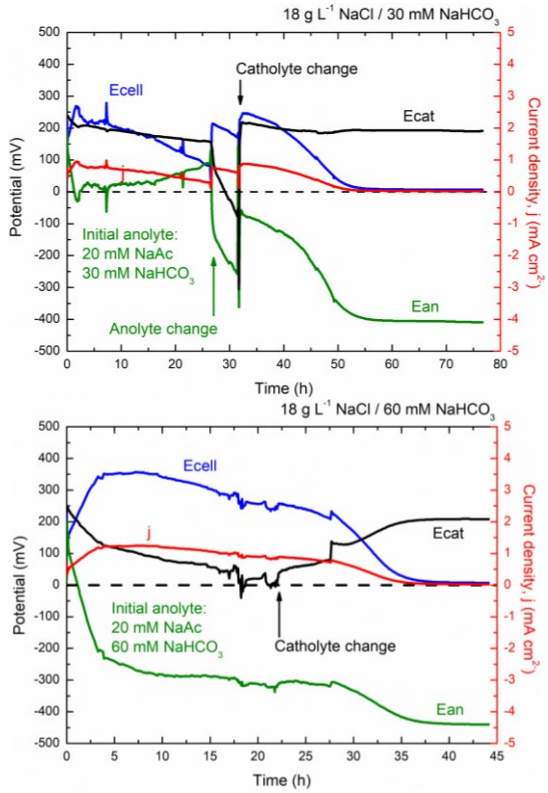

Figure S-58 Record of anodic, cathodic, and cell potentials during the desalination process of Experiments **4** (at the top) and **5** (at the bottom) for the desalination of 18 g L^{-1} NaCl. Additionally, the current density for each experiment is shown.

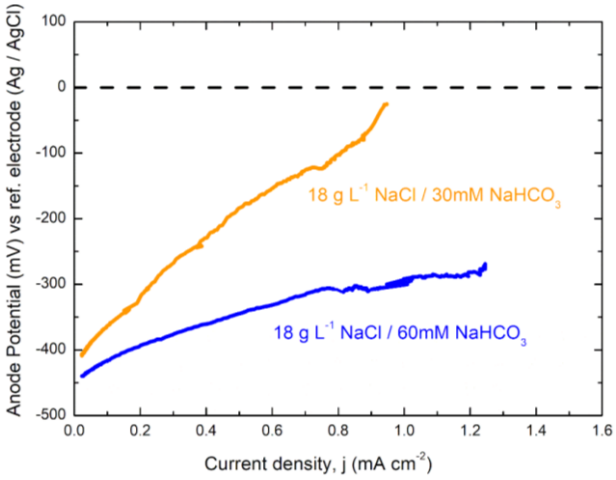

Figure S-59 Anode polarization curves for Experiments **4** (using 30 mM $NaHCO_3$) and **5** (using 60 mM $NaHCO_3$) for 18 g L^{-1} NaCl desalination.

Treatment capacity considerations

The value of the treatment capacity parameter (kg COD m^{-3} d^{-1}) depends on the time. In this study, it was considered that the treatment capacity value changes depending on the final salinity concentration considered for total desalination (in this study, a saline tank with final EC = 1 mS cm^{-1} was considered for a total desalination cycle).

Figure S-60 shows the experimental circulated charge through the external circuit during the desalination time for Experiments **1** and **6** (desalination of 1.3 and 35.0 g L^{-1} NaCl, respectively). For **Exp. 1** (graph on the left), if the desalination reaches a final electrical conductivity value in the saline tank of 0.04 mS cm^{-1}, the desalination time (td) is 22 h, and the load circulated through the circuit is 1011 C. In that case, the treatment capacity of the system is 1.2 kg COD m^{-3} d^{-1} according to the circulated charge. The COD analysis of the anolyte sample obtained at this time (t_d = 22 h) indicated an experimental value of 1.0 kg COD m^{-3} d^{-1}. However, if the desalination reaches a final value of electrical

conductivity in the saline tank of 1 mS cm^{-1}, the desalination time (t_d) is 3.5 h, the load circulated through the circuit is 613 C, and the treatment capacity of the system is 4.7 kg COD m^{-3} d^{-1} according to the circulated charge.

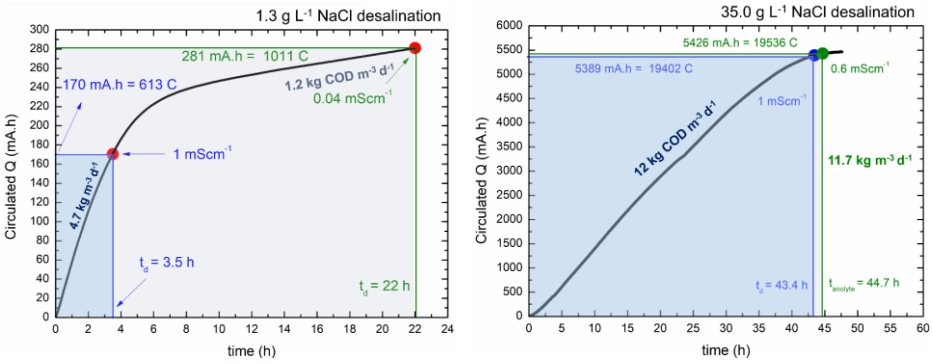

Figure S-60 Circulated charge vs. desalination time for **Experiment 1** (1.3 g L^{-1} NaCl) on the left and **Experiment 6** (35 g L^{-1} NaCl) on the right. The desalination times (td) are indicated (circles) for the different electric conductivity values achieved in the saline tank. According to circulated charge, the treatment capacity value is indicated when desalination ends in saline tank ECf = 1 mS cm^{-1} or ECf < 1 mS cm^{-1}.

For **Exp. 6** (graph on the right), the desalination reached a final electrical conductivity value in the saline tank of 0.6 mS $cm^{-1,}$ the desalination time (t_d) was 44.7 h, and the load circulated through the circuit was 19536 C. In that experiment, the treatment capacity of the system was 11.7 kg COD m^{-3} d^{-1} according to the circulated charge. The COD analysis of the anolyte sample (obtained in t_d = 44.7 h) indicated an experimental value of 13 kg COD m^{-3} d^{-1} (this value is higher than the value according to the circulated load because the Coulombic efficiency was lower in this experiment). If the desalination reaches a final value of electrical conductivity in the saline tank of 1 mS cm^{-1}, the desalination time (t_d) is 43.4 h, the load circulated through the circuit is 19402 C, and the treatment capacity of the system is 12 kg COD m^{-3} d^{-1}.


Dura
72 ms
500

Chapter 7

Screening of Real Wastewater for Use in Real Saline Water Desalination

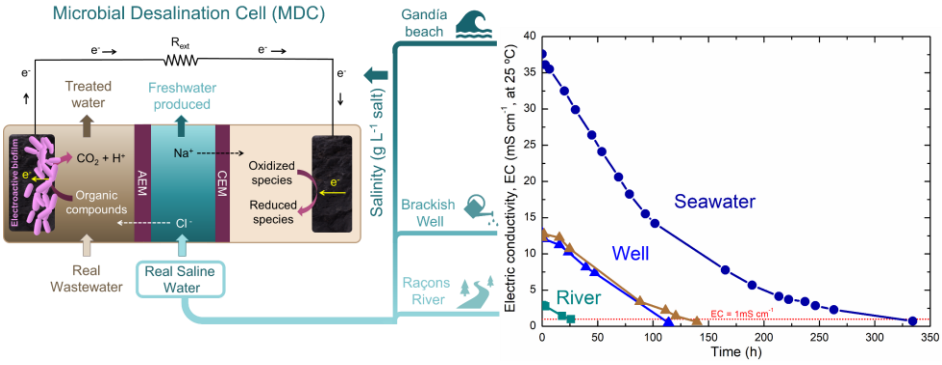

Chapter 7: Screening of Real Wastewater for Use in Real Saline Water Desalination

7.1 Introduction

As indicated in the literature (Yang et al., 2019a), it is difficult to compare the performance of reported MDC systems because various factors influence their performance, as we have seen throughout this thesis. These factors vary between different research groups and sometimes may not be sufficiently detailed in the publications. One of these variables is the actual wastewater and saline water used; the composition and characteristics of these real waters must be as optimal as possible because it defines the environment of the anode chamber where the electroactive microbial community is hosted. Therefore, this variable will directly affect the performance of the bioelectrochemical systems (including MDC systems) and exits divergences in the reported studies in the literature.

Some studies have used real wastewater (ww) from different source as MDC fuel: domestic ww. (Luo et al., 2012b, 2012c; Sophia and Bhalambaal, 2015; Zuo et al., 2018; Salman and Ismail, 2020), petroleum refinery ww. (Sevda et al., 2017), leachate from landfill (Iskander et al., 2018), sewage sludge (Meng et al., 2014; Ebrahimi et al., 2018b), steel plant ww. (Shinde et al., 2018), municipal ww. (Ebrahimi et al., 2018a) or dairy industrial ww. (Khazraee Zamanpour et al., 2017; Bejjanki et al., 2021). Although some of them have used real wastewater for the desalination of synthetic water (that is, using different initial concentrations of NaCl in deionized water), recent studies have reported the desalination of real saline water, such as real seawater with an initial conductivity of 41 $mScm^{-1}$ (Total dissolved solids (TDS) 32310 mgL^{-1}) (Bejjanki et al., 2021) or wetland saline water (initial TDS between 4000-15000 mgL^{-1})(Salman and Ismail, 2020) using real wastewater as fuel for the MDC system, achieving desalination efficiency of 93.7% and coulombic efficiency of 31.14%.

In general, the use of real water (both wastewater and saline) causes a decrease in the desalination performance (Yang et al., 2019a), as indicated in different reviews of MDC systems. This decrease in overall MDC system performance and the variability in results could be explained by the following factors:

- The availability of an easily oxidative substrate: real wastewater contains complex organic matter compared to the synthetic mediums used as recurrent fuel in laboratory with easier biodegradable substrates such as acetate. This major complexity of the fuel is reflected in low degradation rates in the bioelectrochemical systems. The most effective systems will be those tailored for each influent and effluent quality needs. For example, an anaerobic pre-digestion step could reduce the organic matter complexity (hydrolysis of complex organic matter into organic compounds such as volatile fatty acids) in the influent of a MET and thus enhance the performance of the bioelectrochemical reactor (as bioelectrogenic microorganisms degrade preferentially volatile fatty acids). In the case of MDC systems, for complete high saline concentration desalination, a high amount of electric charge from organic compounds oxidation is necessary. However, these higher organic matter concentrations can be results in a decrease in Coulombic efficiencies (defined as the electron recovery as electricity from the removed substrate) due to the stimulation of other microbial processes, such as fermentation and methanogenesis (Logan and Regan, 2006b; Freguia et al., 2007a) and, consequently, decreasing freshwater production.
- Solids or biomass amount: these solids and biomass can lead to clogging (scaling or biofouling) of electrodes or ion exchanges membranes. This fact promotes the competition of bacteria for space on the electrode: non-electrogenic bacteria attached to the electrode could occupy electrode space that electrochemically active bacteria could instead use. Apart of a possible discontinuity in the conductive network of the biofilm, this causes non-

desired reactions or competing processes in the biofilm or by planktonic biomass, such as methanogenesis or other electron acceptors (present in wastewater or even saline stream in the case of MDC) that could compete with the electrode as a final acceptor. This competing process when mixed cultures and complex substrates are used promotes low Coulombic efficiencies values in the range of 5-10 % (Pant et al., 2010; Speers and Reguera, 2012). In contrast, using well-buffered systems, simple compounds and pure electroactive cultures, the Coulombic efficiencies reported values up to 93 % (Speers and Reguera, 2012). In that sense, is interesting the goal of to be able to control these not desired metabolisms by maintaining certain environmental conditions at which electrogens outcompete the rest of the microbial community.

- The buffering capacity: high buffer capacity (Davis et al., 2013; Lu et al., 2016) must be present to overcome a decrease in pH in anode chambers. The production of protons at the vicinity of the anode could affect the viability of the electroactive biofilm if the diffusion within the biofilm is slow (Torres et al., 2008).
- The conductivity: the conductivity of real wastewaters is low compared to the synthetic media with high ionic content. This is one of the constraints of treating wastewater with electrochemical methods. The ohmic losses in these systems, related to the ion migration, are usually high and therefore the anode and cathode distance must be small to minimize this loss. In the specific case of MDC this conductivity could be increased during the desalination process (ion migration from saline chamber to anode chamber).
- Ion composition in saline water: In the case of MDCs, desalinating the ionic composition of the saline stream will affect desalination since, apart from chloride ions, ions such as nitrates or sulfates cross the anion-exchange membrane. The bacterial community can use them as final electron acceptors competing with the electrode.

In this context, the objective of this chapter was **i)** the screening of different available real wastewater as MDC fuel and ii) the verification of the feasibility of the MDC system at laboratory scale by using real saline water with the most adequate real wastewater. The optimal conditions would be used for the operation of pre-pilot scale MDC as part of the MIDES Project. The chapter can be divided in two blocks:

1) In the first block is shown the feasibility of desalination of synthetic brackish water (sodium chloride) with the use of several wastewater sources (industrial, municipal wastewater…) acting as anolyte of the system. The objective is the screening of real wastewater for the choice of one with the best characteristics for optimal desalination of real saline waters (i.e., the wastewater which would achieve the higher freshwater production, expressed as nominal desalination rate (NDR, L $m^{-2}h^{-1}$)).

2) In the second block is shown the feasibility of desalination of real saline water (river, brackish well and seawater) with the use of the most adequate real wastewater.

7.2 Experimental setup.

The microbial desalination cell device description, electrochemical equipment, analytical methods, start-up protocol as well as process parameters used in this study are described in ***Chapter 3 (section 3.3).***

7.2.1 Real desalination cycles

After the start-up protocol (Borjas Hernández, 2016; Borjas et al., 2017), described in ***Chapter 3*** (section 3.3.5) of this thesis, the MDC operates autonomously without any additional energy input for desalination. With this protocol, the inoculation and incubation of the lab scale MDC system with a culture of *Geobacter sulfurreducens* were carried out in 2017. Since that

incubation date, numerous desalination cycles have been carried out under synthetic conditions (both the anolyte and the saline), whose results have been shown in the previous ***Chapters*** (***4,5,6***). After this work period under synthetic conditions, the MDC system was first operated using real wastewater as an anolyte (fuel) to desalinate synthetic saline water (i.e., NaCl) **(Block 1 in Figure 61)**. It should be noted that the different wastewaters tested in the MDC system were not previously recirculated in the system before desalination. This means there was no acclimatization time for the biofilm to the residual water used as fuel. As a final part of this chapter, one of the types of real wastewater was used to real saline water desalination cycles (**block 2 in Figure 61**).

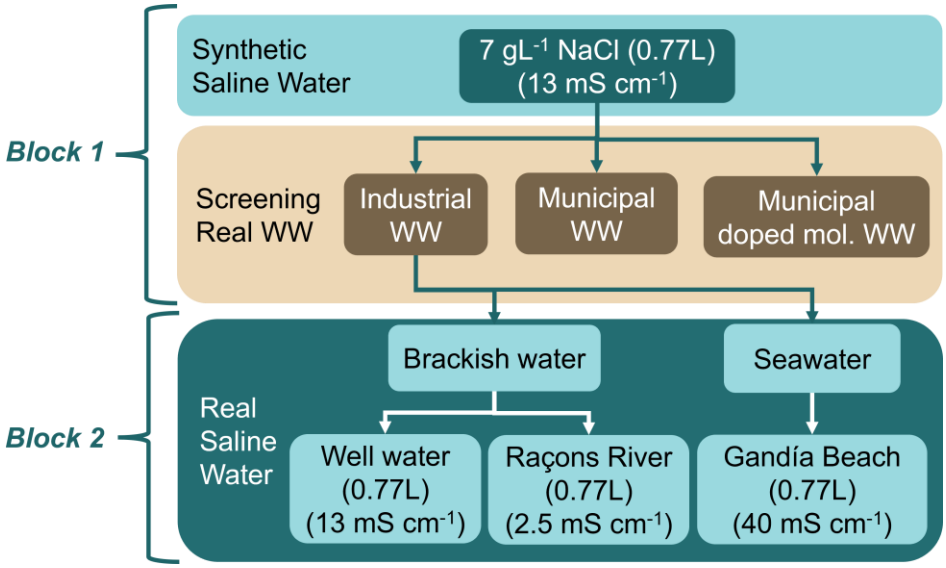

Figure 61. Chronological diagram or road map of desalination cycles followed for finding the optimal conditions in MDC. Divided in **block 1** and **block 2**.WW: wastewater; Municipal doped. mol.: Municipal doped with molasses wastewater.

Block 1: Screening of real wastewater through synthetic brackish water desalination

In this first block of experiments were carried out desalination cycles of synthetic brackish water (7 g L^{-1} NaCl) with different real wastewater acting as an anolyte in the MDC system.

The effluents of the **i)** anaerobic reactors treating municipal and **ii)** molasses-doped municipal (1% v/v) wastewater, and **iii)** the influent of the anaerobic reactor treating industrial (brewery) wastewater (non-digested) have been evaluated as feed for the lab-scale MDC with anode area of 100 cm^2. The municipal and molasses-doped municipal wastewater samples were collected from Chiclana, Cádiz (Spain) and the industrial wastewater samples were collected from the brewery plant Mahou-San Miguel in Alovera, Guadalajara (Spain), and stored at -4ºC until its use. This last wastewater samples were taken from the homogenization tank that feed the anaerobic digester of the brewery plant. **Table 17** collect the physicochemical parameters measured for different samples for each available wastewater type.

Table 17. Physicochemical parameters measured for the raw different wastewater samples.

Parameters	Municipal WW	Municipal + Molasses WW	Industrial WW
pH	7.5	4.4	6.5
EC (mS cm^{-1}, 25 ºC)	0.16	3.3	5.5
TOC (mg L^{-1})	18.1	2408	136
COD (mg L^{-1})	47.0-134	7500	344-3840
VFA (mg L^{-1})	71.1	4446	1000
Acetic acid (mg L^{-1})	36.4	1432	600
Turbity (NTU)	4.38	175	12.4
TSS (mg L^{-1})	3.08 – 73.3	92.4 - 345	41.4
Alkanility (mg L^{-1} $CaCO_3$)	423	315	1808
Cl^- (mg L^{-1})	224	400	540

NO_3^- (mg L^{-1})	n.d	n.d	n.d
NO_2^- (mg L^{-1})	n.d	4.67	n.d
SO_4^{2-} (mg L^{-1})	109	80.0	2.55
HCO_3^- (mg L^{-1})	516	384	2205
HPO_4^{2-} (mg L^{-1})	14.1	4.1	n.d
Na^+ (mg L^{-1})	154	257	1110
NH_4^+ (mg L^{-1})	67.2	22.8	6.75
K^+ (mg L^{-1})	20.6	251	20.2
Ca^{2+}(mg L^{-1})	86.2	230	20.6
Mg^{2+} (mg L^{-1})	19.2	43.7	6.55

*Analysis from external service analytical from IMDEA Water for report of MIDES project.

Synthetic brackish water (7 g L^{-1} NaCl; Volume= 0.77 L, EC=13 mS cm^{-1} at 25 ºC) was used as saline stream in this **block 1**. The initial salt concentration of 7 g L^{-1} of NaCl was chosen as brackish water model (because its complete desalination could be carried out in 24 hours). The following streams (1L) were fed into the anodic chamber of the MDC: **a)** pre-digested municipal wastewater, **b)** pre-digested municipal wastewater doped with molasses and **c)** (non-digested) industrial wastewater from a brewery. These real wastewaters were vacuum filtered before being fed to the MDC. The electrical conductivity of these waters was very low compared to the synthetic medium used in the laboratory. With the objective of comparing the MDC performance with the synthetic wastewater (FWM), bicarbonate buffer was added to the water to increase the electric conductivity (similar to the synthetic water used in previous chapters). This addition of buffer is a strategy used by other authors in their studies to neutralize the pH of the waters under investigation (Shinde et al., 2018). A 2 L solution with potassium ferricyanide in excess was used as catholyte. The use of liquid catholyte (potassium ferricyanide solution) allows the assessment of the performance and efficiency of the MDC device without the limitation imposed by the potential available by the cathode. The ratio of the volume ($V_{anolyte}$: V_{saline}: $V_{catholyte}$) in these experiments was 1.5:1:2.8.

The experimental conditions of this **block 1** are summarized in **Table 18.** The results of these tests were compared to those carried out with synthetic wastewater (freshwater medium with acetate as only electron donor) as anolyte.

Table 18 Initial conditions of anolyte, saline stream and catholyte for the four different desalination cycles using municipal, municipal doped, industrial and synthetic wastewater.

ANOLYTE				
Type of wastewater	Municipal WW	Municipal doped molasses WW	Industrial WW	Synthetic WW
Initial COD (mg L^{-1}) *	922	6550	1232	1170
Initial [Acetic] (mg L^{-1}) *	244	1199	662	1138
pH Raw water	7.55	4.12	7.6	-
EC (mS cm^{-1}, 25 ºC) Raw water	1.3	3.4	4.9	-
pHi*	7.6	7.2	7.7	7.7
ECi (mS cm^{-1}, 25 ºC) *	7.7	8.2	8.7	8.9
Anolyte Volume **	1150 mL			2150 mL
SALINE STREAM				
Type of saline water	Synthetic Brackish Water			
Saline Volume **	0.77 L			
Initial saline concentration	7 g L^{-1} NaCl			
Initial EC (25 ºC)	13 mS cm^{-1}			
CATHOLYTE				
Type of catholyte	$K_3[Fe(CN)_6]$			
Molar concentration (M)	0.06			
Catholyte volume	2150 mL			
GENERAL PARAMETER				
$V_{anolyte}$: V_{saline}: $V_{catholyte}$ **	1.5:1:2.8			2.8:1:2.8
R_{ext} (Ω)	2.5			
Flow rate	95 mL min^{-1}			

NOTE: the initial conditions have been added of a reference desalination cycle using synthetic solutions to compare the performance of the MDC device with the use of real solutions or synthetic solutions. *Collected sample after adding $NaHCO_3$ and 10 min recirculation in MDC system for the homogenisation. ** In the $V_{anolyte}$: V_{saline}: $V_{catholyte}$ volume ratio, the dead and chamber volumes have been considered.

***Block 2:* real saline water desalination with the adequate real wastewater**

In this second block of experiments, desalination cycles were carried out with different real saline water using the most adequate wastewater as anolyte in the MDC system (fuel).

The physicochemical parameters measured for the three raw saline streams are collected in **Table 19.** For these desalination cycles the following streams (with a volume of 0.77 L) were vacuum filtered previously to use as a saline solution. The brackish water streams were collected from a river and well Denia (Comunidad Valenciana, Spain), and seawater from Gandía beach (Comunidad Valenciana, Spain). As anolyte, 5 L of vacuum-filtered industrial wastewater (from a brewery) were used. To compare the MDC performance with the previous initial conditions in **block 1** bicarbonate buffer was added to the water to increase the electric conductivity (similar to the synthetic water used in previous chapters). Finally, 2 L of an excess of potassium ferricyanide solution were used as catholyte for the MDC device. The initial conditions of each of the desalination cycles carried out in this **block 2** are indicated in **Table 20**.

Table 19. Physicochemical parameters measured for the raw saline stream.

Parameters	Raçons River	Well Brackish water	Seawater
pH	7.93	8.41	8.40
Conductivity (20 ºC) mS cm^{-1}	2.75	11.51	40.20
TSS (mg L^{-1})	73.3	18.3	170
TOC (mg L^{-1})	1.90	6.31	<1
COD (mg L^{-1})	8.10	44.0	-
Turbity (NTU)	31.7	4.86	16.5
Alkanility (mg L^{-1} $CaCO_3$)	159	561	106
F^- (mg L^{-1})	n.c	n.c	n.c
Cl^- (mg L^{-1})	797	3108	15075
NO_3^- (mg L^{-1})	5.53	173	n.c
NO_2^- (mg L^{-1})	n.c	n.c	n.c
SO_4^{2-} (mg L^{-1})	114	2752	2924
HCO_3^- (mg L^{-1})	193	685	119
HPO_4^{2-} (mg L^{-1})	n.c	n.c	n.c
Na^+ (mg L^{-1})	441	1978	9102
NH_4^+ (mg L^{-1})	n.c	n.c	n.c

K^+ (mg L^{-1})	17.6	24.1	301
Ca^{2+}(mg L^{-1})	95.9	583	325
Mg^{2+} (mg L^{-1})	55.5	478	1051

*Data included in technical reports of MIDES project. Analysis performed by Water Analysis Lab Unit of IMDEA Water.

Table 20. Initial conditions of anolyte, saline stream and catholyte for the four different desalination cycles using municipal, municipal doped, industrial and synthetic wastewater.

SALINE STREAM				
Type of saline water	Raçons River	Well Brackish Water	Well Brackish Water (r)	Seawater (Gandia beach)
Saline Volume (mL)	0.77			
Initial salt concentration (g L^{-1}) *	1.6	7.8	9.2	24.4
Initial EC (mS cm^{-1} 25 ºC) *	2.8	12.2	12.8	37.6
ANOLYTE				
Type of wastewater	Industrial WW			
COD (mg L^{-1}) of filtered raw water	1453	1996	3452	-
Initial pH of filtered raw water	7.04	7.3	6.68	-
Initial EC (mS cm^{-1}, 25 ºC) of filtered raw water	3.25	3.38	2.92	-
COD (mg L^{-1})*	1498 *a	2110	3212	7883**
Initial pH *	8.08	8.69	8.2	8.04
Initial EC (mS cm^{-1}, 25 ºC)*	7.44	7.66	7.51	7.57
Anolyte Volume (mL)	5150			
CATHOLYTE				
Type of catholyte	$K_3[Fe(CN)_6]$			
Molar concentration (M)**	0.06 M	0.1 M	0.1 M	0.2 M
Catholyte volume (mL)	2150			
GENERAL PARAMETER				
$V_{anolyte}$: V_{saline}: $V_{catholyte}$*	6.7:1:1.6			
R_{ext} (Ω)	2.5			
Flow rate (mL min^{-1})	95			

NOTE: Volume ratio, the dead and chamber volumes have been considered. *An Organic acids measurement as acetic acid (799 mg L^{-1}). *Collected initial sample after adding $NaHCO_3$ (in anolyte case) and 10 min recirculation in MDC system for the homogenisation. **Concentration anolyte/catholyte required to complete the desalination cycle (final EC saline tank = 1mS cm^{-1}).

All the desalination cycles were performance under the same external resistance value (2.5 Ω) and flow rate of tanks recirculation (95 mL min^{-1}). The system was operated at 30°C, maintaining anaerobic conditions in the anolyte

tank during the experiment. The conductivity of saline tank was measured during the desalination process. In the cases where is achieved the complete desalination, the total time for the desalination was determined when saline tank conductivity was equal or below 1 mS cm^{-1}. Initial anolyte and catholyte samples were collected after 10 min of recirculation through the MDC system to homogenisation. Final anolyte and catholyte sample were collect at the end of desalination cycle (final EC saline tank = 1mS cm^{-1}). The samples were kept at 4 ^{0}C until analysis. (***Chapter 3,*** section 3.3.6).

7.3 Results

7.3.1 **Block 1:** Screening of real wastewater

In this **block 1,** the effluents of the anaerobic reactors treating **i)** municipal and **ii)** molasses-doped wastewaters and the **iii)** influent of the anaerobic reactor treating industrial (brewery) wastewater have been evaluated as feed for the MDC at lab-scale (anode area of 100 cm^2).

From the initial analysis of the different samples of wastewaters (**Tables 17 and 18**), it is important to remark:

- the residual water with the lowest pH is the wastewater doped with molasses, while the water with a higher conductivity is the industrial wastewater.

- the water with higher concentration of COD and volatile fatty acids (including acetic acid) is water doped with molasses. Conversely, municipal wastewater has the lowest concentration of organic matter.
- The industrial wastewater has a significant buffer capacity compared to the other streams. The one with the least buffer capacity is water doped with molasses.
- No concentration of nitrates was detected in the samples, and a appreciable concentration of sulphates was obtained in municipal waters.

The conductivity of the saline tank over time for each of the desalination with different types of wastewaters is shown in **Figure 62**. Also, the initial COD concentration available in the different wastewater as well as the water production value (Nominal Desalination Rate, NDR, L m^{-2} h^{-1}) achieved for each desalination cycle is shown.

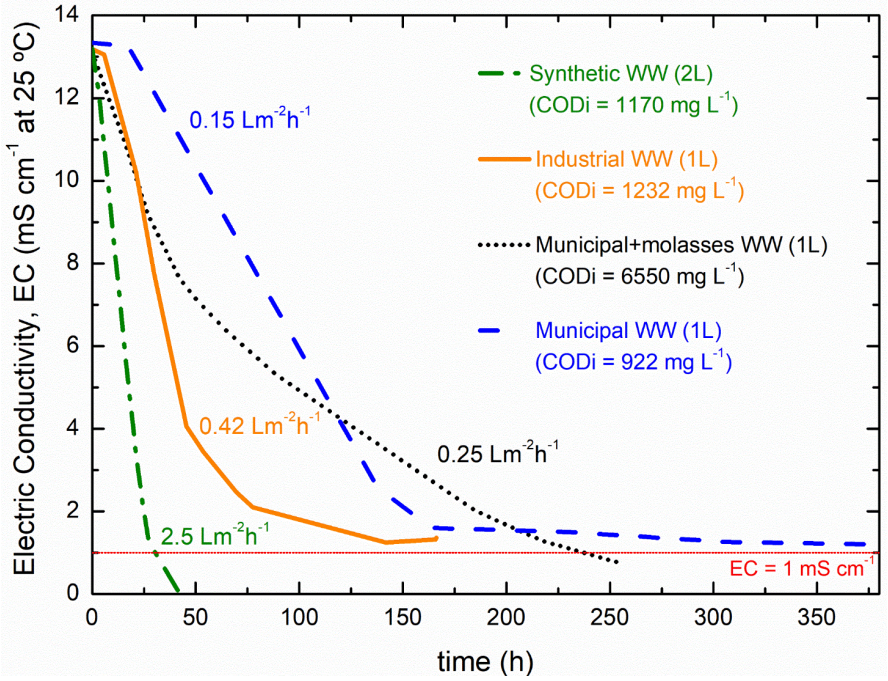

Figure 62. Evolution of electric conductivity (EC at 25 ºC) for each saline tank with the desalination time, using different types of wastewaters as anolyte. Values of NDR (L m^{-2} h^{-1}) are added for each experiment. Red line marks the value of EC saline tank equal to 1 mS cm^{-1}.

In all desalination cycles, NaCl removal exceeds 90%, and current efficiency exceeds 94%. The green dash-dotted line represents the MDC performance in desalinating 7 g L^{-1} NaCl (0.77L) using synthetic water (only acetate as an electron donor) as an anolyte. This curve shows how the cell behaves under controlled conditions compared to the other waters.

Using municipal WW (blue dashed line) or industrial WW (orange line) acting as anolyte, complete desalination could not be achieved (if we considered

a final EC of tank saline solution equal to 1 mS cm^{-1} as complete desalination). On the other hand, municipal water doped with molasses (black dotted line) achieves complete desalination below 1 mS cm^{-1} for the conductivity of the saline stream, as occurs in the desalination cycle using the freshwater medium (only acetate as electron donor) as an anolyte (green dot-dash line). However, although desalination is almost complete using any wastewater, there is a difference in the time used for each desalination cycle. Desalination rates using real wastewater as feed to the MDC bioanode were 5 times lower than those achieved with synthetic media (2.5 L m^{-2} h^{-1} nominal desalination rate, NDR).

The highest water production value, 0.42 L m^{-2} h^{-1}, obtained with real industrial wastewater (from the brewery industry), is the most similar to synthetic water (total desalination time approximately 27 hours). During the desalination process, the maximum current density obtained by the MDC system was 0.5 mA cm^{-2} (**Figure 63**, **table 22**). In this sense, this industrial effluent could be optimal regarding the amount of organic matter (COD = 1232 mg L^{-1}), of which almost half is in the form of volatile fatty acids such as acetic acid to be oxidised for desalination without predigestion. Furthermore, this water has a high buffering capacity (even before adding a buffer to increase the conductivity), so the biofilm performance is not affected by pH changes during the process. Therefore, the real residual water that is optimal for the performance of the MDC is industrial water (brewery), with which the following experiments have been carried out in **block 2.**

However, when desalination is performed with municipal wastewater, the desalination time is significantly increased compared to synthetic water and the lowest water production is obtained (0.15 L m^{-2} h^{-1}). This type of water has less volatile fatty acids, such as acetic acid, and a lower buffering capacity than industrial wastewater. In addition, the sulfate content shown in the analysis of these raw municipal waters could be interfering with the behaviour of the system. This translates into a lower current density during the desalination process (0.25

mA cm^{-1}) and which can cause retro-diffusion effects due to the low current densities reached. On the other hand, if this same municipal water is used but doped with molasses, the biofilm performance is affected by the acidic pH that this water contains (even if the buffer has been added from the beginning, the final pH of the anolyte sample has an acidic pH (**table S-22**), despite having a large amount of organic matter (COD_i = 6550 mg L^{-1}). However, for this desalination cycle, a current density similar to that of industrial water is reached (**Figure 63**), and then drops rapidly in the first hours of desalination. Given the COD content, better performance of the MDC with molasses-doped municipal wastewater was expected compared to the industrial stream. This fact can be explained by the buffering capacity and acidification of the anolyte, which plays a crucial role in desalination.

In general, the low coulombic efficiencies (approx. 23-53%) are comparable with the literature using real wastewater to desalinate synthetic wastewater conditions (Salman and Ismail, 2020), and specific energy production (0.1-0.3 kWh m^{-3}) and treatment capacity (0.7 - 4.9 kg COD m^{-3} d^{-1}) values obtained are lower compared to synthetic water (72% coulombic efficiency, 0.8 kWh m^{-3} and 8 kg COD $m^{-3}d^{-1}$) (**Table S-23**).

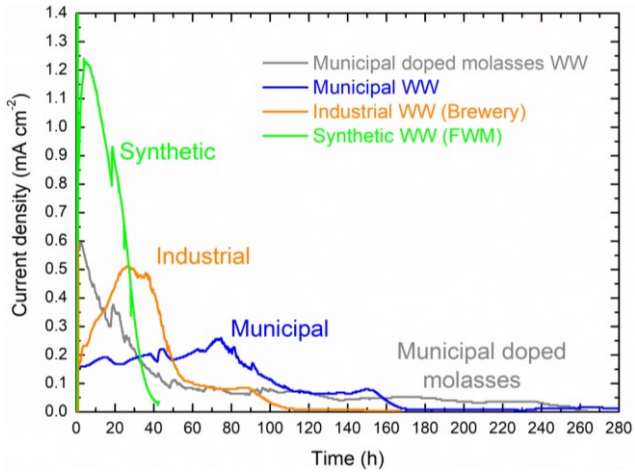

Figure 63. Current density vs the desalination time, using different types of wastewaters as anolyte.

7.3.2 **Block 2:** real saline water desalination with the adequate real wastewater

The final step, shown in this **block 2**, was desalinating different real saline solutions using the industrial wastewater (from the brewery) as an anolyte which offered the best performance in the synthetic brackish water desalination (screening of **block 1**). MDC system completed desalination (final EC saline tank below 1 mS cm^{-1}) of the three different saline streams with different initial compositions using industrial wastewater as anolyte. The following graph (**Figure 64**) shows the evolution of conductivity versus time for the four different desalination cycles: actual river water, real brackish well water and natural seawater.

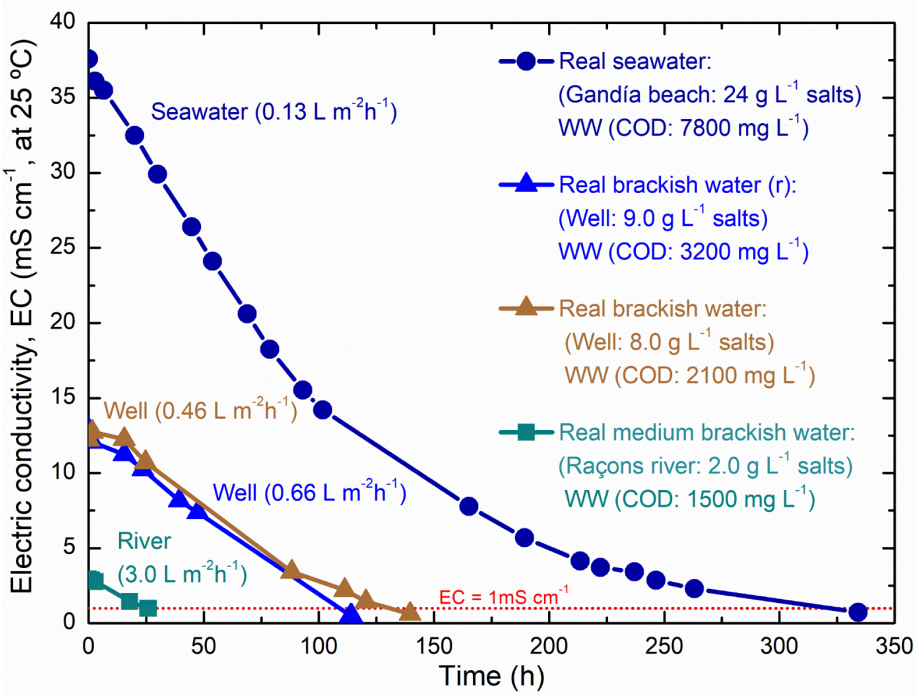

Figure 64. Evolution of electric conductivity (EC mS cm^{-1} at 25 ºC) in saline tank with the desalination time, from desalination cycle with different types of real saline water using industrial wastewater as anolyte.

The river water desalination (initial conductivity of 2.8 mS cm^{-1}), using industrial wastewater with an initial COD of 1500 mg L^{-1}, was completed in 26 hours (**table 21**), and a high nominal value (3 L m^{-2} h^{-1}) was achieved.

On the other hand, the desalination of brackish water from well (12.2 mS cm^{-1}) was achieved in 129 hours with an initial COD of 2100 mg L^{-1}. This last desalination was repeated to carry out a replica experiment with similar initial conductivity of the brackish water from the well (12.8 mS cm^{-1}). In this desalination industrial wastewater had higher initial COD concentration (3200 mg L^{-1}). In both experiments similar NDR values was achieved (0.46 and 0.66 L m^{-2} h^{-1} respectively). Although both desalination cycles reached almost the same current density (0.88 - 0.9 mA cm^{-2}) **(Figure 65)**, the lower value of 0.46 L m^{-2} h^{-1} could be due to osmosis effects caused by the high concentration of catholyte used at the beginning of desalination (**table S-22**) compared to initial conditions of the other desalination cycle (0.66 L m^{-2} h^{-1}) where the osmosis effect is less pronounced. In addition, the available initial COD concentration is lower in the experiment where a lower value was obtained (0.46 L m^{-2} h^{-1}). If we compare these values obtained for the desalination of real brackish water from well (initial conductivity of 12.2 - 12.8 mS cm^{-1}) with the results obtained in **block 1** in synthetic water desalination (13 mS cm^{-1}) using industrial water as anolyte, we can see the similarity of the results obtained in the production of desalinated water (**table 21**).

Finally, the desalination of seawater (37 mS cm^{-1}) was completed in approximately 304 hours, being the necessary initial COD of 7800 mg L^{-1} to complete desalination. As we have already seen in this thesis (***Chapter 6***), in desalination with high initial saline concentrations, the value obtained for desalinated water production was the lowest (**Table 21**).

As in all desalination processes, an excess of substrate and catholyte has been used to complete desalination; the maximum current density reached in each

cycle increases as the initial conductivity of the saline stream increases (internal resistance in the system imposed by the saline compartment decreases).

In general, the low coulombic efficiencies (approx. 10-30%) are comparable with the literature using real wastewater to desalinate real saline water (Salman and Ismail, 2020), specific energy production increase with the initial saline concentration (0.16 - 2.54 kWh m^{-3}) (as it was discussed in ***Chapter 6***) and treatment capacity (19 - 42 kg COD m^{-3} d^{-1}) values obtained are higher compared to previous desalination cycles (**block 1**) (**Table S-23**). This high treatment capacity is according to low coulombic efficiencies values (Salman and Ismail, 2020) due to removal substrate by non-electroactive bacteria and other processes.

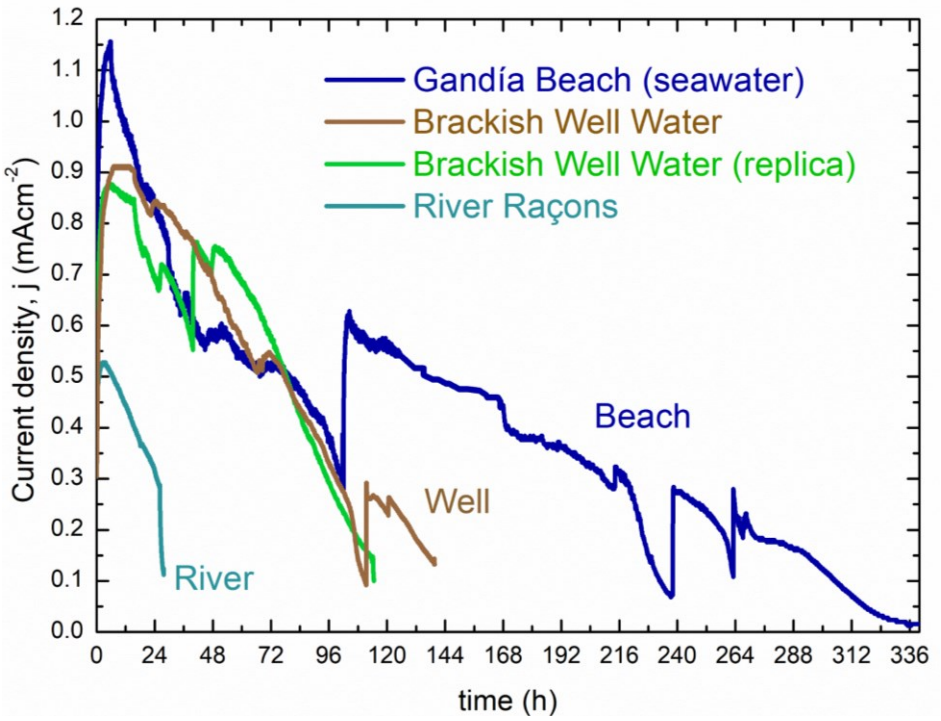

Figure 65. Current density vs the desalination time, using different types of wastewaters as anolyte.

Table 21. Summary of results from lab-scale MDC performance with real wastewaters **(Block 1)** and real saline water **(Block 2).**

	Wastewater type	Saline water type	Initial EC saline tank (mS cm^{-1})	Final EC saline tank (mS cm^{-1})	$j_{máx}$ (mA cm^{-2})	T_d (h)	NDR* (L m^{-2} h^{-1})
BLOCK 1	Synthetic WW (2L)	Synthetic brackish water (0.77L)	13	1	1.10	42	2.5
	Industrial WW (1L)			1.2	0.50	142	0.42
	Municipal doped molasses WW (1L)			1	0.60	256	0.25
	Municipal WW (1L)			1.2	0.25	376	0.15
BLOCK 2	Industrial WW (5L)	Raçons River (0.77L)	2.8	1	0.50	25.4	3.0
		Brackish well (0.77L)	12.2	1	0.9	129	0.46
		Brackish well (r) (0.77L)	12.8	1	0.88	102	0.66
		Seawater (0.77L)	37.6	1	1.15	304	0.13

*Take account the final saline volume (after osmosis effect during desalination process). (r): experiment replica for real brackish well desalination cycle.

7.4 Conclusions and future works

MDC system has completely desalinated synthetic and real salt water with different real wastewater used as fuel without any external energy input. The main difference between the desalination cycles carried out in this chapter is the value of the freshwater production, which varies according to the initial operating conditions, such as the composition of the wastewater (**block 1**) or the initial concentration of salts in the saline stream **(block 2).** As the literature indicates (Yang et al., 2019a), parameters such as desalination efficiency, coulombic efficiencies or COD removal decrease when real water is compared with synthetic water.

With the results obtained in **block 1** (screening of wastewater for acting as anolyte), we proposed that the type of industrial wastewater (from a brewery) was the most suitable to act as an anolyte since it showed a better freshwater production value (0.42 L m^{-2} h^{-1}) for synthetic brackish water. This value was obtained possibly for two reasons: the high available amount of easily oxidizable organic matter (without pre-digestion) and the high buffering capacity for the good performance of the biofilm compared to the other proposed wastewater sources. This type of wastewater was used to validate the pre-pilot and pilot MDC system (a task inside the MIDES project). As we can see in **block 2**, with industrial wastewater, MDC devices can desalinate a wide range of initial salt concentrations in a real saline matrix, where high salinity concentrations require a large amount of initial COD to achieve complete desalination.

It is important to note that these desalinated water production values are calculated for desalination up to 1 mS cm^{-1} of electrical conductivity in the saline stream to compare all the experiments. However, for its use as a pretreatment of reverse osmosis, as suggested in the literature (Mehanna et al., 2010c), this final

conductivity value may be higher (only a pre-desalination, not complete desalination), with which the NDR values may increase.

As future work in this part of the use of real water in the MDC system, it will be the deepening of several aspects: the repercussion in the performance of the system of the majority ions of the real solutions. The study of the structural change in the anodic microbial populations at the beginning and the end of a desalination cycle with a high saline concentration (seawater, for example) where the anolyte solution will suffer an increased change in the electrical conductivity. And finally, the behaviour of the MDC system with the use of industrial brewery water with an ultrafiltration pretreatment would avoid biomass contamination of wastewater.

Supplementary data of Chapter 7

Table S-22. Initial and final values of pH and electric conductivity of the anolyte, catholyte and saline stream for each desalination cycle.

Id.	Anolyte stream				Catholyte stream				Saline stream			
	pH_i	pH_f	EC_i (mS cm^{-1})	EC_f (mS cm^{-1})	pH_i	pH_f	EC_i (mS cm^{-1})	EC_f (mS cm^{-1})	pH_i	pH_f	EC_i (mS cm^{-1})	EC_f (mS cm^{-1})
Real Wastewater screening												
Synthetic WW	7.70	6.92	8.99	10.09	7.45	7.50	23	23.20	5.76	5.40	13.19	0.072
Industrial WW	7.68	7.29	8.72	10.85	8.27	6.62	18.31	18.72	6.32	6.74	13.18	1.2
Municipal+ molasses WW	7.2	4.01	8.16	10.7	7.4	-	18.46	-	5.35	-	13.06	0.7
Municipal WW	7.6	6.27	7.7	10.5	8.02	6.74	18.13	18.07	6.67	5.94	13.26	1.2
Real saline water desalination												
Raçons River	8.08	7.93	7.44	7.33	9.0	8.61	24.1	23.9	7.72	8.55	2.83	0.97
Brackish well	8.69	8.03	7.66	5.71	8.57	8.83	40	44.2	7.12	8.81	12.17	0.62
Brackish well (r)	8.20	8.28	7.5	6.67	8.39	7.68	21.9	39.4	8.08	8.5	14.37	0.51
Seawater	8.04	7.82	7.57	2.77	9.55	-	60.9	-	7.9	7.79	37.6	0.07

*Initial samples (i) were collected after 10 min circulating in the MDC system for homogenization. EC (mS cm^{-1}) measured at 25ºC.

Table S-23.Initial and final values of pH and electric conductivity of the anolyte, catholyte and saline stream for each desalination cycle.

Real Wastewater Type	Real Saline type	CEC (kC m^{-3})	Current efficiency (%)	Coulombic efficiency (%)	SEP (kWh m^{-3})	Treatment Capacity (kg COD m^{-3} d^{-1})
Synthetic WW (2L)	Synthetic brackish water (0.77L)	11095	94	72	0.8	8
Industrial WW (1L)		10514	103	53	0.3	2.6
Muni. doped mol. WW (1L)		10976	99	23	0.2	4.9
Municipal WW (1L)		11515	94	-	0.16	0.7
Industrial WW (5L)	Raçons River (0.77L)	5096	34	20	0.16	22
	Brackish well (0.77L)	33454	32	30	1.67	19
	Brackish well (r) (0.77L)	29923	45	14	1.46	42
	Seawater (beach) (0.77L)	62786	66	10	2.54	38

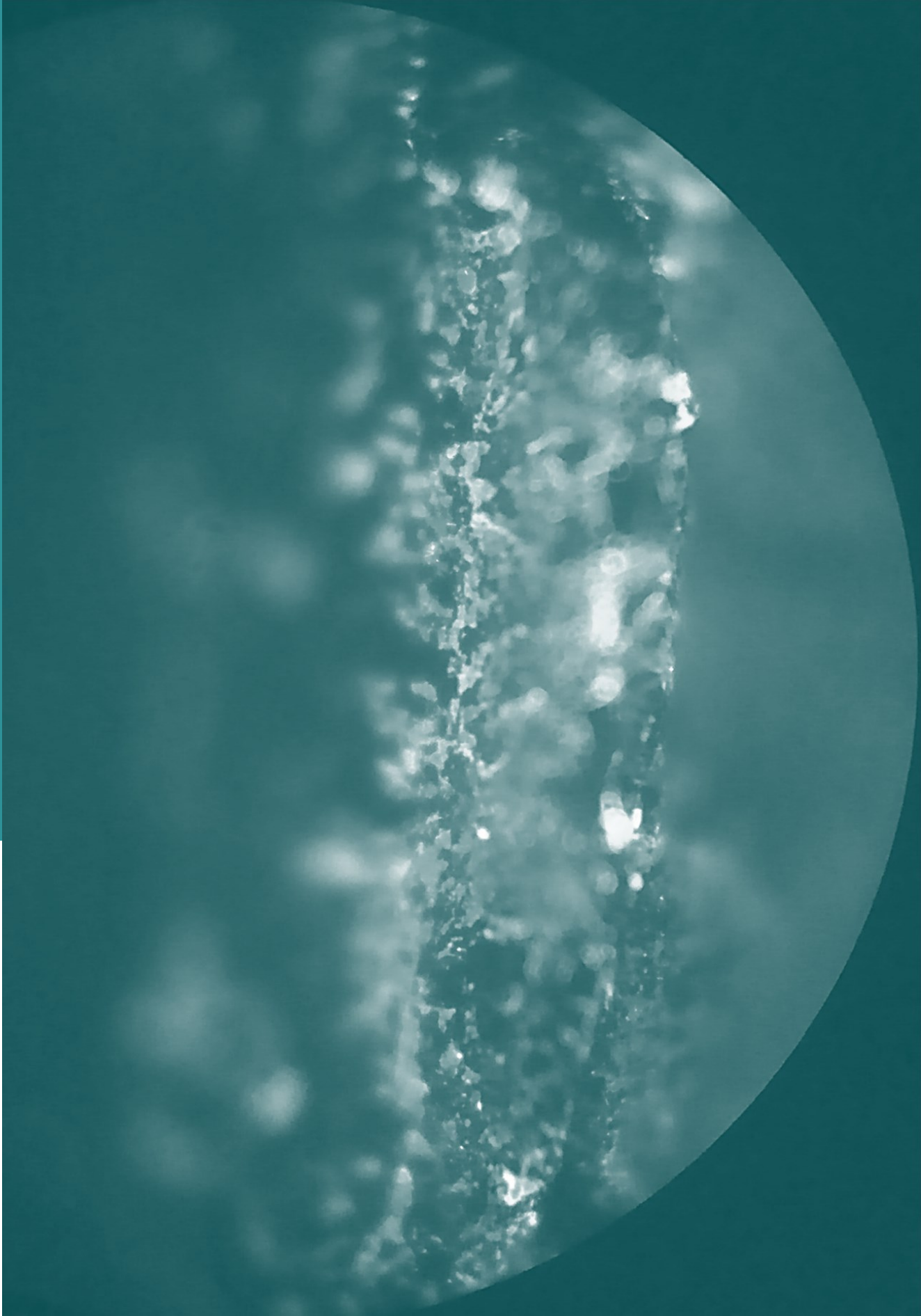

7.5 Appendix Chapter 7

7.5.1 Analysis of bacterial communities from long-term MDC system

On top of the bioelectrochemical performance described in ***Chapter 7***, some preliminary results regarding the analysis of bacterial communities are included as appendix. This analysis was performed on four samples obtained from different elements at MDC: **i)** two different zones from anode, **ii)** cathode, and **iii)** anionic exchange membrane. This MDC was operated for four years, starting with an initial inoculation using a pure culture of *Geobacter sulfurreducens* (March 2017). The operating conditions during such four years were adapting to the needs of the different assays: first, a series of assays were performed using artificial conditions based on freshwater medium as anolyte and synthetic saline water (NaCl) as a saline stream ***(Chapter 4,5,6)***. Then, the MDC was operated under real conditions using real wastewater as anolyte and real streams of saline water ***(Chapter 7)***. The four samples collected from the MDC system were as follows **(Figure App_A)**:

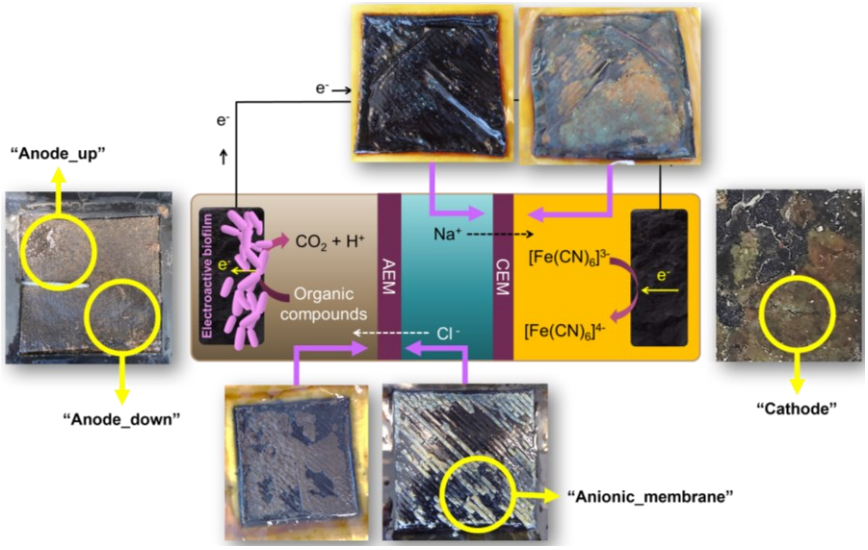

Figure App_A. Photos of the origin and location in the MDC device of the samples taken for the analysis of bacterial communities.

Anode samples: Two felt carbon samples from different anode locations were collected (4 cm^2) and stored at -20 ^{0}C until analysis. The "Anode_down" sample was collected from the lower zone of the anode close to the inlet port of the anodic compartment. The sample "Anode_up" was collected from the upper zone of the anode, close to the oulet port of the anodic compartment.

Cathode sample: A sample of the carbon felt from the cathode electrode was collected (4 cm^2) and stored at -20 ^{0}C until analysis. Such microbial community was in contact with potassium ferricyanide during the whole period.

Saline compartment sample: the biofilm generated on the anionic membrane separating the saline compartment from the anodic compartment was collected. Sample was taken from saline compartment side and stored at -20 ^{0}C until analysis.

Sequencing of full-length 16S rRNA gene from microbial community was performed using a MinION MK1C (Oxford Nanopore Technologies (ONT)) by Microbial Ecology Unit of laboratory of IMDEA Agua. The biofilm samples were collected by a sterile cell-scrappers, then DNA extraction of the samples was performed with the commercial kit DNAeasy PowerBiofilm kit (Qiagen). Aftewards, as the samples contained several PCR inhibitors, these were treated with the commercial kit One-Step PCR Inhibitor Removal Kit (Zymo Research). The DNA extracts obtained were quantified with Qubit 4 DNA Assay Kit (Invitrogen) and the quality was checked with Nanofotometer (EPOCH, BioTek). The sequencing library was was generated using a 16S barcoding kit (SQK-RAB204 from ONT) and it was loaded onto a MinION flow cell (R9.4.1, FLO_MIN106) and this placed into the device MK1C.

A total of 1.67 M of raw data were generated and basecalled by MinKNOW software (v. 22.12.5). After quality filtering an average of 317,330.5 reads per sample were obtained (min:268,173; max:414,378; median Q = 9.7). The reads were analyzed by the EPI2ME interface (v. 3.6.2), the cloud plataform for data

analysis of ONT, using Fastq 16S workflow and the statistic analyses were processed with R software (v.4.2.1).

7.5.2 Results

The analysis of bacterial communities presents in all four samples revealed a diverse profile of bacterial species **(Figure App_B)**. A greater diversity of species was observed in the three samples of carbon felt (Anode_up, Anode_down and Cathode) in comparison with the consortium associated to the anionic membrane (Anionic_membrane). A literature review of the main feature of every specie was included in **Table App_A**).

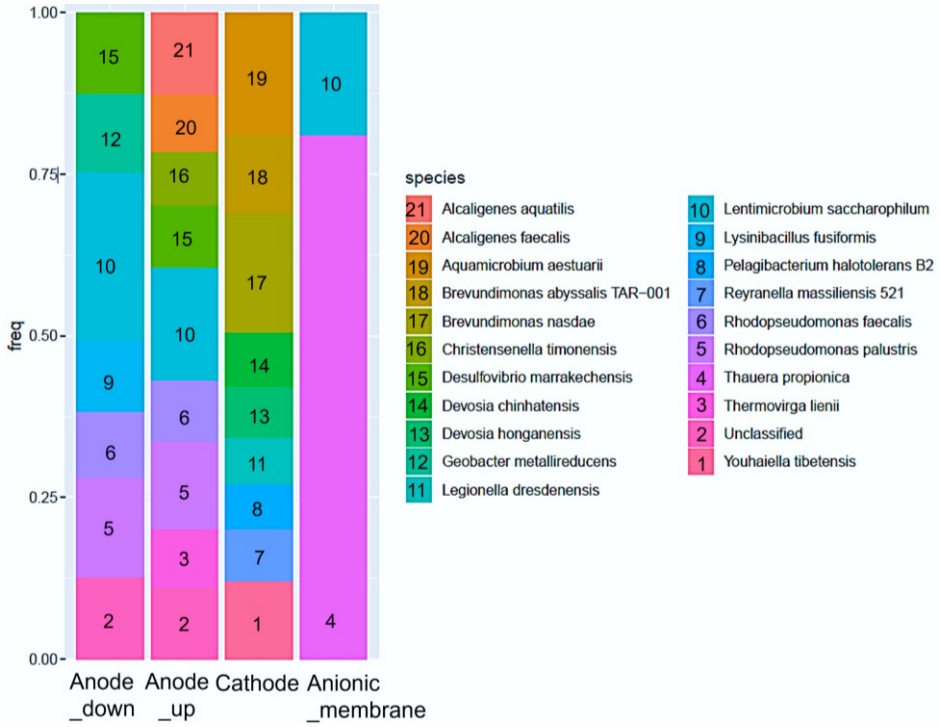

Figure App_B. Bacterial species above 3% relative abundance from the different MDC's samples.

Anodic species (Anode_up / Anode_Down):

The bacterial community in both anodic samples consisted mainly of species previously reported as anaerobes. This is consistent with the fact that the recirculation tank and the anodic compartment were maintained in anaerobic conditions throughout the experimentation. Indeed, a large percentage of such species were previously reported to be isolated from aquatic environments (both freshwater- or marine environments) reflecting the salinity variations from anolyte chamber accepting chlorides, nitrates, or sulfates from the salt compartment. Both anodic samples have similarities in the presence of the following species:

- *Lentimicrobium saccharophilum*: It correspond to the most abundant species in both samples. Typically present in river sediments and in anaerobic sludge blanket reactor treating high-strength starch-based organic wastewater. They are strictly anaerobic with volatile fatty acids as main substrate. It tolerates extreme environmental conditions such as high salt concentration (Sun et al., 2016).
- *Rhodopseudomonas palustris* (Larimer et al., 2004; Xing et al., 2008; Logan et al., 2019; Rengasamy et al., 2021) and *Rhodopseudomonas faecalis* (Zhang et al., 2002): They are classified as Purple non-sulfur phototrophic bacteria. Specifically, *R. palustris ATCC 17001, DX1,* and *R. palustris TIE 1* strains have been reported to be exoelectrogenic and electrotrophic bacteria.
- *Desulfovibrio marrakechensis*: this obligate anaerobe use sulfate as an electron acceptor for respiration (high sulfate concentrations was present in several desalination cycles from our research). They are adapted to extreme salinity environments (4-fold higher than seawater). *Desulfovibrio marrakechensis* was isolated for the first time in waste mills characterized by their high organic content (oils and fats, suspended solids, and

polyphenols), high acidity (municipal wastewater doped with molasses with minimal buffer capacity was used) and high electrical conductivity (Chamkh et al., 2009).

Regarding specific samples, Anode_Down (**Figure App_B**, **Figure App_C**) showed a ca. 5% relative abundance of *Geobacter metallireducens* (one of the first species reported with electroactive activity along with *Geobacter sulfurreducens*)(Lovley and Phillips, 1986; Lovley et al., 1993; Logan et al., 2019; Lovley and Holmes, 2022). Interestingly, *Lysinibacillus fusiformis* is resistant to resistant to multiple metals, and it was present (ca. 4% relative abundance) in this anodic sample. In fact, such specie was isolated for the first time in river sediments and wastewater contaminated with chromium. Indeed, strains *L. fusiformis ZC1* can reduce Cr (VI) using acetate as electron donor. Precisely, *Lysinibacillus sphaericus D-8 and Lysinibacillus sphaericus VA5* have been reported as anodic electroactive species (He et al., 2011b; Hristoskova et al., 2018; Logan et al., 2019; Zhang and Zhang, 2022).

On the other hand, the Anode_Up sample (**Figure App_B**, **Figure App_C**) contained a different profile with *Alcaligenes faecalis* (Rabaey et al., 2004; Zhou et al., 2013; Logan et al., 2019) and *aquatilis* (Durán et al., 2019; Arkatkar et al., 2023)(relative abundance of 4 and 5%, respectively) as main actors. These species were reported as anaerobic and alkaliphilic genus. Indeed, the actual wastewater was doped with bicarbonate buffer, so perhaps this buffer was first neutralized in the lower electrode zone due to bacterial metabolism, and the high alkalinity did reach high electrode areas (anode_up). They are species isolated have been reported in marine environments. *Alcaligenes faecalis subsp. parafaecalis G.* has been reported to be an electroactive species (cathode, electrotrophic bacteria). *Thermovirga lienii* was isolated from the North Sea oil well and is anaerobic (Dahle and Birkeland, 2006), as is *Christensenella timonensis* (Ndongo et al., 2016) isolated from the human gut (possibly from municipal wastewater used as anolyte for several desalination cycles).

Electroactive bacteria like *Geobacter pickeringii* (Shelobolina et al., 2007; Badalamenti and Bond, 2015), or *Geovibrio ferrireducens* (Caccavo Jr. et al., 1996; Conners et al., 2022) were present in both anodic samples (ca. 1- 3% relative abundance). Additional members of electroactive community are shown in **Figure App_C**, and **Table App_B**.

Anionic membrane species

The microbial community present in the surface of the anion membrane (saline compartment side) revealed a lower biodiversity in comparison with communities from electrodes **(Figure App_B, Figure App_D)**.

The most abundant species by far (50%) was *Thauera propionica* (Lovley, 2017; Pal et al., 2018; Yang et al., 2019b). This strain was first isolated in the Ganges River (India). This species has been reported as dominant in bioelectrochemical devices for removing nitrogenous compounds (some of the saline waters used in our saline compartment had high concentrations of nitrate). *Thauera propionica* has also been reported as a species with potential for direct interspecies transfer (DIET) **(Table App_A)**. This species has also been found in both anodic samples but with a relative abundance between 1 and 3%. The species that follow in abundance (11%) was *Lentimicrobium saccharophilum* (Sun et al., 2016). Such bacteria was indeed the most abundant in the two anodic samples of the current study. Other species with 1-2% abundance were anaerobic and denitrifying bacteria (descriptions in **Table App_B**).

Microbial diversity in the cathode

All the species analyzed in the cathodic electrode were different from the species present in both the anodic samples and the saline compartment **(Figure App_B, Figure App_D)**. All species present at the cathode revealed aerobic respiration (the potassium ferricyanide recirculation tank and the cathode

compartment of the bioreactor were not deoxygenated during desalination cycles). Some of these bacteria have previously been isolated in rivers, deep sea waters, or soils near areas contaminated with pesticides **(Table App_A** and **App_B)**. The two species with the highest abundance are *Brevundimonas nasdae* (8.2%) and *Aquamicrobium aestuarii* (8.5%), followed by *Youhaiella tibetensis* (Wang et al., 2015b) and *Brevundimonas abyssalis TAR−001* (both with a relative abundance of 5.3%). The most abundant species, *Aquamicrobium aestuarii*, was isolated from the Yellow Sea in South Korea and is strictly aerobic although it can also reduce nitrate (Lo et al., 2014). The aerobic *Brevundimonas nasdae* species was isolated for the first time from condensed water from the Russian space laboratory MIR (Li et al., 2004; Logan et al., 2019), and the *Brevundimonas abyssalis TAR−001* species was isolated from abyssal depths of the ocean (approx. 1180 m), which is alkali tolerant. *Brevundimonas diminuta ATCC 11568* was reported to be electroactive (Cournet et al., 2010; Tsubouchi et al., 2013; Logan et al., 2019).

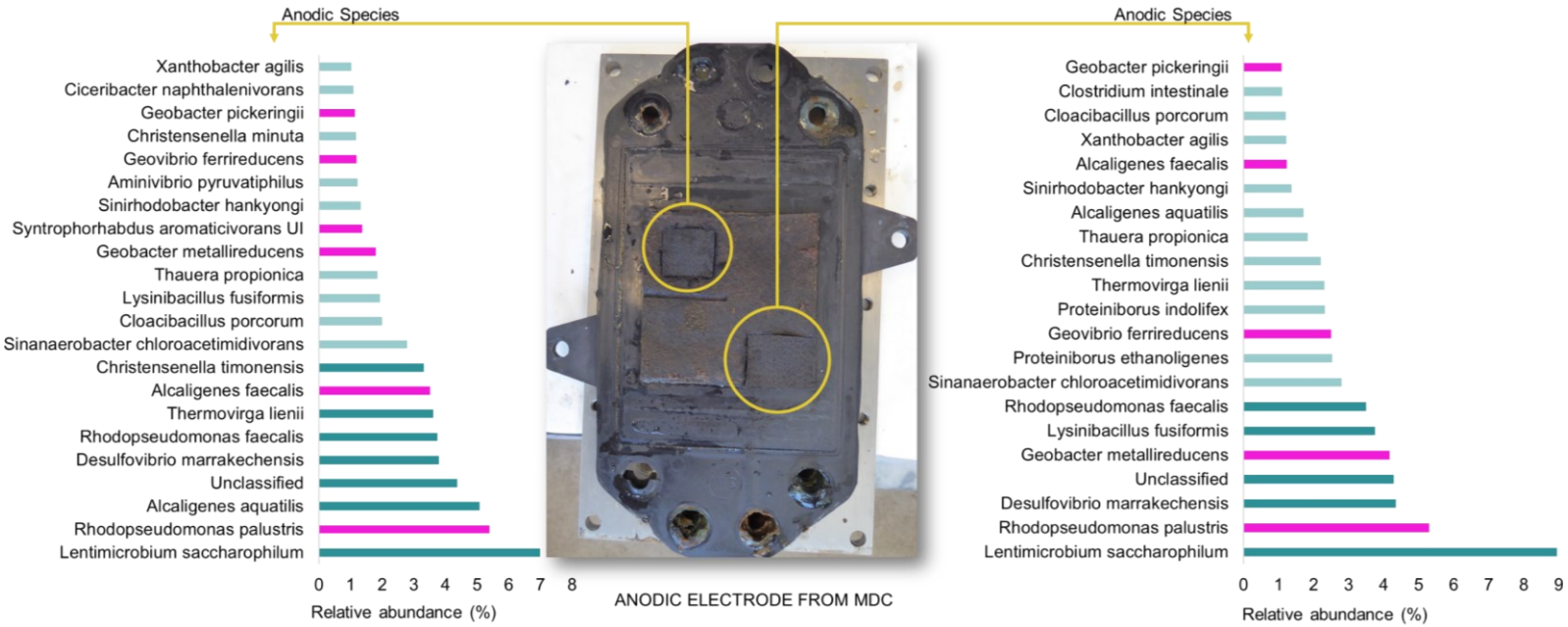

Figure App_C. Profile of the bacterial community present in **left)** carbon felt from the anode (outlet zone) and **right)** carbon felt from the anode (inlet zone). Reported electroactive species are marked in pink. Dark blue species with a relative abundance greater than 3% (as in **Figure App_B**). Light blue shows species that have a relative abundance between 1 – 3%.

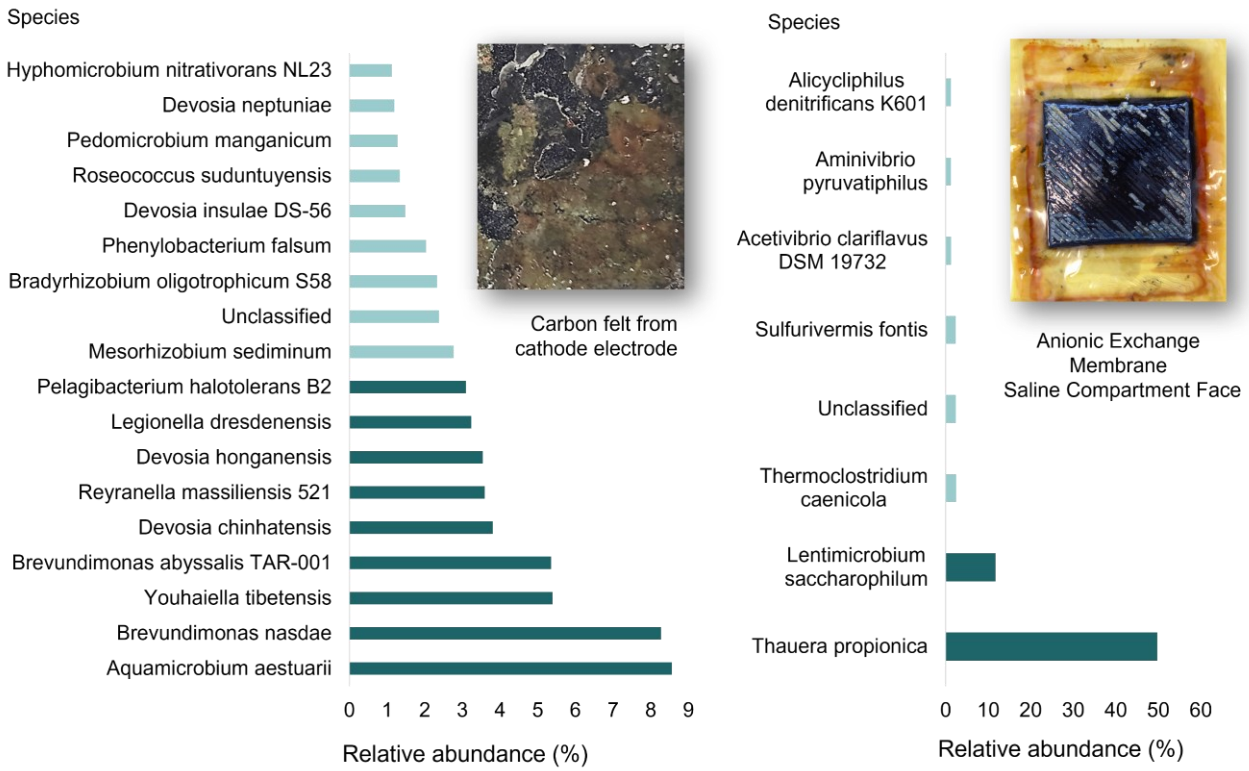

Figure App_D. Profile of the bacterial community present in **left)** carbon felt from the cathode and **right)** surface of the anion membrane (saline compartment side). Those electroactive species are marked in pink. Dark blue species with a relative abundance greater than 3% (as in **Figure App_B**). Light blue corresponds to species that have a relative abundance between 1 – 3%.

Table App_A. Description and main characteristics from bacterial species **above 3% in relative abundance** (electroactive bacteria in pink).

Id	Location	*Specie*	Isolated from	Characteristics	Reference
3	Anode	*Thermovirga lienii*	• North Sea oil well	• Anaerobic • Moderately thermophilic • Degrades amino acids	(Dahle and Birkeland, 2006)
5	Anode	*Rhodopseudomonas palustris*	• Swine waste lagoons • Earthworm droppings • Marine coastal sediments • Pond water	• Purple non-sulfur phototrophic bacteria • Mainly anaerobic • Photoautotrophic, photoheterotrophic, chemoautotrophic, chemoheterotrophic • R. palustris ATCC 17001: exoelectrogenic bacteria • R. palustris DX1: exoelectrogenic bacteria • R. palustris TIE 1: electrotrophic bacteria	(Larimer et al., 2004; Xing et al., 2008; Logan et al., 2019; Rengasamy et al., 2021)
6	Anode	*Rhodopseudomonas faecalis*	• Anaerobic reactor digests chicken faeces • Aquatic environments and soils	• Purple non-sulfur phototrophic bacteria • Anaerobic phototroph. • Optimal growth: 35-40 ^{0}C, pH 6.5-8.5. • Various organic compounds as photosynthetic electron donors and carbon sources. • Sulfate used as sulfur source for growth.	(Zhang et al., 2002)

9	Anode	*Lysinibacillus fusiformis*	• Chromium contaminated wastewater (metal electroplating factory) • River basin sediment	• Strain L. fusiformis ZC1: Cr(VI) reduction ability enhanced by sodium acetate and NADH. Resistance to multiple metals (Cu, Ni, Co, Hg, Cd and Ag) and a metalloid (As). • Carbon Sources: acetate, citrate, formiate, lactate, succinate • Anodic electroactive species: Lysinibacillus sphaericus D-8 Lysinibacillus sphaericus VA5	(He et al., 2011b; Hristoskova et al., 2018; Logan et al., 2019; Zhang and Zhang, 2022)
12	Anode	*Geobacter metallireducens*	• Sediments from Potomac River Estuary in Maryland	• Strict anaerobe • Exoelectrogenic bacteria: oxidizes several short-chain fatty acids, alcohols, and monoaromatic compounds with electron transfer to electrodes or Fe (III) oxides. Acetate oxidized with the reduction of Mn (IV), U (VI), and nitrate. • Electrotrophic bacteria: extract electrons from negatively poised electrodes for the reduction of nitrate.	(Lovley and Phillips, 1986; Lovley et al., 1993; Logan et al., 2019; Lovley and Holmes, 2022)
15	Anode	*Desulfovibrio marrakechensis*	• Oil mill wastewater: high organic content, contaminants such as oils and fats, suspended solids, and polyphenols. High acidity and electrical conductivity	• Obligate anaerobic • Sulfate as an electron acceptor for respiration. • Adaptation to extreme environments: high salinity up to 4 times the salt concentration of seawater,	(Chamkh et al., 2009)
16	Anode	*Christensenella timonensis*	• Human gut	• Anaerobic • Butyric acid production	(Ndongo et al., 2016)

20	Anode	*Alcaligenes faecalis*	• Aquatic environments, sewage and sediment, chemically contaminated soils	• Facultative anaerobic bacteria • Alkaliphilic genera • Alcaligenes faecalis subsp. parafaecalis G.: Electroactive (cathode, electrotrophic bacteria)	(Rabaey et al., 2004; Zhou et al., 2013; Logan et al., 2019)
21	Anode	*Alcaligenes aquatilis*	• Aquatic environments, freshwater and marine habitats	• Strictly anaerobic • Alkalophilic genera • Degradation of polycyclic aromatic hydrocarbons (PAHs) • Nitrogen removal • Physiological responses to withstand environmental stresses.	(Durán et al., 2019; Arkatkar et al., 2023)
4	Anode AEM	*Thauera propionica*	• Ganges river	• Potential of direct interspecies transfer (DIET) • Reported to dominate a nitrogen removing MFC	(Lovley, 2017; Pal et al., 2018; Yang et al., 2019b)
10	Anode AEM	*Lentimicrobium saccharophilum*	• River sediments • Methanogenic granular sludge in mesophilic upflow anaerobic sludge blanket reactor treating high-strength starch-based organic wastewater.	• Strictly anaerobic • Substrate: lactic acid, acetic, propionic, and formic acid • Tolerates extreme environmental conditions, acid pH, high salt concentrations, high temperatures	(Sun et al., 2016)

1	Cathode	*Youhaiella tibetensis*	• Subsurface sediment core of Qiangtang Basin permafrost in China (Tibet plateau)	• Aerobic • Optimum growth: 37 °C, pH 8.0	(Wang et al., 2015b)
7	Cathode	*Reyranella massiliensis 521*	• Cooling towers • Reyran river (France)	• Microaerophilic • Grow: 30 - 35 °C. • NO_3 reduction	(Pagnier et al., 2011)
8	Cathode	*Pelagibacterium halotolerans B2*	• Sea water (East China Sea) depth 70 m (16.7 °C; salinity 33.95%)	• Aerobic • Tolerance to high salt environment • Optimum growth: pH 7.0 / 30 °C	(Xu et al., 2011)
11	Cathode	*Legionella dresdenensis*	• River Elbe (Germany)	• Aerobic	(Lück et al., 2010)
13	Cathode	*Devosia honganensis*	• Waste surface soil of chemical factory (China)	• Strict aerobic • Light yellow-pigmented • Produce yellow-orange pigment • Grow optimally: pH 7.0 / 30 °C	(Zhang et al., 2015)
14	Cathode	*Devosia chinhatensis*	• Soil sample area adjoining an India Pesticide plant (India)	• Aerobic	(Kumar et al., 2008)
17	Cathode	*Brevundimonas nasdae*	• Condensation water from Russian space laboratory Mir	• Aerobic / 30°C • Utilizes acetate, pyruvate, methyl pyruvate, succinate, amino acids. • Produces acid from glucose, galactose, maltose, sucrose	(Li et al., 2004; Logan et al., 2019)

18	Cathode	*Brevundimonas abyssalis TAR−001*	• Deep-sea floor sediments (Japan). Abyssal depths of the ocean (approx. 1180 m)	• Aerobic • Alkali tolerant • Yellowish-white colour • Optimum: 20 °C / pH 7.0–8.0 • Utilizes xylitol, acetic acid, β-hydroxybutyric acid, α-ketoglutaric acid, dl-lactic acid, propionic acid • Brevundimonas diminuta ATCC 11568 (electroactive)	(Cournet et al., 2010; Tsubouchi et al., 2013; Logan et al., 2019)
19	Cathode	*Aquamicrobium aestuarii*	• Yellow Sea • Crude-oil-contaminated tidal flat of the Taean coast (South Korea)	• strictly aerobic • Nitrate reduction • Optimum: 30–35 °C / pH 6.5–7.5	(Lo et al., 2014)

Table App_B Description and main characteristics from species **between 1- 3% in relative abundance**.

Location	Specie	Isolated from	Characteristics	Reference
Anode	*Sinanaerobacter chloroacetimidivorans*	• Anaerobic acetochlor-degrading reactor	• Obligate anaerobic • degrading acetochlor, butachlor (herbicide).	(Bao et al., 2021)
Anode	*Cloacibacillus porcorum*	• Swine intestinal tract on mucin-based media	• Obligately anaerobic • Fermentation amino acids • Fermentation products acetate, propionate, formate • Mucin as carbon source	(Looft et al., 2013)
Anode	*Syntrophorhabdus aromaticivorans UI*	• Anaerobic granular sludge. • Granular activated carbon up-flow anaerobic sludge blanket reactor treating blackwater at 35 °C.	• Anaerobe, mesophilic • Capable of oxidizing phenol in association with an H_2-scavenging methanogen partner. • Hosted the genes for e-pili which made it a potential species for DIET	(Qiu et al., 2008; Nobu et al., 2015; Dang et al., 2022)
Anode	*Sinirhodobacter hankyongi*	• Sludge	• facultative-aerobic • denitrifying bacterium	(Lee et al., 2020)

Anode	*Geovibrio ferrireducens*	• Surface sediment hydrocarbon-contaminated ditch	• Fe(III)-reducing bacterium (strain PAL-1) • Obligately anaerobic • Electron donor: acetate for electron acceptor: ferric pyrophosphate, ferric oxyhydroxide, ferric citrate, Co(III)-EDTA, or elemental sulfur. • Electron donors: proline, hydrogen, lactate, propionate, succinate, fumarate, pyruvate for Fe(III) reduction. • The first bacterium known to couple the oxidation of an amino acid to Fe(III) reduction.	(Caccavo Jr. et al., 1996; Conners et al., 2022)
Anode	*Christensenella minuta*	• Human faeces	• Strictly anaerobic	(Morotomi et al., 2012; Saheb-Alam et al., 2019)
Anode	*Geobacter pickeringii (Strain G13)*	• Sedimentary kaolin clays strata in Georgia, USA	• Closely *Geobacter metallireducens* (95.1%). • Colonies pink on fumarate (high c-type cytochrome content of cells of species of the genus *Geobacter*) • Colonies black on PCFO due to formation of dark coloured Fe(II)-bearing minerals such as magnetite • First *Geobacter* species for which formation of blebs • Optimal growth: 30°C pH 6.6–7.2 • Electron acceptors: Fe(III)-reducing bacteria, PCFO, elemental sulfur, a humic acid analogue, AQDS, fumarate, malate, U(VI). • Electron donors: methanol, ethanol, butanol, glycerol, acetate, lactate, butyrate, pyruvate, succinate, valerate.	(Shelobolina et al., 2007; Badalamenti and Bond, 2015)

Anode	*Ciceribacter naphthalenivorans*	• Sediment of a polychlorinated-dioxin-transforming microcosm	• Synonim: Rhizobium naphthalenivorans • Three strains of aerobic chemoorganotrophic naphthalene-degrading bacteria (designated TSY03bT, TSY04, and TSW01) isolated from sediment of a polychlorinated-dioxin-transforming microcosm were characterized.	(Kaiya et al., 2012; Rahi et al., 2021)
Anode	*Xanthobacter agilis*	• Water samples from a small eutrophic lake (Switzerland)	• Growth formate, acetate, propionate, pyruvate, butyrate, succinate, DL-alanine and aliphatic alcohols. • Mesophilic, optimal 25-30°C, • Strictly aerobic metabolism • Either chemolithoautotrophic, using H_2 as electron donor and CO_2 as carbon source, or chemoorganoheterotrophic.	(Jenni and Aragno, 1987)
Anode	*Proteiniborus ethanoligenes*	• granular sludge from a laboratory-scale UASB hydrogen-producing reactor used to treat food industry wastewater.	• Anaerobic, mesophilic, protein-utilizing bacterial strain, • Optimum growth: 37 °C / pH 8.5–8.8 • Carbon and energy sources: yeast extract and peptone • Fermentation products: ethanol, acetic acid, hydrogen, carbon dioxide. • Nitrate reduction	(Niu et al., 2008)
Anode	*Proteiniborus indolifex*	• Thermophilic industrial-scale biogas plant	• Strictly anaerobic • Cell growth: yeast extract, peptone, meat extract, amino acids, glucose, pyruvate, ribose. • Fermentation products: acetic acid, H2 and CO2 • optimum growth: 35–50 °C / pH 7.6	(Hahnke et al., 2018)
Anode AEM	*Aminivibrio pyruvatiphilus*	• Soil of a rice field (Japan)	• Anaerobic • Ferment amino acids organic acids	(Honda et al., 2013)

AEM	*Thermoclostridium caenicola*	• anaerobic sludge of a cellulose-degrading methanogenic bioreactor	• Obligately anaerobic, thermophilic and chemo-organotrophic. • optimum 60 °C / pH 6.5 • Carbon and energy sources: amygdalin, arabinose, glucose, maltose, mannitol, salicin and starch. • Fermentation products: hydrogen, carbon dioxide, acetate, lactate and ethanol.	(Shiratori et al., 2009)
AEM	*Acetivibrio clariflavus DSM 19732*	• anaerobic sludge of a cellulose-degrading methanogenic bioreactor	• Synonyms: Clostridium clariflavum • bright yellow, the colour of the colonies or pigment • Moderately anaerobic, thermophilic and chemo-organotrophic. • optimum 55–60 °C / pH 7.5 • Salinity (NaCl) growth: 0.4% (w/v). • carbon and energy sources: Cellulose, cellobiose • Fermentation products: hydrogen, carbon dioxide, acetate, lactate, ethanol, formate.	
AEM	*Sulfurivermis fontis*	• Hot spring microbial mat (Japan)	• Facultatively anaerobic • Chemolithoautotrophic: sulfide, thiosulfate, tetrathionate and elemental sulfur as an electron donor for autotrophic growth. Nitrogen source: Nitrate and ammonium • Reduces nitrate as an electron acceptor to support growth • Optimum growth: 42–48 °C / pH 7.2–7.9. No growth: 3% (w/v) NaCl.	(Kojima et al., 2017)
AEM	*Alicycliphilus denitrificans K601*	• At 30 °C from a municipal sewage plant on cyclohexanol as sole carbon source and nitrate as electron acceptor.	• Facultatively denitrifying • Aerobic conditions: used acetate, fumarate, lactate, pyruvate, crotonate, indole, glucose, vanillate, 4-hydroxybenzoate, m-cresol, o-cresol and p-cresol. • Electron acceptors: nitrate, nitrite and oxygen but not sulfate, sulfite or fumarate.	(Mechichi et al., 2003)

Cathode	*Mesorhizobium sediminum*	• Deep-sea sediment (Indian Ocean)	• Aerobic bacterium • Optimal growth: 25–30 °C / pH 6.0 / 3–5 % (w/v) NaCl	(Yuan et al., 2016a)
Cathode	*Bradyrhizobium oligotrophicum S58*	• Rice paddy soil	• Basonym: Agromonas oligotrophica • Aerobe, mesophilic, Oligotrophic	(Ohta and Hattori, 1983; Ramírez-Bahena et al., 2013)
Cathode	*Phenylobacterium falsum*	• Alkaline groundwater (pH 11.4)	• Strictly aerobic • Optimum growth 35 °C / pH 8.0.	(Tiago et al., 2005)
Cathode	*Devosia insulae DS-56*	• Soil from Dokdo (island) Korea	• Aerobic • Optimally: pH 6.5–7.5 / 25°C / 0.5% (w/v) NaCl	(Yoon et al., 2007)
Cathode	*Roseococcus suduntuyensis*	• Surface layer of bottom sediments from the soda lake Shuluutai-Ekhe-Torom (Chita oblast, Eastern Siberia, Russia) with mineralization 30 g/L and a pH 9.2	• Obligate aerobe • Facultative alkaliphile • Optimal growth: pH 8.5–9.0 / 2.0 g/L NaCl / 23–28°C. • Photosynthetic pigments: bacteriochlorophyll • Grows well: sugars, glycerol • Reduces nitrates to nitrites	(Boldareva et al., 2009)
Cathode	*Pedomicrobium manganicum*	• “dirty water” and from drinking water	• Manganese-oxidizing pedomicrobia • Strictly aerobic • Optimal growth: 26-35 0C / pH = 9	(Sly et al., 1988)

Cathode	*Devosia neptuniae*	• Neptunia natans is an aquatic legume indigenous to tropical and subtropical regions and in African soils	• strictly aerobic • carbon sources: several carbohydrates (but not organic acids)	(Rivas et al., 2003)
Cathode	*Hyphomicrobium nitrativorans NL23*	• Methanol-fed denitrification system treating seawater at the Montreal Biodome, (Canada)	• Aerobe • Grow under denitrifying conditions in the presence of nitrate without nitrite accumulation. • pH 7.0–9.5/ 0–1% NaCl / 15–35 °C	(Martineau et al., 2013)

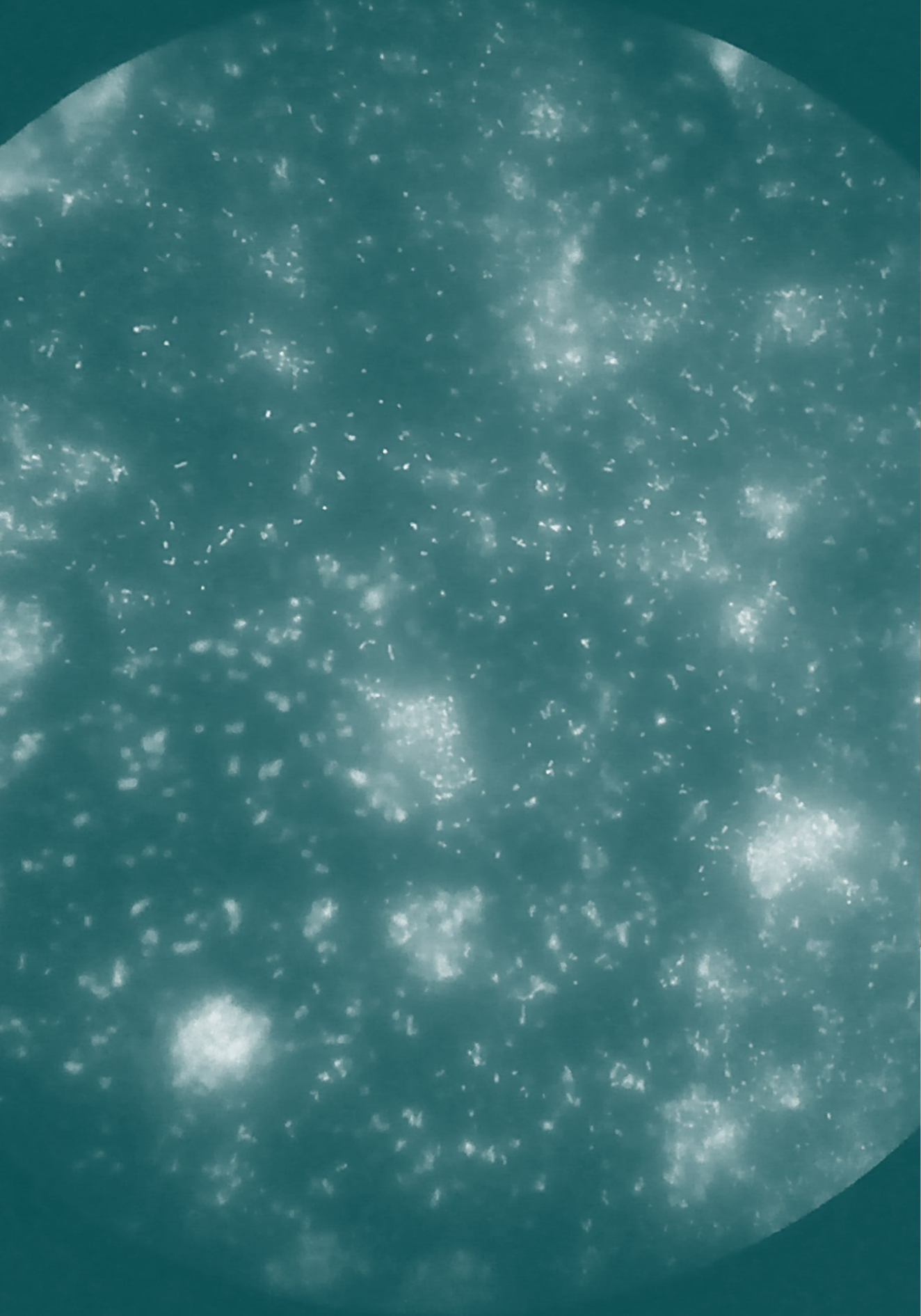

Chapter 8

Study of the Influence of Nanoscale Porosity on the microbial electroactivity between expanded graphite electrodes and *Geobacter sulfurreducens* biofilms

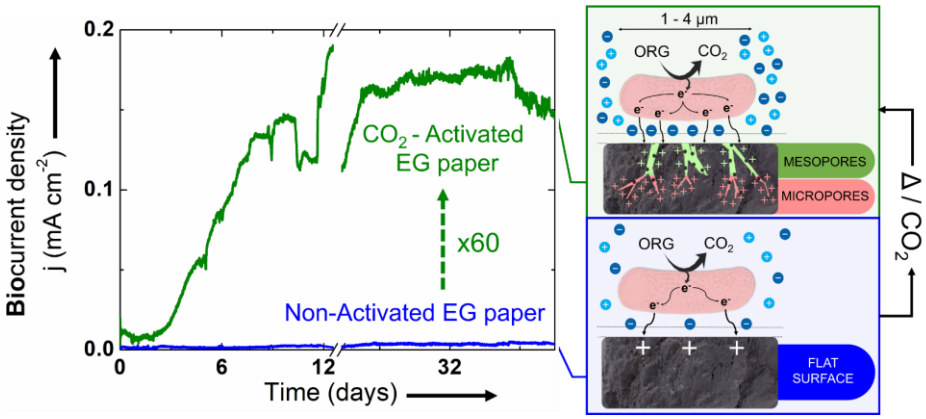

Collaboration with Instituto Universitario de Materiales, Departamento de Química Física, Universidad de Alicante. This chapter has been accepted for publication in *Microbial Biotechnology* (2023). Authors: M. Ramirez-Moreno, R. Berenguer, J.M. Ortiz and A. Esteve-Núñez.

Chapter 8. Study of the Influence of Nanoscale Porosity on the microbial electroactivity between expanded graphite electrodes and *Geobacter sulfurreducens* biofilms

Abstract

Expanded graphite (EG) electrodes gather several advantages for their utilization in microbial electrochemical technologies (MET). Unfortunately, the low microbial electroactivity makes them non-practical for implementing them as electrodes, restricting their use only as current collectors in microbial electrochemical cells. The objective of this work is to explore the enhancement of microbial electroactivity of expanded graphite (commercial PV15) through generation of nanopores by CO_2 treatment at different temperatures and reaction times. The changes on PV15 properties were thoroughly analyzed by TG, XRD, Raman, XPS, gas adsorption, SEM and AFM, while the microbial electroactivity was studied by cyclic voltammetry and chronoamperometry in the presence of *Geobacter sulfurreducens* and acetate as electron donor. Moreover, biofilm formation was studied by SEM and live/dead staining. Results showed that heat treatments at 800-900ºC under a CO_2-containing atmosphere generated a wide range of different nanopores (mainly d < 50 nm) on the PV15 surface without significantly affecting its microstructure and electroconductivity. These nanopores remarkably enhance the electrical double layer capacitance (425 – fold increase) and the microbially-derived electrical current (60 – fold increase) of this material. Given the inaccessibility of micron-sized bacteria to these nanopores, it is suggested that the electric charge exchanged by electroactive microorganisms might be greatly affected by the capability of the electrode to compensate these charges through ion adsorption, a phenomenon that occurs in the nanoporosity. In the studied bioreactor and experimental conditions, the increased microbial current density produced on activated PV15 becomes similar to those of

commercial carbon felts, opening the possibility of using such materials as promising electrodes in MET.

8.1 Introduction

Global challenges in the water-energy-climate nexus demand the development of new technologies and energy sources (UNESCO/UN-Water, 2020). In this context, the emergence of microbial electrochemical technologies (METs) is receiving a growing interest. These technologies use electroactive microorganisms that can exchange electrons with a conductive and/or electroactive material (Lovley, 2006), in most cases, to convert the chemical energy contained in organic compounds into electric energy and/or valuable inorganic and organic chemicals (Logan and Rabaey, 2012), or just to promote microbial metabolism. The practical utilization of these microorganisms is an emerging field that is giving rise to different applications, including energy production (Logan, 2009), wastewater treatment (Aguirre-Sierra et al., 2020), electrobioremediation (Wang et al., 2020a), bioelectrosynthesis (ter Heijne et al., 2017), biosensors (Chung et al., 2020), desalination (Cao et al., 2009; Ramírez-Moreno et al., 2019) among others.

Over the last two decades, the research in this field has proved that the nature of the electrode materials plays a key role in determining the microbial electroactivity (Maestro et al., 2014; Beyenal and Babauta, 2015; Prado et al., 2019) and, therefore, the overall system performance for these applications. In addition, the electrode material is one of the critical factors in determining the cost and sustainability of MET (Rozendal et al., 2008).

Among several candidates, the state-of-the-art for MET is generally based on highly-conductive carbon electrodes. These materials typically exhibit good stability, biocompatibility and a well-developed graphitic structure that ensures a high electrical conductivity, being this property essential for generating electrical

power in different types of MET. Examples of these most used conductive carbon electrodes for electromicrobial applications are generally 3D conformations, dense (sheets, rods, plates, etc.) or porous (papers, felts, cloths, foams, etc.), of graphite, carbon fibers and glassy carbon (Logan, 2010; Alvarez Esquivel et al., 2020). Generally, the dense conformations are prone to provide higher conductivities, while the porous ones expose a higher accessible surface area for an extended biofilm growth, which results in larger microbial currents (Chong et al., 2019). These 3D porous materials, however, usually suffer from clogging, internal acidification and/or unstable responses during operation, among other drawbacks. Hence, for microbial electrochemical applications, it would be desirable to attain the high conductivities of the dense electrode conformations together with the enhanced microbial activities of the porous ones.

In this context, the study of novel approaches and/or strategies to optimize the electrode response in METs becomes key for the implementation of microbial electrochemical technology in real applications. Thus, several modification treatments have been attempted to improve the microbial electroactivity of carbon electrodes, and most of them have been devoted to increasing the conductivity and external surface area. Nonetheless, apart from these properties, carbon materials can exhibit characteristic-rich surface chemistry and nano-sized porous structure, including micropores (d, pore diameter; $d < 2$ nm) and mesopores ($2 < d < 50$ nm), which play a critical role in other electrochemical technologies without bacteria, such as energy storage and conversion, environmental remediation, etc. (Liu and Creager, 2010; Zhang et al., 2014; Momodu et al., 2017). These extraordinary effects of atomic species and nanoscale features can be explained by the fact that they can directly interact with electrons and ions, the main actors in electrochemical processes.

In the case of MET, the influence of electrode porosity on microbial performance has been scarcely studied until now. Thus, Chen et al. reported that microporous and mesoporous activated carbon, used as a bioanode in an

microbial fuel cell (MFC), improves the performance since this nanoscale structure could promote charge transfer and microbial adhesion (Chen et al., 2018). In this sense, it is generally thought that the micro- and meso-porosity, which cannot host micron-sized bacteria, cause any direct effects on the performance of MET (Chong et al., 2019), as the surface is not accessible by microorganisms. However, recent works on the so-called METlands®, for which current production is not essential, have evidenced the better microbial electrochemical performance of some biochars, materials with comparatively much poorer conductivity (Prado et al., 2020b). These findings have led researchers to hypothesize that the large volume of micropores in these materials could enhance the activity of electroactive microorganisms (Schievano et al., 2019; Berenguer et al., 2020). Hence, the study on the influence of nano-scaled porosity of electrodes in the performance of MET is still an unexplored topic with a huge potential impact on this emerging field.

To face this study, ideally, it is necessary to compare carbon materials in which the only difference must be the nanoporosity to avoid any potential interference of other intercorrelated properties, such as surface chemistry, microstructure or conductivity. In fact, it is well known that the change of nanoporosity usually alters these properties. For the aforementioned reason, a suitable choice of the carbon material and the modification technique are necessary to precisely and systematically change the nanoporosity. Furthermore, the choice of carbon material with real applicability in MET may greatly contribute to highlighting the potential of this study.

Particularly, expanded graphite (EG) is a carbon material commonly used in various electrochemical applications/devices, mainly as a bipolar electrode or current collector (Guo et al., 2021; Kim et al., 2021). This is a relatively low-cost material exhibiting great corrosion resistance, high electrical conductivity and density, as well as a matchless simplicity of handling and adaptation to most electrochemical cells. All these features of EG are important advantages for its

utilization in MET. However, it is practically a smooth material with negligible specific surface area, so its predictable low microbial electroactivity may have made it practically useful only as a current collector (for example, in combination with graphite felt). This may also explain why there are few studies analyzing the performance of EGs in microbial electrochemical systems (Alvarez Esquivel et al., 2020; Rajendran et al., 2022).

This work explores the impact of nanoscale porosity from a commercial EG electrode on the electroactivity of *Geobacter sulfurreducens* (1-4 μm size), a model electroactive microorganism (Bond and Lovley, 2003; Ishii et al., 2008; Marsili et al., 2008; Speers and Reguera, 2012). For this purpose, first, the physical activation of EG with CO_2 was investigated, and the effects of activation temperature and time were analyzed. Next, the physicochemical and electrochemical properties of the EGs, before and after CO_2 activation, were characterized by several techniques. Finally, the microbial electroactivity of selected materials was evaluated through cyclic voltammetry and chronoamperometry techniques in a three-electrode bioreactor with a pure *Geobacter sulfurreducens* culture and acetate as electron donor. Moreover, scanning electron microscopy (SEM) and fluorescence laser scanning microscopy (LSM) were used to visualize the colonization and metabolic activity of biofilms on the studied electrodes.

8.2 Experimental

8.2.1 Materials

A commercial EG from SGL-Carbon, called PV15 (SIGRACELL® bipolar plates), was chosen for this study. PV15 materials are flexible, thin (0.6 mm) and flat sheets of fluoropolymer-bonded expanded graphite with a low weight footprint. The electrical resistivity of this material is around 7 10^{-4} Ω cm (in parallel to the surface). Another type of EG was used in this work for comparison

purposes: flexible graphite *Papyex*® (from Mersen), with electrical resistivity of 0.001 Ω cm (parallel). Finally, an isostatically-pressed graphite plate (from Mersen) was used as a control electrode in the growth electroactive biofilm study. The electrical resistivity of this control material is 0.0008 Ω cm (electrode thickness = 5 mm). **Table 24** shows the characteristics of electrode materials provided by manufacturers.

Table 24 Characteristics of electrode materials provided by manufacturers.

Electrode	Company	Thickness (mm)	Electrical resistivity (Ω cm)	Bulk density (g cm^{-3})	Thermal conductivity (W m^{-1} K^{-1})
PV15[a]	SGL Carbon	0.6	0.0007 (in parallel) 0.3 (in perpendicular)	1.75	300
Papyex[b]	Mersen	1	0.001 (in parallel) 0.05 (in perpendicular)	0.7-1.3	Variable (50-150)
Graphite plate (grade 6503)[c]	Mersen	5	0.0008	17.74	200

NOTE: further details available in:

[a]https://www.sglcarbon.com/en/markets-solutions/applications/redox-flow-batteries/#

[b]https://www.mersen.co.uk/sites/uk/files/publications-media/6-gs-papyex-flexible-graphite-mersen.pdf

[c]https://www.mersen.co.uk/sites/uk/files/publications-media/1-markets-energy-solar-carbon-graphite-photovoltaic-mersen.pdf

8.2.2 Physical activation with CO_2

PV15 foils with different porosities were prepared by physical activation (i.e., partial gasification) with CO_2 at different temperatures and for distinct times. To do so, the foils were cut into pieces of 1.2 × 0.7 mm and introduced in the sample holder (alumina) of a simultaneous TGA/DSC 2 thermogravimetric system

(Mettler-Toledo), which enabled monitoring the sample weight-loss during activation. The reactor was initially evacuated with N_2 at room temperature for 10 min, and then heated at 20 ºC min^{-1} under continuous flow of 100 mL (STP) min^{-1} of N_2: CO_2 = 1:9 gas up to the desired activation temperature, ranging from 600 to 900 ºC. Next, the gasification experiments were carried out isothermally at these temperatures by using holding times ranging from 4 to 12 h. In this sense, longer treatments were not studied to avoid the formation of macropores (by excessive widening of porosity), thus, enabling this work to focus only on the effect of the smallest pores (Rodríguez-Reinoso et al., 1995). The influence of both the temperature and time on the activation degree was studied. The obtained samples are referred to as *PV15-T-t*, where *T* is the temperature (in ºC), and *t* is the holding time (in h) in the isothermal treatment.

8.2.3 Physicochemical characterization

The thermal behavior of PV15 was analyzed by thermogravimetry under both N_2 and N_2: CO_2 = 1:9 gas using the same equipment to that of section 2.2. The textural properties of the different samples were characterized by gas adsorption together with the assistance of SEM and atomic force microscopy (AFM). N_2 adsorption-desorption at 196 ºC and CO_2 adsorption at 0 ºC were performed on a Quadrasorb-Kr/MP apparatus (Quantachrome Instruments), after outgassing at 250 ºC under vacuum for 8 h. The specific surface area (S_{BET}) and the total volume of micropores ($V_{DR}(N_2)$) (pore diameter (d) < 2 nm) were calculated according to the BET and the Dubinin–Radushkevich (DR) equations, respectively, from N_2 adsorption/desorption isotherms (between $0.005 < P/P_0 < 0.15$) (D. Lozano-Castello, F. Suarez-García, D. Cazorla-Amoros, 2009). The mesopore volume (V_{mes}) (2 < d < 50 nm) was determined as the difference between the total pore volume ($V_{0.995}$, volume at relative pressure of 0.995) and the micropore volume ($V_{DR}(N_2)$) (D. Lozano-Castello, F. Suarez-García, D. Cazorla-Amoros, 2009). On the other hand, the volume of narrowest micropores

($V_{DR}(CO_2)$) (the so-called ultramicropores, d < 0.7 nm) was derived from the adsorption of CO_2 at 0 ºC also by using the DR equation (P/P_0 < 0.025) (D. Lozano-Castello, F. Suarez-García, D. Cazorla-Amoros, 2009). SEM images were obtained by using a JEOL JSM-840 microscope operating at 15 kV, while topographic information was derived from AFM by using a NTEGRA Prima equipment (NT-MDT SPM).

X-ray diffraction (XRD) measurements were obtained by the aid of a KRISTALLOFLEX K 760−80F diffractometer (Bruker D8-Advance) with a Ni-filtered CuKα radiation (λ = 1.5416 Å) generated at 40 kV and 40 mA. The profile intensities were recorded stepwise within 2θ = 10-60° at a scan rate of 1° min^{-1} and with a scan step of 0.05° in 2θ (step time 3 s). Raman spectra were recorded with a Jasco NRS-5100 dispersive system using a frequency-doubled Nd:YAG laser at 532 nm, with a maximal spectral resolution of 1 cm^{-1}, and a Peltier cooled CCD detector. The electrical conductivity measurements were carried out by using a Lucas Lab resistivity equipment with four probes in-line. In addition, the surface chemistry of the graphite foils was studied by X-ray photoelectron spectroscopy (XPS) in a K-Alpha spectrometer (Thermo-Scientific) with MgKα radiation (1253.6 eV).

8.2.4 Assembly, operation and electrochemical analysis of the bioreactor

The microbial electroactivity of the different PV15 samples (activated and non-activated) was studied in a single-chamber bioreactor using a three-electrode configuration. This experimental setup enabled simultaneous electrochemical control and measurement of the microbial response on different electrode materials under the same physicochemical and biological conditions, thus, ensuring a meaningful performance comparison (Prado et al., 2020a). The schematic diagram of the laboratory assembly is shown in **Figure 66** and a photo of the real laboratory system setup is shown in **Figure S-73(A).**

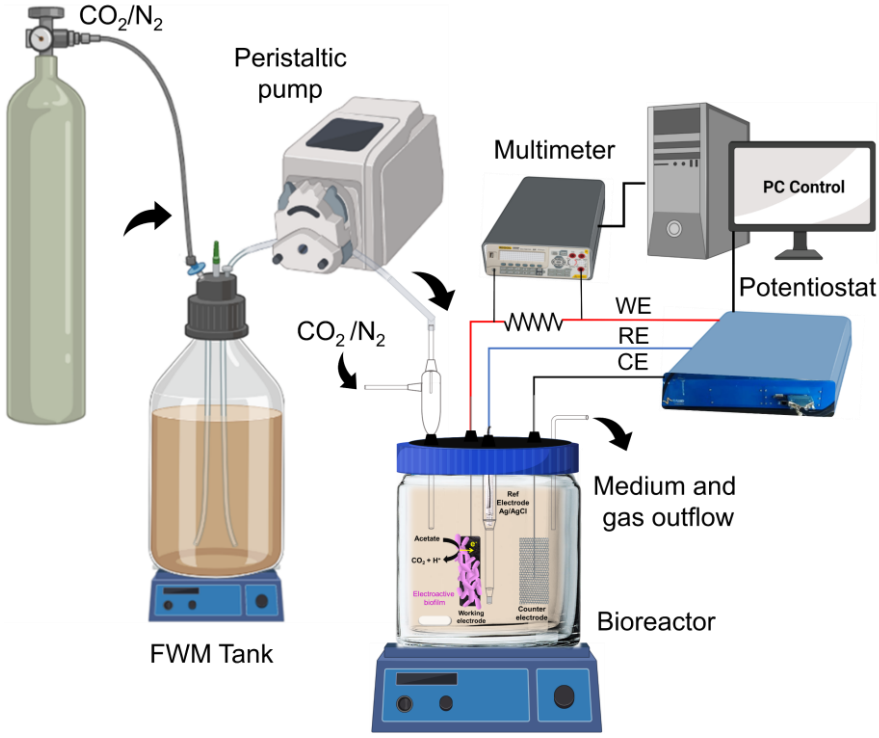

Figure 66. Schematic diagram of the laboratory assembly to study the growth and electroactivity of biofilms on the different studied materials used as working electrodes. Created with Biorender.com.

The 3-electrode bioreactor was assembled into a sterilization hood to avoid contamination (**Figure S-73(B)**). The sterilized bioreactor was filled with a 600 mL freshwater medium (FWM, pH = 7.4, electric conductivity (EC) = 6.2 mS cm^{-1}) composed of vitamins, minerals (Esteve-Nunez et al., 2005) and 20 mM acetate as an electron donor; the polarized electrode was the only electron acceptor. Three types of EG electrodes (PV15, Papyex and CO_2-activated PV15), as well as the isostatic graphite plate, were used as working electrodes. This last material is a well-known carbonaceous surface used as a control electrode to confirm the appropriate behavior of electroactive bacteria in the bioreactor. The counter electrode was a platinized titanium mesh, while the reference electrode was Ag/AgCl (3 M NaCl) (RE-5B BASi, USA). A fritted glass chamber with 3 M NaCl was used as lugging capillary to place the reference electrode (**Figure S-**

73(C and D)). The potential of this reference electrode was checked prior to the experiments.

An optimal connection of the different electrodes is paramount to measuring meaningful and reproducible signals. According to previous works, this was ensured depending on its nature (Prado et al., 2020a). Details of these connections (**Figure S-73(E and F)**) as well as the geometric surface area and resistance of anode electrodes with the connections are provided in the supporting information (**Table S-27**).

After its assembly, the bioreactor was hydraulically connected with a sterilized feeding tank (2 L of FWM without electron acceptor) and electrically connected to a polarization and data acquisition instrument (BioLogic (SP – 150) potentiostat and Keithley Integra Series 2700 Multimeter, respectively) (Prado et al., 2020a) **(Figure 66)**. Then, the whole system was purged with a gas phase of N_2/CO_2 (80%/ 20%) passing through an oxygen filter (Gas Clean Filter System, Agilent Technologies). Before inoculation of the bioreactor, initial CV (scan rates: 5 and 10 mV s^{-1}) was performed (in FWM) to characterize the surface of each working electrode, ensure the proper connections and verify the current intensity absence from other analytes inside the bioreactor. After these abiotic CVs, all the electrodes were simultaneously polarised at + 0.2 V (vs. reference electrode, Ag/AgCl, NaCl 3M). Then, the bioreactor inoculation was carried out by adding 25 % (v/v) of a pure anaerobic exponential-phase culture of *Geobacter sulfurreducens* (strain DL1). After inoculation, the bioreactor was initially operated in batch mode for the first 48 h, and then a constant flux of FWM (0.7 mL min^{-1}) was circulated with a peristaltic pump from the sterilized feeding tank to the bioreactor. With this continuous operation mode, the FWM was renovated inside the bioreactor to maintain the electron-donor substrate and avoid changes in pH due to the metabolism of electroactive bacteria. The current density evolution provided by each anode was recorded over time and calculated with the geometric area of the electrodes. The evolution of biofilm growth was tested by

biotic CV at different times during the experiment. The potential window was between 0.8 V to - 0.8 V (vs. Ag/AgCl; NaCl 3 M reference electrode), and the scan rate was 5 mV s^{-1}. The bioreactor was continuously purged with N_2/CO_2 in the headspace, and the mediums were continuously stirred at a low rate. The temperature was maintained at 30-35 °C in the bioreactor during the entire experiment. During the CV, the low agitation and pumping of the new medium into the reactor were not stopped. In addition, an abiotic control experiment (chronoamperometry without electroactive inoculum) of these activated electrodes was carried out (see **Figure S-77**, Supplementary information).

8.2.5 Biofilms microscopy analysis

SEM (Digital Scanning Microscope DSM-950) was used to visualize the surface morphology of electrodes. The electrode samples were submerged into a fixation solution (Cacodylate buffer, 0.2 M, pH 7.2, containing 5 % glutaraldehyde) for one hour at room temperature. The samples were rinsed in 0.2 M cacodylate buffer for 10 min and then dehydrated at room temperature in an ascending graded ethanol series (25, 50, 70, 90 and 100%; 10 min each stage). Finally, the samples were rinsed in acetone for 10 min and immersed in anhydrous acetone at 4 ºC overnight. The last steps were carried out in the microscopy service of Alcalá University, where the dehydrated samples were dried in CO_2 at the critical point. Also, they were mounted in pins and gold sputter-coated for their visualization.

On the other hand, LSM was used to visualize metabolically active biofilm on the electrode surface. After operation as bioanode, the electrodes were carefully removed from the reactor and fluorescently stained with the LIVE/DEAD BacLight bacterial viability kit (Invitrogen). For this task, 2 µL of a mixture 1:1 of SYTO9: propidium iodide was added to 1 mL of phosphate buffer (90 mM). The electrodes were exposed to this mixture for 15 min at room temperature in the dark before washing with buffer phosphate twice to remove

the excess staining. Fluorescence images were captured using an inverted microscope (Nikon, ECLIPSE, *Ti-S*) so that bacteria with intact cell membranes emit green light. The excitation/emission wavelengths for SYTO 9 and propidium iodide were 488/500–550 nm and 543/600–670 nm. Metabolically active biofilm was observed under different light intensities.

8.3 Results and Discussion

Expanded graphite PV15 was first activated under different conditions and their physicochemical properties and electrochemical behaviour were characterized before and after activation. Then, all materials were tested in presence of the model electroactive microorganism electrochemically analyzed, and biological assays were carried out to study the influence of the materials' nanopores on their microbial electroactivity.

8.3.1 Thermal behaviour and CO_2-activation of expanded graphite PV15

The evolution of the PV15 sample weight (normalized) during heat-treatment under two different atmospheres, i.e., inert (N_2) or reactive (N_2: CO_2), as well as the corresponding derivative curves, are shown in **Figures 67A** and **67B**, respectively. The matching thermograms **(Fig. 67A)** indicate that the thermal behavior of PV15 is practically independent of the atmosphere until ca. 450 ºC. Thus, in both cases, this material decomposes from ca. 330 ºC up to 490 ºC, encompassing two overlapped processes **(Fig. 67B)**. The first process between 300-395 ºC reaches a maximum decomposition rate at 366 ºC whereas the strongest one shows its maximum rate at ca. 450 ºC. However, both figures evidence that the extent of the decomposition between 450-490 ºC is more marked for the CO_2 gas. Thus, the weight-loss up to this temperature is ca. 12.4 and 14.9 % for the N_2 and CO_2 atmosphere, respectively. This reflects the higher reactivity of CO_2 compared to N_2, even at this moderate temperature range. The

weight-loss of the material heated in CO_2 atmosphere practically coincides with the 15 wt.% of binder polymer in PV15, as provided by the company, so the thermal process between 330 - 490 ºC is certainly attributed to the decomposition of this polymer on the surface of this material.

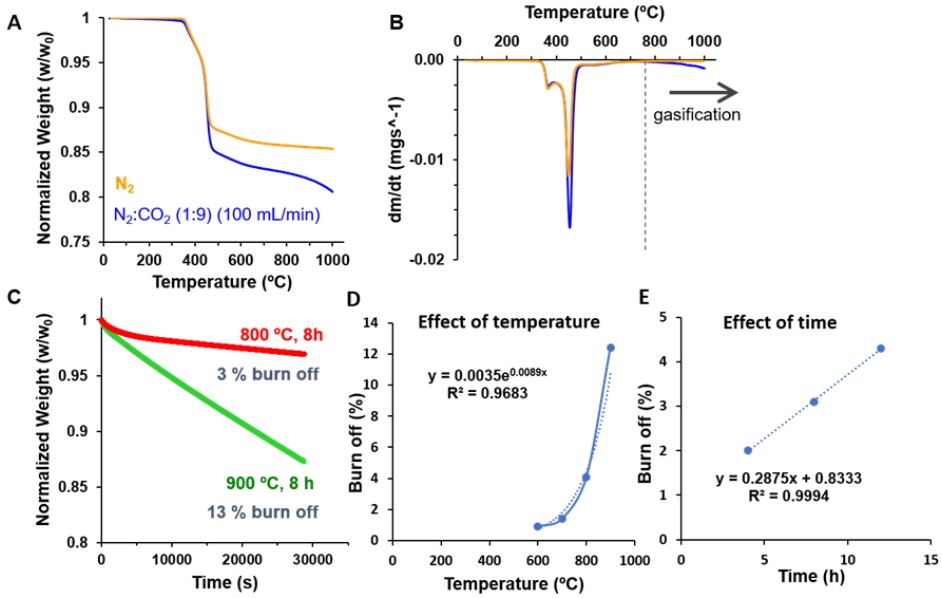

Figure 67. **(A)** Normalised weight loss and **(B)** the corresponding derivative (DTG) curves of PV15 in N_2 and N_2:CO_2 (1:9) atmospheres. Gas flow = 100 mL min^{-1}. Heating rate = 10 ºC min^{-1}. Effect of temperature at constant time (8 h) on **(C)** the weight loss and **(D)** burn off; and **(E)** the effect of time at 800 ºC on the burn off.

Next, from 490 to 700 ºC the material experiences a softer decomposition process, with a 1.6 and 1.9 % weight loss for the N_2 and CO_2 atmospheres, respectively. This process could be related to the release of less accessible inner parts of the polymer alone or pulling out some fragments of graphitic layers on PV15 during decomposition. This is in line with the eruption-like big holes (1-10 µm) observed by SEM on some parts of PV15 surface (see **Figure S-74(A and B)**).

Finally, above 700 ºC, while the weight of PV15 stabilises in N_2 gas, it continues decreasing in CO_2. This weight loss is then ascribed to the gasification

of the graphitic material with CO_2 (see equation 1) (Contescu et al., 2018), a phenomenon that may start around this temperature at the used conditions.

$$C(s) + CO_2\,(g) \rightarrow 2\,CO\,(g) \qquad (1)$$

Hence, the effects of the temperature and reaction time on the gasification of PV15 were studied. In these experiments, the weight of PV15 was monitored upon heating up to a given temperature and, subsequently, during different isothermal conditions (see some examples in **Fig. 67C**). **Table 25** collects the burn-off values (%) of the different samples calculated as the weight loss percentage during these isothermal conditions. In addition, the table also includes the isothermal oxidation rates of PV15 (expressed as variation of weight loss per time, Δwt(%)/Δt(min)) deduced from the obtained burn-off values divided by the corresponding studied reaction times.

Table 25 Burn off (BO) and oxidation rate (OR) calculated at isothermal conditions and textural properties (from gas adsorption) of PV15 and some derivatives obtained under different conditions.

Electrode*	B.O.	O.R.	A_{BET}	$V_{0.995}$	V_{DR} (N_2)	V_{meso}	A_{DR} (CO_2)	V_{DR} (CO_2)
	%	% min^{-1}	m^2 g^{-1}	cm^3 g^{-1}	cm^3 g^{-1}	cm^3 g^{-1}	m^2 g^{-1}	cm^3 g^{-1}
PV15	---	---	0.0	0.000	0.000	0.000	9	0.003
PV15(N_2)	---	---	94	0.101	0.038	0.063	157	0.067
PV15-600-8h	0.8	0.002	83	0.112	0.031	0.081	115	0.049
PV15-700-8h	1.7	0.004	82	0.147	0.033	0.114	88	0.038
PV15-800-8h	5.1	0.011	88	0.152	0.036	0.116	106	0.046
PV15-900-8h	12.4	0.026	40	0.209	0.016	0.191	44	0.019
PV15-800-4h	3.1	0.013	83	0.149	0.033	0.116	83	0.036
PV15-800-12h	7.1	0.010	93	0.178	0.037	0.141	111	0.048

*NOTE: The obtained samples are referred to as *PV15-T-t*, where *T* is the temperature (in ºC), and t is the holding time (in h) in the isothermal treatment.

In general, the relatively low BO and OR values found for PV15 **(Table 25)** are ascribed to the slowness of gasification reaction and therefore, high stability, of graphitic structures in PV15. Nevertheless, both the BO as well as the OR of PV15 increase with temperature and time. Particularly, an exponential increase in burn off and oxidation rate with temperature is observed **(Figure 67D)**. This behavior can be generally represented by the Arrhenius relationship (see equation 2), in agreement with that observed for other carbonaceous materials during CO_2 oxidation (Contescu et al., 2018).

$$rate\ \left(\frac{\%}{min}\right) = \frac{\Delta wt(\%)}{\Delta t(\mathrm{min})} = A\ exp(-\frac{E_{act}}{RT}) \qquad (2)$$

where $\Delta wt/\Delta t$ is the rate of weight loss by chemical reaction at constant temperature T (K), R is the gas constant (8.314 J mol^{-1} K^{-1}), *Eact* is the activation energy, and A is the pre-exponential factor. From the linear representation ln $\Delta wt/\Delta t$ vs. $1/T$, the calculated apparent kinetic parameters for PV15 were *Eact* = 79 kJ mol^{-1} and A = 71.6 min^{-1}. These values agree with those of other carbon materials found in literature (Contescu et al., 2018).

On the other hand, at constant temperature, the burn off of PV15 increases linearly with time **(Figure 67E)**. This behaviour has been observed by other authors (Rodríguez-Reinoso and Molina-Sabio, 1992; Rodríguez-Reinoso et al., 1995; Bergna et al., 2019) and clearly reflects that the gasification rate for the studied material and conditions is constant.

8.3.2 Characterization of expanded graphite PV15 and CO_2-activated derived samples

From the structural point of view, the observed high intensity and remarkably narrow XRD peaks of PV15 **(Figure 68A)** stress the high crystallinity of this carbonaceous material. These peaks, centered at around 2θ = 26.55 and 54.65º, are related to the vertical or horizontal arrangement of graphene sheets aligned along the (002) or (100) planes in graphite, respectively (Rodríguez-Mirasol et al., 1996; Coutinho et al., 2000). Further details on the crystallinity of this material are provided in the SI (**Table S-28**). Because of such a graphitic structure, PV15 exhibits a high conductivity of 123 S cm^{-1} (0.008 Ω cm), which makes it suitable as current collector in electrochemical devices.

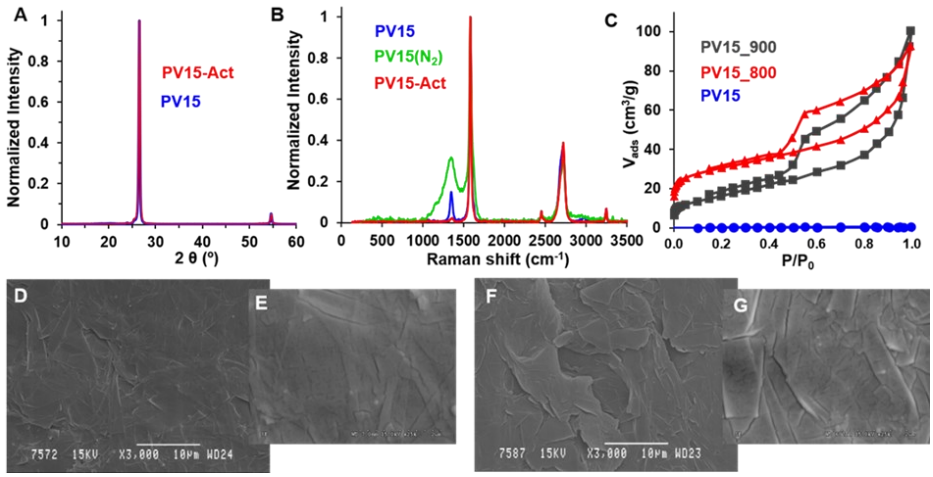

Figure 68. (A) XRD and **(B)** Raman spectra, **(C)** N_2 adsorption-desorption isotherms at -196 ºC of different samples, and **(D-G)** SEM images of PV15 **(D,E)** and PV15-800-8h **(F,G).**

In parallel, two strong bands centered at 1584 and ~2719 cm^{-1} in the Raman spectrum of PV15 **(Figure 68B)**, the so-called the G and 2D bands, have been assigned to the degree of two- and three-dimensionally graphitic orientation, respectively (Rodríguez-Mirasol et al., 1996). Particularly, the Raman shift, high relative intensity and narrowness of these bands found for this material (**Table S-**

28) are also characteristic of a high degree of structural order (Wang et al., 1990; Cuesta et al., 1994). Nevertheless, the so-called D band at 1348 cm^{-1} is indicative of surface structural defects on this graphitic material. In this sense, chemical analysis by XPS evidenced F atoms (15.3 at.%) and aliphatic carbon bonds on PV15 surface (**Table S-29**), confirming the presence of the polyfluorinated binder polymer on this material.

Respect to the textural features, the null N_2 and CO_2 adsorptions on pristine PV15 **(Figure 68C** and **Table 25)** stress the smoothness of this material at the narrowest nano-scale. Moreover, SEM images evidence the overall flat surface of this material at microscale **(Figure 68D** and **68E).** However, the images also show some cracks of 20-50 nm width and laminates on this material. Hence, AFM was used to get further insight into the topography of this sample. Despite apparently flat, the 2D **(Figure 69A)** and 3D **(Figure 69B)** AFM images reveal unevenness of up to 1.2 µm and certainly some roughness on PV15 surface. Specifically, the calculated roughness average (Ra) and root mean square roughness (Rq) were 85.952 and 103.934 nm, respectively.

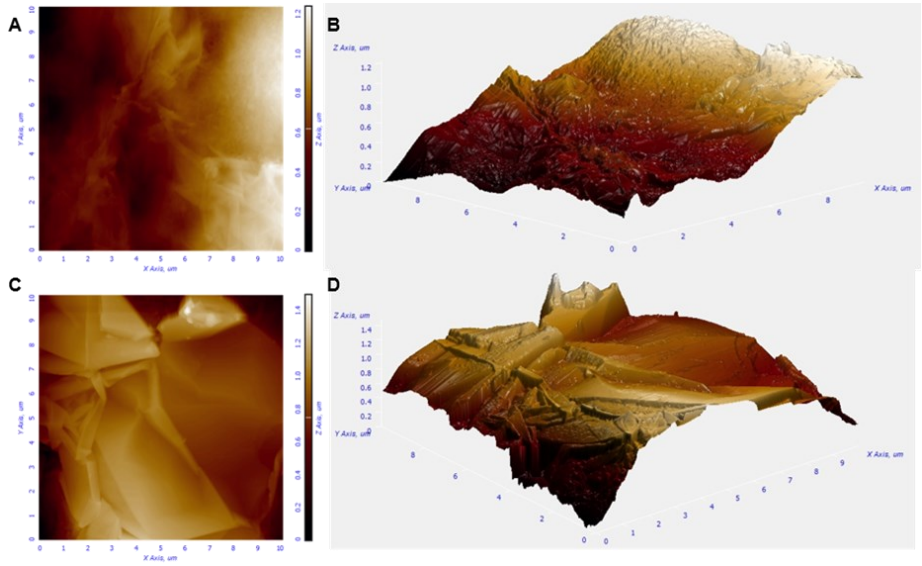

Figure 69. 2D and 3D AFM images of PV15 (10x10 µm) before **(A,B)** and after **(C,D)** CO_2 activation.

Interestingly, the practically identical X-ray diffractograms **(Fig. 68A)** and quite similar G and 2D Raman bands **(Fig. 68B)** observed for PV15 before and after heating in different atmospheres indicated that its inner graphitic structure and therefore, electrical conductivity (140 S cm^{-1} (resistivity = 0.007 Ω cm) for PV15-800-8h), was not significantly affected by the studied thermal treatments. By contrast, the thermal treatments were found to affect mainly the surface of this material. Thus, XPS pointed out that F atoms were released during thermal treatment in both N_2 and CO_2 atmospheres (**Table S-29**), and Raman and textural characterisation highlighted significant differences between the samples heated in these two distinct gases.

On the one hand, while the D band practically vanishes in the case of the CO_2-activated sample, the relative intensity and width of this band remarkably increased for the sample heated under N_2 atmosphere **(Fig. 68B).** Since this contribution is ascribed to the fluoropolymer film, the obtained results suggest that the surface may be cleaned and practically free of defects when heated in CO_2, but a pyrolysed decomposition product seems to remain after treatment in N_2 gas.

On the other hand, the different heat-treatments were found to greatly develop the textural properties of PV15 **(Table 25)**. The observed IV-type shape of N_2 adsorption-desorption isotherms **(Fig. 68C)** reveal the formation of micropores and mesopores (Rouquerol et al., 1994) during heat-treatment. These small pores are generally assigned to the spaces left empty among graphitic foils by the release of the binding polymer and/or the oxidative reaction of graphite with CO_2 (equation 1).

Nonetheless, other phenomena could also contribute to the formation of these small pores. Thus, despite showing the lowest weight loss (i.e., the lowest degree of polymer removal), the sample treated under N_2 gas up to 1000 ºC (PV15(N_2)) was found to develop the largest volume of ultramicropores (0.067 cm^3 g^{-1}) and among the largest volumes of micropores (0.038 cm^3 g^{-1}) in the present study

(Table 25). Since this sample still contains a residue of the carbonised polymer (as deduced from TG and Raman), this higher microporosity may be ascribed to the formation of pores and/or cracks in the polymer film itself by the partial decomposition and/or release of polymer molecules. In fact, the presence of porous and rough deposits on PV15(N_2) was confirmed by SEM and AFM (see **Fig. S-74(B and C)**) and **S-75**). In addition, the incomplete polymer decomposition could also explain the second largest ultramicroporosity found for the CO_2-derived sample obtained at the lowest temperature studied (PV15-600-8h in **Table 25**). However, initial stages of CO_2 gasification should not be ruled out.

As deduced from **Table 25**, the increment in temperature from 600 to 900 ºC and/or time generally increased the total volume of pores ($V_{0.995}$), i.e., degree of activation, on PV15. However, the pore structure was greatly affected by the chosen heating conditions. On the one hand, the volume of ultramicropores first decreased to reach a minimum for the sample obtained at 700 ºC; but it subsequently increased for the sample 800 ºC and it drastically decayed when obtained at 900 ºC. On the other hand, while the volume of mesopores steadily increased with temperature, the volume of micropores increased up to 800 ºC and it remarkably dropped for the sample prepared at 900 ºC (from 40 to 20 % of the total pore volume). On the other hand, at constant temperature of 800 ºC, the increase in reaction time progressively augmented the volume of ultramicro-, micro- and mesopores, at least for the first 12 h of isothermal treatment.

The minimum ultramicroporosity found for PV15-700-8h, suggests the absence or minimisation of porous deposits on this sample and, therefore, the promoted or completely decomposition of the binder polymer from 700 ºC. Next, a higher temperature like 800 ºC may concurrently favor the generation of ultramicropores, and their subsequently widening into micropores and/or mesopores on the graphitic layers by CO_2 gasification (see equation 1). Afterwards, further pore widening seems to be promoted at 900 ºC, increasing

the relative proportion of mesopores. These results point out the interconversion of ultramicropores into micropores and that of micropores into mesopores with the increasing temperature and reaction time (Rodríguez-Mirasol et al., 1993).

Concerning the surface morphology and roughness of CO_2-activated samples (see PV15-800-8h as example), both SEM (**Figures 68F** and **68G**) and AFM (**Figures 69C** and **69D**) images clearly show that heat-treatments in CO_2 efficiently remove the binder polymer to expose the interconnected graphite sheets on the surface of PV15. This is in line with Raman and XPS analyses. Moreover, unlike the case of the treatment in N_2 gas, big holes are not observed in the CO_2-derived samples, so the reaction with CO_2 might facilitate the release of less accessible polymer chains. From the analysis of AFM images, the calculated Ra and Rq for PV15-800-8h were 153.208 and 204.800 nm, respectively. These average-like parameters are approximately twice those found for pristine PV15 and reflect the more abrupt topography resulting from the exposition of graphite sheets (**Figure 69D**).

The obtained results demonstrate that both CO_2 gas and temperatures high enough are necessary to eliminate the polymer from PV15 surface. Although the surface became more abrupt, the average roughness (ca. 85 to 150 nm) did not seem so remarkable, at least respect to the micron-sized electroactive bacteria. By contrast, the main effect of CO_2 reaction has been found the activation of PV15 surface, i.e., the generation of a large volume of pores ranging from 0.7 to 50 nm. These pores are too small, i.e., physically inaccessible for an electroactive bacteria like *Geobacter*, whose dimensions comprise ca. 1-3 μm. Then, the influence of these changes on the microbial electrochemical response was studied. Because of the cleanliness and larger volume of small pores, the samples prepared at 800 and 900 ºC were selected for this study.

8.3.3 Microbial electroactivity

Abiotic control

The first step for studying microbial electroactivity on the surfaces of the different materials was to perform CV on each of the working electrodes before inoculating the reactor. This task was carried out with three purposes: **1)** to corroborate the optimal connection of the electrodes with the current collectors (wires); **2)** to ensure that there were no electron transfer signals with the electrode surface at the beginning of the experiment when electroactive bacteria were not present; and finally, **3)** to study the electrochemical change in the surface of commercial material after CO_2 activation.

The voltammetric response of the pristine and activated electrode surfaces **(Figure 70A)** revealed no peak of current intensity in the potential window analyzed for PV15; furthermore, no species participated in electron transfer with the surface under these initial conditions. In contrast, the green and red voltammetric cycles corresponding to the activated material PV15-900-8h and PV15-800-8h, respectively, present a marked capacitance compared to plain PV15 (i.e., without activation). The CV curves showed a more rectangular shape in the potential windows, which indicated a better current response behavior than non-activated material (since the current depends on the electrode surface area). In order to maximize the capacity of a material, a well-balanced between meso and microporosity is needed (Fuertes et al., 2005). The charge increases markedly after material CO_2 activation, and it is associated with the adsorption of ions in micro and mesopores. The adsorption of ions in micropores is more effective than in larger pores due to confined micropores forcing ions to desolvate partially or entirely (Simon and Gogotsi, 2008). Probably, for this reason, the capacity shown by the material activated at 800 ºC for 8h was somewhat higher compared to that of the material activated at 900 ºC for 8h. In addition, the slightly more tilted CV of PV15-800-8h compared to that of PV15-900-8h may be attributed to the

slightly lower resistance of the former material, which shows a lower activation (burn-off) degree.

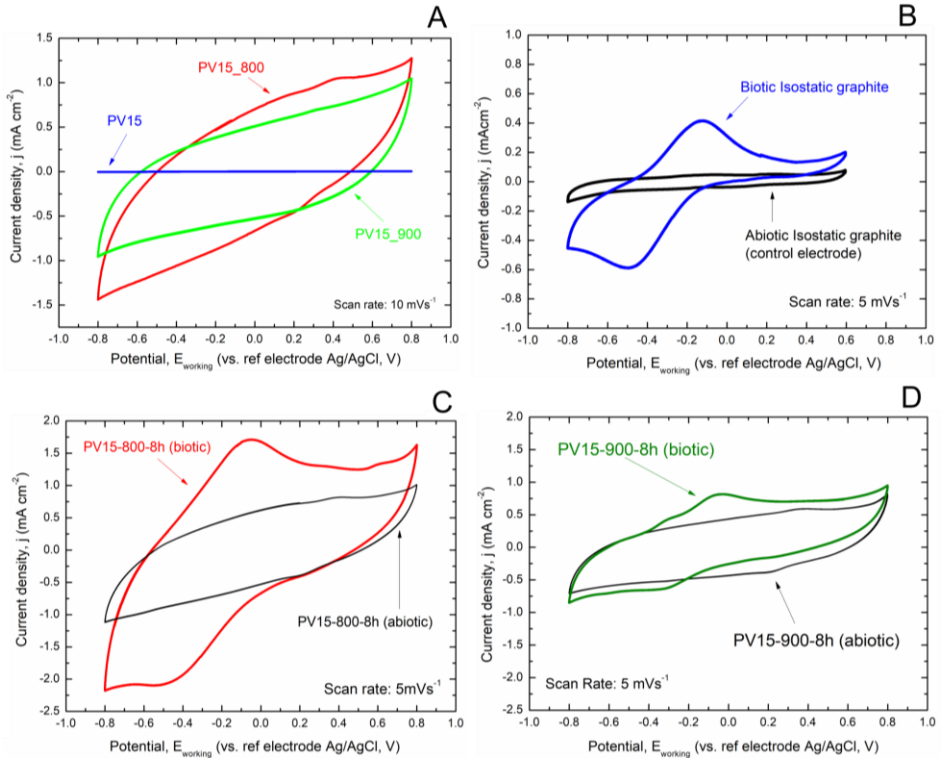

Figure 70. (A) CV for commercial expanded graphite, PV15 (blue line), and activated expanded graphite electrodes at a temperature of 800 ºC during 8h (PV15-800-8h, red line) and 900ºC during 8h (PV15-900-8h, green line) in freshwater media (without *Geobacter sulfurreducens*). CV Scan rate = 10 mV s^{-1}. **(B)** Abiotic initial CV (without *Geobacter sulfurreducens*, black line) and biotic CV after the chronoamperometric experiment (growth of the electroactive biofilm on the surface of the electrode in the presence of *Geobacter sulfurreducens*, blue line) of the control electrode formed by isostatic graphite plate (scan rate = 5 mV s^{-1}). **(C, D)** CV in FWM without *Geobacter* (black line) and after the chronoamperometric experiment with electroactive biofilm on the activated electrodes **(C)** biotic PV15-800-8h (red line) and **(D)** biotic PV15-900-8h (green line) (scan rates = 5 mV s^{-1}).

The electrochemical behavior in the freshwater medium of the abiotic non-activated expanded graphite papers (PV15 and Papyex), isostatic graphite plate, and activated PV15 electrodes through the CV technique is shown in SI **(Figure S-76)** for comparison purposes**.** PV15 voltammetric profile is very similar to Papyex **(Figure S-76(A))** and even to that of the control isostatic graphite plate, although it had a more significant double layer **(Figure S-76(B)).** The more significant double layer of the activated expanded graphites compared to the isostatic graphite plate was also confirmed **(Figure S-76(C)).**

Biological assays: microbial current generation

The objective of this section was to analyze the response of the activated and non-activated materials to the growth of electroactive biofilms of *Geobacter sulfurreducens*. In this sense, we classified the quality of the material according to the current density generated by the electroactive biofilm. The electrons were generated during the oxidation of an organic substrates (i.e., acetate) by electroactive bacteria. The bioreactor was designed to house all the working electrodes in the same physicochemical and biological conditions. All working electrodes were polarized at 0.2 V (vs. Ag /AgCl, 3 M NaCl reference electrode), and the current was recorded for 35 days in the presence of *Geobacter sulfurreducens* inoculum **(Figure 71A)** (see Supplementary Information for abiotic controls and experiment repetitions to ensure reproducibility, **Figure S-77** and **S-78**). It is noteworthy to highlight that this bioelectrochemical reactor is not an MFC. Instead, it is a practical system to study and compare the performance of electroactive bacteria on different materials.

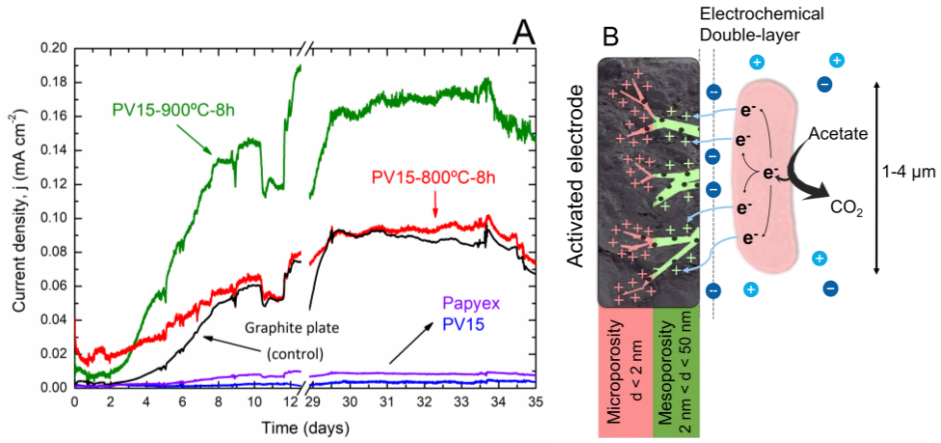

Figure 71. (A) Current density (mA cm^{-2}) generated by *Geobacter sulfurreducens*. Working electrodes were operated at a constant potential of 0.2 V vs. Ag/AgCl, 3 M NaCl reference electrode. **(B)** Proposed effect of nano-scale porosity in the microbial extracellular electron transfer. The size difference between a bacteria (1-4 µm) and nano-scale pores (nm) are represented.

Chronoamperometry showed two explicit scenarios. Firstly, in non-activated expanded graphite materials, an increase in current density was not observed due to the growth of the *Geobacter sulfurreducens* film. However, an increased current was observed during experiments with activated materials, PV15-800-8h and PV15-900-8h, and the control material. As explained before, these currents are related to the different microbiological activity towards acetate oxidation in the aqueous solution (medium). The chronoamperometry of these last materials (activated and electrode control) showed two clear phases of the growth of the electroactive biofilm. The lag phase (the first 2 days) provided a current density almost negligible. The freshwater medium (FWM) circulation through the reactor (t = 48 h) renewed the medium and a second phase was observed. Thus, the current density was increased exponentially, indicating a constant growth of the electroactive biofilm on the surface of the materials. After several days, a stable current density was reached, being j = 0.09 mA cm^{-2} for the activated electrode PV15-800-8h, and j = 0.17 mA cm^{-2} for the activated electrode PV15-900-8h (red and green line in **Figure 71A**, respectively). This current density value indicated

steady-state biofilm formation (the growth and death and/or electroactivity of the bacteria was constant). According to literature, the steady-state current density depends on many parameters such as electrode material, temperature and biofilm composition, and it is considered a feature of a particular electroactive electrode/biofilm system (Logan, 2007). **Table 26** summarizes the steady-state current densities for the studied electrodes and compares them with other reported studies under similar experimental conditions.

Table 26 Summary of current densities for the studied electrodes and other reported studies using a 3-electrode set-up and polarized at 0.2 V vs. Ag/AgCl.

Anode material	Pore size	Inoculum	Substrate	j (mA cm^{-2})	Ref.
Carbon fiber	6.8 µm	Wastewater	Acetate 10 mM	j (max) = 3.0	(He et al., 2011a)
	0.4 µm			j (max) = 1.7	
Commercial Carbon felt	47 µm	Wastewater	Acetate 10 mM	j (max) = 1.2	(Chen et al., 2011a)
NCP-CFM	38 µm			j (max) = 0.5	
2D-ECFM	0.6 µm			j (max) = 0.17	
Carbon felt	20-200 µm	Sludge	Food waste	j (max) = 0.3	(Blanchet et al., 2016)
Non-porous ITO	-	S. oneidensis	-	j (max) = 0.00005	(Wenzel et al., 2018)
Polystyrene microspheres	80-140 µm			j (max) = 0.03	
Nanoparticle suspension (nanoporous)	10-100 nm			j (max) = 0.006	
Papyex (Mersen)	-	G. sulfurreducens	Acetate 20 mM	j (steady-state) = 0.008	This study
PV15 (SGL Carbon)				j (steady-state) = 0.003	
PV15-800-8h	< 50 nm			j (steady-state) = 0.10	
PV15-900-8h				j (steady-state) = 0.17	

*NCP-CFM (Natural cellulose paper – Carbon nanofiber mat). * 2D-ECFM (Electrospun-carbon nanofiber). *ITO (non-porous indium tin oxide).

Interestingly, introducing micro- and mesoporosity in PV15 improves biofilm activity (60-fold) compared to plain EG. The electrode activated at 800 °C (for 8 h), with the largest volume of micropores, reaches almost the same steady-state current as the control electrode. However, the electrode activated at 900 ºC with many micropores and a higher volume of mesopores reached ca. 0.2 mA cm^{-2} (in steady-state), which is almost double the current density provided by previous electrode materials. Even if the microbial current density could be slightly lower compared to the electric current provided by reported materials in the literature (see **Table 26**), the use of these activated materials could significantly decrease the internal resistances (i.e., and high costs associated to the use of the state-of-the-art electrodes in METs.

A similar improvement in bioelectricity production has been observed in systems where the anode material in the presence of carbon nanotubes (CNTs) improved the extracellular electron transfer (Ma and Hou, 2019), as microporosity was increased after modification. In this work, the authors claimed that the carbon nanotube-chitosan (CNT-CS) layer with mesoporous and microporous structure provides a strong interaction with microbial films (Xie et al., 2011), facilitating electron transfer between biofilm and the conductive surface. However, the nature of this strong interaction was not described or defined.

Despite this work is focused on the study and demonstration of the phenomenon itself (neither it has been intended nor the experiments have been designed to study its mechanism), potential reasonable explanations can be suggested. Thus, taking into account that micro and mesoporosity in the material are not accessible to microorganisms, a possible hypothesis for this improvement in current production could be that the number of electrons exchanged by electroactive microorganisms could be determined by the number of surface charges that must be compensated by ion adsorption on the electrode pores (**Figure 71B**). In this sense, the highest current density produced by bacteria has

been observed for the electrode prepared at the highest activation temperature (PV15-900-8h), which shows the largest number of total pores ($V_{0.995}$ in **Table 25**). Nonetheless, this bioelectrode also exhibits the highest proportion of mesopores (V_{meso} in **Table 25**), so not only micropores but also bigger nanopores might play an important role. In fact, it is well known that mesopores are essential for faster ion diffusion into electrode inner micropores to produce larger currents in distinct electrochemical applications (Liu and Creager, 2010; Zhang et al., 2014; Momodu et al., 2017). On the other hand, previous studies in abiotic media showed that the adsorption of proteins, like *cit c*, is promoted in nanostructured carbon films with increasing pore sizes between 30 – 150 nm (Vijayaraj et al., 2010). Hence, given the fact that *cit c* is considered to be a protein involved in direct EET by electroactive bacteria (Busalmen et al., 2008), it is proposed that the presence of mesopores or bigger nanopores in the studied activated samples may somehow facilitate the physicochemical interaction and/or EET with *Geobacter*'s proteins.

The electrochemical characterization of biofilm development on the electrode surfaces during experiments was carried out by CV. **Figure 70** compares the biofilm evolution on the surface of the activated electrode PV15-800-8h (**Figure 70C**) and PV15-900-8h (**Figure 70D**) before inoculation of the bioreactor (black line) and at the steady-state (constant current density in the chronoamperometry) (colored line). The same procedure was carried out with the control electrode (**Figure 70B**). The CV at steady-state current density showed the characteristic turnover signal obtained when the extracellular electron transfer capacity (EET) of electroactive bacteria occurs (in the presence of an electron donor) (Maestro et al., 2014). The signal showed a redox couple attributed to the electron transfer from the electron donor (acetate) to the carbonaceous surface, mediated by the C-type cytochromes of the electroactive bacteria (Richter et al., 2009; Prado et al., 2019).

The difference between the CVs of colonized materials was remarkable. The activated electrode PV15-900-8h revealed the highest steady-state current density during chronoamperometry, but a lower response in current density value throughout the entire potential window analyzed. However, this current density value was higher for the activated material PV15-800-8h, which showed a lower current density during the biofilm growth experiment. This effect could be due to a higher surface area of the PV15-800-8h material (**Table 25**), which contains a larger volume of micropores on its surface (i.e., effect of the electrical double-layer capacity of the modified electrode due to surface area increase).

After the electrochemical analysis, the materials were duly prepared for their visualization with SEM and LSM microscopic techniques. The obtained SEM and LSM images of the activated electrode PV15-800-8h before the biotic chronoamperometry showed the absence of any biofilm on its surface **(Figure 72A** and **72C**, respectively). On the contrary, after the chronoamperometric experiment, the same electrode surface exhibited a clear biofilm distinguishing the characteristic bacillus-shape of *Geobacter sulfurreducens* **(Figure 72B).** Moreover, the presence of green fluorescence clusters of live bacterial cells was observed in the LSM image of this electrode after biological assays **(Figure 72D).** Similar images were obtained for the activated electrode PV15-900-8h. These results corroborate the formation of a *Geobacter sulfurreducens* biofilm on the electroactive electrode surfaces.

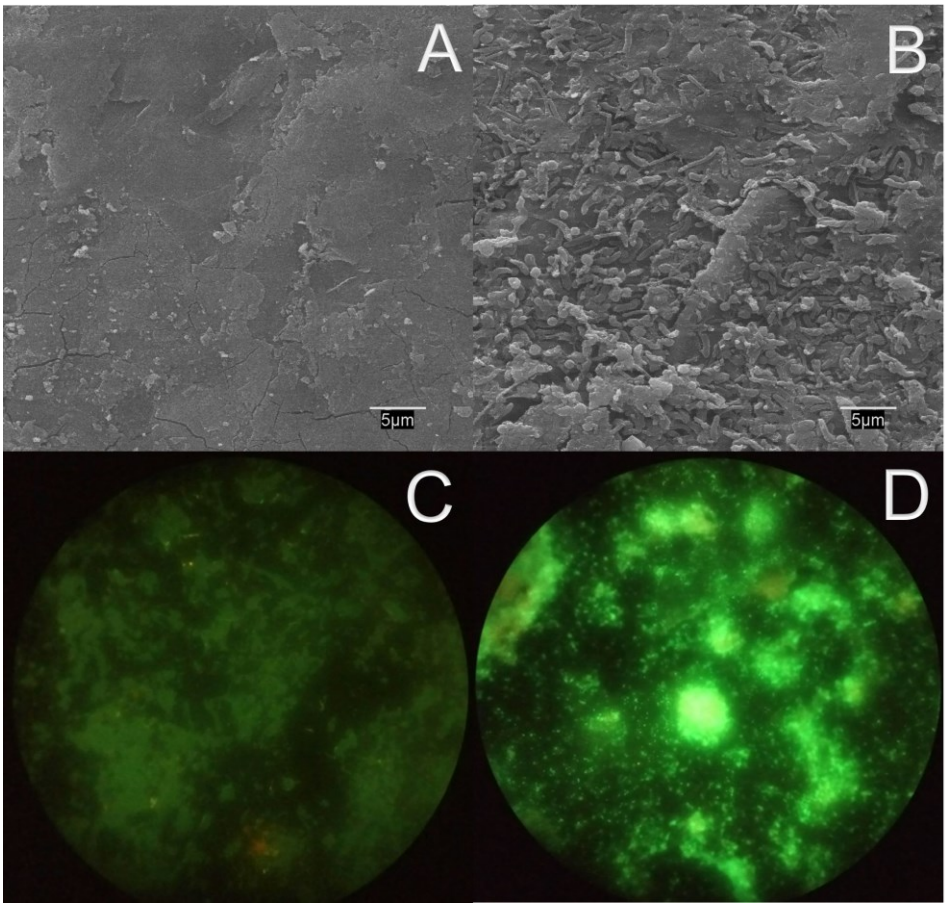

Figure 72. Verification of biofilm growth: SEM images of the surface of the activated electrode PV15-800-8h, **(A)** before and **(B)** after the chronoamperometry in the presence of electroactive bacteria; and fluorescence (LSM) images of the same electrode **(C)** before and **(D)** after this chronoamperometric experiment. Bacteria with intact cell membrane stain green.

8.4 Conclusions

This work presents a systematic study on the CO_2-activation of PV15 commercial expanded graphite including microbial electroactivity responses in presence of this upgraded material. Thus, this contribution tackles two poorly-studied but interesting topics in MET, i.e., the effect of nano-scale porosity in the response of electroactive bacteria and the potential use of EG as bioelectrode. The

obtained results indicate that PV15 gasifies in CO_2 atmosphere from 700 ºC, progressively increasing the volume and mean diameter of nanopores with the temperature and reaction time. Apart from the changes in textural properties and the removal of binder polymer, these treatments do not significantly affect the microstructure and electrical conductivity of PV15.

Voltammetric characterization of the materials under abiotic conditions reveals that CO_2-activation causes a huge increase in the electrical double layer capacitance (EDLC) of PV15 (up to 425 times) as the main electrochemical consequence of nanopores generation. In addition, under biotic conditions, this technique also evidences that the extracellular electron transfer (EET) of *Geobacter sulfurreducens* on PV15 was greatly promoted after CO_2-activation. Furthermore, chronoamperometries and microscopy analysis have demonstrated that CO_2-activation treatments greatly promote the growth and bioelectricity production (up to 60 times) of *Geobacter sulfurreducens*.

From (i) the consistency of nanopores generation and remarkable EDLC enhancement, (ii) the insignificant modification of other properties, as well as (iii) the inaccessibility of bacteria to the created nanopores; the observed effective redox coupling between *Geobacter* and CO_2-activated PV15 samples points out a direct effect of nanoporosity on microbial electroactivity. It is proposed that the capability of electroactive microorganisms to transfer electrons with carbon surfaces may be greatly affected by the availability of sites (nanopores) to accommodate or compensate electric charge in the electrode surface. Moreover, these pores could also promote the interaction or EET with bacteria proteins ranging nanoscale dimensions. Nevertheless, the understanding of the mechanisms of this promoted activity needs further studies.

The present research not only presents a new strategy to enhance the performance of bioelectrodes, but it also suggests that activated EG electrodes could be good candidates for the simplification and cost reduction of different bioelectrochemical systems.

Supplementary data of Chapter 8

I. Assembly and connections of the electrochemical bioreactor.

II. Characterisation of PV15 and derived CO_2-activated samples

III. Comparison of microbial electroactivity: commercial materials versus activated materials

I. Assembly and connections of the electrochemical bioreactor

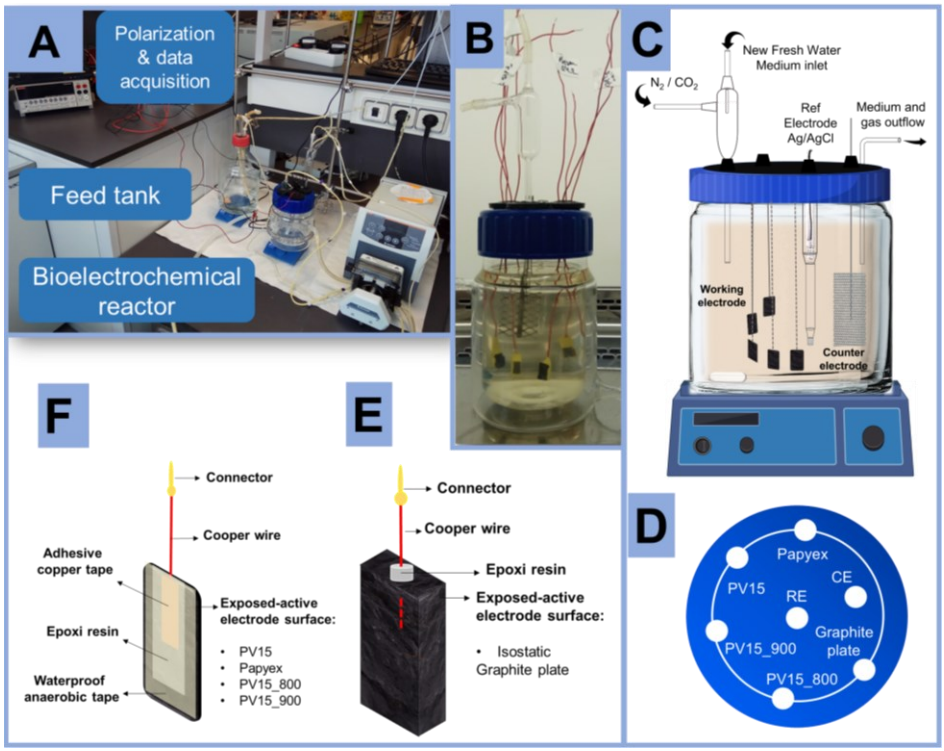

Figure S-73. **A)** Photo of the laboratory system setup, from right to left: peristaltic pump, bioreactor, feed tank, Keithley multimeter. **B)** Photo of the 3-electrode bioreactor in the sterilization chamber. **C)** Diagram of the 3-electrode bioreactor and the assembly of the different electrodes. **D)** Scheme of the bioreactor top cap and the position of the different working electrodes made with different materials. CE = counter electrode, RE = reference electrode. **E)** Type of connection mode for the control electrode based on isostatic graphite plate. **F)** Type of connection made for working electrodes based on expanded graphites (activated and non-activated).

Table S-27 Materials used as working electrodes in this work, showing details of their geometric areas and electrode-connection resistances.

Working Anode Electrode	Type Material	Enterprise	Geometric Area Electrode (cm^2)	Resistance with connection (Ω)
PV15-800°C-8h	Activated EG	-	0.6	2.4
PV15-900°C-8h	Activated EG	-	0.6	3.7

PV15	Commercial EG	SGL-Carbon	3.6	1.8
Papyex	Commercial EG	Mersen	3.6	1.7
Control electrode	Isostatic Graphite plate	Mersen	11.54	1.3

II. Characterisation of PV15 and derived CO_2-activated samples

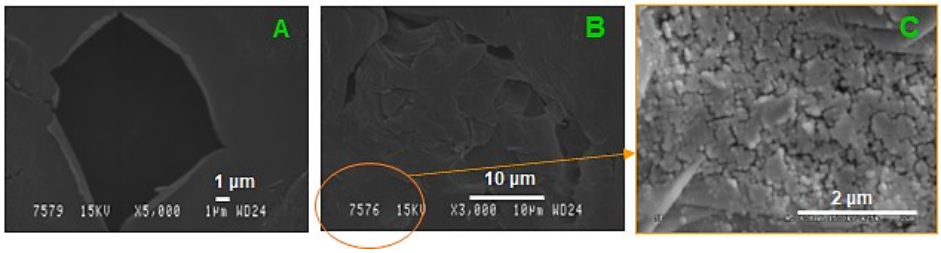

Figure S-74. SEM images showing big holes (1-10 µm) **(A,B)** and porous deposits **(B,C)** on PV15(N_2) surface.

Table S-28 Crystallinity (position of the 002 and 100 peaks, and calculated crystallite dimensions of the graphite in the vertical (La) or horizontal (Lc) directions) and microstructure (Raman shift and width of the G and D bands) from XRD and Raman characterization, respectively.

Electrode	XRD				Raman		
	002 (2θ)	*Lc* (Å)	*100* (2θ)	*La* (Å)	ν_G (cm^{-1})	$\Delta\nu_G$ (cm^{-1})	$\Delta\nu_D$ (cm^{-1})
PV15	26.540	388	54.666	389	1583.6	21.5	41.5
PV15(N_2)	nd*	nd	nd	nd	1584.5	141.8	35.4
PV15-800-8h	26.540	343	54.667	373	1583.9	23.4	36.6

*nd = non determined

Table S-29 Surface chemical composition (wt. %) of some PV15 samples determined by X-ray photoelectron spectroscopy (XPS).

Electrode	C	O	F
PV15	80.1	4.6	15.3
PV15(N_2)	98.1	1.9	---
PV15-800-8h	99.1	1.0	---

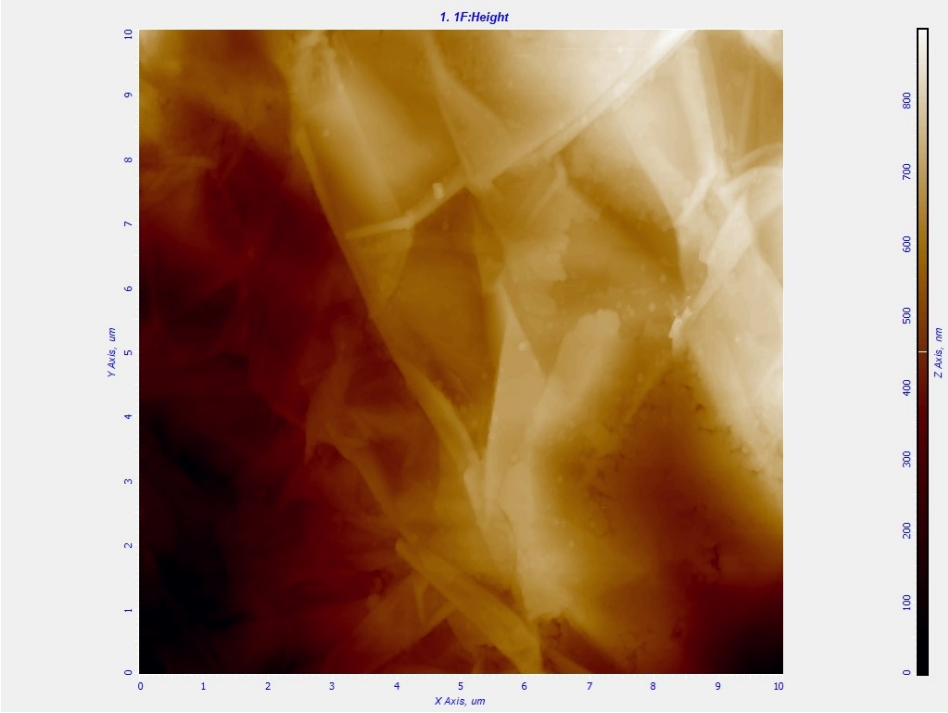

Figure S-75. 2D AFM image of PV15(N_2) which shows the presence of undecomposed deposits.

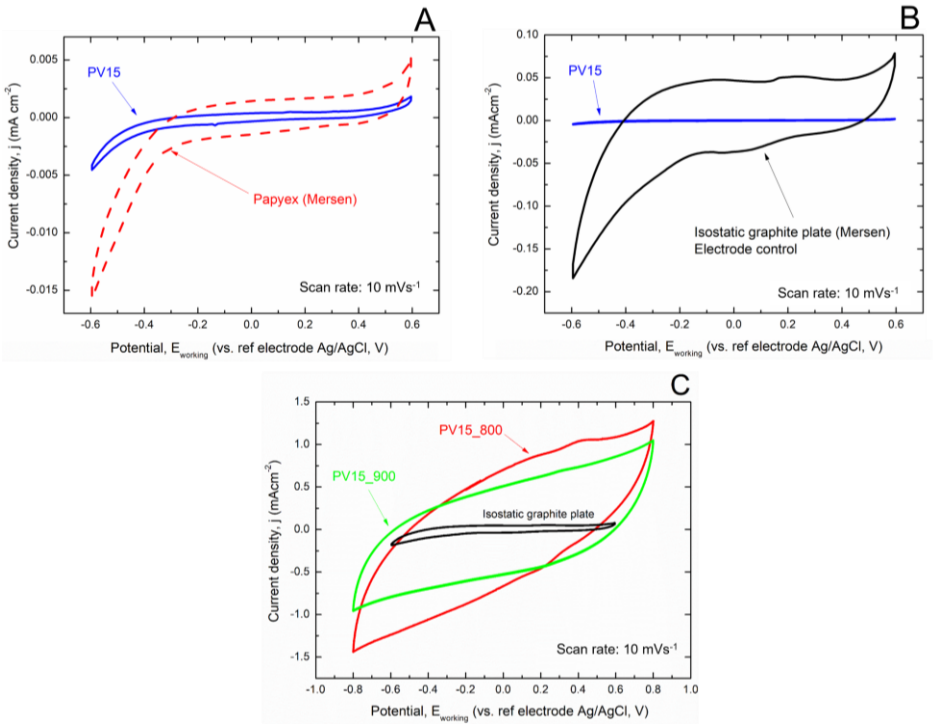

Figure S-76.Abiotic initial cyclic voltammetry (without bioreactor inoculation) performed in FWM for: **(A)** PV15 electrode (blue line); Papyex electrode (red dash). **(B)** PV15 electrode (blue line) and control electrode, isostatic graphite plate (black line). **(C)** Isostatic graphite plate as control electrode (black line) versus activated expanded graphite paper PV15-800-8h (red line) and PV15-900-8h (green line).

III. Comparison of microbial electroactivity: commercial materials versus activated materials

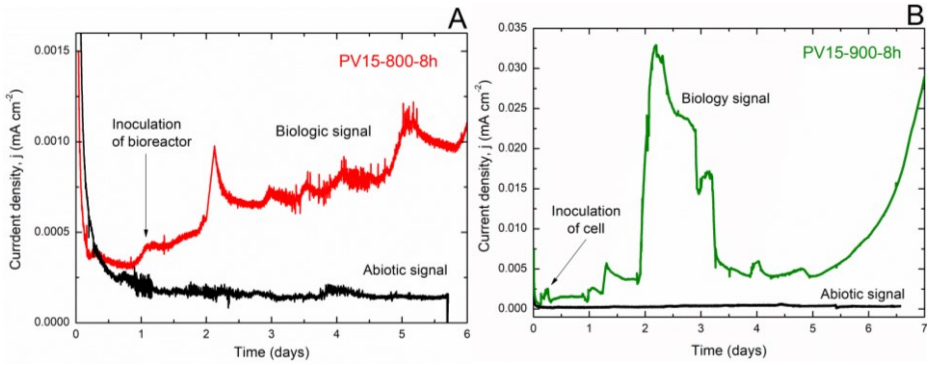

Figure S-77. Chronoamperometry at 0.2 V (vs. Ag /AgCl, 3M NaCl reference electrode) to perform the abiotic tests of the activated materials **(A)** PV15-800-8h **(B)** PV15-900-8h in the freshwater medium during 6 days approximately. **(A)** Current density (biology response) from electrobacteria after inoculation of the cell for PV15-800-8h (red line) and abiotic signal for the same system without electroactive bacteria (black line). **(B)** Current density (biology response) from electrobacteria after inoculation of the cell for PV15-900-8h (green line) and abiotic signal for the same system without electroactive bacteria (black line).

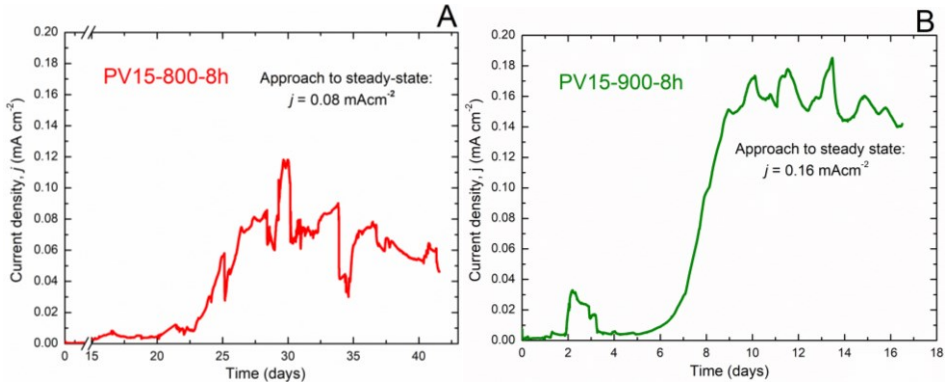

Figure S-78. Chronoamperometry during the repeated experiment to study microbial electroactivity on the surfaces of activated electrodes. **(A)** Chronoamperometry with the polarization (0.2 V vs. Ag /AgCl, 3M NaCl reference electrode) of the electrode composed of the activated material PV15-800-8h. **(B)** Chronoamperometry with the polarization (0.2 V vs. Ag /AgCl, 3M NaCl reference electrode) of the electrode composed of the activated material PV15-900-8h.

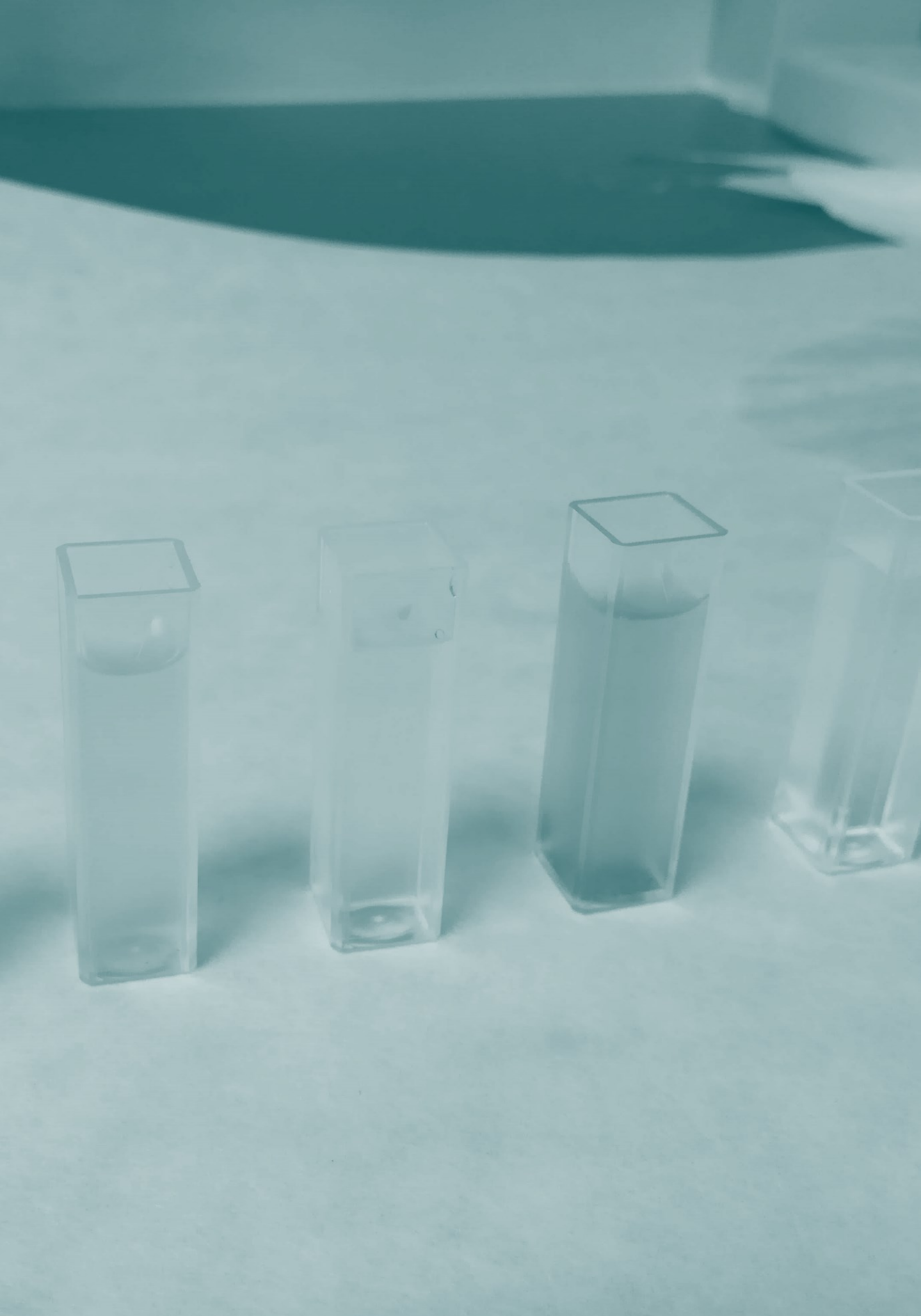

Chapter 9

General discussion, conclusions and future work

Chapter 9: General discussion, conclusions, and future work

The general discussion, conclusions and future work of this thesis will be presented for offering answers to the following issues:

I. Is MDC technology capable of simultaneously treating wastewater, generating power, and desalinating saline water in the same device.

II. What are the main considerations to set up an MDC system.

III. What is the practical implication of the present thesis.

IV. How important is to establish criteria to compare experimental results among MDC devices reported in literature.

V. Towards future scale-up and implementation of MDC technology: what are the main design considerations, limitations, and challenges.

I. Is MDC technology capable of simultaneously treating wastewater, generating power, and desalinating saline water in the same device. What could be the repercussion of this capacity.

Cao et al. (2009) reported the first proof of concept regarding water desalination through microbial electrochemical tools. Indeed, they presented the original concept of a Microbial Desalination Cell (MDC) capable of completely desalinating saline water using chemical energy contained in wastewater. Moreover, this concept is able to generate electric power simultaneously, unlike conventional desalination technologies such as reverse osmosis or electrodialysis. In this sense, the energy recovered from the wastewater by electroactive bacteria is used to **i)** provide energy for the desalination process (ion migration) and **ii)** simultaneous energy production in the MDC device (electric energy is converted/diffused into heat energy in the external resistor).

In the present thesis, complete desalination was achieved (value of 1 mS cm^{-1} as a final reference value in saline compartment) in a laboratory-scale MDC bioreactor (cross section of 100 cm^2) without the need for external energy input. Thus, we have evaluated the impact of using different catholytes (air cathode versus Ferricyanide, ***Chapter 4)***, external resistance values (0.1 Ohms to 100 Ohms, ***Chapter 5),*** and initial salinities (2.5 mS cm^{-1} to 57.8 mS cm^{-1}, ***Chapter 6***). Moreover, complete desalination was also achieved using both real saline streams and real industrial wastewater from brewery sector ***(Chapter 7),*** confirming its technical feasibility under real scenarios.

Thus, the lab – scale MDC device has been used to study the performance and compare it with the available literature, as well as visualize the influence of experimental conditions in the behaviour of the MDC system: energy, water treatment capacity and desalination parameters (described in ***Chapter 3***). With these systematic studies, the general objective described for this thesis (***Chapter***

2) has been achieved: to provide a detailed study of the operation and limitations of this technology.

Beyond the scientific importance of any technological advance (whether on a laboratory or pilot scale within any level of technical maturity, TRL), we must not forget the possible impact of these studies on the environment and quality of life.

As is well known, high-quality and safe drinking water is essential for health and public welfare and an important economic factor. In practice, it would be possible to obtain drinking water under the concept of the MIDES project (implementation of MDC technology as pre-treatment to reverse osmosis) since reverse osmosis technology and disinfection are implemented as post-treatment to the MDC system, ensuring the quality of treated water, even if there are minor leaks or cross-contamination in the microbial desalination cell device. However, for the commercial development of MDC technology, greater social acceptance of drinking water production using waste will be necessary (Salinas-Rodríguez et al., 2021).

The advantage of these bioelectrochemical systems capable of using wastewater to obtain energy and thus drive the desalination process (which is the primary function that has been explored throughout this thesis) can also open the discussion about the potential of these systems energetically self-sufficient for use in other applications beyond the production of freshwater:

- The use focused on treating industrial or domestic wastewater: the energy required to carry out the treatment in these systems is less than conventional treatment technologies, and aeration of the wastewater or external energy input to the system is not required.
- The use for electro-bioremediation purposes: saline water treatment from the galvanic, mining, and petrochemical industries.

- As a pretreatment to conventional biological wastewater treatments: these treatments are inefficient when the salt concentration is high, which can affect microorganisms, producing the effect of plasmolysis, inhibiting their action.
- The MDC system process for desalination includes the reuse of wastewater as a renewable energy source for the ion migration process and a reusable water source after treatment; the use of biocathodes is interesting since they can take advantage of the remaining dissolved organic matter and the nutrients of the already treated wastewater to produce biomass in the form of microalgae or other microorganisms that could later be used to produce bioenergy or the production of high added value products. In summary, in this technology, the waste produced in other processes becomes our resource and they can selective recovery of high-added value resources from wastewater, such as volatile fatty acids, nutrients and metals. With this application, the circularity of critical resources could be increased, turning these devices into possible tools towards a circular economy. Nowadays, implementing "closing loops" in industrial ecosystems implies a reduction in the use of current resources, with more efficient use of flows with renewable resources. With this kind of implementation, it is possible to reintroduce waste into the production cycle with a reduction in environmental impacts (reduction in waste generation, avoiding the use of fossil fuels and greenhouse gas emissions), as well as save in operating and energy costs due to better use of resources, even new jobs position (Stahel, 2016).

Finally, is interesting to highlight that some aspects of the desalination process with these systems meet the requirements of the so-called "Twelve Principles of Green Chemistry", which is a guiding framework for the design and development of new products and processes from a sustainable point of view to reduce or eliminate the use and generation of hazardous substances (Anastas and Eghbali, 2010): The reduction of energy consumption in the desalination process and water treatment can make at room temperature and pressure and neutral pH,

which leads to a minimization of the environmental and economic impact. The reduction of auxiliary substances using, for example, biocathodes where the oxygen molecule acts as the last electron acceptor. The use of selective biocatalysts such as the different electroactive microorganisms. The production of innocuous molecules in the anodic and cathodic reactions involved in the process.

II. What are the main considerations to set up an MDC system.

MDC systems are versatile and complex devices, with many factors influencing their performance simultaneously (Jingyu et al., 2017), such as design and geometry reactor or operational conditions (***Chapter 1)***. The initial saline composition (e.g., initial ion concentration), anolyte composition (e.g., available substrate, buffer capacity and conductivity), and catholyte composition (e.g., final electron acceptor or conductivity) could determine the overall system performance. These factors will affect the internal resistance, electrochemical performance, bacterial community, membrane scaling and biofouling processes, and other driving forces of desalination, such as diffusion and osmotic pressure. For all these reasons, the operation conditions must be clearly defined, as almost all the factors are interrelated.

The first consideration would be to determine the main objective of the MDC system: **i)** to maximize the energy production (Specific Energy Production, kWh m^{-3}) or **ii)** to maximize freshwater production (NDR, Nominal Desalination Rate L m^{-2} h^{-1}). In this sense, it would be necessary to use high or low resistance values in the external circuit of the device (***Chapter 5)***.

In the case of maximizing freshwater production, the main objective would be to achieve the highest current density in the MDC device (i.e., short circuit condition). This is achieved under a low external resistance value. This high current density is used for the migration of ions from the central saline

compartment to the adjacent compartments. Therefore, rapid desalination of the central compartment is produced, and, in addition, undesired effects such as back-diffusion or osmosis processes that reduce desalination efficiency are avoided ***(Chapter 4 and Chapter 6).***

Those systems operating under condition seeking for maximum current density are controlled by the bioavailability of the organic substrate (electron donor) and the buffering capacity of the anolyte. The buffer capacity counteracts the acidification of the biofilm, especially in the first stage of the desalination performance ***(Chapter 6 and Chapter 7)***, when the highest current densities are reached (batch mode). A fair strategy would be to select microbial communities from bioanode capable to cope with the salinity shift in the anode compartment during anion migration ***(Chapter 6)***. Regarding the cathode ***(Chapter 4)***, it is key to achieve a high value of cathodic potential during the desalination process and this was precisely the case when potassium ferricyanide was used instead of air diffusion cathodes (due to faster kinetic at neutral pH). Therefore, the desalination of brackish and seawater revealed a better performance concerning all parameters (energy, treatment and desalination) by reducing potassium ferricyanide in comparison with oxygen reduction reaction at neutral pH (ORR).

In addition, in order to obtaining a high current density, the MDC system must have a proper configuration to minimize losses of the available electrochemical potential. Since the first MDC proof of concept (Cao et al., 2009), configuration, design and geometry modifications have been explored in order to avoid the limitations of these systems: low production of desalinated water, acidification, cathode with low potentials ***(Chapter 1)***. However, all these modifications are based on adding membranes and compartments which decreases the available potential in the cell by increasing the internal resistance, thus decreasing the current density and water production. So, it is essential to use ion exchange membranes with low electrical resistance values, high ionic permeability and low water transport capacity ***(Chapter 4*** and ***Chapter 6)*** to

improve the MDC performance. Furthermore, the physicochemical characteristics of anodes used in these bioelectrochemical devices play an essential role in their performance and efficiency ***(Chapter 8)***.

Another important factor that affects the internal resistance is the ohmic drop of aqueous media due low conductivity in catholyte, anolyte and saline stream (three-compartment configuration in our case). Indeed, the evolution of electric conductivity of saline stream controls the MDC system performance in batch mode operation. ***Chapter 6*** specifically reveals how the salinity of the central saline compartment controls the behaviour of an MDC operated under non-limiting conditions for substrate and catholyte (i.e., excess of electron donor and electron acceptors). In fact, desalination in the saline compartment makes conductivity to decrease leading to higher values of internal resistance and, consequently, a decrease in the available cell potential, which negatively affect the desalination process.

Such bottleneck will not be an issue when MDC is not expected to perform a complete desalination, a real situation if MDC is implemented as a pretreatment for RO technology to decrease the energy consumption associated to RO. This strategy or merging MDC and RO, can desalinate a high salinity stream (e.g., 35 mS cm^{-1}) by reaching high electrical current density values at the beginning of the desalination process ***(Chapter 6)***. In this first stage, the MDC desalination process is faster, leading to vast reduction in electric conductivity to approximately 10 mS cm^{-1} (correspondents with the value of electric conductivity for brackish water). Then the partially desalinated water can be entirely desalinated by RO, reducing the energy required for desalination from 3.5 $kWhm^{-3}$ to 0.5 $kWhm^{-3}$ according to MIDES project.

III. Which is the practical implication of the present thesis.

Microbial Electrochemical Technologies (MET) are a multidisciplinary research field, combining microbiology, electrochemistry, physical phenomena, and membrane technology concepts; so many processes and phenomena can co-occur in these systems. This fact makes it difficult to control the conditions through the experimental design, and understanding the behaviour of the system is always a challenge. In order to reduce the number of variables , we followed a similar approach that (Cao et al., 2009) used in their pioneer work: the use of potassium ferricyanide to provide high potential and avoid limitations in the cathode reaction ***(Chapter 6)***. In this manner, it is easier to explain other constraints, such as internal resistance from the conductivity of the saline compartment, anolyte buffer capacity or physical transport phenomena like back-diffusion. Unfortunately, the use redox mediators are not sustainable and must be regenerated; however, their use is helpful to **i)** illustrate the performance of MDC systems, **ii)** to obtain information about their ideal performance and **iii)** to understand the main limitations of the technology ***(Chapter 4-6)***. In this sense, it is envisaged the possibility of using sustainable and non-toxic redox mediators (for example, quinone derivatives, as used in organic redox flow batteries) in MDC systems for scaling-up purposes.

Sometimes, electrochemistry concepts are not always properly understood, especially if microorganisms are involved. To avoid misconceptions, this thesis provides an exhaustive and detailed explanation of the electrochemical behaviour of MDC operating in different experimental conditions ***(Chapter 5)***. Furthermore, the continuous monitoring of the cell potentials, anode, cathode, and current density showed in experimental chapters greatly helps to understand what is happening in the cell in real time during the desalination process. Thus, it is possible to clarify and understand the processes that occur during the desalination process, opening the possibility of overcoming the main limitations for

implementation at a real scale. In addition, it is important to indicate that the electric conductivity variation in the saline chamber of MDC can be used to predict electrochemical performance under non-limiting conditions for anolyte and catholyte ***(Chapter 5).***

In addition, all research developed during this thesis offered valuable information for the multidisciplinary team of scientist and engineers working in MIDES to scale-up the technology. Before starting the MIDES project, the desalinated water production in the most significant scaled-up MDC reported was 0.077 L m^{-2} h^{-1} (i.e., freshwater production per square meter of membrane and hour) for partial desalination of synthetic seawater (Zhang and He, 2015). Although complete desalination in MDCs was achieved without an external electrical source, the freshwater production was still 200 times lower than in conventional desalination systems (for RO = 15–20 L m^{-2} h^{-1}). Preliminary results from one of the MDC pilot constructed in MIDES project (Demo Site 1, Denia, Spain) revealed a complete synthetic brackish water desalination (initial electric conductivity of 4.2 mS cm^{-1}) showing a nominal desalination rate (NDR) of 4.1 L m^{-2} h^{-1}. In addition, this value was comparable to the lab scale results (4.6 L m^{-2} h^{-1} for an initial electric conductivity of 5.6 mS) and pre-pilot scale MDC systems (6.2 L m^{-2} h^{-1} for an initial electric conductivity of 3.2 mS cm^{-1}). Such results assures a good correlation for the future of the scale-up of the MDC system (Salinas-Rodríguez et al., 2021). In conclusion, the scientific background obtained in the thesis has been used to support engineering tasks for design, construction and operation of scaled-up MDC pilot plants during MIDES project, so contributing to the implementation of MDC technology at largest scale so far.

Finally, for the economic scale-up and commercialization of these systems, there must be a compromise between efficiency and cost. In this sense, a large part of the costs is due to the materials used as electrodes. A strategy to simplify the assembly and cost of the systems by exploring upgraded materials to host electroactive bacteria was deeply treated in ***Chapter 8***. Research included in this

last chapter revealed how changing a single feature of a commercial carbonaceous material (e.g., the porosity at the nanoscale) could enhance the electroactive response of the microbial community.

IV. How important is to establish criteria to compare experimental results among MDC devices reported in literature.

After reviewing the state of the art of MDC ***(Chapter 1)***, a number of multiple configurations, designs, and conditions of operation can be identified to affect the final performance of the system (the desalination, treatment, and energy production parameters). This fact represents two sides of the same coin: a positive one revealing how numerous factors can be still optimized for the proper performance of the system (materials, inoculum, configuration, etc.); on the other side, the comparison among reported experimental systems in literature becomes tedious and complicated.

Consequently, the main objective of ***Chapter 4*** was to properly explore two similar MDCs operating with two different catholyte strategies to compare performance and desalination efficiencies for understanding the impact of how a single parameter. The following experimental chapters ***(Chapters 5 and 6)*** present a comparative table including this thesis research and the most similar MDC systems reported in the bibliography. In order to compare them in a rationale and adequate mode, the chosen criteria were: **i)** systems have a 3-chamber configuration, **ii)** low external resistance (promoting desalinated water production instead of energy production) and **iii)** potassium ferricyanide redox mediator or the ORR as a cathodic strategy.

On the other hand, probably, there is now agreement regarding criteria to consider certain issues (e.g., what is a complete cycle of desalination***, Chapter 6).*** These criteria directly affect water and energy production values, and it complicates the comparison of MDC performance reported in the literature. Thus,

more systematic studies under the same criteria should be carried out. In this sense, ***Chapter 4*** includes those results from the collaboration of two independent laboratories (IMDEA Water and Leitat) after following the same criteria of desalination cycle (electric conductivity below 1 mS cm^{-1}). The very same criteria were followed in the next Chapters ***(Chapters 5-7)***.

V. Towards future scale-up and implementation of MDC technology: what are the main design considerations, limitations, and challenges.

As indicated in ***Chapter 1*** of this thesis, problems related to water stress and energy depletion have forced the search for practical solutions in recent decades, among which is the desalination of water with lower energy consumption. MDC technology has promising potential as a sustainable process for water desalination, compared to more conventional technologies of desalination (eg. RO or thermal processes). MDCs could be either operated as a stand-alone technology for water treatment and recycling or, alternatively, they could also be integrated with the traditional membrane-based RO plants as a strategy for reducing energy requirements by decreasing the salinity of the feeding water. A future effort must be made to demonstrate the technical/economic feasibility of MDC technology (Salinas-Rodríguez et al., 2021), in terms of catholyte regeneration (e.g. redox-mediators), membranes and electrodes development, capital and operation costs, and appropriate niches.

One of the main bottlenecks of this technology is the choice of the cathodic reaction (***Chapter 4)*** due to the high impact in the available potential to promote ion migration (i.e., desalination). The strategy of using air cathodes and ORR as the cathodic reaction is conditioned, among other factors, by the catalytic load of the electrode (Zhao et al., 2006). The bibliography shows the effort to improve the implementation of the ORR using transition metals, trying to avoid using precious metals. In spite of the good performance using ferricyanide, such

catholyte was chosen in a proof-of-concept context with the main objective of demonstrating a new concept of sustainable desalination technology. Thus, as highlighted in in ***chapter 4***, using liquid catholyte in MDC technology increases brackish and seawater desalination performance (high values of treated, desalinated water production and energy production) compared with air diffusion cathode due to a higher potential provided by the system. However, implementing this type of mediator has many economic and sustainable barriers. One of the drawbacks is its depletion, and it must regenerate. For this reason, it will only be feasible implementation if a strategy is developed that allows their regeneration simply and economically. Some proposed alternatives are integrating renewable energy (i.e., photovoltaic, wind energy) or using specific biocathodes for regeneration. Using an air diffusion cathode with the help of inexpensive materials (iron-doped carbon nanofibers) for ORR has shown good performance to provide enough electrical potential to drive the brackish water desalination process. Unfortunately, it is not sufficient to complete seawater desalination. In this sense, this kind of cathode could be interesting for applications where the complete desalination process is not mandatory (for example, pre-treatment of RO). As possible future actions, this concept could be developed on a large scale for its validation in a pilot plant during long-term assays.

The ion exchange membranes (IEM) are critical elements of MDC technology. However, the membranes available on the market are currently designed and manufactured for different application areas (i.e., energy systems, electrodialysis). Therefore, designing and developing specific IEM for desalination in these bioelectrochemical devices as well as the reduction in production costs would be desirable. In MDC long-term tests, the AEM biofouling (Luo et al., 2012b) and inorganic scaling due to divalent cations (Ca^{2+} and Mg^{2+}) on the CEM (Ping et al., 2013) inhibits ion transfer and increases system resistance leading to significant performance limitations (Chen et al., 2012a; Luo et al., 2012a). The action of replacing the membranes recovered the

performance of the system, but this increases costs (Zhang et al., 2016b). Properties such as mechanical stability, low back-diffusion rates and water loss could be improved. In high-salinity water desalination, unfavourable back diffusion (Davis et al., 2013; Werner et al., 2013) of organic or inorganic substrate from the anode to the desalination chamber could occur due to the greater osmotic water flux generated by concentration gradient (Ping et al., 2016). Furthermore, microbial growth in the saline chamber was reported and, consequently, desalination efficiency became reduced (Ping et al., 2013). This IEM development with anti-biofouling properties (such as antibiotic coating or carbon-based nanomaterials) would achieve more resistance against typical fouling in these systems which can decrease system performance, even if capital costs are slightly increased (Judd, 2008; Logan and Elimelech, 2012).

The use of real wastewater and seawater in these systems revealed a lower performance MDC in comparison with synthetic water. Few studies have employed actual wastewater and saline water (Jacobson et al., 2011b; Luo et al., 2012b; Sophia and Bhalambaal, 2015; Sevda et al., 2017). However, our research (***Chapter 7***) revealed how the MDC achieved lower desalinated water production values (NDR, $Lm^{-2}h^{-1}$) using real water (wastewater) compared to the use of synthetic water (only acetate as electron donor). One of the reasons for this behaviour is the increased complexity of the available substrate for electroactive biofilm. To overcome this limitation, to pre-digest wastewater by using commercially available processes was suggested. For example, MDC installed after an anaerobic digestion process which supply easily degradable carbon sources (e.g., volatile fatty acids). In addition, with a similar value of COD in real wastewater, factors such as the buffer capacity of wastewater take control of the performance of the system, as discussed in ***Chapter 6***. Finally, in real water, different microorganisms with other respiration mechanisms will compete with electroactive bacteria. The available substrate for electroactive bacteria will be

reduced, coulombic efficiencies will be decreased, and then, the overall MDC performance.

The limitation of the organic substrate could be a negative factor for the performance of the MDC system and its future implementation, especially in isolated or remote areas. For this reason, the study of alternative organic substrates for the operation of MDC (for example, microalgae, agricultural residues, etc.) could be interesting. MDC technology must be built in strategic and previously studied locations close to sources of sewage and saline waters. In this sense, it would be interesting to apply MDC technology in wastewater treatment plants where, due to the high salinity of the effluent, a desalination process is required (i.e., tertiary treatment), obtaining regenerated water for irrigation after the process.

Finally, other key elements are the electrodes and current collectors. In this sense, the electrodes should have a great electric conductivity and high surface area. Moreover, the carbonaceous materials must be biocompatible, flexible, chemically and mechanically resistant and cost-effective for their implementation (it contributes significantly to the total capital costs of the system). Among other studies already reported in the literature, this thesis explores the modification of commercial current collectors (carbon materials) to produce a customized porous structure in the surface (***Chapter 8***), in order to improve microbial adhesion and increase performance. This strategy could bring new advances for microbial desalination, reducing their costs (by not having to use several materials to form an anode) and maintaining optimal performance for technology scale-up.

References

References

Abdelkareem, M. A., El Haj Assad, M., Sayed, E. T., and Soudan, B. (2018). Recent progress in the use of renewable energy sources to power water desalination plants. *Desalination* 435, 97–113. doi:10.1016/j.desal.2017.11.018.

Abu Reesh, I. M., Sevda, S., and He, Z. (2016). Evolution of Seawater Desalination and Petroleum Refinery Wastewater Treatment in a Microbial Desalination Cell. in *Qatar Foundation Annual Research Conference Proceedings Volume 2016 Issue 1* (Hamad bin Khalifa University Press (HBKU Press)), EEOP3220. doi:10.5339/qfarc.2016.EEOP3220.

Aguirre-Sierra, A., Bacchetti-De Gregoris, T., Berná, A., Salas, J. J., Aragón, C., and Esteve-Núñez, A. (2016). Microbial electrochemical systems outperform fixed-bed biofilters in cleaning up urban wastewater. *Environ. Sci. Water Res. Technol.* 2, 984–993. doi:10.1039/C6EW00172F.

Aguirre-Sierra, A., Bacchetti-De Gregoris, T., Salas, J. J., de Deus, A., and Esteve-Núñez, A. (2020). A new concept in constructed wetlands: assessment of aerobic electroconductive biofilters. *Environ. Sci. Water Res. Technol.* 6, 1312–1323. doi:10.1039/C9EW00696F.

Al-Karaghouli, A., and Kazmerski, L. L. (2013). Energy consumption and water production cost of conventional and renewable-energy-powered desalination processes. *Renew. Sustain. Energy Rev.* 24, 343–356. doi:10.1016/j.rser.2012.12.064.

Allen, J. W. A., Sawyer, E. B., Ginger, M. L., Barker, P. D., and Ferguson, S. J. (2009). Variant c -type cytochromes as probes of the substrate specificity of the E. coli cytochrome c maturation (Ccm) apparatus. *Biochem. J.* 419, 177–186. doi:10.1042/BJ20081999.

Alvarez Esquivel, D. Y., Brown, R. K., Knohl, S., and Schröder, U. (2020). Developing Cheap and Mass-Producible Graphite-Filled Paper as an Anode Material for Microbial Electrochemical Technologies. *ChemElectroChem*, 1851–1859. doi:10.1002/celc.201902087.

An, Z., Zhang, H., Wen, Q., Chen, Z., and Du, M. (2014a). Desalination combined with copper(II) removal in a novel microbial desalination cell. *Desalination* 346, 115–121. doi:10.1016/j.desal.2014.05.012.

An, Z., Zhang, H., Wen, Q., Chen, Z., and Du, M. (2014b). Desalination combined with hexavalent chromium reduction in a microbial desalination cell. *Desalination* 354, 181–188. doi:10.1016/j.desal.2014.10.006.

Anastas, P., and Eghbali, N. (2010). Green Chemistry: Principles and Practice. *Chem. Soc. Rev.* 39, 301–312. doi:10.1039/B918763B.

Angosto, J. M., Fernández-López, J. A., and Godínez, C. (2015). Brewery and liquid manure wastewaters as potential feedstocks for microbial fuel cells: a performance study. *Environ. Technol.* 36, 68–78. doi:10.1080/09593330.2014.937769.

Arana, T. J., and Gude, V. G. (2018). A microbial desalination process with microalgae biocathode using sodium bicarbonate as an inorganic carbon source. *Int.*

Biodeterior. Biodegrad. 130, 91–97. doi:10.1016/j.ibiod.2018.04.003.

Arkatkar, A., Mungray, A. K., and Sharma, P. (2023). Effect of treatment on electron transfer mechanism in microbial fuel cell. *Energy Sources, Part A Recover. Util. Environ. Eff.* 45, 3843–3858. doi:10.1080/15567036.2019.1668878.

Asensio, Y., Llorente, M., Fernández, P., Tejedor-Sanz, S., Ortiz, J. M., Ciriza, J. F., et al. (2021a). Upgrading fluidized bed bioelectrochemical reactors for treating brewery wastewater by using a fluid-like electrode. *Chem. Eng. J.* 406, 127103. doi:10.1016/j.cej.2020.127103.

Asensio, Y., Llorente, M., Tejedor-Sanz, S., Fernández-Labrador, P., Manchon, C., Ortiz, J. M., et al. (2021b). Microbial electrochemical fluidized bed reactor (ME-FBR): An energy-efficient advanced solution for treating real brewery wastewater with different initial organic loading rates. *J. Environ. Chem. Eng.* 9, 106619. doi:10.1016/j.jece.2021.106619.

Ashwaniy, V. R. V., and Perumalsamy, M. (2017). Reduction of organic compounds in petro-chemical industry effluent and desalination using Scenedesmus abundans algal microbial desalination cell. *J. Environ. Chem. Eng.* 5, 5961–5967. doi:10.1016/j.jece.2017.11.017.

Aulenta, F., Reale, P., Canosa, A., Rossetti, S., Panero, S., and Majone, M. (2010). Characterization of an electro-active biocathode capable of dechlorinating trichloroethene and cis-dichloroethene to ethene. *Biosens. Bioelectron.* 25, 1796–1802. doi:10.1016/j.bios.2009.12.033.

Aulenta, F., Tucci, M., Cruz Viggi, C., Dolfing, J., Head, I. M., and Rotaru, A. E. (2021). An underappreciated DIET for anaerobic petroleum hydrocarbon-degrading microbial communities. *Microb. Biotechnol.* 14, 2–7. doi:10.1111/1751-7915.13654.

Aulenta, F., Verdini, R., Zeppilli, M., Zanaroli, G., Fava, F., Rossetti, S., et al. (2013). Electrochemical stimulation of microbial cis-dichloroethene (cis-DCE) oxidation by an ethene-assimilating culture. *N. Biotechnol.* 30, 749–755. doi:10.1016/j.nbt.2013.04.003.

Badalamenti, J. P., and Bond, D. R. (2015). Complete Genome of Geobacter pickeringii G13 T , a Metal-Reducing Isolate from Sedimentary Kaolin Deposits. *Genome Announc.* 3. doi:10.1128/genomeA.00038-15.

Bao, Y., Liu, J., Zhang, X., Lei, P., Qiu, J., He, J., et al. (2021). Sinanaerobacter chloroacetimidivorans gen. nov., sp. nov., an obligate anaerobic bacterium isolated from anaerobic sludge. *Antonie Van Leeuwenhoek* 114, 1609–1617. doi:10.1007/s10482-021-01627-2.

Bashyam, R., and Zelenay, P. (2006). A class of non-precious metal composite catalysts for fuel cells. *Nature* 443, 63–66. doi:10.1038/nature05118.

Bejjanki, D., Muthukumar, K., Radhakrishnan, T. K., Alagarsamy, A., Pugazhendhi, A., and Naina Mohamed, S. (2021). Simultaneous bioelectricity generation and water desalination using Oscillatoria sp. as biocatalyst in photosynthetic microbial desalination cell. *Sci. Total Environ.* 754, 142215. doi:10.1016/j.scitotenv.2020.142215.

Berenguer, R., Marzorati, S., Rago, L., Cristiani, P., Pivato, A., Nuñez, A. E., et al.

(2020). Electroactive Biochar : Sustainable and Scalable Environmental Applications of Microbial Electrochemical Technologies. *Microb. Electrochem. Technol.*, 360–382. doi:10.1201/9780429487118-24.

Bergna, D., Hu, T., Prokkola, H., Romar, H., and Lassi, U. (2019). Effect of Some Process Parameters on the Main Properties of Activated Carbon Produced from Peat in a Lab-Scale Process. *Waste Biomass Valorization 2019 116* 11, 2837–2848. doi:10.1007/S12649-019-00584-2.

Beyenal, H., and Babauta, J. (2015). *Biofilms in Bioelectrochemical Systems*. Hoboken, NJ, USA: John Wiley & Sons, Inc doi:10.1002/9781119097426.

Blanchet, E., Erable, B., De Solan, M.-L., and Bergel, A. (2016). Two-dimensional carbon cloth and three-dimensional carbon felt perform similarly to form bioanode fed with food waste. *Electrochem. commun.* 66, 38–41. doi:10.1016/j.elecom.2016.02.017.

Blázquez, E., Gabriel, D., Baeza, J. A., and Guisasola, A. (2016). Treatment of high-strength sulfate wastewater using an autotrophic biocathode in view of elemental sulfur recovery. *Water Res.* 105, 395–405. doi:10.1016/j.watres.2016.09.014.

Boldareva, E. N., Turova, T. P., Kolganova, T. V., Moskalenko, A. A., Makhneva, Z. K., and Gorlenko, V. M. (2009). [Roseococcus suduntuyensis sp. nov., a new aerobic bacteriochlorophyll A-containing bacterium isolated from a low-mineralized soda lake of Eastern Siberia]. *Mikrobiologiia* 78, 106–16. doi:10.1134/S0026261709010123/METRICS.

Bond, D. R. (2002). Electrode-Reducing Microorganisms That Harvest Energy from Marine Sediments. *Science (80-.).* 295, 483–485. doi:10.1126/science.1066771.

Bond, D. R., and Lovley, D. R. (2003). Electricity Production by Geobacter sulfurreducens Attached to Electrodes. *Appl. Environ. Microbiol.* 69, 1548–1555. doi:10.1128/AEM.69.3.1548-1555.2003.

Borjas Hernández, L. Z. (2016). Physiological and Operation Strategies for Optimizing Geobacter – based Electrochemical Systems. Available at: https://ebuah.uah.es/dspace/handle/10017/26339 [Accessed March 27, 2023].

Borjas, Z., Esteve-Núñez, A., and Ortiz, J. M. (2017). Strategies for merging microbial fuel cell technologies in water desalination processes: Start-up protocol and desalination efficiency assessment. *J. Power Sources* 356, 519–528. doi:10.1016/j.jpowsour.2017.02.052.

Borjas, Z., Ortiz, J., Aldaz, A., Feliu, J., and Esteve-Núñez, A. (2015). Strategies for Reducing the Start-up Operation of Microbial Electrochemical Treatments of Urban Wastewater. *Energies* 8, 14064–14077. doi:10.3390/en81212416.

Borràs, E., Aliaguilla, M., Bossa, N., Martinez-Crespiera, S., Huidobro, L., Schweiss, R., et al. (2021). Nanomaterials-based air-cathodes use in microbial desalination cells for drinking water production: Synthesis, performance and release assessment. *J. Environ. Chem. Eng.* 9, 105779. doi:10.1016/j.jece.2021.105779.

Bosch-Jimenez, P., Martinez-Crespiera, S., Amantia, D., Della Pirriera, M., Forns, I., Shechter, R., et al. (2017). Non-precious metal doped carbon nanofiber air-cathode for Microbial Fuel Cells application: Oxygen reduction reaction characterization and long-term validation. *Electrochim. Acta* 228, 380–388.

doi:10.1016/j.electacta.2016.12.175.

Brastad, K. S., and He, Z. (2013). Water softening using microbial desalination cell technology. *Desalination* 309, 32–37. doi:10.1016/j.desal.2012.09.015.

Bretschger, O., Obraztsova, A., Sturm, C. A., Chang, I. S., Gorby, Y. A., Reed, S. B., et al. (2007). Current Production and Metal Oxide Reduction by Shewanella oneidensis MR-1 Wild Type and Mutants. *Appl. Environ. Microbiol.* 73, 7003–7012. doi:10.1128/AEM.01087-07.

Busalmen, J. P., Esteve-Núñez, A., Berná, A., and Feliu, J. M. (2008). C-Type Cytochromes Wire Electricity-Producing Bacteria to Electrodes. *Angew. Chemie Int. Ed.* 47, 4874–4877. doi:10.1002/anie.200801310.

Caccavo Jr., F., Coates, J. D., Rossello-Mora, R. A., Ludwig, W., Schleifer, K. H., Lovley, D. R., et al. (1996). Geovibrio ferrireducens , a phylogenetically distinct dissimilatory Fe(III)-reducing bacterium. *Arch. Microbiol.* 165, 370–376. doi:10.1007/s002030050340.

Cahoon, L. A., and Freitag, N. E. (2018). The electrifying energy of gut microbes. *Nat. 2021 5627725* 562, 43–44. doi:10.1038/d41586-018-06180-z.

Call, D., and Logan, B. E. (2008). Hydrogen Production in a Single Chamber Microbial Electrolysis Cell Lacking a Membrane. *Environ. Sci. Technol.* 42, 3401–3406. doi:10.1021/es8001822.

Cao, X., Huang, X., Liang, P., Xiao, K., Zhou, Y., Zhang, X., et al. (2009). A New Method for Water Desalination Using Microbial Desalination Cells. *Environ. Sci. Technol.* 43, 7148–7152. doi:10.1021/es901950j.

Cao, X., Song, H., Yu, C., and Li, X. (2015). Simultaneous degradation of toxic refractory organic pesticide and bioelectricity generation using a soil microbial fuel cell. *Bioresour. Technol.* 189, 87–93. doi:10.1016/j.biortech.2015.03.148.

Capodaglio, A. G., Molognoni, D., Dallago, E., Liberale, A., Cella, R., Longoni, P., et al. (2013). Microbial fuel cells for direct electrical energy recovery from urban wastewaters. *Sci. World J.* 2013. doi:10.1155/2013/634738.

Carmo, M., Fritz, D. L., Mergel, J., and Stolten, D. (2013). A comprehensive review on PEM water electrolysis. *Int. J. Hydrogen Energy* 38, 4901–4934. doi:10.1016/j.ijhydene.2013.01.151.

Cath, T., Childress, A., and Elimelech, M. (2006). Forward osmosis: Principles, applications, and recent developments. *J. Memb. Sci.* 281, 70–87. doi:10.1016/j.memsci.2006.05.048.

Cecconet, D., Devecseri, M., Callegari, A., and Capodaglio, A. G. (2018). Effects of process operating conditions on the autotrophic denitrification of nitrate-contaminated groundwater using bioelectrochemical systems. *Sci. Total Environ.* 613–614, 663–671. doi:10.1016/j.scitotenv.2017.09.149.

Cercado-Quezada, B., Delia, M.-L., and Bergel, A. (2010). Testing various food-industry wastes for electricity production in microbial fuel cell. *Bioresour. Technol.* 101, 2748–2754. doi:10.1016/j.biortech.2009.11.076.

Chamkh, F., Sproer, C., Lemos, P. C., Besson, S., El Asli, A.-G., Bennisse, R., et al. (2009). Desulfovibrio marrakechensis sp. nov., a 1,4-tyrosol-oxidizing, sulfate-reducing bacterium isolated from olive mill wastewater. *Int. J. Syst. Evol.*

Microbiol. 59, 936–942. doi:10.1099/ijs.0.003822-0.

Chandrasekhar, K., and Venkata Mohan, S. (2012). Bio-electrochemical remediation of real field petroleum sludge as an electron donor with simultaneous power generation facilitates biotransformation of PAH: Effect of substrate concentration. *Bioresour. Technol.* 110, 517–525. doi:10.1016/j.biortech.2012.01.128.

Chen, Q., Pu, W., Hou, H., Hu, J., Liu, B., Li, J., et al. (2018). Activated microporous-mesoporous carbon derived from chestnut shell as a sustainable anode material for high performance microbial fuel cells. *Bioresour. Technol.* 249, 567–573. doi:10.1016/j.biortech.2017.09.086.

Chen, S., He, G., Carmona-Martinez, A. A., Agarwal, S., Greiner, A., Hou, H., et al. (2011a). Electrospun carbon fiber mat with layered architecture for anode in microbial fuel cells. *Electrochem. commun.* 13, 1026–1029. doi:10.1016/j.elecom.2011.06.009.

Chen, S., Liu, G., Zhang, R., Qin, B., and Luo, Y. (2012a). Development of the Microbial Electrolysis Desalination and Chemical-Production Cell for Desalination as Well as Acid and Alkali Productions. *Environ. Sci. Technol.* 46, 2467–2472. doi:10.1021/es203332g.

Chen, S., Liu, G., Zhang, R., Qin, B., Luo, Y., and Hou, Y. (2012b). Improved performance of the microbial electrolysis desalination and chemical-production cell using the stack structure. *Bioresour. Technol.* 116, 507–511. doi:10.1016/j.biortech.2012.03.073.

Chen, S., Luo, H., Hou, Y., Liu, G., Zhang, R., and Qin, B. (2015). Comparison of the removal of monovalent and divalent cations in the microbial desalination cell. *Front. Environ. Sci. Eng.* 9, 317–323. doi:10.1007/s11783-013-0596-y.

Chen, S., Rotaru, A.-E., Liu, F., Philips, J., Woodard, T. L., Nevin, K. P., et al. (2014a). Carbon cloth stimulates direct interspecies electron transfer in syntrophic co-cultures. *Bioresour. Technol.* 173, 82–86. doi:10.1016/j.biortech.2014.09.009.

Chen, S., Rotaru, A.-E., Shrestha, P. M., Malvankar, N. S., Liu, F., Fan, W., et al. (2014b). Promoting Interspecies Electron Transfer with Biochar. *Sci. Rep.* 4, 5019. doi:10.1038/srep05019.

Chen, X., Liang, P., Wei, Z., Zhang, X., and Huang, X. (2012c). Sustainable water desalination and electricity generation in a separator coupled stacked microbial desalination cell with buffer free electrolyte circulation. *Bioresour. Technol.* 119, 88–93. doi:10.1016/j.biortech.2012.05.135.

Chen, X., Sun, H., Liang, P., Zhang, X., and Huang, X. (2016). Optimization of membrane stack configuration in enlarged microbial desalination cells for efficient water desalination. *J. Power Sources* 324. doi:10.1016/j.jpowsour.2016.05.065.

Chen, X., Xia, X., Liang, P., Cao, X., Sun, H., and Huang, X. (2011b). Stacked Microbial Desalination Cells to Enhance Water Desalination Efficiency. *Environ. Sci. Technol.* 45, 2465–2470. doi:10.1021/es103406m.

Chen, X., Zhou, H., Zuo, K., Zhou, Y., Wang, Q., Sun, D., et al. (2017). Self-sustaining advanced wastewater purification and simultaneous in situ nutrient recovery in a novel bioelectrochemical system. *Chem. Eng. J.* 330, 692–697. doi:10.1016/j.cej.2017.07.130.

Cheng, S., Liu, H., and Logan, B. E. (2006). Power densities using different cathode catalysts (Pt and CoTMPP) and polymer binders (Nafion and PTFE) in single chamber microbial fuel cells. *Environ. Sci. Technol.* 40, 364–369. doi:10.1021/es0512071.

Cheng, S., Xing, D., Call, D. F., and Logan, B. E. (2009). Direct Biological Conversion of Electrical Current into Methane by Electromethanogenesis. *Environ. Sci. Technol.* 43, 3953–3958. doi:10.1021/es803531g.

Chong, P., Erable, B., and Bergel, A. (2019). Effect of pore size on the current produced by 3-dimensional porous microbial anodes: A critical review. *Bioresour. Technol.* 289, 121641. doi:10.1016/j.biortech.2019.121641.

Chung, T. H., Meshref, M. N. A., and Dhar, B. R. (2020). Microbial electrochemical biosensor for rapid detection of naphthenic acid in aqueous solution. *J. Electroanal. Chem.* 873, 114405. doi:10.1016/j.jelechem.2020.114405.

Clauwaert, P., Rabaey, K., Aelterman, P., De Schamphelaire, L., Pham, T. H., Boeckx, P., et al. (2007). Biological Denitrification in Microbial Fuel Cells. *Environ. Sci. Technol.* 41, 3354–3360. doi:10.1021/es062580r.

Clauwaert, P., Tolêdo, R., van der Ha, D., Crab, R., Verstraete, W., Hu, H., et al. (2008). Combining biocatalyzed electrolysis with anaerobic digestion. *Water Sci. Technol.* 57, 575–579. doi:10.2166/wst.2008.084.

Cohen, B. (1931). Thirty-second Annual Meeting of the Society of American Bacteriologists. *J. Bacteriol.* 21, 1–60.

Cologgi, D. L., Lampa-Pastirk, S., Speers, A. M., Kelly, S. D., and Reguera, G. (2011). Extracellular reduction of uranium via Geobacter conductive pili as a protective cellular mechanism. *Proc. Natl. Acad. Sci.* 108, 15248–15252. doi:10.1073/pnas.1108616108.

Conners, E. M., Rengasamy, K., and Bose, A. (2022). Electroactive biofilms: how microbial electron transfer enables bioelectrochemical applications. *J. Ind. Microbiol. Biotechnol.* 49, 12. doi:10.1093/jimb/kuac012.

Contescu, C., Adhikari, S., Gallego, N., Evans, N., and Biss, B. (2018). Activated Carbons Derived from High-Temperature Pyrolysis of Lignocellulosic Biomass. *C* 4, 51. doi:10.3390/c4030051.

Coppi, M. V., Leang, C., Sandler, S. J., and Lovley, D. R. (2001). Development of a Genetic System for Geobacter sulfurreducens. *Appl. Environ. Microbiol.* 67, 3180–3187. doi:10.1128/AEM.67.7.3180-3187.2001.

Cornejo, P. K., Santana, M. V. E., Hokanson, D. R., Mihelcic, J. R., and Zhang, Q. (2014). Carbon footprint of water reuse and desalination: a review of greenhouse gas emissions and estimation tools. *J. Water Reuse Desalin.* 4, 238–252. doi:10.2166/wrd.2014.058.

Cosert, K. M., and Reguera, G. (2019). Voltammetric study of conductive planar assemblies of Geobacter nanowire pilins unmasks their ability to bind and mineralize divalent cobalt. *J. Ind. Microbiol. Biotechnol.* 46, 1239–1249. doi:10.1007/s10295-019-02167-5.

Costa, N. L., Clarke, T. A., Philipp, L.-A., Gescher, J., Louro, R. O., and Paquete, C. M. (2018). Electron transfer process in microbial electrochemical technologies: The

role of cell-surface exposed conductive proteins. *Bioresour. Technol.* 255, 308–317. doi:10.1016/j.biortech.2018.01.133.

Council Directive 75/440/EEC of 16 June 1975 concerning the quality required of surface water intended for the abstraction of drinking water in the Member States (OJ L 194 25.07.1975 p. 26) (2006). in *Documents in European Community Environmental Law* (Cambridge University Press), 839–844. doi:10.1017/CBO9780511610851.052.

Cournet, A., Délia, M.-L., Bergel, A., Roques, C., and Bergé, M. (2010). Electrochemical reduction of oxygen catalyzed by a wide range of bacteria including Gram-positive. *Electrochem. commun.* 12, 505–508. doi:10.1016/j.elecom.2010.01.026.

Coutinho, A. . R., Rocha, J. . D., and Luengo, C. . A. (2000). Preparing and characterizing biocarbon electrodes. *Fuel Process. Technol.* 67, 93–102. doi:10.1016/S0378-3820(00)00091-6.

Cruz Viggi, C., Presta, E., Bellagamba, M., Kaciulis, S., Balijepalli, S. K., Zanaroli, G., et al. (2015). The "Oil-Spill Snorkel": an innovative bioelectrochemical approach to accelerate hydrocarbons biodegradation in marine sediments. *Front. Microbiol.* 6, 881. doi:10.3389/fmicb.2015.00881.

Cruz Viggi, C., Rossetti, S., Fazi, S., Paiano, P., Majone, M., and Aulenta, F. (2014). Magnetite Particles Triggering a Faster and More Robust Syntrophic Pathway of Methanogenic Propionate Degradation. *Environ. Sci. Technol.* 48, 7536–7543. doi:10.1021/es5016789.

Cuesta, A., Dhamelincourt, P., Laureyns, J., Martínez-Alonso, A., and Tascón, J. M. D. (1994). Raman microprobe studies on carbon materials. *Carbon N. Y.* 32, 1523–1532. doi:10.1016/0008-6223(94)90148-1.

Cusick, R. D., and Logan, B. E. (2012). Phosphate recovery as struvite within a single chamber microbial electrolysis cell. *Bioresour. Technol.* 107, 110–115. doi:10.1016/j.biortech.2011.12.038.

D. Lozano-Castello, F. Suarez-García, D. Cazorla-Amoros, A. L.-S. (2009). "Porous Texture of Carbons," in *Carbons for Electrochemical Energy Storage and Conversion Systems*, eds. F. Beguin and E. Frackowiak (Boca Raton: CRC Press), 115–162.

Dahle, H., and Birkeland, N.-K. (2006). Thermovirga lienii gen. nov., sp. nov., a novel moderately thermophilic, anaerobic, amino-acid-degrading bacterium isolated from a North Sea oil well. *Int. J. Syst. Evol. Microbiol.* 56, 1539–1545. doi:10.1099/ijs.0.63894-0.

Dang, H., Yu, N., Mou, A., Zhang, L., Guo, B., and Liu, Y. (2022). Metagenomic insights into direct interspecies electron transfer and quorum sensing in blackwater anaerobic digestion reactors supplemented with granular activated carbon. *Bioresour. Technol.* 352, 127113. doi:10.1016/j.biortech.2022.127113.

David White, James Drummond, and Fuqua, C. (2012). *The Physiology and Biochemistry of Prokaryotes*. 4th ed. Oxford University Press, 2012.

Davis, J. B., and Yarbrough, H. F. (1962). Preliminary Experiments on a Microbial Fuel Cell. *Science (80-.).* 137, 615–616. doi:10.1126/science.137.3530.615.

Davis, R. J., Kim, Y., and Logan, B. E. (2013). Increasing Desalination by Mitigating

Anolyte pH Imbalance Using Catholyte Effluent Addition in a Multi-Anode Bench Scale Microbial Desalination Cell. *ACS Sustain. Chem. Eng.* 1, 1200–1206. doi:10.1021/sc400148j.

Davis, T. A., Genders, J. D., and Pletcher, D. (1997). A first course in ion permeable membranes. 1–5.

Deutzmann, J. S., Sahin, M., and Spormann, A. M. (2015). Extracellular Enzymes Facilitate Electron Uptake in Biocorrosion and Bioelectrosynthesis. *MBio* 6, 1–8. doi:10.1128/mBio.00496-15.

Dhakal, N., Salinas-Rodriguez, S. G., Hamdani, J., Abushaban, A., Sawalha, H., Schippers, J. C., et al. (2022). Is Desalination a Solution to Freshwater Scarcity in Developing Countries? *Membranes (Basel).* 12, 1–15. doi:10.3390/membranes12040381.

Di Lorenzo, M., Thomson, A. R., Schneider, K., Cameron, P. J., and Ieropoulos, I. (2014). A small-scale air-cathode microbial fuel cell for on-line monitoring of water quality. *Biosens. Bioelectron.* 62, 182–188. doi:10.1016/j.bios.2014.06.050.

Domínguez-Garay, A., Berná, A., Ortiz-Bernad, I., and Esteve-Núñez, A. (2013). Silica Colloid Formation Enhances Performance of Sediment Microbial Fuel Cells in a Low Conductivity Soil. *Environ. Sci. Technol.* 47, 2117–2122. doi:10.1021/es303436x.

Domínguez-Garay, A., Boltes, K., and Esteve-Núñez, A. (2016). Cleaning-up atrazine-polluted soil by using Microbial Electroremediating Cells. *Chemosphere* 161, 365–371. doi:10.1016/j.chemosphere.2016.07.023.

Domínguez-Garay, A., and Esteve-Núñez, A. (2018). Designing strategies for operating Microbial Electrochemical Systems to clean up polluted soils under non-flooded conditions. *Bioelectrochemistry* 124, 142–148. doi:10.1016/j.bioelechem.2018.03.006.

Domínguez-Garay, A., Quejigo, J. R., Dörfler, U., Schroll, R., and Esteve-Núñez, A. (2018). Bioelectroventing: an electrochemical-assisted bioremediation strategy for cleaning-up atrazine-polluted soils. *Microb. Biotechnol.* 11, 50–62. doi:10.1111/1751-7915.12687.

Domínguez Garay, A. (2016). Bioelectrochemically-assisted remediation: a novel strategy for cleaning-up polluted soils.

Dong, Y., Liu, J., Sui, M., Qu, Y., Ambuchi, J. J., Wang, H., et al. (2017). A combined microbial desalination cell and electrodialysis system for copper-containing wastewater treatment and high-salinity-water desalination. *J. Hazard. Mater.* 321, 307–315. doi:10.1016/j.jhazmat.2016.08.034.

Donnan, F. G. (1995). Theory of membrane equilibria and membrane potentials in the presence of non-dialysing electrolytes. A contribution to physical-chemical physiology. *J. Memb. Sci.* 100, 45–55. doi:10.1016/0376-7388(94)00297-C.

Durán, R. E., Méndez, V., Rodríguez-Castro, L., Barra-Sanhueza, B., Salvà-Serra, F., Moore, E. R. B., et al. (2019). Genomic and Physiological Traits of the Marine Bacterium Alcaligenes aquatilis QD168 Isolated From Quintero Bay, Central Chile, Reveal a Robust Adaptive Response to Environmental Stressors. *Front. Microbiol.* 10, 528. doi:10.3389/fmicb.2019.00528.

Ebrahimi, A., Najafpour, G. D., and Yousefi Kebria, D. (2018a). Performance of microbial desalination cell for salt removal and energy generation using different catholyte solutions. *Desalination* 432, 1–9. doi:10.1016/j.desal.2018.01.002.

Ebrahimi, A., Yousefi Kebria, D., and Darzi, G. N. (2018b). Improving bioelectricity generation and COD removal of sewage sludge in microbial desalination cell. *Environ. Technol. (United Kingdom)* 39, 1188–1197. doi:10.1080/09593330.2017.1323958.

Ebrahimi, A., Yousefi Kebria, D., and Najafpour Darzi, G. (2017). Enhancing biodegradation and energy generation via roughened surface graphite electrode in microbial desalination cell. *Water Sci. Technol.* 76, 1206–1214. doi:10.2166/wst.2017.280.

Edel, M., Horn, H., and Gescher, J. (2019). Biofilm systems as tools in biotechnological production. *Appl. Microbiol. Biotechnol.* 103, 5095–5103. doi:10.1007/s00253-019-09869-x.

Elimelech, M., and Phillip, W. A. (2011). The Future of Seawater Desalination: Energy, Technology, and the Environment. *Science (80-.).* 333, 712–717. doi:10.1126/science.1200488.

ElMekawy, A., Hegab, H. M., and Pant, D. (2014). The near-future integration of microbial desalination cells with reverse osmosis technology. *Energy Environ. Sci.* 7, 3921–3933. doi:10.1039/C4EE02208D.

Erable, B., Etcheverry, L., and Bergel, A. (2011). From microbial fuel cell (MFC) to microbial electrochemical snorkel (MES): maximizing chemical oxygen demand (COD) removal from wastewater. *Biofouling* 27, 319–326. doi:10.1080/08927014.2011.564615.

Esteve-Nunez, A., Rothermich, M., Sharma, M., and Lovley, D. (2005). Growth of Geobacter sulfurreducens under nutrient-limiting conditions in continuous culture. *Environ. Microbiol.* 7, 641–648. doi:10.1111/j.1462-2920.2005.00731.x.

Esteve-Núñez, A., Sosnik, J., Visconti, P., and Lovley, D. R. (2008). Fluorescent properties of c-type cytochromes reveal their potential role as an extracytoplasmic electron sink in Geobacter sulfurreducens. *Environ. Microbiol.* 10, 497–505. doi:10.1111/J.1462-2920.2007.01470.X.

Estévez-Canales, M. (2016). Novel bioelectrochemical approaches for exploring extracellular electron transfer in Geobacter sulfurreducens.

Estevez-Canales, M., Berná, A., Borjas, Z., and Esteve-Núñez, A. (2015a). Screen-Printed Electrodes: New Tools for Developing Microbial Electrochemistry at Microscale Level. *Energies* 8, 13211–13221. doi:10.3390/en81112366.

Estevez-Canales, M., Kuzume, A., Borjas, Z., Füeg, M., Lovley, D., Wandlowski, T., et al. (2015b). A severe reduction in the cytochrome C content of G eobacter sulfurreducens eliminates its capacity for extracellular electron transfer. *Environ. Microbiol. Rep.* 7, 219–226. doi:10.1111/1758-2229.12230.

European Environment Agency (EEA) (2019). National emissions reported to the UNFCCC and to the EU Greenhouse Gas Monitoring Mechanism.

Ewusi-Mensah, D., Huang, J., Chaparro, L. K., Rodenas, P., Ramírez-Moreno, M., Ortiz, J. M., et al. (2021). Algae-Assisted Microbial Desalination Cell: Analysis of

Cathode Performance and Desalination Efficiency Assessment. *Processes* 9, 2011. doi:10.3390/pr9112011.

Fernandez-Gatell, M., Sanchez-Vila, X., and Puigagut, J. (2022). Mec-Based Biosensor for Continuous Assessment of Microbial Activity and Biomass in Freshwater Ecosystems. *SSRN Electron. J.* doi:10.2139/SSRN.4012476.

Forrestal, C., Xu, P., and Ren, Z. (2012). Sustainable desalination using a microbial capacitive desalination cell. *Energy Environ. Sci.* 5, 7161. doi:10.1039/c2ee21121a.

Franks, A. E., and Nevin, K. P. (2010). Microbial Fuel Cells, A Current Review. *Energies* 3, 899–919. doi:10.3390/en3050899.

Freguia, S., Rabaey, K., Yuan, Z., and Keller, J. (2007a). Electron and Carbon Balances in Microbial Fuel Cells Reveal Temporary Bacterial Storage Behavior During Electricity Generation. *Environ. Sci. Technol.* 41, 2915–2921. doi:10.1021/es062611i.

Freguia, S., Rabaey, K., Yuan, Z., and Keller, J. (2007b). Non-catalyzed cathodic oxygen reduction at graphite granules in microbial fuel cells. *Electrochim. Acta* 53, 598–603. doi:10.1016/j.electacta.2007.07.037.

Freguia, S., Rabaey, K., Yuan, Z., and Keller, J. (2008). Sequential anode–cathode configuration improves cathodic oxygen reduction and effluent quality of microbial fuel cells. *Water Res.* 42, 1387–1396. doi:10.1016/j.watres.2007.10.007.

Fuertes, A. B., Lota, G., Centeno, T. A., and Frackowiak, E. (2005). Templated mesoporous carbons for supercapacitor application. *Electrochim. Acta* 50, 2799–2805. doi:10.1016/j.electacta.2004.11.027.

Fujimoto, K., Ueda, Y., Inohara, D., Fujii, Y., and Nakayama, M. (2020). Cobalt-doped electrolytic manganese dioxide as an efficient bifunctional catalyst for oxygen evolution/reduction reactions. *Electrochim. Acta* 354, 136592. doi:10.1016/j.electacta.2020.136592.

Gangadharan, P., and Nambi, I. M. (2015). Hexavalent chromium reduction and energy recovery by using dual-chambered microbial fuel cell. *Water Sci. Technol.* 71, 353–358. doi:10.2166/wst.2014.524.

Ge, X., Sumboja, A., Wuu, D., An, T., Li, B., Goh, F. W. T., et al. (2015). Oxygen Reduction in Alkaline Media: From Mechanisms to Recent Advances of Catalysts. *ACS Catal.* 5, 4643–4667. doi:10.1021/acscatal.5b00524.

Ge, Z., Dosoretz, C. G., and He, Z. (2014). Effects of number of cell pairs on the performance of microbial desalination cells. *Desalination* 341, 101–106. doi:10.1016/j.desal.2014.02.029.

Gholizadeh, A., Ebrahimi, A. A., Salmani, M. H., and Ehrampoush, M. H. (2017). Ozone-cathode microbial desalination cell; An innovative option to bioelectricity generation and water desalination. *Chemosphere* 188, 470–477. doi:10.1016/j.chemosphere.2017.09.009.

Global Water Intelligence (2020). 32nd Worldwide Desalting Plant Inventory Media Analytics Ltd.

Gorby, Y. A., Yanina, S., McLean, J. S., Rosso, K. M., Moyles, D., Dohnalkova, A., et al. (2006). Electrically conductive bacterial nanowires produced by Shewanella oneidensis strain MR-1 and other microorganisms. *Proc. Natl. Acad. Sci.* 103,

11358–11363. doi:10.1073/pnas.0604517103.

Gregory, K. B., Bond, D. R., and Lovley, D. R. (2004). Graphite electrodes as electron donors for anaerobic respiration. *Environ. Microbiol.* 6, 596–604. doi:10.1111/j.1462-2920.2004.00593.x.

Gregory, K. B., and Lovley, D. R. (2005). Remediation and Recovery of Uranium from Contaminated Subsurface Environments with Electrodes. *Environ. Sci. Technol.* 39, 8943–8947. doi:10.1021/es050457e.

Gubler, L. (2018). "Polymer Electrolyte Materials for Electrochemical Energy Devices," in *Reference Module in Chemistry, Molecular Sciences and Chemical Engineering* (Elsevier), 1–12. doi:10.1016/B978-0-12-409547-2.14285-4.

Gude, V. G., Kokabian, B., and Gadhamshetty, V. (2013). Beneficial bioelectrochemical systems for energy, water, and biomass production. *J. Microb. Biochem. Technol.* 5, 6. doi:10.4172/1948-5948.S6-005.

Gude, V. G., Nirmalakhandan, N., and Deng, S. (2010). Renewable and sustainable approaches for desalination. *Renew. Sustain. Energy Rev.* 14, 2641–2654. doi:10.1016/j.rser.2010.06.008.

Güler, E., Elizen, R., Vermaas, D. A., Saakes, M., and Nijmeijer, K. (2013). Performance-determining membrane properties in reverse electrodialysis. *J. Memb. Sci.* 446, 266–276. doi:10.1016/j.memsci.2013.06.045.

Guo, S., Yang, H., Liu, M., Feng, X., Gao, Y., Bai, Y., et al. (2021). Al-Storage Behaviors of Expanded Graphite as High-Rate and Long-Life Cathode Materials for Rechargeable Aluminum Batteries. *ACS Appl. Mater. Interfaces* 13, 22549–22558. doi:10.1021/acsami.1c04466.

Hahnke, S., Langer, T., and Klocke, M. (2018). Proteiniborus indolifex sp. nov., isolated from a thermophilic industrial-scale biogas plant. *Int. J. Syst. Evol. Microbiol.* 68, 824–828. doi:10.1099/ijsem.0.002591.

Harnisch, F., and Freguia, S. (2012). A Basic Tutorial on Cyclic Voltammetry for the Investigation of Electroactive Microbial Biofilms. *Chem. - An Asian J.* 7, 466–475. doi:10.1002/asia.201100740.

Harnisch, F., Wirth, S., and Schröder, U. (2009). Effects of substrate and metabolite crossover on the cathodic oxygen reduction reaction in microbial fuel cells: Platinum vs. iron(II) phthalocyanine based electrodes. *Electrochem. commun.* 11, 2253–2256. doi:10.1016/j.elecom.2009.10.002.

Haruta, S., and Kanno, N. (2015). Survivability of Microbes in Natural Environments and Their Ecological Impacts. *Microbes Environ.* 30, 123–125. doi:10.1264/jsme2.ME3002rh.

Hassan, R. Y. A., Febbraio, F., and Andreescu, S. (2021). Microbial Electrochemical Systems: Principles, Construction and Biosensing Applications. *Sensors 2021, Vol. 21, Page 1279* 21, 1279. doi:10.3390/S21041279.

He, G., Gu, Y., He, S., Schröder, U., Chen, S., and Hou, H. (2011a). Effect of fiber diameter on the behavior of biofilm and anodic performance of fiber electrodes in microbial fuel cells. *Bioresour. Technol.* 102, 10763–10766. doi:10.1016/j.biortech.2011.09.006.

He, M., Li, X., Liu, H., Miller, S. J., Wang, G., and Rensing, C. (2011b). Characterization

and genomic analysis of a highly chromate resistant and reducing bacterial strain Lysinibacillus fusiformis ZC1. *J. Hazard. Mater.* 185, 682–688. doi:10.1016/j.jhazmat.2010.09.072.

He, Z., and Angenent, L. T. (2006). Application of Bacterial Biocathodes in Microbial Fuel Cells. *Electroanalysis* 18, 2009–2015. doi:10.1002/elan.200603628.

Hemalatha, M., Butti, S. K., Velvizhi, G., and Venkata Mohan, S. (2017). Microbial mediated desalination for ground water softening with simultaneous power generation. *Bioresour. Technol.* 242, 28–35. doi:10.1016/j.biortech.2017.05.020.

Hernandez, M. E., and Newman, D. K. (2001). Extracellular electron transfer. *Cell. Mol. Life Sci.* 58, 1562–1571. doi:10.1007/PL00000796.

Hoareau, M., Erable, B., and Bergel, A. (2019). Microbial electrochemical snorkels (MESs): A budding technology for multiple applications. A mini review. *Electrochem. commun.* 104, 106473. doi:10.1016/j.elecom.2019.05.022.

Holmes, D. E., Bond, D. R., O?Neil, R. A., Reimers, C. E., Tender, L. R., and Lovley, D. R. (2004). Microbial Communities Associated with Electrodes Harvesting Electricity from a Variety of Aquatic Sediments. *Microb. Ecol.* 48, 178–190. doi:10.1007/s00248-003-0004-4.

Holmes, D. E., Chaudhuri, S. K., Nevin, K. P., Mehta, T., Methe, B. A., Liu, A., et al. (2006). Microarray and genetic analysis of electron transfer to electrodes in Geobacter sulfurreducens. *Environ. Microbiol.* 8, 1805–1815. doi:10.1111/j.1462-2920.2006.01065.x.

Holmes, D. E., Zhou, J., Ueki, T., Woodard, T., and Lovley, D. R. (2021). Mechanisms for Electron Uptake by Methanosarcina acetivorans during Direct Interspecies Electron Transfer. *MBio* 12. doi:10.1128/mBio.02344-21.

Honda, T., Fujita, T., and Tonouchi, A. (2013). Aminivibrio pyruvatiphilus gen. nov., sp. nov., an anaerobic, amino-acid-degrading bacterium from soil of a Japanese rice field. *Int. J. Syst. Evol. Microbiol.* 63, 3679–3686. doi:10.1099/ijs.0.052225-0.

Hristoskova, S., Bardarov, I., Yankov, D., Danova, S., Hubenova, Y., and Mitov, M. (2018). Identification of bacterial community in a sediment microbial fuel cell. *Bulg. Chem. Commun.* 50B, 147–153.

Huang, L., Wang, Q., Jiang, L., Zhou, P., Quan, X., and Logan, B. E. (2015). Adaptively Evolving Bacterial Communities for Complete and Selective Reduction of Cr(VI), Cu(II), and Cd(II) in Biocathode Bioelectrochemical Systems. *Environ. Sci. Technol.* 49, 9914–9924. doi:10.1021/acs.est.5b00191.

IDA Desalination & Reuse Handbook 2021–2022 (2022). Oxford: Media Analytics Ltd.,.

Ieropoulos, I. A., Ledezma, P., Stinchcombe, A., Papaharalabos, G., Melhuish, C., and Greenman, J. (2013). Waste to real energy: the first MFC powered mobile phone. *Phys. Chem. Chem. Phys.* 15, 15312. doi:10.1039/c3cp52889h.

Ihsanullah, I., Atieh, M. A., Sajid, M., and Nazal, M. K. (2021). Desalination and environment: A critical analysis of impacts, mitigation strategies, and greener desalination technologies. *Sci. Total Environ.* 780, 146585. doi:10.1016/j.scitotenv.2021.146585.

Inoue, K., Leang, C., Franks, A. E., Woodard, T. L., Nevin, K. P., and Lovley, D. R. (2011). Specific localization of the c-type cytochrome OmcZ at the anode surface

in current-producing biofilms of Geobacter sulfurreducens. *Environ. Microbiol. Rep.* 3, 211–217. doi:10.1111/j.1758-2229.2010.00210.x.

Ishii, S., Watanabe, K., Yabuki, S., Logan, B. E., and Sekiguchi, Y. (2008). Comparison of electrode reduction activities of Geobacter sulfurreducens and an enriched consortium in an air-cathode microbial fuel cell. *Appl. Environ. Microbiol.* 74, 7348–7355. doi:10.1128/AEM.01639-08.

Iskander, S. M., Novak, J. T., and He, Z. (2018). Enhancing forward osmosis water recovery from landfill leachate by desalinating brine and recovering ammonia in a microbial desalination cell. *Bioresour. Technol.* 255, 76–82. doi:10.1016/j.biortech.2018.01.097.

Jacobson, K. S., Drew, D. M., and He, Z. (2011a). Efficient salt removal in a continuously operated upflow microbial desalination cell with an air cathode. *Bioresour. Technol.* 102, 376–380. doi:10.1016/j.biortech.2010.06.030.

Jacobson, K. S., Drew, D. M., and He, Z. (2011b). Use of a Liter-Scale Microbial Desalination Cell As a Platform to Study Bioelectrochemical Desalination with Salt Solution or Artificial Seawater. *Environ. Sci. Technol.* 45, 4652–4657. doi:10.1021/es200127p.

Jafary, T., Al-Mamun, A., Alhimali, H., Baawain, M. S., Rahman, S., Tarpeh, W. A., et al. (2020). Novel two-chamber tubular microbial desalination cell for bioelectricity production, wastewater treatment and desalination with a focus on self-generated pH control. *Desalination* 481, 114358. doi:10.1016/j.desal.2020.114358.

Jafary, T., Daud, W. R. W., Aljlil, S. A., Ismail, A. F., Al-Mamun, A., Baawain, M. S., et al. (2018). Simultaneous organics, sulphate and salt removal in a microbial desalination cell with an insight into microbial communities. *Desalination* 445, 204–212. doi:10.1016/j.desal.2018.08.010.

Jenni, B., and Aragno, M. (1987). Xanthobacter agilis sp. nov., a Motile, Dinitrogen-Fixing, Hydrogen-Oxidizing Bacterium. *Syst. Appl. Microbiol.* 9, 254–257. doi:10.1016/S0723-2020(87)80030-9.

Jiang, C., Yang, Q., Wang, D., Zhong, Y., Chen, F., Li, X., et al. (2017). Simultaneous perchlorate and nitrate removal coupled with electricity generation in autotrophic denitrifying biocathode microbial fuel cell. *Chem. Eng. J.* 308, 783–790. doi:10.1016/j.cej.2016.09.121.

Jin, X., Angelidaki, I., and Zhang, Y. (2016). Microbial Electrochemical Monitoring of Volatile Fatty Acids during Anaerobic Digestion. *Environ. Sci. Technol.* 50, 4422–4429. doi:10.1021/acs.est.5b05267.

Jingyu, H., Ewusi-Mensah, D., and Norgbey, E. (2017). Microbial desalination cells technology: a review of the factors affecting the process, performance and efficiency. *Desalin. Water Treat.* 87, 140–159. doi:10.5004/dwt.2017.21302.

Judd, S. (2008). The status of membrane bioreactor technology. *Trends Biotechnol.* 26, 109–116. doi:10.1016/j.tibtech.2007.11.005.

Kadier, A., Simayi, Y., Abdeshahian, P., Azman, N. F., Chandrasekhar, K., and Kalil, M. S. (2016). A comprehensive review of microbial electrolysis cells (MEC) reactor designs and configurations for sustainable hydrogen gas production. *Alexandria Eng. J.* 55, 427–443. doi:10.1016/J.AEJ.2015.10.008.

Kaiya, S., Rubaba, O., Yoshida, N., Yamada, T., and Hiraishi, A. (2012). Characterization of Rhizobium naphthalenivorans sp. nov. with special emphasis on aromatic compound degradation and multilocus sequence analysis of housekeeping genes. *J. Gen. Appl. Microbiol.* 58, 211–224. doi:10.2323/jgam.58.211.

Kalleary, S., Mohammed Abbas, F., Ganesan, A., Meenatchisundaram, S., Srinivasan, B., Packirisamy, A. S. B., et al. (2014). Biodegradation and bioelectricity generation by Microbial Desalination Cell. *Int. Biodeterior. Biodegradation* 92, 20–25. doi:10.1016/j.ibiod.2014.04.002.

Kato, S. (2015). Biotechnological Aspects of Microbial Extracellular Electron Transfer. *Microbes Environ.* 30, 133–139. doi:10.1264/jsme2.ME15028.

Kato, S., Hashimoto, K., and Watanabe, K. (2012). Microbial interspecies electron transfer via electric currents through conductive minerals. *Proc. Natl. Acad. Sci.* 109, 10042–10046. doi:10.1073/pnas.1117592109.

Kelly, P. T., and He, Z. (2014). Understanding the application niche of microbial fuel cells in a cheese wastewater treatment process. *Bioresour. Technol.* 157, 154–160. doi:10.1016/j.biortech.2014.01.085.

Khawaji, A. D., Kutubkhanah, I. K., and Wie, J.-M. (2008). Advances in seawater desalination technologies. *Desalination* 221, 47–69. doi:10.1016/j.desal.2007.01.067.

Khazraee Zamanpour, M., Kariminia, H.-R., and Vosoughi, M. (2017). Electricity generation, desalination and microalgae cultivation in a biocathode-microbial desalination cell. *J. Environ. Chem. Eng.* 5, 843–848. doi:10.1016/j.jece.2016.12.045.

Khilari, S., Pandit, S., Varanasi, J. L., Das, D., and Pradhan, D. (2015). Bifunctional Manganese Ferrite/Polyaniline Hybrid as Electrode Material for Enhanced Energy Recovery in Microbial Fuel Cell. *ACS Appl. Mater. Interfaces* 7, 20657–20666. doi:10.1021/acsami.5b05273.

Kim, B. H., and Gadd, G. M. (2019). *Prokaryotic Metabolism and Physiology*. Cambridge University Press doi:10.1017/9781316761625.

Kim, S., Kim, Y. J., and Ryu, W.-H. (2021). Controllable Insertion Mechanism of Expanded Graphite Anodes Employing Conversion Reaction Pillars for Sodium-Ion Batteries. *ACS Appl. Mater. Interfaces* 13, 24070–24080. doi:10.1021/acsami.1c05928.

Kim, Y., and Logan, B. E. (2011). Series Assembly of Microbial Desalination Cells Containing Stacked Electrodialysis Cells for Partial or Complete Seawater Desalination. *Environ. Sci. Technol.* 45, 5840–5845. doi:10.1021/es200584q.

Kim, Y., and Logan, B. E. (2013a). Microbial desalination cells for energy production and desalination. *Desalination* 308, 122–130. doi:10.1016/j.desal.2012.07.022.

Kim, Y., and Logan, B. E. (2013b). Simultaneous removal of organic matter and salt ions from saline wastewater in bioelectrochemical systems. *Desalination* 308, 115–121. doi:10.1016/j.desal.2012.07.031.

Kojima, H., Watanabe, M., and Fukui, M. (2017). Sulfurivermis fontis gen. nov., sp. nov., a sulfur-oxidizing autotroph, and proposal of Thioprofundaceae fam. nov. *Int. J. Syst. Evol. Microbiol.* 67, 3458–3461. doi:10.1099/ijsem.0.002137.

Kokabian, B., Ghimire, U., and Gude, V. G. (2018a). Water deionization with renewable energy production in microalgae - microbial desalination process. *Renew. Energy* 122, 354–361. doi:10.1016/j.renene.2018.01.061.

Kokabian, B., and Gude, V. G. (2013). Photosynthetic microbial desalination cells (PMDCs) for clean energy, water and biomass production. *Environ. Sci. Process. Impacts* 15, 2178–2185. doi:10.1039/c3em00415e.

Kokabian, B., and Gude, V. G. (2015). Sustainable photosynthetic biocathode in microbial desalination cells. *Chem. Eng. J.* 262, 958–965. doi:10.1016/j.cej.2014.10.048.

Kokabian, B., Gude, V. G., Smith, R., and Brooks, J. P. (2018b). Evaluation of anammox biocathode in microbial desalination and wastewater treatment. *Chem. Eng. J.* 342, 410–419. doi:10.1016/j.cej.2018.02.088.

Kokabian, B., Smith, R., Brooks, J. P., and Gude, V. G. (2018c). Bioelectricity production in photosynthetic microbial desalination cells under different flow configurations. *J. Ind. Eng. Chem.* 58, 131–139. doi:10.1016/j.jiec.2017.09.017.

Kölbel, J., Strong, C., Noe, C., and Reig, P. (2018). Mapping Public Water Management By Harmonizing and Sharing Corporate Water Risk Information. *World Resour. Inst.*, 1–20. Available at: www.wri.org/publication/mapping-public-water.

Kondaveeti, S., Kakarla, R., and Min, B. (2018). "Physicochemical Parameters Governing Microbial Fuel Cell Performance," in *Microbial Fuel Cell* (Cham: Springer International Publishing), 189–208. doi:10.1007/978-3-319-66793-5_10.

Kotloski, N. J., and Gralnick, J. A. (2013). Flavin Electron Shuttles Dominate Extracellular Electron Transfer by Shewanella oneidensis. *MBio* 4, 553–565. doi:10.1128/mBio.00553-12.

Kumar, M., Verma, M., and Lal, R. (2008). Devosia chinhatensis sp. nov., isolated from a hexachlorocyclohexane (HCH) dump site in India. *Int. J. Syst. Evol. Microbiol.* 58, 861–865. doi:10.1099/ijs.0.65574-0.

Larimer, F. W., Chain, P., Hauser, L., Lamerdin, J., Malfatti, S., Do, L., et al. (2004). Complete genome sequence of the metabolically versatile photosynthetic bacterium Rhodopseudomonas palustris. *Nat. Biotechnol.* 22, 55–61. doi:10.1038/nbt923.

Lee, H.-J., Sarfert, F., Strathmann, H., and Moon, S.-H. (2002). Designing of an electrodialysis desalination plant. *Desalination* 142, 267–286. doi:10.1016/S0011-9164(02)00208-4.

Lee, Y. W., Hoang, T. S., Rhee, M.-S., Lee, S. Y., and Im, W.-T. (2020). Sinirhodobacter hankyongi sp. nov., a novel denitrifying bacterium isolated from sludge. *Int. J. Syst. Evol. Microbiol.* 70, 668–674. doi:10.1099/ijsem.0.003814.

Lefebvre, O., Tan, Z., Kharkwal, S., and Ng, H. Y. (2012). Effect of increasing anodic NaCl concentration on microbial fuel cell performance. *Bioresour. Technol.* 112, 336–340. doi:10.1016/j.biortech.2012.02.048.

Lefèvre, M., Proietti, E., Jaouen, F., and Dodelet, J.-P. (2009). Iron-Based Catalysts with Improved Oxygen Reduction Activity in Polymer Electrolyte Fuel Cells. *Science (80-.).* 324, 71–74. doi:10.1126/science.1170051.

Lejarazu-Larrañaga, A., Molina, S., Ortiz, J. M., Navarro, R., and García-Calvo, E. (2020a). Circular economy in membrane technology: Using end-of-life reverse

osmosis modules for preparation of recycled anion exchange membranes and validation in electrodialysis. *J. Memb. Sci.* 593, 117423. doi:10.1016/j.memsci.2019.117423.

Lejarazu-Larrañaga, A., Molina, S., Ortiz, J. M., Riccardelli, G., and García-Calvo, E. (2020b). Influence of acid/base activation treatment in the performance of recycled electromembrane for fresh water production by electrodialysis. *Chemosphere* 248, 126027. doi:10.1016/j.chemosphere.2020.126027.

Li, H., Chang, J., Liu, P., Fu, L., Ding, D., and Lu, Y. (2015). Direct interspecies electron transfer accelerates syntrophic oxidation of butyrate in paddy soil enrichments. *Environ. Microbiol.* 17, 1533–1547. doi:10.1111/1462-2920.12576.

Li, Y., Kawamura, Y., Fujiwara, N., Naka, T., Liu, H., Huang, X., et al. (2004). Sphingomonas yabuuchiae sp. nov. and Brevundimonas nasdae sp. nov., isolated from the Russian space laboratory Mir. *Int. J. Syst. Evol. Microbiol.* 54, 819–825. doi:10.1099/ijs.0.02829-0.

Li, Z., Zhang, Y., Leduc, P. R., and Gregory, K. B. (2011). Microbial electricity generation via microfluidic flow control. *Biotechnol. Bioeng.* 108, 2061–2069. doi:10.1002/BIT.23156.

Liang, Y., Feng, H., Shen, D., Li, N., Long, Y., Zhou, Y., et al. (2016). A high-performance photo-microbial desalination cell. *Electrochim. Acta* 202, 197–202. doi:10.1016/j.electacta.2016.03.177.

Lin, W. C., Coppi, M. V., and Lovley, D. R. (2004). Geobacter sulfurreducens Can Grow with Oxygen as a Terminal Electron Acceptor. *Appl. Environ. Microbiol.* 70, 2525–2528. doi:10.1128/AEM.70.4.2525-2528.2004.

Liu, B., and Creager, S. (2010). Silica-sol-templated mesoporous carbon as catalyst support for polymer electrolyte membrane fuel cell applications. *Electrochim. Acta* 55, 2721–2726. doi:10.1016/j.electacta.2009.12.044.

Liu, F., Rotaru, A.-E., Shrestha, P. M., Malvankar, N. S., Nevin, K. P., and Lovley, D. R. (2012). Promoting direct interspecies electron transfer with activated carbon. *Energy Environ. Sci.* 5, 8982. doi:10.1039/c2ee22459c.

Liu, F., Rotaru, A.-E., Shrestha, P. M., Malvankar, N. S., Nevin, K. P., and Lovley, D. R. (2015a). Magnetite compensates for the lack of a pilin-associated c -type cytochrome in extracellular electron exchange. *Environ. Microbiol.* 17, 648–655. doi:10.1111/1462-2920.12485.

Liu, G., Zhou, Y., Luo, H., Cheng, X., Zhang, R., and Teng, W. (2015b). A comparative evaluation of different types of microbial electrolysis desalination cells for malic acid production. *Bioresour. Technol.* 198, 87–93. doi:10.1016/j.biortech.2015.08.149.

Liu, H., and Logan, B. E. (2004). Electricity Generation Using an Air-Cathode Single Chamber Microbial Fuel Cell in the Presence and Absence of a Proton Exchange Membrane. *Environ. Sci. Technol.* 38, 4040–4046. doi:10.1021/es0499344.

Liu, X.-W., Sun, X.-F., Huang, Y.-X., Sheng, G.-P., Zhou, K., Zeng, R. J., et al. (2010). Nano-structured manganese oxide as a cathodic catalyst for enhanced oxygen reduction in a microbial fuel cell fed with a synthetic wastewater. *Water Res.* 44, 5298–5305. doi:10.1016/J.WATRES.2010.06.065.

Liu, X., Huang, L., Rensing, C., Ye, J., Nealson, K. H., and Zhou, S. (2021). Syntrophic interspecies electron transfer drives carbon fixation and growth by Rhodopseudomonas palustris under dark, anoxic conditions. *Sci. Adv.* 7. doi:10.1126/sciadv.abh1852.

Lo, N., Jin, H. M., and Jeon, C. O. (2014). Photobacterium aestuarii sp. nov., a marine bacterium isolated from a tidal flat. *Int. J. Syst. Evol. Microbiol.* 64, 625–630. doi:10.1099/ijs.0.056861-0.

Logan, B. E. (2007). *Microbial Fuel Cells*. Hoboken, NJ, USA: John Wiley & Sons, Inc. doi:10.1002/9780470258590.

Logan, B. E. (2009). Exoelectrogenic bacteria that power microbial fuel cells. *Nat. Rev. Microbiol.* 7, 375–381. doi:10.1038/nrmicro2113.

Logan, B. E. (2010). Scaling up microbial fuel cells and other bioelectrochemical systems. *Appl. Microbiol. Biotechnol.* 85, 1665–1671. doi:10.1007/s00253-009-2378-9.

Logan, B. E., Call, D., Cheng, S., Hamelers, H. V. M., Sleutels, T. H. J. A., Jeremiasse, A. W., et al. (2008). Microbial Electrolysis Cells for High Yield Hydrogen Gas Production from Organic Matter. *Environ. Sci. Technol.* 42, 8630–8640. doi:10.1021/es801553z.

Logan, B. E., and Elimelech, M. (2012). Membrane-based processes for sustainable power generation using water. *Nature* 488, 313–319. doi:10.1038/nature11477.

Logan, B. E., Hamelers, B., Rozendal, R., Schröder, U., Keller, J., Freguia, S., et al. (2006). Microbial fuel cells: Methodology and technology. *Environ. Sci. Technol.* 40, 5181–5192. doi:10.1021/es0605016.

Logan, B. E., and Rabaey, K. (2012). Conversion of Wastes into Bioelectricity and Chemicals by Using Microbial Electrochemical Technologies. *Science (80-.).* 337, 686–690. doi:10.1126/science.1217412.

Logan, B. E., and Regan, J. M. (2006a). Electricity-producing bacterial communities in microbial fuel cells. *Trends Microbiol.* 14, 512–518. doi:10.1016/j.tim.2006.10.003.

Logan, B. E., and Regan, J. M. (2006b). Microbial Fuel Cells—Challenges and Applications. *Environ. Sci. Technol.* 40, 5172–5180. doi:10.1021/es0627592.

Logan, B. E., Rossi, R., Ragab, A., and Saikaly, P. E. (2019). Electroactive microorganisms in bioelectrochemical systems. *Nat. Rev. Microbiol.* 17, 307–319. doi:10.1038/s41579-019-0173-x.

Looft, T., Levine, U. Y., and Stanton, T. B. (2013). Cloacibacillus porcorum sp. nov., a mucin-degrading bacterium from the swine intestinal tract and emended description of the genus Cloacibacillus. *Int. J. Syst. Evol. Microbiol.* 63, 1960–1966. doi:10.1099/ijs.0.044719-0.

Lovley, D. R. (2006). Bug juice: harvesting electricity with microorganisms. *Nat. Rev. Microbiol.* 4, 497–508. doi:10.1038/nrmicro1442.

Lovley, D. R. (2017). Syntrophy Goes Electric: Direct Interspecies Electron Transfer. *Annu. Rev. Microbiol.* 71, 643–664. doi:10.1146/annurev-micro-030117-020420.

Lovley, D. R., Giovannoni, S. J., White, D. C., Champine, J. E., Phillips, E. J. P., Gorby,

Y. A., et al. (1993). Geobacter metallireducens gen. nov. sp. nov., a microorganism capable of coupling the complete oxidation of organic compounds to the reduction of iron and other metals. *Arch. Microbiol.* 159, 336–344. doi:10.1007/BF00290916.

Lovley, D. R., and Holmes, D. E. (2022). Electromicrobiology: the ecophysiology of phylogenetically diverse electroactive microorganisms. *Nat. Rev. Microbiol.* 20, 5–19. doi:10.1038/s41579-021-00597-6.

Lovley, D. R., Holmes, D. E., and Nevin, K. P. (2004). "Dissimilatory Fe(III) and Mn(IV) Reduction," in *Advances in Microbial Physiology* (Academic Press), 219–286. doi:10.1016/S0065-2911(04)49005-5.

Lovley, D. R., and Phillips, E. J. P. (1986). Organic Matter Mineralization with Reduction of Ferric Iron in Anaerobic Sediments. *Appl. Environ. Microbiol.* 51, 683–689. doi:10.1128/AEM.51.4.683-689.1986.

Lovley, D. R., and Phillips, E. J. P. (1988). Novel Mode of Microbial Energy Metabolism: Organic Carbon Oxidation Coupled to Dissimilatory Reduction of Iron or Manganese. *Appl. Environ. Microbiol.* 54, 1472–1480. doi:10.1128/aem.54.6.1472-1480.1988.

Lovley, D. R., Stolz, J. F., Nord, G. L., and Phillips, E. J. P. (1987). Anaerobic production of magnetite by a dissimilatory iron-reducing microorganism. *Nature* 330, 252–254. doi:10.1038/330252a0.

Lovley, D. R., Ueki, T., Zhang, T., Malvankar, N. S., Shrestha, P. M., Flanagan, K. A., et al. (2011). "Geobacter," in *Advances in Microbial Physiology* (Academic Press), 1–100. doi:10.1016/B978-0-12-387661-4.00004-5.

Lu, L., and Ren, Z. J. (2016). Microbial electrolysis cells for waste biorefinery: A state of the art review. *Bioresour. Technol.* 215, 254–264. doi:10.1016/j.biortech.2016.03.034.

Lu, M., and Li, S. F. Y. (2012). Cathode Reactions and Applications in Microbial Fuel Cells: A Review. *Crit. Rev. Environ. Sci. Technol.* 42, 2504–2525. doi:10.1080/10643389.2011.592744.

Lu, Y., Abu-Reesh, I. M., and He, Z. (2016). Treatment and desalination of domestic wastewater for water reuse in a four-chamber microbial desalination cell. *Environ. Sci. Pollut. Res.*, 1–10. doi:10.1007/s11356-016-6910-z.

Lu, Y., Luo, H., Yang, K., Liu, G., Zhang, R., Li, X., et al. (2017). Formic acid production using a microbial electrolysis desalination and chemical-production cell. *Bioresour. Technol.* 243, 118–125. doi:10.1016/j.biortech.2017.06.059.

Lück, P. C., Jacobs, E., Röske, I., Schröter-Bobsin, U., Dumke, R., and Gronow, S. (2010). Legionella dresdenensis sp. nov., isolated from river water. *Int. J. Syst. Evol. Microbiol.* 60, 2557–2562. doi:10.1099/ijs.0.017863-0.

Luo, H., Jenkins, P. E., and Ren, Z. (2011). Concurrent Desalination and Hydrogen Generation Using Microbial Electrolysis and Desalination Cells. *Environ. Sci. Technol.* 45, 340–344. doi:10.1021/es1022202.

Luo, H., Li, H., Lu, Y., Liu, G., and Zhang, R. (2017). Treatment of reverse osmosis concentrate using microbial electrolysis desalination and chemical production cell. *Desalination* 408, 52–59. doi:10.1016/j.desal.2017.01.003.

Luo, H., Xu, P., Jenkins, P. E., and Ren, Z. (2012a). Ionic composition and transport

mechanisms in microbial desalination cells. *J. Memb. Sci.* 409–410, 16–23. doi:10.1016/j.memsci.2012.02.059.

Luo, H., Xu, P., and Ren, Z. (2012b). Long-term performance and characterization of microbial desalination cells in treating domestic wastewater. *Bioresour. Technol.* 120, 187–193. doi:10.1016/j.biortech.2012.06.054.

Luo, H., Xu, P., Roane, T. M., Jenkins, P. E., and Ren, Z. (2012c). Microbial desalination cells for improved performance in wastewater treatment, electricity production, and desalination. *Bioresour. Technol.* 105, 60–66. doi:10.1016/j.biortech.2011.11.098.

Ma, C.-Y., and Hou, C.-H. (2019). Enhancing the water desalination and electricity generation of a microbial desalination cell with a three-dimensional macroporous carbon nanotube-chitosan sponge anode. *Sci. Total Environ.* 675, 41–50. doi:10.1016/j.scitotenv.2019.04.174.

MacHarg, J. P., Seacord, T. F., and Sessions, B. (2008). ADC baseline tests reveal trends in membrane performance. *Desalin. Water Reuse* 18, 1–9. Available at: www.unionpump.com [Accessed February 11, 2019].

Maestro, B., Ortiz, J. M., Schrott, G., Busalmen, J. P., Climent, V., and Feliu, J. M. (2014). Crystallographic orientation and electrode nature are key factors for electric current generation by Geobacter sulfurreducens. *Bioelectrochemistry* 98, 11–19. doi:10.1016/j.bioelechem.2014.02.001.

Malakootian, M., Mahdizadeh, H., Nasiri, A., Mirzaienia, F., Hajhoseini, M., and Amirmahani, N. (2018). Investigation of the efficiency of microbial desalination cell in removal of arsenic from aqueous solutions. *Desalination* 438, 19–23. doi:10.1016/j.desal.2018.03.025.

Manchon, C., Muniesa-Merino, F., Serna, D., Asensio, Y., Wardman, C., and Esteve-Nuñez, A. (2023). Fluid-like electrodes and Purple Phototrophic Bacteria: bridging the gap in wastewater biorefineries. *Chem. Eng. J.* 453, 139828. doi:10.1016/j.cej.2022.139828.

Marsili, E., Rollefson, J. B., Baron, D. B., Hozalski, R. M., and Bond, D. R. (2008). Microbial biofilm voltammetry: Direct electrochemical characterization of catalytic electrode-attached biofilms. *Appl. Environ. Microbiol.* 74, 7329–7337. doi:10.1128/AEM.00177-08.

Martineau, C., Villeneuve, C., Mauffrey, F., and Villemur, R. (2013). Hyphomicrobium nitrativorans sp. nov., isolated from the biofilm of a methanol-fed denitrification system treating seawater at the Montreal Biodome. *Int. J. Syst. Evol. Microbiol.* 63, 3777–3781. doi:10.1099/ijs.0.048124-0.

Mashkour, M., Rahimnejad, M., Raouf, F., and Navidjouy, N. (2021). A review on the application of nanomaterials in improving microbial fuel cells. *Biofuel Res. J.* 8, 1400–1416. doi:10.18331/BRJ2021.8.2.5.

Mathews, C. K., Van Holde, K. E. (Kensal E., Ahern, K. G., and González de Buitrago, J. M. (2002). *Bioquímica*. 3rd ed. Addison Wesley.

McCarty, P. L., Bae, J., and Kim, J. (2011). Domestic wastewater treatment as a net energy producer-can this be achieved? *Environ. Sci. Technol.* 45, 7100–7106. doi:10.1021/es2014264.

Mechichi, T., Stackebrandt, E., and Fuchs, G. (2003). Alicycliphilus denitrificans gen.

nov., sp. nov., a cyclohexanol-degrading, nitrate-reducing β-proteobacterium. *Int. J. Syst. Evol. Microbiol.* 53, 147–152. doi:10.1099/ijs.0.02276-0.

Mehanna, M. A., Saito, T., Yang, J., Hickner, M., Cao, X., Huang, X., et al. (2010a). From an air-cathode microbial fuel cell (MFC) to an air-cathode microbial desalination cell (MDC). in *Abstracts of Papers, 239th ACS National Meeting, San Francisco, CA, United States, March 21-25, 2010* (American Chemical Society), ENVR-525.

Mehanna, M., Kiely, P. D., Call, D. F., and Logan, B. E. (2010b). Microbial Electrodialysis Cell for Simultaneous Water Desalination and Hydrogen Gas Production. *Environ. Sci. Technol.* 44, 9578–9583. doi:10.1021/es1025646.

Mehanna, M., Saito, T., Yan, J., Hickner, M., Cao, X., Huang, X., et al. (2010c). Using microbial desalination cells to reduce water salinity prior to reverse osmosis. *Energy Environ. Sci.* 3, 1114. doi:10.1039/c002307h.

Meng, F., Jiang, J., Zhao, Q., Wang, K., Zhang, G., Fan, Q., et al. (2014). Bioelectrochemical desalination and electricity generation in microbial desalination cell with dewatered sludge as fuel. *Bioresour. Technol.* 157, 120–126. doi:10.1016/j.biortech.2014.01.056.

Meng, F., Zhao, Q., Na, X., Zheng, Z., Jiang, J., Wei, L., et al. (2017). Bioelectricity generation and dewatered sludge degradation in microbial capacitive desalination cell. *Environ. Sci. Pollut. Res.* 24, 5159–5167. doi:10.1007/s11356-016-6853-4.

Methé, B. A., Nelson, K. E., Eisen, J. A., Paulsen, I. T., Nelson, W., Heidelberg, J. F., et al. (2003). Genome of Geobacter sulfurreducens: Metal Reduction in Subsurface Environments. *Science (80-.).* 302, 1967–1969. doi:10.1126/science.1088727.

Mohanakrishna, G., Seelam, J. S., Vanbroekhoven, K., and Pant, D. (2015). An enriched electroactive homoacetogenic biocathode for the microbial electrosynthesis of acetate through carbon dioxide reduction. *Faraday Discuss.* 183, 445–462. doi:10.1039/C5FD00041F.

Momodu, D., Madito, M., Barzegar, F., Bello, A., Khaleed, A., Olaniyan, O., et al. (2017). Activated carbon derived from tree bark biomass with promising material properties for supercapacitors. *J. Solid State Electrochem.* 21, 859–872. doi:10.1007/s10008-016-3432-z.

Morel, A., Zuo, K., Xia, X., Wei, J., Luo, X., Liang, P., et al. (2012). Microbial desalination cells packed with ion-exchange resin to enhance water desalination rate. *Bioresour. Technol.* 118, 43–48. doi:10.1016/j.biortech.2012.04.093.

Morotomi, M., Nagai, F., and Watanabe, Y. (2012). Description of Christensenella minuta gen. nov., sp. nov., isolated from human faeces, which forms a distinct branch in the order Clostridiales, and proposal of Christensenellaceae fam. nov. *Int. J. Syst. Evol. Microbiol.* 62, 144–149. doi:10.1099/ijs.0.026989-0.

Moruno, F. L., Rubio, J. E., Atanassov, P., Cerrato, J. M., Arges, C. G., and Santoro, C. (2018a). Microbial desalination cell with sulfonated sodium (poly(ether ether ketone) as cation exchange membranes for enhancing power generation and salt reduction. *Bioelectrochemistry* 121, 176–184. doi:10.1016/j.bioelechem.2018.02.004.

Moruno, F. L., Rubio, J. E., Santoro, C., Atanassov, P., Cerrato, J. M., and Arges, C. G.

(2018b). Investigation of patterned and non-patterned poly(2,6-dimethyl 1,4-phenylene) oxide based anion exchange membranes for enhanced desalination and power generation in a microbial desalination cell. *Solid State Ionics* 314, 141–148. doi:10.1016/j.ssi.2017.11.004.

Moya, A. A. (2016). A numerical comparison of optimal load and internal resistances in ion-exchange membrane systems under reverse electrodialysis conditions. *Desalination* 392, 25–33. doi:10.1016/j.desal.2016.04.016.

Myers, C. R., and Nealson, K. H. (1988). Bacterial Manganese Reduction and Growth with Manganese Oxide as the Sole Electron Acceptor. *Science (80-.).* 240, 1319–1321. doi:10.1126/science.240.4857.1319.

Ndongo, S., Dubourg, G., Khelaifia, S., Fournier, P.-E., and Raoult, D. (2016). Christensenella timonensis, a new bacterial species isolated from the human gut. *New Microbes New Infect.* 13, 32–33. doi:10.1016/j.nmni.2016.05.010.

Nevin, K. P., Hensley, S. A., Franks, A. E., Summers, Z. M., Ou, J., Woodard, T. L., et al. (2011). Electrosynthesis of Organic Compounds from Carbon Dioxide Is Catalyzed by a Diversity of Acetogenic Microorganisms. *Appl. Environ. Microbiol.* 77, 2882–2886. doi:10.1128/AEM.02642-10.

Nevin, K. P., Woodard, T. L., Franks, A. E., Summers, Z. M., and Lovley, D. R. (2010). Microbial Electrosynthesis: Feeding Microbes Electricity To Convert Carbon Dioxide and Water to Multicarbon Extracellular Organic Compounds. *MBio* 1. doi:10.1128/mBio.00103-10.

Niu, L., Song, L., and Dong, X. (2008). Proteiniborus ethanoligenes gen. nov., sp. nov., an anaerobic protein-utilizing bacterium. *Int. J. Syst. Evol. Microbiol.* 58, 12–16. doi:10.1099/ijs.0.65108-0.

Nobu, M. K., Narihiro, T., Hideyuki, T., Qiu, Y.-L., Sekiguchi, Y., Woyke, T., et al. (2015). The genome of S yntrophorhabdus aromaticivorans strain UI provides new insights for syntrophic aromatic compound metabolism and electron flow. *Environ. Microbiol.* 17, 4861–4872. doi:10.1111/1462-2920.12444.

Ohta, H., and Hattori, T. (1983). Agromonas oligotrophica gen. nov., sp. nov., a nitrogen-fixing oligotrophic bacterium. *Antonie Van Leeuwenhoek* 49, 429–446. doi:10.1007/BF00399322.

Olabi, A. G., Elsaid, K., Rabaia, M. K. H., Askalany, A. A., and Abdelkareem, M. A. (2020). Waste heat-driven desalination systems: Perspective. *Energy* 209, 118373. doi:10.1016/j.energy.2020.118373.

Ortiz, J. M., Sotoca, J. A., Expósito, E., Gallud, F., García-García, V., Montiel, V., et al. (2005). Brackish water desalination by electrodialysis: batch recirculation operation modeling. *J. Memb. Sci.* 252, 65–75. doi:10.1016/j.memsci.2004.11.021.

Pagnier, I., Raoult, D., and La Scola, B. (2011). Isolation and characterization of Reyranella massiliensis gen. nov., sp. nov. from freshwater samples by using an amoeba co-culture procedure. *Int. J. Syst. Evol. Microbiol.* 61, 2151–2154. doi:10.1099/ijs.0.025775-0.

Pal, D., Bhardwaj, A., Sudan, S. K., Kaur, N., Kumari, M., Bisht, B., et al. (2018). Thauera propionica sp. nov., isolated from downstream sediment sample of the river Ganges, Kanpur, India. *Int. J. Syst. Evol. Microbiol.* 68, 341–346.

doi:10.1099/ijsem.0.002508.

Pant, D., Van Bogaert, G., Diels, L., and Vanbroekhoven, K. (2010). A review of the substrates used in microbial fuel cells (MFCs) for sustainable energy production. *Bioresour. Technol.* 101, 1533–1543. doi:10.1016/j.biortech.2009.10.017.

Paquete, C. M., Rosenbaum, M. A., Bañeras, L., Rotaru, A.-E., and Puig, S. (2022). Let's chat: Communication between electroactive microorganisms. *Bioresour. Technol.* 347, 126705. doi:10.1016/j.biortech.2022.126705.

Parot, S., Délia, M.-L., and Bergel, A. (2008). Forming electrochemically active biofilms from garden compost under chronoamperometry. *Bioresour. Technol.* 99, 4809–4816. doi:10.1016/j.biortech.2007.09.047.

Patil, S. A., Arends, J. B. A., Vanwonterghem, I., van Meerbergen, J., Guo, K., Tyson, G. W., et al. (2015). Selective Enrichment Establishes a Stable Performing Community for Microbial Electrosynthesis of Acetate from CO 2. *Environ. Sci. Technol.* 49, 8833–8843. doi:10.1021/es506149d.

Peixoto, L., Min, B., Martins, G., Brito, A. G., Kroff, P., Parpot, P., et al. (2011). In situ microbial fuel cell-based biosensor for organic carbon. *Bioelectrochemistry* 81, 99–103. doi:10.1016/j.bioelechem.2011.02.002.

Peñacoba-Antona, L., Gómez-Delgado, M., and Esteve-Núñez, A. (2021a). Multi-Criteria Evaluation and Sensitivity Analysis for the Optimal Location of Constructed Wetlands (METland) at Oceanic and Mediterranean Areas. *Int. J. Environ. Res. Public Health* 18, 5415. doi:10.3390/ijerph18105415.

Peñacoba-Antona, L., Senán-Salinas, J., Aguirre-Sierra, A., Letón, P., Salas, J. J., García-Calvo, E., et al. (2021b). Assessing METland® Design and Performance Through LCA: Techno-Environmental Study With Multifunctional Unit Perspective. *Front. Microbiol.* 12, 1331. doi:10.3389/fmicb.2021.652173.

Peñacoba Antona, L. (2021). Validating full scale METland solutions for decentralized sustainable wastewater treatment: techno-environmental and geospatial analysis.

Perona-Vico, E., Feliu-Paradeda, L., Puig, S., and Bañeras, L. (2020). Bacteria coated cathodes as an in-situ hydrogen evolving platform for microbial electrosynthesis. *Sci. Rep.* 10, 19852. doi:10.1038/s41598-020-76694-y.

Ping, Q., Cohen, B., Dosoretz, C., and He, Z. (2013). Long-term investigation of fouling of cation and anion exchange membranes in microbial desalination cells. *Desalination* 325, 48–55. doi:10.1016/j.desal.2013.06.025.

Ping, Q., and He, Z. (2013). Improving the flexibility of microbial desalination cells through spatially decoupling anode and cathode. *Bioresour. Technol.* 144, 304–310. doi:10.1016/j.biortech.2013.06.117.

Ping, Q., Porat, O., Dosoretz, C. G., and He, Z. (2016). Bioelectricity inhibits back diffusion from the anolyte into the desalinated stream in microbial desalination cells. *Water Res.* 88, 266–273. doi:10.1016/j.watres.2015.10.018.

Post, J. W., Veerman, J., Hamelers, H. V. M., Euverink, G. J. W., Metz, S. J., Nymeijer, K., et al. (2007). Salinity-gradient power: Evaluation of pressure-retarded osmosis and reverse electrodialysis. *J. Memb. Sci.* 288, 218–230. doi:10.1016/j.memsci.2006.11.018.

Potter, M. C. (1910). On the difference of potential due to the vital activity of

microorganisms. *Proc. Univ. Durham Phil. Soc* 3, 245–249.

Potter, M. C. (1911). Electrical effects accompanying the decomposition of organic compounds. *Proc. R. Soc. London. Ser. B, Contain. Pap. a Biol. Character* 84, 260–276. doi:10.1098/rspb.1911.0073.

Pous, N., Balaguer, M. D., Colprim, J., and Puig, S. (2018). Opportunities for groundwater microbial electro-remediation. *Microb. Biotechnol.* 11, 119–135. doi:10.1111/1751-7915.12866.

Pous, N., Casentini, B., Rossetti, S., Fazi, S., Puig, S., and Aulenta, F. (2015). Anaerobic arsenite oxidation with an electrode serving as the sole electron acceptor: A novel approach to the bioremediation of arsenic-polluted groundwater. *J. Hazard. Mater.* 283, 617–622. doi:10.1016/j.jhazmat.2014.10.014.

Pous, N., Puig, S., Coma, M., Balaguer, M. D., and Colprim, J. (2013). Bioremediation of nitrate-polluted groundwater in a microbial fuel cell. *J. Chem. Technol. Biotechnol.* 88, 1690–1696. doi:10.1002/jctb.4020.

Pradhan, H., and Ghangrekar, M. M. (2014). Multi-chamber microbial desalination cell for improved organic matter and dissolved solids removal from wastewater. *Water Sci. Technol.* 70, 1948–1954. doi:10.2166/wst.2014.438.

Prado, A., Berenguer, R., Berná, A., and Esteve-Núñez, A. (2020a). Simultaneous characterization of porous and non-porous electrodes in microbial electrochemical systems. *MethodsX* 7, 101021. doi:10.1016/j.mex.2020.101021.

Prado, A., Berenguer, R., and Esteve-Núñez, A. (2019). Electroactive biochar outperforms highly conductive carbon materials for biodegrading pollutants by enhancing microbial extracellular electron transfer. *Carbon N. Y.* 146, 597–609. doi:10.1016/j.carbon.2019.02.038.

Prado, A., Ramírez-Vargas, C. A., Arias, C. A., and Esteve-Núñez, A. (2020b). Novel bioelectrochemical strategies for domesticating the electron flow in constructed wetlands. *Sci. Total Environ.* 735, 139522. doi:10.1016/j.scitotenv.2020.139522.

Prado de Nicolás, A. (2021). Exploring Metland Technology: Treating Wastewater By Integrating Electromicrobiology Into Nature-based Solution.

Prévoteau, A., Carvajal-Arroyo, J. M., Ganigué, R., and Rabaey, K. (2020). Microbial electrosynthesis from CO2: forever a promise? *Curr. Opin. Biotechnol.* 62, 48–57. doi:10.1016/j.copbio.2019.08.014.

Prévoteau, A., and Rabaey, K. (2017). Electroactive Biofilms for Sensing: Reflections and Perspectives. *ACS Sensors* 2, 1072–1085. doi:10.1021/acssensors.7b00418.

Puig, S., Serra, M., Vilar-Sanz, A., Cabré, M., Bañeras, L., Colprim, J., et al. (2011). Autotrophic nitrite removal in the cathode of microbial fuel cells. *Bioresour. Technol.* 102, 4462–4467. doi:10.1016/j.biortech.2010.12.100.

Pun, Á., Boltes, K., Letón, P., and Esteve-Nuñez, A. (2019). Detoxification of wastewater containing pharmaceuticals using horizontal flow bioelectrochemical filter. *Bioresour. Technol. Reports* 7, 100296. doi:10.1016/j.biteb.2019.100296.

Qin, B., Luo, H., Liu, G., Zhang, R., Chen, S., Hou, Y., et al. (2012). Nickel ion removal from wastewater using the microbial electrolysis cell. *Bioresour. Technol.* 121, 458–461. doi:10.1016/j.biortech.2012.06.068.

Qiu, Y.-L., Hanada, S., Ohashi, A., Harada, H., Kamagata, Y., and Sekiguchi, Y. (2008). Syntrophorhabdus aromaticivorans gen. nov., sp. nov., the First Cultured Anaerobe Capable of Degrading Phenol to Acetate in Obligate Syntrophic Associations with a Hydrogenotrophic Methanogen. *Appl. Environ. Microbiol.* 74, 2051–2058. doi:10.1128/AEM.02378-07.

Qu, Y., Feng, Y., Liu, J., He, W., Shi, X., Yang, Q., et al. (2013). Salt removal using multiple microbial desalination cells under continuous flow conditions. *Desalination* 317, 17–22. doi:10.1016/j.desal.2013.02.016.

Qu, Y., Feng, Y., Wang, X., Liu, J., Lv, J., He, W., et al. (2012). Simultaneous water desalination and electricity generation in a microbial desalination cell with electrolyte recirculation for pH control. *Bioresour. Technol.* 106, 89–94. doi:10.1016/j.biortech.2011.11.045.

Quejigo, J. R., Tejedor-Sanz, S., Schroll, R., and Esteve-Núñez, A. (2019). Electrodes boost microbial metabolism to mineralize antibiotics in manure. doi:10.1016/j.bioelechem.2019.04.008.

Rabaey, K. (2009). Bioelectrochemical Systems: From Extracellular Electron Transfer to Biotechnological Application. *Water Intell. Online* 8. doi:10.2166/9781780401621.

Rabaey, K., Boon, N., Siciliano, S. D., Verhaege, M., and Verstraete, W. (2004). Biofuel Cells Select for Microbial Consortia That Self-Mediate Electron Transfer. *Appl. Environ. Microbiol.* 70, 5373–5382. doi:10.1128/AEM.70.9.5373-5382.2004.

Rabaey, K., Rodríguez, J., Blackall, L. L., Keller, J., Gross, P., Batstone, D., et al. (2007). Microbial ecology meets electrochemistry: electricity-driven and driving communities. *ISME J.* 1, 9–18. doi:10.1038/ismej.2007.4.

Rabaey, K., and Rozendal, R. A. (2010). Microbial electrosynthesis — revisiting the electrical route for microbial production. *Nat. Rev. Microbiol.* 8, 706–716. doi:10.1038/nrmicro2422.

Rabaey, K., and Verstraete, W. (2005). Microbial fuel cells: novel biotechnology for energy generation. *Trends Biotechnol.* 23, 291–298. doi:10.1016/j.tibtech.2005.04.008.

Rahi, P., Khairnar, M., Hagir, A., Narayan, A., Jain, K. R., Madamwar, D., et al. (2021). Peteryoungia gen. nov. with four new species combinations and description of Peteryoungia desertarenae sp. nov., and taxonomic revision of the genus Ciceribacter based on phylogenomics of Rhizobiaceae. *Arch. Microbiol.* 203, 3591–3604. doi:10.1007/s00203-021-02349-9.

Rahman, S., Al-Mamun, A., Jafary, T., Alhimali, H., and Baawain, M. S. (2021a). Effect of internal and external resistances on desalination in microbial desalination cell. *Water Sci. Technol.* 83, 2389–2403. doi:10.2166/wst.2021.145.

Rahman, S., Jafary, T., Al-Mamun, A., Baawain, M. S., Choudhury, M. R., Alhaimali, H., et al. (2021b). Towards upscaling microbial desalination cell technology: A comprehensive review on current challenges and future prospects. *J. Clean. Prod.* 288, 125597. doi:10.1016/j.jclepro.2020.125597.

Rajendran, J., Shetty, B. H., Ganapathy, D., Murugan, P., Atchudan, R., Umapathy, D., et al. (2022). Thermally Expanded Graphite Incorporated with PEDOT:PSS Based

Anode for Microbial Fuel Cells with High Bioelectricity Production. *J. Electrochem. Soc.* 169, 017515. doi:10.1149/1945-7111/ac4b23.

Ramírez-Bahena, M.-H., Chahboune, R., Peix, A., and Velázquez, E. (2013). Reclassification of Agromonas oligotrophica into the genus Bradyrhizobium as Bradyrhizobium oligotrophicum comb. nov. *Int. J. Syst. Evol. Microbiol.* 63, 1013–1016. doi:10.1099/ijs.0.041897-0.

Ramírez-Moreno, M., Esteve-Núñez, A., and Ortiz, J. M. (2021a). Desalination of brackish water using a microbial desalination cell: Analysis of the electrochemical behaviour. *Electrochim. Acta* 388, 138570. doi:10.1016/j.electacta.2021.138570.

Ramírez-Moreno, M., Rodenas, P., Aliaguilla, M., Bosch-Jimenez, P., Borràs, E., Zamora, P., et al. (2019). Comparative Performance of Microbial Desalination Cells Using Air Diffusion and Liquid Cathode Reactions: Study of the Salt Removal and Desalination Efficiency. *Front. Energy Res.* 7, 135. doi:10.3389/fenrg.2019.00135.

Ramírez-Moreno, M., Rodenas, P., Aliaguilla, M., Bosch-Jimenez, P., Borràs, E., Zamora, P., et al. (2021b). "Microbial desalination cell design & bioengineering assays: Main concepts," in *Microbial Desalination Cells for Low Energy Drinking Water* (IWA Publishing), 15–40. doi:10.2166/9781789062120_0015.

Ramírez-Vargas, C. A., Arias, C. A., Carvalho, P., Zhang, L., Esteve-Núñez, A., and Brix, H. (2019). Electroactive biofilm-based constructed wetland (EABB-CW): A mesocosm-scale test of an innovative setup for wastewater treatment. *Sci. Total Environ.* 659, 796–806. doi:10.1016/j.scitotenv.2018.12.432.

Ramírez-Vargas, C., Prado, A., Arias, C., Carvalho, P., Esteve-Núñez, A., and Brix, H. (2018). Microbial Electrochemical Technologies for Wastewater Treatment: Principles and Evolution from Microbial Fuel Cells to Bioelectrochemical-Based Constructed Wetlands. *Water* 10, 1128. doi:10.3390/w10091128.

Reguera, G., McCarthy, K. D., Mehta, T., Nicoll, J. S., Tuominen, M. T., and Lovley, D. R. (2005). Extracellular electron transfer via microbial nanowires. *Nature* 435, 1098–1101. doi:10.1038/nature03661.

Reguera, G., Nevin, K. P., Nicoll, J. S., Covalla, S. F., Woodard, T. L., and Lovley, D. R. (2006). Biofilm and Nanowire Production Leads to Increased Current in Geobacter sulfurreducens Fuel Cells. *Appl. Environ. Microbiol.* 72, 7345–7348. doi:10.1128/AEM.01444-06.

Reimers, C. E., Tender, L. M., Fertig, S., and Wang, W. (2001). Harvesting Energy from the Marine Sediment−Water Interface. *Environ. Sci. Technol.* 35, 192–195. doi:10.1021/es001223s.

Ren, H., Lee, H.-S., and Chae, J. (2012). Miniaturizing microbial fuel cells for potential portable power sources: promises and challenges. *Microfluid. Nanofluidics* 13, 353–381. doi:10.1007/s10404-012-0986-7.

Ren, Z., Ward, T. E., and Regan, J. M. (2007). Electricity Production from Cellulose in a Microbial Fuel Cell Using a Defined Binary Culture. *Environ. Sci. Technol.* 41, 4781–4786. doi:10.1021/es070577h.

Rengasamy, K., Ranaivoarisoa, T., Bai, W., and Bose, A. (2021). Magnetite nanoparticle

anchored graphene cathode enhances microbial electrosynthesis of polyhydroxybutyrate by Rhodopseudomonas palustris TIE-1. *Nanotechnology* 32, 035103. doi:10.1088/1361-6528/abbe58.

Rezk, H., Sayed, E. T., Al-Dhaifallah, M., Obaid, M., El-Sayed, A. H. M., Abdelkareem, M. A., et al. (2019). Fuel cell as an effective energy storage in reverse osmosis desalination plant powered by photovoltaic system. *Energy* 175, 423–433. doi:10.1016/j.energy.2019.02.167.

Richter, H., Nevin, K. P., Jia, H., Lowy, D. A., Lovley, D. R., and Tender, L. M. (2009). Cyclic voltammetry of biofilms of wild type and mutant Geobacter sulfurreducens on fuel cell anodes indicates possible roles of OmcB, OmcZ, type IV pili, and protons in extracellular electron transfer. *Energy Environ. Sci.* 2, 506–516. doi:10.1039/B816647A.

Richter, K., Schicklberger, M., and Gescher, J. (2012). Dissimilatory Reduction of Extracellular Electron Acceptors in Anaerobic Respiration. *Appl. Environ. Microbiol.* 78, 913–921. doi:10.1128/AEM.06803-11.

Rivas, R., Willems, A., Subba-Rao, N. S., Mateos, P. F., Dazzo, F. B., Kroppenstedt, R. M., et al. (2003). Description of Devosia neptuniae sp. nov. that Nodulates and Fixes Nitrogen in Symbiosis with Neptunia natans, an Aquatic Legume from India. *Syst. Appl. Microbiol.* 26, 47–53. doi:10.1078/072320203322337308.

Rodenas Motos, P., ter Heijne, A., van der Weijden, R., Saakes, M., Buisman, C. J. N., and Sleutels, T. H. J. A. (2015). High rate copper and energy recovery in microbial fuel cells. *Front. Microbiol.* 6, 527. doi:10.3389/fmicb.2015.00527.

Rodrigo, J., Boltes, K., and Esteve-Nuñez, A. (2014). Microbial-electrochemical bioremediation and detoxification of dibenzothiophene-polluted soil. *Chemosphere* 101, 61–65. doi:10.1016/j.chemosphere.2013.11.060.

Rodrigo Quejigo, J. (2017). Bioelectroventing: cleaning-up polluted sites using electrodes to stimulate microbial remediation activities.

Rodrigo Quejigo, J., Domínguez-Garay, A., Dörfler, U., Schroll, R., and Esteve-Núñez, A. (2018). Anodic shifting of the microbial community profile to enhance oxidative metabolism in soil. *Soil Biol. Biochem.* 116, 131–138. doi:10.1016/j.soilbio.2017.09.012.

Rodrigo Quejigo, J., Dörfler, U., Schroll, R., and Esteve-Núñez, A. (2016). Stimulating soil microorganisms for mineralizing the herbicide isoproturon by means of microbial electroremediating cells. *Microb. Biotechnol.* 9, 369–380. doi:10.1111/1751-7915.12351.

Rodríguez-Mirasol, J., Cordero, T., and Rodríguez, J. J. (1993). Preparation and characterization of activated carbons from eucalyptus kraft lignin. *Carbon N. Y.* 31, 87–95. doi:10.1016/0008-6223(93)90160-C.

Rodríguez-Mirasol, J., Cordero, T., and Rodríguez, J. J. (1996). High-temperature carbons from kraft lignin. *Carbon N. Y.* 34, 43–52. doi:10.1016/0008-6223(95)00133-6.

Rodríguez-Reinoso, F., and Molina-Sabio, M. (1992). Activated carbons from lignocellulosic materials by chemical and/or physical activation: an overview. *Carbon N. Y.* 30, 1111–1118. doi:10.1016/0008-6223(92)90143-K.

Rodríguez-Reinoso, F., Molina-Sabio, M., and González, M. T. (1995). The use of steam and CO2 as activating agents in the preparation of activated carbons. *Carbon N. Y.* 33, 15–23. doi:10.1016/0008-6223(94)00100-E.

Rollefson, J. B., Stephen, C. S., Tien, M., and Bond, D. R. (2011). Identification of an Extracellular Polysaccharide Network Essential for Cytochrome Anchoring and Biofilm Formation in Geobacter sulfurreducens. *J. Bacteriol.* 193, 1023–1033. doi:10.1128/JB.01092-10.

Rotaru, A.-E. E., Woodard, T. L., Nevin, K. P., and Lovley, D. R. (2015). Link between capacity for current production and syntrophic growth in Geobacter species. *Front. Microbiol.* 6, 744. doi:10.3389/fmicb.2015.00744.

Rotaru, A.-E., Shrestha, P. M., Liu, F., Markovaite, B., Chen, S., Nevin, K. P., et al. (2014). Direct Interspecies Electron Transfer between Geobacter metallireducens and Methanosarcina barkeri. *Appl. Environ. Microbiol.* 80, 4599–4605. doi:10.1128/AEM.00895-14.

Rotaru, A. E., Yee, M. O., and Musat, F. (2021). Microbes trading electricity in consortia of environmental and biotechnological significance. *Curr. Opin. Biotechnol.* 67, 119–129. doi:10.1016/j.copbio.2021.01.014.

Rouquerol, J., Avnir, D., Everett, D. H., Fairbridge, C., Haynes, M., Pernicone, N., et al. (1994). "Guidelines for the Characterization of Porous Solids," in *Studies in Surface Science and Catalysis* (De Gruyter), 1–9. doi:10.1016/S0167-2991(08)63059-1.

Rozendal, R. A., Hamelers, H. V. M. M., Rabaey, K., Keller, J., and Buisman, C. J. N. N. (2008). Towards practical implementation of bioelectrochemical wastewater treatment. *Trends Biotechnol.* 26, 450–459. doi:10.1016/j.tibtech.2008.04.008.

Rozendal, R. A., Leone, E., Keller, J., and Rabaey, K. (2009). Efficient hydrogen peroxide generation from organic matter in a bioelectrochemical system. *Electrochem. commun.* 11, 1752–1755. doi:10.1016/j.elecom.2009.07.008.

Russell, J. B., and Cook, G. M. (1995). Energetics of bacterial growth: balance of anabolic and catabolic reactions. *Microbiol. Rev.* 59, 48–62. doi:10.1128/MMBR.59.1.48-62.1995.

Sabina, K., Fayidh, M. A., Archana, G., Sivarajan, M., Babuskin, S., Babu, P. A. S., et al. (2014). Microbial desalination cell for enhanced biodegradation of waste engine oil using a novel bacterial strain Bacillus subtilis moh3. *Environ. Technol. (United Kingdom)* 35, 2194–2203. doi:10.1080/09593330.2014.896951.

Saeed, H. M., Husseini, G. A., Yousef, S., Saif, J., Al-Asheh, S., Abu Fara, A., et al. (2015). Microbial desalination cell technology: A review and a case study. *Desalination* 359, 1–13. doi:10.1016/j.desal.2014.12.024.

Saheb-Alam, S., Persson, F., Wilén, B., Hermansson, M., and Modin, O. (2019). Response to starvation and microbial community composition in microbial fuel cells enriched on different electron donors. *Microb. Biotechnol.* 12, 962–975. doi:10.1111/1751-7915.13449.

Salehmin, M. N. I., Lim, S. S., Satar, I., and Daud, W. R. W. (2021). Pushing microbial desalination cells towards field application: Prevailing challenges, potential mitigation strategies, and future prospects. *Sci. Total Environ.* 759, 143485.

doi:10.1016/j.scitotenv.2020.143485.

Salinas-Rodríguez, S. G., Arévalo, J., Ortiz, J. M., Borràs-Camps, E., Monsalvo-Garcia, V., Kennedy, M. D., et al. (2021). *Microbial Desalination Cells for Low Energy Drinking Water*. , eds. S. G. Salinas-Rodríguez, J. Arévalo, J. M. Ortiz, E. Borràs-Camps, V. Monsalvo-Garcia, M. D. Kennedy, et al. London: IWA Publishing doi:10.2166/9781789062120.

Saline Agriculture Worldwide Classification of saline water - Salt Farm Foundation. Available at: https://www.salineagricultureworldwide.com/classification-of-saline-water [Accessed August 16, 2022].

Salman, H. H., and Ismail, Z. Z. (2020). Desalination of actual wetland saline water associated with biotreatment of real sewage and bioenergy production in microbial desalination cell. *Sep. Purif. Technol.* 250, 117110. doi:10.1016/j.seppur.2020.117110.

Santoro, C., Talarposhti, M. R., Kodali, M., Gokhale, R., Serov, A., Merino-Jimenez, I., et al. (2017). Microbial Desalination Cells with Efficient Platinum-Group-Metal-Free Cathode Catalysts. *ChemElectroChem* 4, 3322–3330. doi:10.1002/celc.201700626.

Sara, T.-S., Patricia, F.-L., Carlos, M., and Abraham, E.-N. (2020). Fluidized bed cathodes as suitable electron donors for bacteria to remove nitrogen and produce biohydrogen. *Electrochem. commun.* 116, 106759. doi:10.1016/j.elecom.2020.106759.

Sayed, E. T., Shehata, N., Abdelkareem, M. A., and Atieh, M. A. (2020). Recent progress in environmentally friendly bio-electrochemical devices for simultaneous water desalination and wastewater treatment. *Sci. Total Environ.* 748, 141046. doi:10.1016/j.scitotenv.2020.141046.

Schievano, A., Berenguer, R., Goglio, A., Bocchi, S., Marzorati, S., Rago, L., et al. (2019). Electroactive Biochar for Large-Scale Environmental Applications of Microbial Electrochemistry. *ACS Sustain. Chem. Eng.* 7, 18198–18212. doi:10.1021/acssuschemeng.9b04229.

Schmidt, J. J. (2019). "Valuing water," in *Water Politics* (Paris: Routledge), 15–27. doi:10.4324/9780429453571-2.

Schröder, U. (2007). Anodic electron transfer mechanisms in microbial fuel cells and their energy efficiency. *Phys. Chem. Chem. Phys.* 9, 2619–2629. doi:10.1039/B703627M.

Schröder, U., Harnisch, F., and Angenent, L. T. (2015). Microbial electrochemistry and technology: Terminology and classification. *Energy Environ. Sci.* 8. doi:10.1039/c4ee03359k.

Sevda, S., and Abu-Reesh, I. M. (2018). Improved salt removal and power generation in a cascade of two hydraulically connected up-flow microbial desalination cells. *J. Environ. Sci. Heal. Part A* 53, 326–337. doi:10.1080/10934529.2017.1400805.

Sevda, S., Abu-Reesh, I. M., Yuan, H., and He, Z. (2017). Bioelectricity generation from treatment of petroleum refinery wastewater with simultaneous seawater desalination in microbial desalination cells. *Energy Convers. Manag.* 141, 101–107. doi:10.1016/j.enconman.2016.05.050.

Sevda, S., Yuan, H., He, Z., and Abu-Reesh, I. M. (2015). Microbial desalination cells as a versatile technology: Functions, optimization and prospective. *Desalination* 371, 9–17. doi:10.1016/j.desal.2015.05.021.

Sharma, S., Hammed, A., and Simsek, H. (2019). "Microbial Desalination Cells," in *Bioelectrochemical Interface Engineering* (Wiley), 235–249. doi:10.1002/9781119611103.ch13.

Sharon, H., and Reddy, K. S. (2015). A review of solar energy driven desalination technologies. *Renew. Sustain. Energy Rev.* 41, 1080–1118. doi:10.1016/j.rser.2014.09.002.

Shehab, N. A., Amy, G. L., Logan, B. E., and Saikaly, P. E. (2014). Enhanced water desalination efficiency in an air-cathode stacked microbial electrodeionization cell (SMEDIC). *J. Memb. Sci.* 469, 364–370. doi:10.1016/j.memsci.2014.06.058.

Shelobolina, E. S., Nevin, K. P., Blakeney-Hayward, J. D., Johnsen, C. V., Plaia, T. W., Krader, P., et al. (2007). Geobacter pickeringii sp. nov., Geobacter argillaceus sp. nov. and Pelosinus fermentans gen. nov., sp. nov., isolated from subsurface kaolin lenses. *Int. J. Syst. Evol. Microbiol.* 57, 126–135. doi:10.1099/ijs.0.64221-0.

Shen, J., Huang, L., Zhou, P., Quan, X., and Puma, G. L. (2017). Correlation between circuital current, Cu(II) reduction and cellular electron transfer in EAB isolated from Cu(II)-reduced biocathodes of microbial fuel cells. *Bioelectrochemistry* 114, 1–7. doi:10.1016/j.bioelechem.2016.11.002.

Shi, L., Dong, H., Reguera, G., Beyenal, H., Lu, A., Liu, J., et al. (2016). Extracellular electron transfer mechanisms between microorganisms and minerals. *Nat. Rev. Microbiol.* 14, 651–662. doi:10.1038/nrmicro.2016.93.

Shinde, O. A., Bansal, A., Banerjee, A., and Sarkar, S. (2018). Bioremediation of steel plant wastewater and enhanced electricity generation in microbial desalination cell. *Water Sci. Technol.* 77, 2101–2112. doi:10.2166/wst.2018.126.

Shiratori, H., Sasaya, K., Ohiwa, H., Ikeno, H., Ayame, S., Kataoka, N., et al. (2009). Clostridium clariflavum sp. nov. and Clostridium caenicola sp. nov., moderately thermophilic, cellulose-/cellobiose-digesting bacteria isolated from methanogenic sludge. *Int. J. Syst. Evol. Microbiol.* 59, 1764–1770. doi:10.1099/ijs.0.003483-0.

Shrestha, P. M., and Rotaru, A.-E. (2014). Plugging in or going wireless: strategies for interspecies electron transfer. *Front. Microbiol.* 5, 237. doi:10.3389/fmicb.2014.00237.

Simon, P., and Gogotsi, Y. (2008). Materials for electrochemical capacitors. *Nat. Mater.* 7, 845–854. doi:10.1038/nmat2297.

Sly, L. I., Arunpairojana, V., and Hodgkinson, M. C. (1988). Pedomicrobium manganicum from Drinking-Water Distribution Systems with Manganese-Related "Dirty Water" Problems. *Syst. Appl. Microbiol.* 11, 75–84. doi:10.1016/S0723-2020(88)80051-1.

Sood, A., and Smakhtin, V. (2014). Can Desalination and Clean Energy Combined Help to Alleviate Global Water Scarcity? *JAWRA J. Am. Water Resour. Assoc.* 50, 1111–1123. doi:10.1111/jawr.12174.

Sophia, A. C., and Bhalambaal, V. M. (2015). Utilization of coconut shell carbon in the anode compartment of microbial desalination cell (MDC) for enhanced desalination

and bio-electricity production. *J. Environ. Chem. Eng.* 3, 2768–2776. doi:10.1016/j.jece.2015.10.026.

Sophia, A. C., Bhalambaal, V. M., Lima, E. C., and Thirunavoukkarasu, M. (2016). Microbial desalination cell technology: Contribution to sustainable waste water treatment process, current status and future applications. doi:10.1016/j.jece.2016.07.024.

Speers, A. M., and Reguera, G. (2012). Electron Donors Supporting Growth and Electroactivity of Geobacter sulfurreducens Anode Biofilms. *Appl. Environ. Microbiol.* 78, 437–444. doi:10.1128/AEM.06782-11.

Sporer, A. J., Kahl, L. J., Price-Whelan, A., and Dietrich, L. E. P. (2017). Redox-Based Regulation of Bacterial Development and Behavior. *Annu. Rev. Biochem.* 86, 777–797. doi:10.1146/annurev-biochem-061516-044453.

Stahel, W. R. (2016). The circular economy. *Nature* 531, 435–438. doi:10.1038/531435a.

Steidl, R. J., Lampa-Pastirk, S., and Reguera, G. (2016). Mechanistic stratification in electroactive biofilms of Geobacter sulfurreducens mediated by pilus nanowires. *Nat. Commun.* 7, 12217. doi:10.1038/ncomms12217.

Steinbusch, K. J. J., Hamelers, H. V. M., Schaap, J. D., Kampman, C., and Buisman, C. J. N. (2010). Bioelectrochemical Ethanol Production through Mediated Acetate Reduction by Mixed Cultures. *Environ. Sci. Technol.* 44, 513–517. doi:10.1021/es902371e.

Strathmann, H. (2010). Electrodialysis, a mature technology with a multitude of new applications. *Desalination* 264, 268–288. doi:10.1016/j.desal.2010.04.069.

Strycharz, S. M., Woodard, T. L., Johnson, J. P., Nevin, K. P., Sanford, R. A., Löffler, F. E., et al. (2008). Graphite Electrode as a Sole Electron Donor for Reductive Dechlorination of Tetrachlorethene by Geobacter lovleyi. *Appl. Environ. Microbiol.* 74, 5943–5947. doi:10.1128/AEM.00961-08.

Summers, Z. M., Fogarty, H. E., Leang, C., Franks, A. E., Malvankar, N. S., and Lovley, D. R. (2010). Direct Exchange of Electrons Within Aggregates of an Evolved Syntrophic Coculture of Anaerobic Bacteria. *Science (80-.).* 330, 1413–1415. doi:10.1126/science.1196526.

Sun, L., Toyonaga, M., Ohashi, A., Tourlousse, D. M., Matsuura, N., Meng, X.-Y., et al. (2016). Lentimicrobium saccharophilum gen. nov., sp. nov., a strictly anaerobic bacterium representing a new family in the phylum Bacteroidetes, and proposal of Lentimicrobiaceae fam. nov. *Int. J. Syst. Evol. Microbiol.* 66, 2635–2642. doi:10.1099/ijsem.0.001103.

Tabares, M., Dulay, H., and Reguera, G. (2020). Geobacter sulfurreducens. *Trends Microbiol.* 28, 327–328. doi:10.1016/j.tim.2019.11.004.

Tandukar, M., Huber, S. J., Onodera, T., and Pavlostathis, S. G. (2009). Biological Chromium(VI) Reduction in the Cathode of a Microbial Fuel Cell. *Environ. Sci. Technol.* 43, 8159–8165. doi:10.1021/es9014184.

Tejedor-Sanz, S. (2016). Merging microbial electrochemical systems with conventional reactor designs for treating wastewater.

Tejedor-Sanz, S., Fernández-Labrador, P., Hart, S., Torres, C. I., and Esteve-Núñez, A. (2018). Geobacter Dominates the Inner Layers of a Stratified Biofilm on a Fluidized

Anode During Brewery Wastewater Treatment. *Front. Microbiol.* 9, 378. doi:10.3389/fmicb.2018.00378.

Tejedor-Sanz, S., Quejigo, J. R., Berná, A., and Esteve-Núñez, A. (2017). The Planktonic Relationship Between Fluid-Like Electrodes and Bacteria: Wiring in Motion. *ChemSusChem* 10, 693–700. doi:10.1002/cssc.201601329.

Tejedor-Sanz, S., Stevens, E. T., Li, S., Finnegan, P., Nelson, J., Knoesen, A., et al. (2022). Extracellular electron transfer increases fermentation in lactic acid bacteria via a hybrid metabolism. *Elife* 11. doi:10.7554/eLife.70684.

ter Heijne, A., Geppert, F., Sleutels, T. H. J. A., Batlle-Vilanova, P., Liu, D., and Puig, S. (2017). "Mixed Culture Biocathodes for Production of Hydrogen, Methane, and Carboxylates," in *Advances in biochemical engineering/biotechnology* (Springer Science and Business Media Deutschland GmbH), 203–229. doi:10.1007/10_2017_15.

The Environmental, and Protection Agency (2014). "Summary for Policymakers," in *Climate Change 2013 – The Physical Science Basis* (Cambridge University Press), 1–30. doi:10.1017/CBO9781107415324.004.

Thrash, J. C., Van Trump, J. I., Weber, K. A., Miller, E., Achenbach, L. A., and Coates, J. D. (2007). Electrochemical Stimulation of Microbial Perchlorate Reduction. *Environ. Sci. Technol.* 41, 1740–1746. doi:10.1021/es062772m.

Tiago, I., Mendes, V., Pires, C., Morais, P. V., and Veríssimo, A. (2005). Phenylobacterium falsum sp. nov., an Alphaproteobacterium isolated from a nonsaline alkaline groundwater, and emended description of the genus Phenylobacterium. *Syst. Appl. Microbiol.* 28, 295–302. doi:10.1016/j.syapm.2005.02.005.

Torres, C. I., Marcus, A. K., and Rittmann, B. E. (2008). Proton transport inside the biofilm limits electrical current generation by anode-respiring bacteria. *Biotechnol. Bioeng.* 100, 872–881. doi:10.1002/BIT.21821.

Tsubouchi, T., Shimane, Y., Usui, K., Shimamura, S., Mori, K., Hiraki, T., et al. (2013). Brevundimonas abyssalis sp. nov., a dimorphic prosthecate bacterium isolated from deep-subsea floor sediment. *Int. J. Syst. Evol. Microbiol.* 63, 1987–1994. doi:10.1099/ijs.0.043364-0.

Tsurumaru, H., Ito, N., Mori, K., Wakai, S., Uchiyama, T., Iino, T., et al. (2018). An extracellular [NiFe] hydrogenase mediating iron corrosion is encoded in a genetically unstable genomic island in Methanococcus maripaludis. *Sci. Rep.* 8, 15149. doi:10.1038/s41598-018-33541-5.

Tucci, M., Carolina, C. V., Resitano, M., Matturro, B., Crognale, S., Pietrini, I., et al. (2021a). Simultaneous removal of hydrocarbons and sulfate from groundwater using a "bioelectric well." *Electrochim. Acta* 388, 138636. doi:10.1016/j.electacta.2021.138636.

Tucci, M., Cruz Viggi, C., Esteve Núñez, A., Schievano, A., Rabaey, K., and Aulenta, F. (2021b). Empowering electroactive microorganisms for soil remediation: Challenges in the bioelectrochemical removal of petroleum hydrocarbons. *Chem. Eng. J.* 419, 130008. doi:10.1016/j.cej.2021.130008.

UNESCO/UN-Water (2020). *The United Nations world water development report 2020:*

water and climate change - UNESCO Digital Library. Paris Available at: https://unesdoc.unesco.org/ark:/48223/pf0000372985 [Accessed July 15, 2020].

Varanasi, J. L., Veerubhotla, R., and Das, D. (2017). Diagnostic tools for the assessment of MFC. *Microb. Fuel Cell A Bioelectrochemical Syst. that Convert. Waste to Watts*, 249–268. doi:10.1007/978-3-319-66793-5_13.

Veerman, J., and Vermaas, D. A. (2016). "Reverse electrodialysis," in *Sustainable Energy from Salinity Gradients* (Elsevier), 77–133. doi:10.1016/B978-0-08-100312-1.00004-3.

Viggi, C. C., Colantoni, S., Falzetti, F., Bacaloni, A., Montecchio, D., and Aulenta, F. (2020). Conductive Magnetite Nanoparticles Enhance the Microbial Electrosynthesis of Acetate from CO 2 while Diverting Electrons away from Methanogenesis. *Fuel Cells* 20, 98–106. doi:10.1002/fuce.201900152.

Vij, V., Sultan, S., Harzandi, A. M., Meena, A., Tiwari, J. N., Lee, W.-G., et al. (2017). Nickel-Based Electrocatalysts for Energy-Related Applications: Oxygen Reduction, Oxygen Evolution, and Hydrogen Evolution Reactions. *ACS Catal.* 7, 7196–7225. doi:10.1021/acscatal.7b01800.

Vijayaraj, M., Gadiou, R., Anselme, K., Ghimbeu, C., Vix-Guterl, C., Orikasa, H., et al. (2010). The Influence of Surface Chemistry and Pore Size on the Adsorption of Proteins on Nanostructured Carbon Materials. *Adv. Funct. Mater.* 20, 2489–2499. doi:10.1002/adfm.201000288.

Vilajeliu-Pons, A., Puig, S., Salcedo-Dávila, I., Balaguer, M. D., and Colprim, J. (2017). Long-term assessment of six-stacked scaled-up MFCs treating swine manure with different electrode materials. *Environ. Sci. Water Res. Technol.* 3, 947–959. doi:10.1039/C7EW00079K.

Virdis, B., Rabaey, K., Rozendal, R. A., Yuan, Z., and Keller, J. (2010). Simultaneous nitrification, denitrification and carbon removal in microbial fuel cells. *Water Res.* 44, 2970–2980. doi:10.1016/j.watres.2010.02.022.

Voordeckers, J. W., Kim, B.-C., Izallalen, M., and Lovley, D. R. (2010). Role of Geobacter sulfurreducens Outer Surface c -Type Cytochromes in Reduction of Soil Humic Acid and Anthraquinone-2,6-Disulfonate. *Appl. Environ. Microbiol.* 76, 2371–2375. doi:10.1128/AEM.02250-09.

Wang, A.-J., Cheng, H.-Y., Liang, B., Ren, N.-Q., Cui, D., Lin, N., et al. (2011). Efficient Reduction of Nitrobenzene to Aniline with a Biocatalyzed Cathode. *Environ. Sci. Technol.* 45, 10186–10193. doi:10.1021/es202356w.

Wang, H., and Ren, Z. J. (2013). A comprehensive review of microbial electrochemical systems as a platform technology. *Biotechnol. Adv.* 31, 1796–1807. doi:10.1016/j.biotechadv.2013.10.001.

Wang, H., and Ren, Z. J. (2014). Bioelectrochemical metal recovery from wastewater: A review. *Water Res.* 66, 219–232. doi:10.1016/j.watres.2014.08.013.

Wang, Q., Huang, L., Yu, H., Quan, X., Li, Y., Fan, G., et al. (2015a). Assessment of five different cathode materials for Co(II) reduction with simultaneous hydrogen evolution in microbial electrolysis cells. *Int. J. Hydrogen Energy* 40, 184–196. doi:10.1016/j.ijhydene.2014.11.014.

Wang, X., Aulenta, F., Puig, S., Esteve-Núñez, A., He, Y., Mu, Y., et al. (2020a).

Microbial electrochemistry for bioremediation. *Environ. Sci. Ecotechnology* 1, 100013. doi:10.1016/j.ese.2020.100013.

Wang, Y., Alsmeyer, D. C., and McCreery, R. L. (1990). Raman spectroscopy of carbon materials: structural basis of observed spectra. *Chem. Mater.* 2, 557–563. doi:10.1021/cm00011a018.

Wang, Y., Huang, F., Nogi, Y., Pang, S., Wang, P., and Lv, J. (2015b). Youhaiella tibetensis gen. nov., sp. nov., isolated from subsurface sediment. *Int. J. Syst. Evol. Microbiol.* 65, 2048–2055. doi:10.1099/ijs.0.000219.

Wang, Y., Xu, A., Cui, T., Zhang, J., Yu, H., Han, W., et al. (2020b). Construction and application of a 1-liter upflow-stacked microbial desalination cell. *Chemosphere* 248, 126028. doi:10.1016/j.chemosphere.2020.126028.

Wang, Z., Cao, C., Zheng, Y., Chen, S., and Zhao, F. (2014). Abiotic Oxygen Reduction Reaction Catalysts Used in Microbial Fuel Cells. *ChemElectroChem* 1, 1813–1821. doi:10.1002/celc.201402093.

Webster, D. P., TerAvest, M. A., Doud, D. F. R., Chakravorty, A., Holmes, E. C., Radens, C. M., et al. (2014). An arsenic-specific biosensor with genetically engineered Shewanella oneidensis in a bioelectrochemical system. *Biosens. Bioelectron.* 62, 320–324. doi:10.1016/j.bios.2014.07.003.

Wei, M., Harnisch, F., Vogt, C., Ahlheim, J., Neu, T. R., and Richnow, H. H. (2015). Harvesting electricity from benzene and ammonium-contaminated groundwater using a microbial fuel cell with an aerated cathode. *RSC Adv.* 5, 5321–5330. doi:10.1039/C4RA12144A.

Weiner, A. M., McGovern, R. K., and Lienhard V, J. H. (2015). A new reverse electrodialysis design strategy which significantly reduces the levelized cost of electricity. *J. Memb. Sci.* 493, 605–614. doi:10.1016/j.memsci.2015.05.058.

Wen, Q., Zhang, H., Chen, Z., Li, Y., Nan, J., and Feng, Y. (2012). Using bacterial catalyst in the cathode of microbial desalination cell to improve wastewater treatment and desalination. *Bioresour. Technol.* 125, 108–113. doi:10.1016/j.biortech.2012.08.140.

Wen, Q., Zhang, H., Yang, H., Chen, Z., Nan, J., and Feng, Y. (2014). Improving desalination by coupling membrane capacitive deionization with microbial desalination cell. *Desalination* 354, 23–29. doi:10.1016/j.desal.2014.09.027.

Wenzel, T., Härtter, D., Bombelli, P., Howe, C. J., and Steiner, U. (2018). Porous translucent electrodes enhance current generation from photosynthetic biofilms. *Nat. Commun.* 9, 1–9. doi:10.1038/s41467-018-03320-x.

Werner, C. M., Logan, B. E., Saikaly, P. E., and Amy, G. L. (2013). Wastewater treatment, energy recovery and desalination using a forward osmosis membrane in an air-cathode microbial osmotic fuel cell. *J. Memb. Sci.* 428, 116–122. doi:10.1016/j.memsci.2012.10.031.

Xiao, Y., Zhang, E., Zhang, J., Dai, Y., Yang, Z., Christensen, H. E. M., et al. (2017). Extracellular polymeric substances are transient media for microbial extracellular electron transfer. *Sci. Adv.* 3, e1700623. doi:10.1126/sciadv.1700623.

Xie, X., Hu, L., Pasta, M., Wells, G. F., Kong, D., Criddle, C. S., et al. (2011). Three-dimensional carbon nanotube-textile anode for high-performance microbial fuel

cells. *Nano Lett.* 11, 291–296. doi:10.1021/nl103905t.

Xing, D., Zuo, Y., Cheng, S., Regan, J. M., and Logan, B. E. (2008). Electricity Generation by Rhodopseudomonas palustris DX-1. *Environ. Sci. Technol.* 42, 4146–4151. doi:10.1021/es800312v.

Xu, X.-W., Huo, Y.-Y., Wang, C.-S., Oren, A., Cui, H.-L., Vedler, E., et al. (2011). Pelagibacterium halotolerans gen. nov., sp. nov. and Pelagibacterium luteolum sp. nov., novel members of the family Hyphomicrobiaceae. *Int. J. Syst. Evol. Microbiol.* 61, 1817–1822. doi:10.1099/ijs.0.023325-0.

Yang, E., Chae, K.-J., Choi, M.-J., He, Z., and Kim, I. S. (2019a). Critical review of bioelectrochemical systems integrated with membrane-based technologies for desalination, energy self-sufficiency, and high-efficiency water and wastewater treatment. *Desalination* 452, 40–67. doi:10.1016/j.desal.2018.11.007.

Yang, E., Choi, M.-J., Kim, K.-Y., Chae, K.-J., and Kim, I. S. (2015). Effect of initial salt concentrations on cell performance and distribution of internal resistance in microbial desalination cells. *Environ. Technol.* 36, 852–860. doi:10.1080/09593330.2014.964333.

Yang, E., Choi, M.-J., Kim, K.-Y., and Kim, I. S. (2013). Improvement of biohydrogen generation and seawater desalination in a microbial electrodialysis cell by installing the direct proton transfer pathway between the anode and cathode chambers. *Desalin. Water Treat.* 51, 6362–6369. doi:10.1080/19443994.2013.780997.

Yang, E., Choi, M.-J., Kim, K.-Y., and Kim, I. S. (2014). Microbial desalination cell for concurrent hydrogen peroxide production and desalination. *J. Environ. Eng. Sci.* 9, 197–206. doi:10.1680/jees.14.00006.

Yang, N., Zhan, G., Li, D., Wang, X., He, X., and Liu, H. (2019b). Complete nitrogen removal and electricity production in Thauera-dominated air-cathode single chambered microbial fuel cell. *Chem. Eng. J.* 356, 506–515. doi:10.1016/j.cej.2018.08.161.

Ye, B., Luo, H., Lu, Y., Liu, G., Zhang, R., and Li, X. (2017). Improved performance of the microbial electrolysis desalination and chemical-production cell with enlarged anode and high applied voltages. *Bioresour. Technol.* 244, 913–919. doi:10.1016/j.biortech.2017.08.049.

Yee, M. O., Deutzmann, J., Spormann, A., and Rotaru, A. E. (2020). Cultivating electroactive microbes-from field to bench. *Nanotechnology* 31. doi:10.1088/1361-6528/ab6ab5.

Yoon, J.-H., Kang, S.-J., Park, S., and Oh, T.-K. (2007). Devosia insulae sp. nov., isolated from soil, and emended description of the genus Devosia. *Int. J. Syst. Evol. Microbiol.* 57, 1310–1314. doi:10.1099/ijs.0.65028-0.

Yu, H., Feng, C., Liu, X., Yi, X., Ren, Y., and Wei, C. (2016). Enhanced anaerobic dechlorination of polychlorinated biphenyl in sediments by bioanode stimulation. *Environ. Pollut.* 211, 81–89. doi:10.1016/j.envpol.2015.12.039.

Yuan, C.-G., Jiang, Z., Xiao, M., Zhou, E.-M., Kim, C.-J., Hozzein, W. N., et al. (2016a). Mesorhizobium sediminum sp. nov., isolated from deep-sea sediment. *Int. J. Syst. Evol. Microbiol.* 66, 4797–4802. doi:10.1099/ijsem.0.001432.

Yuan, H., Abu-Reesh, I. M., and He, Z. (2015). Enhancing desalination and wastewater

treatment by coupling microbial desalination cells with forward osmosis. *Chem. Eng. J.* 270, 437–443. doi:10.1016/j.cej.2015.02.059.

Yuan, H., Hou, Y., Abu-Reesh, I. M., Chen, J., and He, Z. (2016b). Oxygen reduction reaction catalysts used in microbial fuel cells for energy-efficient wastewater treatment: a review. *Mater. Horizons* 3, 382–401. doi:10.1039/C6MH00093B.

Yuan, H., Sun, S., Abu-Reesh, I. M., Badgley, B. D., and He, Z. (2017). Unravelling and Reconstructing the Nexus of Salinity, Electricity, and Microbial Ecology for Bioelectrochemical Desalination. *Environ. Sci. Technol.* 51, 12672–12682. doi:10.1021/acs.est.7b03763.

Zhan, G., Zhang, L., Li, D., Su, W., Tao, Y., and Qian, J. (2012). Autotrophic nitrogen removal from ammonium at low applied voltage in a single-compartment microbial electrolysis cell. *Bioresour. Technol.* 116, 271–277. doi:10.1016/j.biortech.2012.02.131.

Zhang, B., and He, Z. (2012). Integrated salinity reduction and water recovery in an osmotic microbial desalination cell. *RSC Adv.* 2, 3265. doi:10.1039/c2ra20193c.

Zhang, B., and He, Z. (2013). Improving water desalination by hydraulically coupling an osmotic microbial fuel cell with a microbial desalination cell. *J. Memb. Sci.* 441, 18–24. doi:10.1016/j.memsci.2013.04.005.

Zhang, B., Zheng, X., Voznyy, O., Comin, R., Bajdich, M., García-Melchor, M., et al. (2016a). Homogeneously dispersed multimetal oxygen-evolving catalysts. *Science* 352, 333–7. doi:10.1126/science.aaf1525.

Zhang, D., Yang, H., Huang, Z., Zhang, W., and Liu, S.-J. (2002). Rhodopseudomonas faecalis sp. nov., a phototrophic bacterium isolated from an anaerobic reactor that digests chicken faeces. *Int. J. Syst. Evol. Microbiol.* 52, 2055–2060. doi:10.1099/00207713-52-6-2055.

Zhang, F., Chen, M., Zhang, Y., and Zeng, R. J. (2012). Microbial desalination cells with ion exchange resin packed to enhance desalination at low salt concentration. *J. Memb. Sci.* 417–418, 28–33. doi:10.1016/j.memsci.2012.06.009.

Zhang, F., and He, Z. (2015). Scaling up microbial desalination cell system with a post-aerobic process for simultaneous wastewater treatment and seawater desalination. *Desalination* 360, 28–34. doi:10.1016/j.desal.2015.01.009.

Zhang, H., Wen, Q., An, Z., Chen, Z., and Nan, J. (2016b). Analysis of long-term performance and microbial community structure in bio-cathode microbial desalination cells. *Environ. Sci. Pollut. Res.* 23, 5931–5940. doi:10.1007/s11356-015-5794-7.

Zhang, J., Xiang, J., Dong, Z., Liu, Y., Wu, Y., Xu, C., et al. (2014). Biomass derived activated carbon with 3D connected architecture for rechargeable lithium−sulfur batteries. *Electrochim. Acta* 116, 146–151. doi:10.1016/j.electacta.2013.11.035.

Zhang, L., Song, M., Chen, X.-L., Xu, R.-J., Chen, K., Li, S.-P., et al. (2015). Devosia honganensis sp. nov., isolated from the soil of a chemical factory. *Antonie Van Leeuwenhoek* 108, 1301–1307. doi:10.1007/s10482-015-0582-4.

Zhang, T., Gannon, S. M., Nevin, K. P., Franks, A. E., and Lovley, D. R. (2010). Stimulating the anaerobic degradation of aromatic hydrocarbons in contaminated sediments by providing an electrode as the electron acceptor. *Environ. Microbiol.*

12, 1011–1020. doi:10.1111/j.1462-2920.2009.02145.x.

Zhang, T., and Zhang, H. (2022). Electrochemical analysis for the rapid screening of copper-tolerant bacteria. *Bioelectrochemistry* 148, 108276. doi:10.1016/j.bioelechem.2022.108276.

Zhang, X. (2019). Electroactive biofilms: novel tools and insights towards charge storage. Available at: https://biblio.ugent.be/publication/8630340/file/8630343.pdf [Accessed February 14, 2022].

Zhang, X., Philips, J., Roume, H., Guo, K., Rabaey, K., and Prévoteau, A. (2017). Rapid and Quantitative Assessment of Redox Conduction Across Electroactive Biofilms by using Double Potential Step Chronoamperometry. *ChemElectroChem* 4, 1026–1036. doi:10.1002/celc.201600853.

Zhang, Y., and Angelidaki, I. (2013). A new method for in situ nitrate removal from groundwater using submerged microbial desalination–denitrification cell (SMDDC). *Water Res.* 47, 1827–1836. doi:10.1016/j.watres.2013.01.005.

Zhao, F., Harnisch, F., Schröder, U., Scholz, F., Bogdanoff, P., and Herrmann, I. (2006). Challenges and Constraints of Using Oxygen Cathodes in Microbial Fuel Cells. *Environ. Sci. Technol.* 40, 5193–5199. doi:10.1021/es060332p.

Zhou, M., Wang, H., Hassett, D. J., and Gu, T. (2013). Recent advances in microbial fuel cells (MFCs) and microbial electrolysis cells (MECs) for wastewater treatment, bioenergy and bioproducts. *J. Chem. Technol. Biotechnol.* 88, 508–518. doi:10.1002/jctb.4004.

Zhu, T., Zhang, Y., Bu, G., Quan, X., and Liu, Y. (2016). Producing nitrite from anodic ammonia oxidation to accelerate anammox in a bioelectrochemical system with a given anode potential. *Chem. Eng. J.* 291, 184–191. doi:10.1016/j.cej.2016.01.099.

Zhuang, Z., Yang, G., Mai, Q., Guo, J., Liu, X., and Zhuang, L. (2020). Physiological potential of extracellular polysaccharide in promoting Geobacter biofilm formation and extracellular electron transfer. *Sci. Total Environ.* 741, 140365. doi:10.1016/j.scitotenv.2020.140365.

Zuo, K., Cai, J., Liang, S., Wu, S., Zhang, C., Liang, P., et al. (2014). A Ten Liter Stacked Microbial Desalination Cell Packed With Mixed Ion-Exchange Resins for Secondary Effluent Desalination. *Environ. Sci. Technol.* 48, 9917–9924. doi:10.1021/es502075r.

Zuo, K., Chang, J., Liu, F., Zhang, X., Liang, P., and Huang, X. (2017). Enhanced organics removal and partial desalination of high strength industrial wastewater with a multi-stage microbial desalination cell. *Desalination* 423, 104–110. doi:10.1016/j.desal.2017.09.018.

Zuo, K., Chen, M., Liu, F., Xiao, K., Zuo, J., Cao, X., et al. (2018). Coupling microfiltration membrane with biocathode microbial desalination cell enhances advanced purification and long-term stability for treatment of domestic wastewater. *J. Memb. Sci.* 547, 34–42. doi:10.1016/j.memsci.2017.10.034.

Zuo, K., Liu, F., Ren, S., Zhang, X., Liang, P., and Huang, X. (2016). A novel multi-stage microbial desalination cell for simultaneous desalination and enhanced organics and nitrogen removal from domestic wastewater. *Environ. Sci. Water Res. Technol.* 2, 832–837. doi:10.1039/C6EW00196C.

Zuo, K., Yuan, L., Wei, J., Liang, P., and Huang, X. (2013). Competitive migration behaviors of multiple ions and their impacts on ion-exchange resin packed microbial desalination cell. *Bioresour. Technol.* 146, 637–642. doi:10.1016/j.biortech.2013.07.139.

Nomenclature

List of abbreviations

Abbreviations	Definition (units)
ACN	Acrylonitrile
AEM	Anion Exchange membrane
AFM	Atomic Force Microscopy
ATP	Adenosine triphosphate
BES	Bioelectrochemical systems
BO	Burn Off
BOD	Biological Oxygen Demand
BPM	Bipolar Membrane
CA	Chronoamperometry
CE	Counter Electrode
CEC	Circulated Electric Charge (C m^{-3})
CEM	Cation Exchange Membrane
CIET	Conductive-particle-mediated Interspecies Electron Transfer
Cit-c	C-type cytochrome
CNF	Carbon-nanofibers
CNT-CS	Carbon Nanotubes - Chitosan
CNTs	Carbon Nanotubes
COD	Chemical Oxygen Demand (mg L^{-1})
CV	Cyclic Voltammetry
CW	Constructed Wetland
CW-MFC	Constructed Wetland -MFC
DEET	Direct Extracellular Electron Transfer
DIET	Direct Interspecies Electron Transfer
DS	Desalting Cycle
DTG	Derivative Thermogravimetry

EAB	Electroactive bacteria
EC	Electric conductivity (mS cm^{-1})
EC_f	Final Electric conductivity (mS cm^{-1})
ECFM	Electrospun - Carbon - Nanofiber
EC_i	Initial Electric conductivity (mS cm^{-1})
EC_m	Medium Electric conductivity (mS cm^{-1})
ED	Electrodialysis
EDLC	Electrical Double Layer Capacitance
EDN	Electron donor
EET	Extracellular Electron Transfer
EG	Expanded Graphite
EPS	Exopolysaccharides
FO	Forward Osmosis
FWM	Fresh Water Medium
GHG	Greenhouse Gas Emissions
HFM-MDC	Hollow Fiber Microfiltration Membrane MDC
HPLC	High-performance liquid chromatography
HRT	Hydraulic Retention Time
IDA	International Desalination Association
IEET	Indirect Extracellular Electron Transfer
IEM	Ion-exchange membrane
IER	Ion-exchange resin
ITO	Non-porous indium tin oxide
LCA	Life Cycle Assessment
LSM	Fluorescence Laser Scanning Microscopy
MCDC	Microbial Capacitive Desalination Cell
MDC	Microbial Desalination Cell
MEC	Microbial Electrolysis Cell
MED	Multi-Effect Distillation
MEDC	Microbial Electrodialysis Cell
MEDCC	Microbial Electrolysis Desalination and Chemical - Production Cell

MEET	Microbial Extracellular Electron Transfer
ME-FBR	Microbial Electrochemical Fluidized bed reactor
MES	Microbial Electron Sink
MESyn	Microbial Electrosynthesis
MET	Microbial Electrochemical Technologies
MFC	Microbial Fuel Cell
MHC	Multi-heme c-type Cytochromes
MIDES	Microbial Desalination for Low Energy Drinking Water
M–MDC	Multi-stage MDCs
MSF	Multi-stage Flash
MW	Molecular Weight
NADH	Nicotinamide adenine dinucleotide
NCP-CFM	Natural Cellulose Paper – Carbon Nanofiber Material
NDR	Nominal Desalination Rate (L m^{-2} h^{-1})
NF	Nanofiltration
OCP / OCV	Open Circuit Potential / Open Circuit Voltage (V)
OD	Optical density
OMCs	Outer-membrane multiheme c-type cytochrome
OMV	Outer-membrane vesicles
OR	Oxidation Rate
ORR	Oxygen Reduction Reaction
OsMDC	Osmotic MDC
OX	Oxidized specie
PAH	Polycyclic Aromatic Hydrocarbons
PBS	Phosphate Buffer Solution
P-MDC	Photosynthetic MDC
PPB	Purple Phototrophic Bacteria
PPY	Polypyrrole
PVDF	Polyvinylidene Fluoride
RE	Reference Electrode
RED	Reduced specie

rMDC	Recirculation MDC
R-MDC	Ion-exchange resin packed MDC
RO	Reverse Osmosis
SDG	Sustainable Developments Goals
SEM	Scanning Electron Microscopy
SEP	Specific energy production (kWh m-3)
SHE	Standard Hydrogen Electrode
SI	Supplementary Information
sMDC	Stacked MDC
SMDDC	Submerged Microbial Desalination-Denitrification Cell
sMFC	Sedimentary MFC
SR	Salt removal (%)
STP	Standard temperature and pressure
T	Temperature
TDS	Total Dissolved Solids (mg L^{-1})
TEA	Terminal Electron Acceptor
TG	Thermogravimetry
TGA/DSC	Thermogravimetric Analyzer / Differential Scanning Calorimeter
TOC	Total Organic Carbon (mg L^{-1})
TSS	Total Suspended Solids (mg L^{-1})
UDCF	Unidirectional Carbon Fiber
UMDC	Tubular up-flow MDC
UN	United Nations
UV	Ultraviolet
VFA	Volatile Fatty Acids
WE	Working Electrode
WP	Work Package
WW	Wastewater
XPS	X-ray photoelectron spectroscopy
XRD	X-ray diffraction

List of symbols and subscripts

Symbols / subscripts	Definition (units)
E^0	Standard potential (V)
$E^{0'}$	Formal standard potential (V)
V_{an}: V_{sal}: V_{cat}	Tank Volume ratio between anolyte, saline and catholyte
j	Current density (mA cm^{-2})
j_{max}	Maximum current density (mA cm^{-2})
j_{pa} / j_{pc}	Anodic / Cathodic Current peak
I	Electric current (A)
A_e	Geometric electrode surface area (cm^2)
η_{cb}	Current efficiency (%)
E_{cell}	Electric potential provided by the MDC device (V)
E_{app}	Electric potential applied (V)
Q_t	Desalinated water volume (L)
υ	Stoichiometric coefficient
z	Salt ion valence
F	Faraday constant (96485 C mol^{-1} of electrons).
c_s^i	Molar salt concentrations in the saline tank at the beginning desalination cycle (mol m^{-3})
c_s^f	Molar salt concentrations in the saline tank at the final desalination cycle (mol m^{-3})
A_m	Geometric area of membrane surface (m^2)
t_d	Desalination time (h)
T_{NaCl}	Salt removal rate (mg NaCl h^{-1})
Δ *COD*	Consumption of chemical oxygen demand in desalination cycle (kg)
V_A	Liquid in the anode compartment (m^3)
V_s	Liquid in the middle desalination compartment (m^3)

COD_{rate}	Chemical Oxygen Demand removal rate / Treatment capacity (kg COD m^{-3} day^{-1})
η_{Cb}	Coulombic efficiency (%)
$Pm\ (Ac)$	Molecular weight of acetate (59 g mol^{-1})
$Pm\ (O_2)$	Molecular weight of oxygen (32 g mol^{-1})
b	Number of moles of electrons produced per moles of acetate (b= 8 moles of electrons per mol of acetate oxidised to CO_2). Or number of moles of electrons per mol of oxygen consumed (b= 4 moles of electrons per mol of oxygen consumed towards CO_2).
Q_{An}	Volume of anolyte tank (L)
$\Delta[Ac]$	Change in concentration of acetate in desalination cycle
R_{ext}	External resistance/ load (Ω)
E_{emf}	Electromotive force (V)
E_{η}	Overpotential of electrodes
E_{Ω}	Voltage lost across internal resistances
$\Delta E^{0'}$	Different potential (standard conditions, neutral pH) (V)
$\Delta G^{0'}$	Gibbs free energy change (standard conditions, neutral pH) (kJ mol^{-1})
E_a	Anode potential (V)
E_c	Cathode potential (V)
R_{memb}	Sum of electric resistances of ion exchange membranes (Ω)
R_{saline}	Electric resistance due to saline chamber (Ω)
EC	Electric conductivity
P_{cell}	Electric power (W)
Q	Total circulated charge (C)
n	Number of electrons transferred in redox reaction
L	Thickness of saline compartment (cm)
E_{drop}	Potential drop (V)
E_{load}	Potential load (V)
C_0	Initial concentration

C_{ox}	Oxidized specie
C_{red}	Reduced specie
$a^2_{H_2O}$	Activity of product / reagent
R	Gas constant (8.314 J mol^{-1} K^{-1})
p_{O_2}	Partial pressure
d	Pore diameter
t	Holding time (h) in isothermal treatment
P	Pressure (atm)
S_{BET} or A_{BET}	Specific surface area or apparent surface area
A_{DR}	Surface area
V_{DR} (N_2)	Total volume micropore
V_{DR} (CO_2)	Volume of narrowest micropore or ultramicropore
$V_{0.995}$	Total Volume of pores at relative pressure of 0.995
V_{meso}	Mesopore volume
E_{act}	Activation energy
A	Pre-exponential factor
$\Delta wt/\Delta t$	Rate of weight loss

Seawater desalination and the reuse of treated water have been proposed as solutions to alleviate the problems associated with the worldwide scarcity of water resources, which is one of the most significant challenges of the 21st century. While conventional desalination processes are technologically feasible, they suffer from high energy consumption, hindering their widespread adoption.

Microbial Desalination Cell (MDC) technology is a sustainable and energy-self-sufficient bioelectrochemical approach that simultaneously treats wastewater, produces power, and desalinates water within the same device, without the need for external power input. The desalination process in the MDC device is driven by the energy provided by electroactive microorganisms through the degradation of organic matter contained in the wastewater. However, the implementation of MDC technology on a larger scale depends on overcoming its limitations. Research efforts are needed to unlock the full potential of MDC technology forward the sustainable desalination in a water-scarce world.

Universidad de Alcalá